



Thèse présentée pour obtenir le grade de
Docteur de l'Université de Strasbourg
Discipline : Chimie
Spécialité : Chimie-Physique
Présentée par : Artur Ciesielski

Supramolecular nanochemistry: from self-assembly to responsive architectures

*Nanochemistry Laboratory, Institut de Science et d'Ingénierie Supramoléculaires (ISIS),
Université de Strasbourg (France)*

Membres du Jury

Prof. Steven De Feyter, Katholieke Universiteit Leuven - Rapporteur externe

Dr. Vincenzo Palermo, Consiglio Nazionale delle Ricerche - Rapporteur externe

Prof. Vincent Ball, Université de Strasbourg - Rapporteur interne

Prof. Jack M. Harrowfield, Université de Strasbourg - Rapporteur invité

Prof. Paolo Samorì, Université de Strasbourg - Directeur de thèse

Table of Contents

Abbreviations	I
Abstract	III
Résumé	X
1 Two dimensional supramolecular architectures probed by STM	1
1.1 Introduction	1
1.2 Hydrogen-bonding Interactions	4
1.2.1 Weak Hydrogen-bonding interactions	5
1.2.2 Carboxylic Acids as Di-hapto Hydrogen-bonding moieties	9
1.2.3 Combined Di-hapto Hydrogen-bond and van der Waals Interactions	14
1.2.4 Tri-hapto Hydrogen-bonding moieties	17
1.2.5 Tetra-hapto Hydrogen-bonding moieties	19
1.2.6 Strength of Hydrogen-bonding interactions	21
1.3 Metallo-Ligand Interactions	23
1.4 Van der Waals interactions	27
References	32
2 Scanning Tunneling Microscopy	39
2.1 Introduction to STM	39
2.2 Working Principle of STM	40
2.3 Set-Up of Scanning Tunneling Microscope	44
2.4 Operation Modes of STM	45
2.5 STM Tips.....	46
2.6 Concentration of investigated solutions.....	47
References	50
3 Methods	51
3.1 STM at the solid-liquid interface	51
3.2 Substrate	52
3.3 Solvent.....	54
References	56

4 1D coordination networks at the solid-liquid interface	58
4.1 Introduction	59
4.2 Results and discussion	63
4.3 Conclusions	68
4.4 Experimental procedures	69
References	70
5 Self-assembled architectures based on H-bonding	72
5.1 Mono-component 2D supramolecular porous networks	73
5.1.1 Introduction.....	74
5.1.2 Results and discussion	75
5.1.3 Conclusions	82
5.1.4 Experimental procedures	82
References	83
5.2 1D supramolecular helical polymers	86
5.2.1 Introduction.....	87
5.2.2 Results and discussion	89
5.2.3 Conclusions	97
5.2.4 Experimental procedures	98
References	99
5.3 H-bonded bi-component supramolecular 1D polymers	103
5.3.1 Introduction.....	104
5.3.2 Results and discussion	106
5.3.3 Conclusions	111
5.3.4 Experimental procedures	112
References	113
5.4 Self-assembly of N^9-alkylguanines at the solid-liquid interface	116
5.4.1 Introduction.....	117
5.4.2 Results and discussion	118
5.4.3 Conclusions	125
5.4.4 Experimental procedures	125
References	126

6 Dynamers at the solid-liquid interface	129
6.1 Reversible assembly/re-assembly process between two highly ordered supramolecular guanine motifs .	130
6.1.1 Introduction.....	131
6.1.2 Results and discussion	133
6.1.3 Conclusions	138
6.1.4 Experimental procedures	138
References	139
6.2 Modulating the self-assembly at the solid-liquid interface by pH-mediated conformational switching	142
6.2.1 Introduction.....	143
6.2.2 Results and discussion	144
6.2.3 Conclusions	148
6.2.4 Experimental procedures	149
References	150
6.3 3D responsive self-assembled monolayers: positioning molecular functions onto the surface	152
6.3.1 Introduction.....	153
6.3.2 Results and discussion	157
6.3.3 Conclusions	163
6.3.4 Experimental procedures	164
References	164
Conclusions and Perspectives	167
Acknowledgments	171
List of Publications	172

Abbreviations

Å	Ångström
A	Acceptor
AA	Acceptor-acceptor
ADA	Acceptor-donor-acceptor
ADAD	Acceptor-donor-acceptor-donor
AFM	Atomic force microscopy
BTP	2,6-bis(1-phenyl-1,2,3-triazol-4-yl)pyridine
°C	Centigrade degree
COSY	Correlation spectroscopy
D	Donor
DD	Donor-donor
DAD	Donor-acceptor-donor
DADA	Donor-acceptor-donor-acceptor
GMP	Guanosine monophosphate
HBC	Hexabenzocoronene
HOMO	Highest occupied molecular orbital
HOPG	Highly oriented pyrolytic graphite
HR-MS	High-resolution mass spectroscopy
L	Litre
LDOS	Local density of states
LUMO	Lowest unoccupied molecular orbital
MD	Molecular dynamics
MS	Mass spectroscopy
nm	Nanometer
NMR	Nuclear magnetic resonance
NOESY	Nuclear Overhauser effect spectroscopy
OF	Oligofluorene
OLED	Organic light emitting diode
OPV	Oligophenylenevinylene
pA	Picoamperes
PSS	Photostationary state
Pt/Ir	Platinum-iridium
PTCDI	Perylene-3,4,9,10-tetracarboxylic di-imide
SAM	Self-assembled monolayer

STM	Scanning tunneling microscopy
TCB	1,2,4-trichlorobenzene
TMA	Trimesic acid
TPT	1,3,5-tris(4-pyridyl)-2,4,6-triazine
TPTC	Terphenyl-3,5,3',5'-tetracarboxylic acid
TSB	(1,3,5-tris[(E)-2-(3,5-didecyloxyphenyl)-ethenyl]benzene
TTF	Tetrathiafulvalene
UHV	Ultra-high vacuum
UV	Ultraviolet
UV-Vis	Ultraviolet-visible
V	Volts
WKB	Wentzel-Kramers-Brillouin

Abstract

Supramolecular chemistry is one of the most important innovations in inorganic, organic and bio-chemistry in the last few decades.^[1] Supramolecular chemistry relies on the use of non-covalent interactions to self-assemble, with a precision on the sub-nanometer scale, chemical entities forming materials with pre-programmed chemical and physical properties: thus supramolecular chemistry is key to nanoscience and nanotechnology. Supramolecular chemistry offers high control over the process of molecular self-assembly: due to its unique nature it combines reversibility, directionality, specificity and cooperativity. Supramolecular chemistry has been mastered so far in particular in solution, in 3D crystals^[2, 3] and in 2D at surfaces under ultra-high vacuum environment.^[4, 5] In 2D at the solid-liquid interface, an environment under which much wet chemistry can be performed, these concepts have not been fully exploited yet.

Since nearly three decades surfaces and interfaces can be mapped with a sub-nanometer spatial resolution making use of Scanning Probe Microscopies. In this frame, the invention of Scanning Tunneling Microscopy (STM) in 1981^[6] and later Atomic Force Microscopy (AFM) in 1986^[7] boosted the scope to nanoscience and nanotechnology. These two techniques, especially STM, made it possible to visualize and manipulate single molecules, therefore study a variety of physico-chemical properties and processes of nanostructured materials. STM can operate under various environmental conditions including ultra-high vacuum (UHV), gas stream, air and liquid, thus making it possible to investigate structure and reactivity in 2D with a single molecules resolution. Over the past two decades, numerous examples of STM visualization of molecule and architectures thereof have been reported^[8, 9] for various materials type including liquid-crystals, conductive molecular crystals, proteins and self-assembled monolayers.

In this thesis we focused our attention on self-assembly of different molecular systems leading to the formation of supramolecular nanostructures resulting from a balance between intra- and inter-molecular interactions as well as interfacial forces. The structural and dynamic properties have been studied at the sub-nanometer scale using the Scanning Tunneling Microscopy (STM).

The nanostructures which were developed in the context of this work are not only of interest as an exercise of nanoscale controlled self-assembly at surfaces but also as potential candidates for applications in electronics.

To explore the use of different non-covalent interactions leading to the formation of functional supramolecular assemblies, we studied the following systems:

- An optically active anthracene based moiety bearing two ethynyl groups equipped with a monodentate (pyridine) and a tridentate (terpyridine) poles, known to form 1D coordination polymers in the presence of metal ions.^[10]
- A hexatopic diacetylamino-pyridine molecules which can adopt a three-fold symmetry and form 2D porous network at the solid substrates by formation multiple hydrogen bonds.^[11]
- A rigid molecule bearing two pyridin-2(1H)-one units, in order to form 1D supramolecular hydrogen-bonded helical polymers at the solid-liquid interface.
- A ditopic molecular components, bearing complementary hydrogen-bonding recognition groups, known to form 1D bi-component hydrogen-bonded supramolecular polymers.^[11-13]
- A N⁹-substituted guanine molecules, in order to exploit recognition of hydrogen bonds between nucleobases and formation of so-called G-quadruplexes.^[14-17]
- 2,6-bis(1-phenyl-1,2,3-triazol-4-yl)pyridine (BTP) based components functionalized with long aliphatic chains, known to change geometrical conformation in the presence of metal ions or by protonation.^[18]
- Oligofluorene based component equipped with azobenzene functional unit, capable to undergo photoisomerisation and to change geometrical conformation upon irradiation with ultra-violet (UV) light.

Regarding anthracene derivatives,^[10, 19] we focused our attention, collaboration with the group of Prof. Mir Wais Hosseini from Université de Strasbourg (France) on component 9-(3'-pyridylethynyl)-10-[3'-ethynyl-2,2':6',2''-terpyridine]-anthracene. The combination of neutral molecules, with metal cations leads to the formation of 1D directional coordination networks. The charge balance imposes the presence of anions. When using weakly coordinating anions, the latter usually occupy the empty space between 1D networks, and often do not interact with the cationic part of the assembly. For the design principle, the formation of 1D directional

coordination networks requires metal centers offering four free coordination sites. This was studied using a Pd(II) cation associated with the weakly coordinating BF_4^- anion. A further possibility, consisting in combining two coordinating anions, such as chloride, with a dicationic metal center adopting the octahedral coordination geometry, such as Co(II), was also explored. The packing of the free molecule on graphite surfaces was studied by STM at the solid-liquid interface.

Two-dimensional supramolecular networks, especially those with void spaces, known as 2D porous networks,^[20, 21] have received an increasing amount of attention due to their templating properties, as well as frameworks for storage and studies on space confinement properties. Such structures, formed by physisorption of the building blocks on atomically flat conductive surfaces, can be investigated with the aid of STM. Robustness and long range crystallinity are some of the properties sought when engineering such 2D molecular networks, which can ultimately physisorb in a wide variety of substrates to tune physico-chemical, electrical and properties at solid-liquid interfaces, expanding the toolbox of functional self-assembled monolayers (SAMs). So far, from 2D networks formed by multiple hydrogen bonds, metal-ligand coordination or van der Waals interactions, no one has yet presented the necessary properties to form robust porous networks without the presence of polymorphism. Polymorphism, the ability to form multiple 2D architectures from the same building-blocks, is so far the main factor in decreasing the robustness of 2D porous networks, even when pre-programming strong consecutive hydrogen-bonds. In the collaboration with the group of Prof. Jean-Marie Lehn from Université de Strasbourg (France), we have identified a highly crystalline 2D network which only exhibits a limited amount of polymorphism at (sub-) monolayer concentrations. The network is formed by an hexatopic diacetylamino-pyridine molecule which can adopt a three-fold symmetry.

Supramolecular polymers combine pre-programmed geometries, stabilities and peculiar mechanical properties as direct results of the joint effect of non-covalent primary and their related secondary interactions holding together functionalized molecular modules.^[22, 23] Through the simultaneous use of multiple and interdigitated H-bonds bridging conformationally rigid molecular modules, it is possible to increase the strength of these interactions and to achieve a full control over the geometry of the supramolecular architecture.^[24] With the group of Prof. Jean-Marie Lehn, we have also studied a functionalized molecular module capable of self-

associating through self-complementary H-bonding patterns comprising interdigitated four strong and two medium strength H-bonds to form dimers with the significant strength. The self-association of these conformationally rigid phenylpyrimidine based dimers through directional H-bonding between two lateral pyridin-2(1H)-one units of neighboring molecules allowed the formation of two differently ordered supramolecular polymers as computationally confirmed by all-electron density functional studies. In particular, a concentration dependent study by Scanning Tunneling Microscopy (STM) at the solid-liquid interface revealed the controlled molecular self-assembly on graphite forming either highly compact linear supramolecular arrays laterally interacting via van der Waals forces to generate micrometer-sized 2D nanopatterns, or hundreds of nanometers long helical supramolecular polymers with a high shape persistence.

Together with the group of Prof. Jean-Marie Lehn, we also explored by STM imaging at the liquid–solid interface at room temperature the formation of supramolecular hydrogen-bonded polymers with either a linear or a *zig-zag* geometry on highly oriented pyrolytic graphite (HOPG) surfaces.^[13] To this end, we used the ditopic molecular components, bearing complementary hydrogen-bonding recognition groups: either a Janus-type cyanuric wedge or barbituric wedge (ADA-ADA-array) and a corresponding (DAD-DAD-array) receptor unit. These molecules were selected because they are known to form 1D supramolecular polymeric strands in solution by polyassociation through sextuple hydrogen bonding between their respective recognition sites.

Among all nucleobases, guanine is very versatile: depending on the experimental conditions it can undergo different self-assembly pathways.^[14] In the presence of certain metal ions, guanines can form G-quartet based architectures such as octamers or columnar polymeric aggregates. In the absence of metal templates, guanines can self-assemble, both in solution and in the solid state, into ribbon-like architectures. More interestingly, these ribbons also exhibit rectifying properties. A field-effect transistor based on this supramolecular structures, was described. In collaboration with Prof. Gian Piero Spada from University of Bologna (Italy), we decided to extend our studies at the solid-liquid interface to physisorbed monolayers of N^9 -alkylguanines because the absence of the sugar when compared to the previously studied guanosines and the presence of an aliphatic side-group can be foreseen to favor the molecular adsorption on graphite. We performed a sub-molecularly resolved STM study of physisorbed monolayers on graphite of a series of N^9 -alkylguanines with linear alkyl side-chains from $-C_2H_5$ up to $-C_{18}H_{37}$. Furthermore, we have also studied the metal-templated reversible

assembly/reassembly process of a N⁹-alkylguanine into highly ordered quartets and ribbons, achieving a submolecular resolution STM visualization of such a process at the solid-liquid interface on HOPG surfaces.^[17]

In recent years, the field of materials chemistry has greatly benefited from methodology development in organic synthesis. In particular the advent of “click chemistry” has had a tremendous impact on synthetic macromolecular and supramolecular chemistry.^[25, 26] Due to the high yield, click chemistry is typically used in materials chemistry for the construction of a large variety of architectures, including linear polymers and block copolymers, hyperbranched polymers and dendrimers, macrocycles as well as catenanes and rotaxanes among others. However, the connecting triazole moiety is usually not involved in the design and mostly serves as a mere connecting unit. We have recently engaged with the group of Prof. Stefan Hecht from Humboldt University in Berlin (Germany), in a program to utilize click chemistry to construct (macro)molecules of defined shape, thereby using the 2,6-bis(1-phenyl-1,2,3-triazol-4-yl)pyridines (BTP) motif as the key structural feature. Due to lone pair repulsion, the extended *syn,syn* conformation of the BTP scaffold is strongly destabilized and hence the BTP prefers to adopt the thermodynamically favored, kinked *anti,anti* conformation, in analogy to bipyridines or terpyridines. We have successfully taken advantage of this conformational preference to design helically folding oligomers and polymers. Furthermore, we explored the switchable self-assembly behaviour of BTP-derivatives at the liquid-solid interface by using STM.

So far, several example of chemically controlled switching of small molecules physisorbed flat at the solid-liquid interface have been presented. The final section of this thesis will be dedicated to illustrating how such molecular switches, when designed ingeniously, can also be powered by nature’s most abundant and powerful energy source, i.e. light. Azobenzene, a well known photochromic system that attracted a great deal in the last few decades was never observed switching at the solid-liquid interface by STM. This is because the non planar *cis* isomer was found to desorb from the surface. Also in collaboration with the group of Prof. Stefan Hecht, we designed and characterized by the means of STM three-dimensional (3D) light responsive monolayers physisorbed on the surface at the solid-liquid interface. As a model system we have chosen oligofluorene derivative, equipped in the α and ω position with two carboxylic acid groups, and exposing in the bridge sp³ carbon both a long alkyl chains and photo-switchable azobenzene unit. Oligofluorene platform act as a scaffold to control the

position of the functional group, i.e. the azobenzene unit, relative to the surface and determine their size spacing between adjacent azobenzenes, resulting in arrays of functional 3D molecular switches operating at the solid-liquid interface.

Overall in these thesis we made use of various pre-programed weak interactions to form ordered motifs and scaffolds, and explored the bi-stable nature of different (supra)molecular systems at surfaces, under STM control. The finding reported are both instructive to the field of nanoscience as well as of potential interest for technological applications, eg. in nanoelectronics.

References

- [1] J. M. Lehn, *Science* **1993**, *260*, 1762.
- [2] G. M. Whitesides, J. P. Mathias, C. T. Seto, *Science* **1991**, *254*, 1312.
- [3] M. C. Etter, *Acc. Chem. Res.* **1990**, *23*, 120.
- [4] J. A. Theobald, N. S. Oxtoby, M. A. Phillips, N. R. Champness, P. H. Beton, *Nature* **2003**, *424*, 1029.
- [5] L. M. A. Perdigao, E. W. Perkins, J. Ma, P. A. Staniec, B. L. Rogers, N. R. Champness, P. H. Beton, *J. Phys.Chem. B* **2006**, *110*, 12539.
- [6] G. Binnig, H. Rohrer, C. Gerber, E. Weibel, *Phys. Rev. Lett.* **1982**, *49*, 57.
- [7] G. Binnig, C. F. Quate, C. Gerber, *Phys. Rev. Lett.* **1986**, *56*, 930.
- [8] S. De Feyter, F. C. De Schryver, *Chem. Soc. Rev.* **2003**, *32*, 139.
- [9] P. Samorì, (ed). *Scanning Probe Microscopy beyond Imaging.; Wiley-VCH, New York* **2006**.
- [10] M. Surin, P. Samorì, A. Jouaiti, N. Kyritsakas, M. W. Hosseini, *Angew. Chem. Int. Ed.* **2007**, *46*, 245.
- [11] V. Berl, M. Schmutz, M. J. Krische, R. G. Khoury, J. M. Lehn, *Chem. Eur. J.* **2002**, *8*, 1227.
- [12] E. Kolomiets, E. Buhler, S. J. Candau, J. M. Lehn, *Macromolecules* **2006**, *39*, 1173.
- [13] A. Ciesielski, G. Schaeffer, A. Petitjean, J. M. Lehn, P. Samorì, *Angew. Chem. Int. Ed.* **2009**, *48*, 2039.
- [14] J. T. Davis, *Angew. Chem. Int. Ed.* **2004**, *43*, 668.
- [15] J. T. Davis, G. P. Spada, *Chem. Soc. Rev.* **2007**, *36*, 296.

- [16] R. Otero, W. Xu, M. Lukas, R. E. A. Kelly, E. Laegsgaard, I. Stensgaard, J. Kjems, L. N. Kantorovich, F. Besenbacher, *Angew. Chem. Int. Ed.* **2008**, *47*, 9673.
- [17] A. Ciesielski, S. Lena, S. Masiero, G. P. Spada, P. Samorì, *Angew. Chem. Int. Ed.* **2010**, *49*, 1963.
- [18] L. Piot, R. M. Meudtner, T. El Malah, S. Hecht, P. Samorì, *Chem. Eur. J.* **2009**, *15*, 4788.
- [19] A. Ciesielski, L. Piot, P. Samorì, A. Jouaiti, M. W. Hosseini, *Adv. Mater.* **2009**, *21*, 1131.
- [20] J. Adisoejoso, K. Tahara, S. Okuhata, S. Lei, Y. Tobe, S. De Feyter, *Angew. Chem. Int. Ed.* **2009**, *48*, 7353.
- [21] K. Tahara, S. Okuhata, J. Adisoejoso, S. B. Lei, T. Fujita, S. De Feyter, Y. Tobe, *J. Am. Chem. Soc.* **2009**, *131*, 17583.
- [22] T. F. A. Greef, E. W. Meijer, *Nature* **2008**, *453*, 171.
- [23] J. A. A. W. Elemans, A. E. Rowan, R. J. M. Nolte, *J. Mater. Chem.* **2003**, *13*, 2661.
- [24] J. M. MacLeod, O. Ivasenko, D. F. Perepichka, F. Rosei, *Nanotechnology* **2007**, *18*, 424031.
- [25] J. F. Lutz, *Angew. Chem. Int. Ed.* **2007**, *46*, 1018.
- [26] D. Fournier, R. Hoogenboom, U. S. Schubert, *Chem. Soc. Rev.* **2007**, *36*, 1369.

Résumé

La chimie supramoléculaire est l'une des innovations les plus importantes dans les dernières décennies concernant les domaines de la chimie inorganique, organiques et biochimie.^[1] La chimie supramoléculaire repose sur l'utilisation des interactions non-covalentes pour auto-assembler, avec une précision sous-nanométrique, des entités chimiques en forme de matériaux avec des propriétés chimiques et physiques pré-programmés: la chimie supramoléculaire ainsi est la clé pour les nanosciences et la nanotechnologie. La chimie supramoléculaire offre un excellent contrôle sur le processus d'auto-assemblage moléculaire: sa nature unique combine la réversibilité, la directivité, la spécificité et la coopérativité. La chimie supramoléculaire a été appliqué à ce jour particulièrement à des solution, des cristaux 3D^[2-3] et en 2D sur des surfaces dans un environnement ultra-vide.^[4-5] En 2D à l'interface solide-liquide, un environnement dans lequel beaucoup de chimie humide peut être effectuée, ces concepts n'ont pas encore été pleinement exploités.

Les concepts les plus fondamentaux de la chimie supramoléculaire ont été introduites au 19e siècle, lorsque quelques-uns des ces principes ont été proposés. En particulier, l'idée de la chimie de coordination a été formulée par Alfred Werner en 1893,^[6] tandis que le concept de serrure-et-clés a été présenté par Emil Fisher en 1894.^[7] Le mot "Supramolecule" est apparu dans la littérature en 1937,^[8] quand K. L. Wolf et ses collaborateurs ont introduit le terme "Übermolekül" pour décrire l'interaction intermoléculaire survenant entre les espèces chimiques telles que les dimères d'acides carboxyliques. Cependant, soutenue par un plus grand nombre d'exemples démontrant l'importance des interactions non-covalentes, le concept de la chimie supramoléculaire a été introduit que par Jean-Marie Lehn dans la «chimie des assemblages moléculaires et de la liaison intermoléculaire" en 1979,^[9] ou comme la chimie "au-delà de la molécule".^[1] D'autres définitions de la chimie supramoléculaire comprennent "la chimie de la liaison non-covalente" et "chimie non-moléculaire".

A l'origine la chimie supramoléculaire a été définie en termes d'interactions non-covalentes entre une molécule «hôte» et une molécule «guest». Toutefois, l'expansion rapide de la chimie supramoléculaire au cours des 30 dernières années a abouti à l'évolution du principe «hôte-guest". La chimie supramoléculaire englobe désormais non seulement les systèmes de

reconnaissance "hôte-guest", mais aussi des systèmes de reconnaissance moléculaire appelées "auto-processus" comme l'auto-assemblage et l'auto-organisation de dispositifs moléculaires. La chimie supramoléculaire est l'une des innovations les plus importantes dans les domaines de la chimie inorganique, organique et bio-chimie dans les dernières décennies.

La chimie supramoléculaire est basée sur l'utilisation des interactions non-covalentes pour diriger l'auto-assemblage, avec une précision à l'échelle sous-nanométrique. Des entités chimiques pré-programmés forment des matériaux avec des propriétés chimiques et physiques désirés: la chimie supramoléculaire est ainsi la clé de la nanoscience et de la nanotechnologie. La chimie supramoléculaire permet de contrôler de manière précise le processus d'auto-assemblage moléculaire: en raison de sa nature unique, elle allie la réversibilité, la directivité, la spécificité et la coopérativité. L'événement de reconnaissance mutuelle entre les molécules (ou entre sites complémentaires) peut être basé sur différents types d'interactions intermoléculaires réversibles.

La "boîte à outils" des interactions non-covalentes contient différents types de liaisons : les liaisons d'hydrogène, les interactions électrostatiques, les interactions π - π , les interactions de van der Waals, les interactions métalliques et les interactions de coordination. En termes d'énergie d'interaction, les liaisons de van der Waals sont les plus faibles (environ 0,5 à 2 kcal mol⁻¹) et plutôt difficile à mesurer. L'énergie des liaisons d'hydrogène varie de faible à fort (env. 10-40 kcal mol⁻¹).^[10] Les interactions métalliques peuvent être aussi fort que les interactions d'hydrogène. Les interactions électrostatiques peuvent être très fortes (environ 50 kcal mol⁻¹). Les liaisons de coordination sont les plus fortes parmi les interactions non-covalentes (environ 30-70 kcal mol⁻¹).^[11]

Depuis presque trois décennies, des surfaces et interfaces peuvent être analysé avec un précision sous-nanométrique en utilisant des microscopies à champ proche. Dans ce cadre, l'invention de la microscopie à effet tunnel (STM) en 1981^[12] et plus tard la microscopie à force atomique (AFM) en 1986^[13] ont eu des grands impacts aux nanosciences et aux nanotechnologies. Ces deux techniques, en particulier le STM, ont permis de visualiser et manipuler des molécules individuelles, et d'étudier une variété de propriétés physico-chimiques et des processus ayant lieu à l'échelle nanométrique des matériaux nanostructurés. Le STM peut être utilisé – avec précision moléculaire - dans différentes conditions expérimentales y compris dans l'ultra-vide (UHV), sous flux de gaz, dans l'air et dans un liquide, permettant d'étudier la structure et la réactivité en

2D pour une multitude de systèmes. Au cours des deux dernières décennies, de nombreux exemples de visualisation par STM de molécules individuelles et d'architectures de celles-ci ont été rapportés ^[14-15] pour de divers types de matériaux, y compris les cristaux liquides, conducteurs cristaux moléculaires, des protéines et des monocouches auto-assemblées.

Dans cette thèse, nous avons concentré notre attention sur l'auto-assemblage de différents systèmes moléculaires résultant en la formation de nanostructures supramoléculaires à cause d'un équilibre entre les interactions intra-et inter-moléculaires ainsi que les forces interfaciales. Les propriétés structurales et dynamiques ont été étudiées à l'échelle sous-nanométrique en utilisant la microscopie à effet tunnel (STM). Les nanostructures qui ont été créées et étudiées dans le cadre de ce travail ne sont pas seulement d'intérêt comme un exercice d'auto-assemblage contrôlé à l'échelle nanométrique sur des surfaces, mais aussi comme des candidats possibles pour des applications électroniques. Pour explorer l'utilisation de différentes interactions non-covalentes pour la formation des assemblages supramoléculaires fonctionnels, nous avons étudié les systèmes suivants:

- Un système optiquement actif à base d'anthracène portant deux groupes d'éthynyle équipé d'un monodentate (pyridine) et un tridenté (terpyridine), connus pour former des polymères 1D de coordination en présence d'ions métalliques.^[16-17]
- Une molécule hexatopique à base de diacétylamino-pyridine qui peut adopter une symétrie d'ordre 3 et qui peut former des réseaux poreux à des surfaces de substrats solides par la formation de liaisons hydrogène multiples.^[18]
- Une molécule rigide portant deux unités pyridin-2 (1H)-one, afin de former des polymères supramoléculaires 1D stabilisés par des liaisons hydrogène hélicoïdaux à l'interface solide-liquide.
- Une composante ditopique moléculaire, contenant des groupes complémentaires pour des liaisons d'hydrogène, connue pour former des polymères supramoléculaires bi-composante 1D par liaisons hydrogène.^[18-20]

- Un molecule N⁹-substitué à base de guanine, afin d'exploiter la reconnaissance de liaisons hydrogène entre les bases nucléiques et la formation de ce qu'on appelle G-quadruplex, présents dans les structures télomériques de l'ADN de l'homme.^[21-25]
- Des composants basé sur le BTP, fonctionnalisés avec de longues chaînes aliphatiques. Ces systèmes sont connus pour changer de conformation géométrique en présence d'ions métalliques ou par protonation.^[26]
- Oligofluorene based component equipped with azobenzene functional unit, capable to undergo photoisomerisation and to change geometrical conformation upon irradiation with ultra-violet (UV) light.

En ce qui concerne les dérivés de l'anthracène,^[16-17] nous avons concentré notre attention – en collaboration avec le groupe du Prof Mir Wais Hosseini de l'Université de Strasbourg (France) – sur la composante 9-(3'-pyridylethynyl) -10 - [3'-éthynyle- 2,2 ': 6', 2"-terpyridine]-anthracène. La combinaison de molécules neutres, avec des cations métalliques conduit à la formation de réseaux 1D de coordination directionnelle polycationiques. Le bilan des charges impose la présence d'anions. Lors de l'utilisation d'anions de coordination faible, ceux-ci occupent généralement l'espace vide entre les réseaux 1D, et n'interagissent souvent pas avec la partie cationique de l'assemblage. La formation de réseaux de coordination 1D directionnelle n'est possible qu'avec des centres métalliques offrant quatre sites de coordination libres. Ceci a été étudié en utilisant un cation Pd (II) associé à l'anion faible BF⁴⁻. Une autre possibilité, consistant en la combinaison de deux anions de coordination, tels que le chlorure, avec un centre métallique dicationique qui adopte la géométrie de coordination octaédrique, tels que Co (II), a également été examinée. L'assemblage de la molécule libre sur des surfaces de graphite a été étudiée par STM à l'interface solide-liquide, en appliquant une goutte d'une solution fortement concentrée de l'anthracène neutre dissolu dans du 1-phenyloctane. Selon nos observations antérieures basées sur des molécules similaires,^[16] la combinaison des molécules neutres avec Pd (II) ou Co (II) conduit à la formation d'un réseau de coordination 1D sur une surface de graphite.

Des réseaux supramoléculaires bidimensionnel, en particulier ceux avec des pores vides, connu sous le nom réseaux 2D poreux,^[27-28] ont reçu une attention croissante en raison de leurs propriétés de gabarits. De telles structures, formées par physisorption des blocs de construction sur des surfaces conductrices atomiquement plats, peuvent être étudiés à l'aide de microscopie à effet tunnel (STM). La stabilité et la cristallinité à long distance sont quelques-unes des propriétés recherchées pour de tels réseaux moléculaires, qui peuvent être physisorbé sur une grande variété de substrats pour ajuster les propriétés physico-chimiques, électriques et des propriétés aux interfaces solide-liquide, en élargissant la panoplie des techniques d'auto-monocouches assemblées (SAM). Jusqu'à présent, les réseaux 2D formés par des liaisons hydrogène multiples, la coordination métal-ligand ou de van der Waals, n'ont pas encore présenté les propriétés nécessaires pour former des réseaux solides poreux sans la présence du polymorphisme. Le polymorphisme, c'est-à-dire la capacité de former de multiples architectures 2D des mêmes blocs de construction, est jusqu'à présent le principal facteur de diminution de la stabilité des réseaux poreux 2D, même si on utilisé des fortes liaisons d'hydrogène. En collaboration avec un groupe du professeur Jean-Marie Lehn de l'Université de Strasbourg (France), nous avons identifié un réseau hautement cristallin 2D qui présente seulement une quantité limitée de polymorphisme au lors de concentrations (sous-)monocouche. Le réseau est formé par une molécule hexatopic diacetylaminopyridine qui peut adopter une symétrie d'ordre 3. En étudiant deux systèmes moléculaires équipée de différentes chaînes alkyl, $-C_3H_7$ et $-C_9H_{19}$, la formation du réseau peut être attribuée à la formation des liaisons hydrogène.

Les polymères supramoléculaires combinent une géométrie pré-programmés avec une stabilité particulière et des propriétés mécaniques qui résultent directement de l'effet combiné des interactions primaires non-covalentes et leurs interactions secondaires liés tenant ensemble des modules moléculaires fonctionnalisés.^[29-30] Grâce à l'utilisation simultanée des interactions d'hydrogène multiples et entrelacés entre des modules moléculaire conformationnellement rigide, il est possible d'augmenter la force de ces interactions et de parvenir à un contrôle sur la géométrie de l'architecture supramoléculaire.^[31] Avec un groupe du Professeur Jean-Marie Lehn de l'Université de Strasbourg (France), nous avons étudié un module moléculaire fonctionnalisé capable d'auto-association à travers quatre interactions fortes et deux liaisons d'hydroène moyennes à former des dimères avec une stabilité significative. L'auto-association de ces dimères rigides de phenylpyrimidine par le biais de d'interactions d'hydrogène directionnels

entre deux unités pyridin-2-(1H)-one latéraux de molécules voisines a permis la formation de deux classes différentes de polymères supramoléculaires comme confirmé par simulations DFT. En particulier, une étude par microscopie à effet tunnel (STM) de la dépendance de la concentration à l'interface solide-liquide a révélé l'auto-assemblage moléculaire contrôlé sur le graphite, formant soit des structures linéaires compacts latéralement interagissant via des forces de van der Waals pour générer des nanomotifs de taille micrométrique 2D, ou des polymères supramoléculaires hélicoïdales de longueur de centaines de nanomètres.

Les polymères supramoléculaires peuvent montrer simultanément des propriétés des matériaux accordables avec faible viscosité de fond.^[29] Leurs caractéristiques mécaniques résultent des interactions secondaires, en particulier la force, la réversibilité, et la directivité de ces interactions. La génération des motifs ordonnés stabilisée par des liaisons hydrogène sur une surface solide exige le réglage fin des interactions entre les molécules voisines et les interactions adsorbat-substrat. La formation contrôlée d'architectures ordonnées de plusieurs composants à l'interface solide-liquide à partir d'une solution concentrée est défavorisée thermodynamiquement. En collaboration avec le groupe du Professeur Jean-Marie Lehn de l'Université de Strasbourg (France), nous avons étudié et visualisé par STM la formation des polymères supramoléculaires à l'interface liquide-solide à température ambiante, observant soit une géométrie linéaire ou une géométrie en *zig-zag* sur des surfaces de graphite pyrolytique (HOPG).^[20] À cette fin, nous avons utilisé des composants ditopiques moléculaires, portant des groupes à reconnaissance complémentaires pour former des liaisons d'hydrogène: soit un type Janus cyanurique ou d'un coin barbiturique (ADA-ADA-array) et une unité de récepteur correspondante (DAD-DAD-array). Ces molécules ont été choisies parce qu'elles sont connues pour former des polymères supramoléculaires 1D en solution par polyassociation par le biais de liaisons hydrogène sextuple entre leurs sites de reconnaissance respectifs.

Parmi tous les nucléobases, guanine est très polyvalente: en fonction des conditions expérimentales, différentes voies d'auto-assemblage peuvent être observées.^[24] En présence de certains ions métalliques, des guanines peuvent former des architectures basées sur le G-quartet telles que des octamères ou des agrégats polymériques colonnaires. En l'absence de métaux, des guanines sans C (8) (qui est un substituant stériquement exigeant) peut s'auto-assembler, à la fois en solution et à l'état solide, dans des architectures de type ruban. Pour les dérivés de la

guanosine physisorbées à la surface, des rubans thermodynamiquement stables sont caractérisés par des liaisons hydrogène cycliques de type NH (2)-O (6) et NH (1)-N (7). Plus intéressant encore, ces rubans présentent également des propriétés de redressement. Un transistor à effet de champ basé sur cette structure supramoléculaire, a été décrit. Jusqu'à présent, les architectures supramoléculaires auto-assemblées à la base de guanine ont été étudiées avec microscopie à effet tunnel (STM) sous ultra-vide (UHV).^[21-22] Contrairement, à l'interface solide-liquide les efforts ont été principalement orientés vers l'étude des monocouches de guanosine lipophile.^[32-35] En collaboration avec le professeur Gian Piero Spada de l'Université de Bologne (Italie), nous avons décidé d'étendre nos études à l'interface solide-liquide de monocouches physisorbées des N⁹-alkylguanines parce que l'absence du sucre par rapport à la guanosine déjà étudiées et la présence d'un side-groupe aliphatique peut être prévue pour favoriser l'adsorption moléculaire sur le graphite. Nous avons réalisé une étude STM avec résolution sous-moléculaire de monocouches physisorbées sur le graphite d'une série de N⁹-alkylguanines alkyle linéaire avec des chaînes latérales de-C₂H₅ à-C₁₈H₃₇. En plus, nous avons également étudié l'assemblage/desassemblage d'un N⁹-alkylguanine en quartets ordonnés ou rubans, en fonction de la présence/absence de métaux, visualisant avec une résolution submoléculaire par STM ce processus à l'interface solide-liquide sur des surfaces HOPG.^[25]

Ces dernières années, le domaine de la chimie des matériaux a beaucoup bénéficié du développement de la méthodologie en synthèse organique. En particulier, l'avènement de la chimie "click" a eu un impact considérable sur la chimie macromoléculaire et supramoléculaire synthétique.^[36-37] En raison du haut rendement la chimie à 'click' est généralement utilisée en chimie des matériaux pour la construction d'une grande variété d'architectures, y compris les polymères linéaires et copolymères à blocs, polymères hyperbranchés et les dendrimères, macrocycles ainsi que caténanes et rotaxanes entre autres. Cependant, la unité de liaison triazole n'est généralement pas impliquée dans le design et sert principalement comme une simple unité de raccordement. Nous avons récemment commencé, avec le groupe du Prof Stefan Hecht de l'Université Humboldt à Berlin (Allemagne), un programme à utiliser pour construire la chimie du 'click' pour des (macro) molécules de forme définie, utilisant le motif 2,6-bis (1-phényl - 1,2,3-triazole-4-yl) pyridines (BTP) comme principale caractéristique structurale. En raison de la répulsion entre les paires d'électrons libres, la conformation syn,syn du BTP est fortement déstabilisée et, par conséquent, le BTP préfère d'adopter la conformation thermodynamiquement

favorisée anti,anti par analogie avec les bipyridines ou terpyridines. Nous avons réussi à prendre avantage de cette préférence conformationnelle à la conception d'oligomères et polymères hélicoïdales. En outre, nous avons exploré le comportement commutable de l'auto-assemblage des dérivés du BTP à l'interface liquide-solide à l'aide de la STM.

Jusqu'à présent, plusieurs exemples de commutation contrôlée par voie chimique de petites molécules physisorbées à l'interface solide-liquide ont été présentés. La dernière section de cette thèse est consacrée à l'illustration de la façon dont ces commutateurs moléculaires, quand ils sont conçus de manière maligne, peuvent également être alimentés par la source d'énergie de la nature la plus abondante et puissante : la lumière. L'azobenzène, un système photochromique bien connu qui a attiré beaucoup d'intérêt dans les dernières décennies n'a jamais été observé de commuter à l'interface solide-liquide par STM. C'est parce que la forme non-plate de l'isomère cis desorbe de la surface. En collaboration avec le groupe du Prof. Stefan Hecht, nous avons conçu et caractérisé par les moyens de STM des monocouches sensibles à la lumière, physisorbées à l'interface solide-liquide. Comme système modèle nous avons choisi un dérivé d'oligofluorene qui a été fonctionnalisé avec deux groupes d'acide carboxylique dans les positions ω et α et qui contenait une unité de « pont » de carbone alkyle sp^3 et une unité d'azobenzène photo-commutable. La plate-forme d'oligofluorene fonctionne comme un échafaudage pour contrôler la position des groupes fonctionnels, c'est à dire l'unité azobenzène, par rapport à la surface et pour déterminer leur l'espacement entre azobenzènes adjacents, résultant dans un réseau régulier d'interrupteurs moléculaires fonctionnels 3D fonctionnant à l'interface solide-liquide.

Nous avons étudié l'auto-assemblage sur des surfaces de différents systèmes moléculaires en nanostructures supramoléculaire, obtenue en équilibrant le rôle des interactions intramoléculaires, intermoléculaires, et interfaciales. A l'interface solide-liquide des structures supramoléculaires, formées par des interactions non-covalentes comme les interactions de coordination, liaison d'hydrogène et de van der Waals ont été étudiés à l'aide de la microscopie à effet tunnel (STM). Dans cette thèse, nous avons prouvé que la combinaison de la chimie supramoléculaire des surfaces et des interfaces avec les microscopies à sonde à balayage offre un niveau de contrôle élevé sur la nanofabrication ascendante des matériaux fonctionnels. L'utilisation de l'approche supramoléculaire a permis de localiser des groupes fonctionnels dans

les systèmes à deux dimensions avec un degré élevé de précision, ainsi que de « imprimer » un réseau pré-défini sur une surface. Les enquêtes STM à l'interface solide-liquide ont permis l'exploration de ces structures et des processus dynamiques avec une résolution sub-moléculaire. En utilisant cet approche, nous avons réussi à fabriquer pour la première fois un système de "dynamers" sur une surface.

En résumé, nous avons donné de nombreux détails sur la façon dont les molécules simples, décorées avec des unités de reconnaissance moléculaire, sont capables de s'auto-organiser en matériaux cristallins 2D supramoléculaires. Cela ouvre la voie vers des échafaudages supramoléculaire, c'est à dire l'utilisation du module moléculaire conçu à subir des événements de reconnaissance et d'intégrer des unités fonctionnelles, pour former des architectures pré-programmés avec une précision sub-ångström. Ceci permettra de développer des matériaux fonctionnelles avec des propriétés contrôlées avec un haut degré de précision. Des matériaux supramoléculaires, c. à d. des substances basées sur des interactions réversibles et dynamiques non-covalentes ont également la capacité intrinsèque d'à la fois pouvoir reconnaître et échanger leurs unités de bases. Ils sont des matériaux intrinsèquement dynamiques et pourraient en principe choisir leurs constituants en réponse à des stimuli externes. L'augmentation de leur complexité, étant l'un des plus grands défis en science des matériaux, peut être poursuivi à travers l'auto-assemblage en exploitant les interactions qui agissent d'une manière hiérarchique, contrôlant sur différents échelles le degré de l'ordre moléculaire de l'échelle moléculaire à l'échelle mésoscopique. Cela conduit à l'élaboration de matériaux intelligents ainsi que des méta-matériaux. Ces deux types de matériaux ("matériaux smart" et "meta-matériaux") sont caractérisés par leur capacité de transformer l'énergie : la transformation des stimuli externes dans la propriété "smart" ou "meta" (des photons en électrons, la chaleur en électrons, des électrons en déplacement, les électrons dans des algorithmes), ce qui rend les matériaux supramoléculaires d'excellents candidats pour de telles tâches complexes. Le contrôle sur le degré de la cristallinité en 2D est l'un des premiers objectifs pour de futures études de microscopie à effet tunnel. D'un grand intérêt est également la caractérisation de l'auto-assemblage 2D au niveau des interfaces courbes tel que les micelles, membranes, les nanotubes et des interfaces rugueuses, qui sont des objets représentant de l'espace courbe que nous habitons.

- [1] J. M. Lehn, *Science* **1993**, *260*, 1762-1763.
- [2] G. M. Whitesides, J. P. Mathias, C. T. Seto, *Science* **1991**, *254*, 1312-1319.
- [3] M. C. Etter, *Acc. Chem. Res.* **1990**, *23*, 120-126.
- [4] J. A. Theobald, N. S. Oxtoby, M. A. Phillips, N. R. Champness, P. H. Beton, *Nature* **2003**, *424*, 1029-1031.
- [5] L. M. A. Perdigo, E. W. Perkins, J. Ma, P. A. Staniec, B. L. Rogers, N. R. Champness, P. H. Beton, *J. Phys. Chem. B* **2006**, *110*, 12539-12542.
- [6] A. Werner, *Zeitschr. Anorg. Chem.* **1893**, *3*, 267.
- [7] E. Fisher, *Ber. Deutsch. Chem. Ges.* **1894**, *27*, 2985.
- [8] K. L. Wolf, H. Frahm, H. Harms, *Z. Phys. Chem. (B)* **1937**, *36*, 237.
- [9] J.-M. Lehn, *Pure Appl. Chem.* **1979**, *51*, 979-997.
- [10] G. R. Desiraju, *Acc. Chem. Res.* **2002**, *35*, 565-573.
- [11] M. W. Hosseini, *CrystEngComm* **2004**, *6*, 318-322.
- [12] G. Binning, H. Rohrer, C. Gerber, E. Weibel, *Phys. Rev. Lett.* **1982**, *49*, 57-61.
- [13] G. Binnig, C. F. Quate, C. Gerber, *Phys. Rev. Lett.* **1986**, *56*, 930.
- [14] S. De Feyter, F. C. De Schryver, *Chem. Soc. Rev.* **2003**, *32*, 139-150.
- [15] P. Samorì, (ed). *Scanning Probe Microscopy beyond Imaging.*; Wiley-VCH, New York **2006**.
- [16] M. Surin, P. Samorì, A. Jouaiti, N. Kyritsakas, M. W. Hosseini, *Angew. Chem. Int. Ed.* **2007**, *46*, 245-249.
- [17] A. Ciesielski, L. Piot, P. Samorì, A. Jouaiti, M. W. Hosseini, *Adv. Mater.* **2009**, *21*, 1131-1136.
- [18] V. Berl, M. Schmutz, M. J. Krische, R. G. Khoury, J. M. Lehn, *Chem. Eur. J.* **2002**, *8*, 1227-1244.
- [19] E. Kolomiets, E. Buhler, S. J. Candau, J. M. Lehn, *Macromolecules* **2006**, *39*, 1173-1181.
- [20] A. Ciesielski, G. Schaeffer, A. Petitjean, J. M. Lehn, P. Samorì, *Angew. Chem. Int. Ed.* **2009**, *48*, 2039-2043.
- [21] R. Otero, W. Xu, M. Lukas, R. E. A. Kelly, E. Laegsgaard, I. Stensgaard, J. Kjems, L. N. Kantorovich, F. Besenbacher, *Angew. Chem. Int. Ed.* **2008**, *47*, 9673-9676.

- [22] R. Otero, M. Schock, L. M. Molina, E. Laegsgaard, I. Stensgaard, B. Hammer, F. Besenbacher, *Angew. Chem. Int. Ed.* **2005**, *44*, 2270-2275.
- [23] J. T. Davis, G. P. Spada, *Chem. Soc. Rev.* **2007**, *36*, 296-313.
- [24] J. T. Davis, *Angew. Chem. Int. Ed.* **2004**, *43*, 668-698.
- [25] A. Ciesielski, S. Lena, S. Masiero, G. P. Spada, P. Samorì, *Angew. Chem. Int. Ed.* **2010**, *49*, 1963-1966.
- [26] L. Piot, R. M. Meudtner, T. El Malah, S. Hecht, P. Samorì, *Chem. Eur. J.* **2009**, *15*, 4788-4792.
- [27] K. Tahara, S. Okuhata, J. Adisojoso, S. B. Lei, T. Fujita, S. De Feyter, Y. Tobe, *J. Am. Chem. Soc.* **2009**, *131*, 17583-17590.
- [28] J. Adisojoso, K. Tahara, S. Okuhata, S. Lei, Y. Tobe, S. De Feyter, *Angew. Chem. Int. Ed.* **2009**, *48*, 7353-7357.
- [29] T. F. A. Greef, E. W. Meijer, *Nature* **2008**, *453*, 171-173.
- [30] J. A. A. W. Elemans, A. E. Rowan, R. J. M. Nolte, *J. Mater. Chem.* **2003**, *13*, 2661-2670.
- [31] J. M. MacLeod, O. Ivasenko, D. F. Perepichka, F. Rosei, *Nanotechnology* **2007**, *18*, 424031-424040.
- [32] S. Lena, S. Masiero, S. Pieraccini, G. P. Spada, *Chem. Eur. J.* **2009**, *15*, 7792-7806.
- [33] S. Lena, G. Brancolini, G. Gottarelli, P. Mariani, S. Masiero, A. Venturini, V. Palermo, O. Pandoli, S. Pieraccini, P. Samorì, G. P. Spada, *Chem. Eur. J.* **2007**, *13*, 3757-3764.
- [34] G. Gottarelli, S. Masiero, E. Mezzina, S. Pieraccini, J. P. Rabe, P. Samorì, G. P. Spada, *Chem. Eur. J.* **2000**, *6*, 3242-3248.
- [35] T. Giorgi, S. Lena, P. Mariani, M. A. Cremonini, S. Masiero, S. Pieraccini, J. P. Rabe, P. Samorì, G. P. Spada, G. Gottarelli, *J. Am. Chem. Soc.* **2003**, *125*, 14741-14749.
- [36] J. F. Lutz, *Angew. Chem. Int. Ed.* **2007**, *46*, 1018-1025.
- [37] D. Fournier, R. Hoogenboom, U. S. Schubert, *Chem. Soc. Rev.* **2007**, *36*, 1369-1380.

Chapter 1

Two dimensional supramolecular architectures probed by STM

1.1 Introduction

The principles of *supramolecular chemistry* date back to the 19th century, when some of the most basic concepts were introduced. In particular, the idea of coordination chemistry was formulated by Alfred Werner in 1893,^[1] while the lock-and-key concept was introduced by Emil Fisher in 1894.^[2] The word “Supramolecule” appeared in the literature in 1937,^[3] when K. L. Wolf and co-workers introduced the term “Übermolekül” to describe the intermolecular interaction occurring between chemical species such as dimers of carboxylic acids. However, supported by an increased number of examples demonstrating the importance of non-covalent interactions, the concept of supramolecular chemistry was introduced only by Jean-Marie Lehn as the “chemistry of molecular assemblies and of the intermolecular bond” in 1979,^[4] or as the “chemistry beyond the molecule”.^[5] Other definitions of supramolecular chemistry include “the chemistry of non-covalent bond” and “non-molecular chemistry”.

Originally supramolecular chemistry was defined in terms of the non-covalent interactions between a “host” and a “guest” molecule. However, the rapid expansion in supramolecular chemistry over the past 30 years has resulted in *evolution* of “host-guest” principle. Supramolecular chemistry now encompasses not only “host-guest” systems but also molecular recognition, so-called “self-processes” such as self-assembly and self-organization to molecular devices and machines. Supramolecular chemistry is one of the most important innovations in

inorganic, organic and bio-chemistry in the last decades. Basic yet key questions have been raised on supramolecular chemistry, including: “*How does matter become complex? What are the steps and the processes that lead from the elementary particle to the thinking organism, the (present!) entity of highest complexity? And there are two linked questions: an ontogenetic one, how has this happened, how has matter become complex in the history of the universe leading up to the evolution of the biological world, and an epigenetic one, what other and what higher forms of complex matter can there be to evolve, are there to be created?*”^[6] Despite it is still not yet possible to answer to all those questions, this may become possible since the field of supramolecular chemistry is continuously expanding, leading to new inventions, discoveries and what is even more important, understanding the processes observed in *Nature*. Thanks to the “invention” of supramolecular chemistry we have been able to design systems which are mimicking the ones observed in *Nature*, which was not possible by using the concepts of “*old fashion*” chemistry.

Supramolecular chemistry relies on the use of non-covalent interactions to self-assemble, with a precision in the sub-nanometer scale, chemical entities forming materials with pre-programmed chemical and physical properties: thus supramolecular chemistry is key to nanoscience and nanotechnology. Supramolecular chemistry offers high control over the process of molecular self-assembly: due to its unique nature it combines reversibility, directionality, specificity and cooperativity. The recognition event between the molecules (or between complementary sites) may take place through a variety of reversible intermolecular interactions (Fig. 1.1).

The “toolbox” of non-covalent interactions is composed of hydrogen-bonding, electrostatic interactions, π - π interactions, van der Waals interactions, metal-metal interactions and coordination bonding. In terms of energy, van der Waals interactions are the weakest (ca. 0.5-2 kcal mol⁻¹) and rather difficult to measure. H-bonding ranges from weak to strong (ca. 1-40 kcal mol⁻¹).^[7] Metal-metal interactions might be as strong as H-bonding. Electrostatic interactions may be substantially strong (ca. 50 kcal mol⁻¹). Coordination bond is the strongest among non-covalent interactions (ca. 30-70 kcal mol⁻¹).^[8]

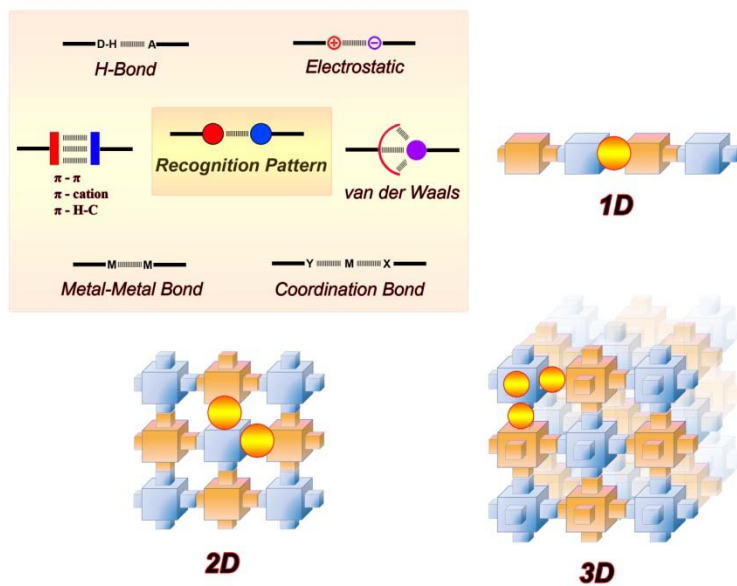


Figure 1.1 Schematic representation of “toolbox” of reversible non-covalent interactions.^[8]

With the invention of Scanning Tunneling Microscopy (STM) in 1981, it became possible to image surfaces with sub-nanometer resolution.^[9, 10] In recent years, the field of chemistry has benefited from this development more than any other discipline of science. The majority of results giving high resolution insight into the world of supramolecular chemistry were indeed obtained by using STM.

In this chapter we will focus our attention on 2D supramolecular architectures visualized by STM mostly at the solid-liquid interface. We will also discuss the role of the non-covalent interactions like: H-bonding, metallo-ligand and van der Waals interactions, in the process of supramolecular engineering.

1.2 Hydrogen-bonding Interactions

*“The discovery of the Hydrogen Bond
could have won someone the Nobel Prize,
but it didn’t.”*

G. A. Jeffrey, Wolfram Saenger, 1991

Hydrogen-bonding is one of the mostly employed non-covalent interaction in supramolecular chemistry.^[11-13] In particular, the association of molecules bearing complementary recognition groups is the most straightforward pathway for pre-programming network self-assembly of multiple components,^[14, 15] both in solution and in the solid state.^[16-18] H-bonding interactions benefit among others from a wide range on interaction energies, depending on the nature, the number (i.e. multiplicity) and the position of consecutive strong hydrogen-bond donor (D) and acceptors (A) moieties determining the impact of both primary and secondary interactions. G. A. Jeffrey^[19] reported that the energy per single A---D pair in the solution quantified by typical methods like NMR or UV-Vis amounts to 1.0 - 1.4 kcal mol⁻¹ per hydrogen-bond. In the case of three parallel H-bonds in ADA---DAD pairs, ab-initio calculated interaction energies can rise to 18 kcal/mol^[20] and up to 26 kcal mol⁻¹ in DDD-AAA pairs.^[21, 22] For four consecutive H-bonds, AADD---DDAA (i.e. a tetra-hapto moiety) in ureidopyrimidone dimers,^[23, 24] the association energy gives a record value of 47 kcal mol⁻¹. The computed geometries and harmonic vibrational frequencies of the H-bonded structures, calculated using ab initio methods, are in a good agreement with experimental data.^[23, 25-27] However energetic values must be taken with caution, since hydrogen-bonds are highly dependent on the molecular environment, which may completely differ within a supramolecular architecture. Therefore the presented values may be regarded as upper limits of the stabilization due to the hydrogen-bond itself. In the following paragraphs we will focus on the advantages and disadvantages of the use of different hydrogen-bond motifs for the formation of stable networks.

1.2.1 Weak Hydrogen-bond interactions.

While strong complementary hydrogen-bonds may be the motif of choice for engineering architectures,^[20, 28, 29] weak hydrogen-bonds can readily direct the formation of 2D crystalline structures.^[30-32] For instance, the self-association of small alkyl-substituted bisurea derivatives^[32] at the interface between highly oriented pyrolytic graphite (HOPG) and a solution in 1-octanol leads to the formation of a lamellar structures. Figure 1.2a shows a STM current image, which reveals a closely packed arrangement of molecules on the graphite substrate with a sub-molecular resolution. In general, the contrast of STM current images can be interpreted in terms of the distribution of the electron density in the frontier molecular orbitals of the adsorbate, therefore organic molecules once adsorbed on HOPG surface, appears brighter than the HOPG itself. Interesting situation is taking place in case of small aromatic organic molecules possessing alkyl or alkoxy substituents in their structures. Local density of states (LDOS) of aromatic molecules (units) is greater than the one of aliphatic molecules (units), therefore tunneling current recorded over the aromatic part of the molecule is typically much higher than the one recorded over the aliphatic part. Because of this reason, the urea groups can be distinguished from the remainder of the molecules. They are lined up and appear as two parallel rows within a lamella. Lamellae are separated from each other by small dark lines. The alkyl chains are clearly visible and their orientation can easily be assigned. The alkyl spacer between both urea moieties makes an angle of 3-5° with the outermost alkyl chains of the molecule, which are lying parallel to each other. The apparent conformation of a single molecule within the STM image can easily be correlated with the shape of a molecular model, which permits the orientation of the molecules on the graphite surface, including the orientation of the urea groups, to be determined. Therefore, carbonyl groups of the left row of urea groups point to the upper side of the image, and the carbonyl groups of the right row of urea groups point to the lower side of the image. Within the lamella the molecules are held together by H-bonding interactions between urea groups of adjacent molecules.

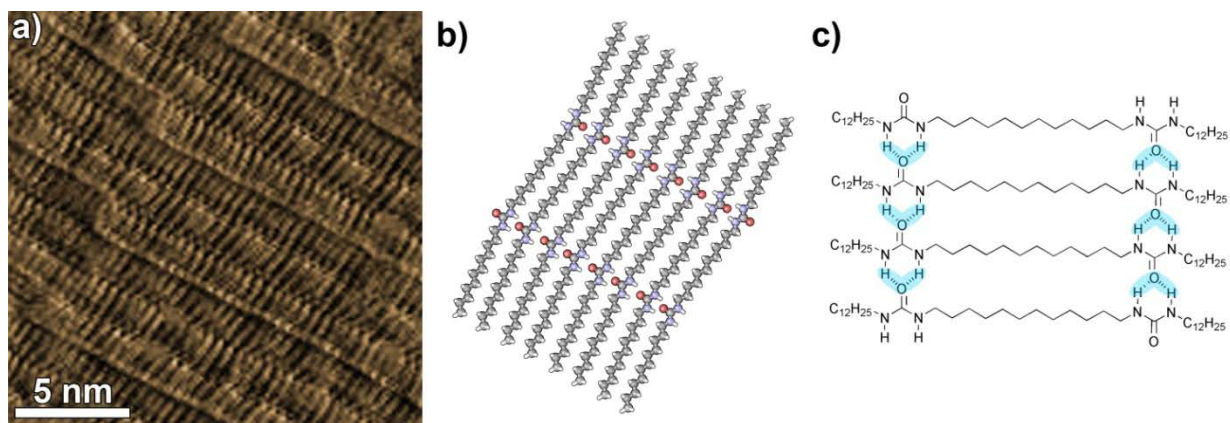


Figure 1.2 (a) STM image of alkyl-substituted bisurea derivative physisorbed on HOPG surface; (b) proposed molecular packing motif; (c) schematic representation of the self-assembly based on alkyl-substituted bisurea derivatives, intermolecular H-bonds were marked in blue.^[32]

Amide groups may also be used for the formation of interlamellar hydrogen-bonds to the point of using peptides for hydrogen-bond recognition.^[33] This is especially important when a specific arrangement of the lamella tilting angle (with respect to graphite) is desired. Of particular interest is the use of interlamellar spacing dictated by amide units to control the π - π stacking. Using this strategy, TTF (tetrathiafulvalene) derivatives exposing an amido group in the side chain was found to physisorb on HOPG from solutions in 1-octanoic acid in a head-to-head and tail-to-tail motif (Fig. 1.3), with lamellar structures stabilized by intermolecular hydrogen-bonds.^[34] In the case of a monoalkylated TTF derivative, multilayer structures are formed at the interface. The single amide functionality is then sufficient to force π - π stacking of the TTF moieties via intermolecular hydrogen-bonding and to overcome the intrinsic tendency of TTF to adsorb flat on the graphite substrate. These results are in line with those obtained by using urea groups^[35, 36] or nucleosides^[37] to template the self-assembly of oligothiophenes and for scaffolding.

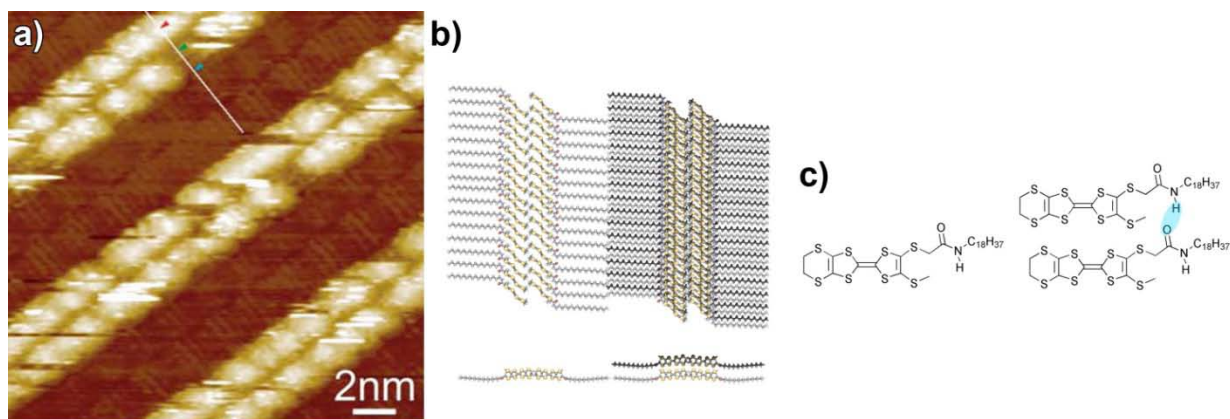


Figure 1.3 (a) STM image of TTF lamellar structures formed on HOPG surface; (b) proposed molecular assembly of TTF molecules; (c) schematic representation of TTF self-assembly, intermolecular H-bonds were marked in blue.^[34]

The self-association of oligopyridine derivatives at the interface between highly oriented pyrolytic graphite (HOPG) and a solution in 1,2,4-trichlorobenzene (TCB) leads to the formation of a lattice, which is held together by eight weak H-bonding interactions per molecule (Fig. 1.4).^[31] Nevertheless, such weak intermolecular interactions will hardly rule over van der Waals and adsorption energies (which steer close-packed molecular tiling) making pattern engineering with weak hydrogen-bonds a challenging topic.

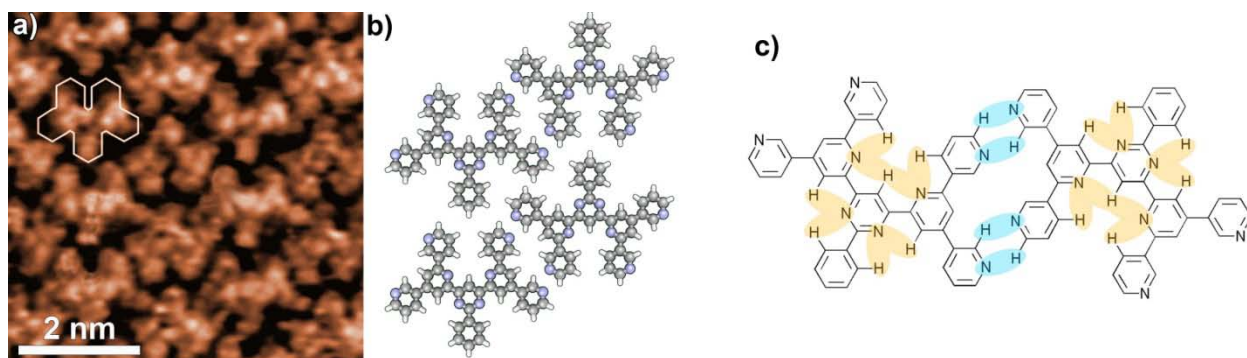


Figure 1.4 (a) STM image of oligopyridine derivative physisorbed on HOPG surface; (b) proposed molecular packing motif; (c) schematic representation of oligopyridine dimer, intermolecular H-bonds were marked in blue, whereas intramolecular H-bonds in orange.^[31]

Astonishingly, the use single hydrogen-bonds, was found being sufficient to form robust 2D porous networks. The bi-component network of 1,3,5-tris(4-pyridyl)-2,4,6-triazine (TPT) and trimesic acid (TMA) with a 6-fold symmetry has been described by Lackinger et al.^[38] Figure 1.5 reports a representative STM image of the monolayer. Each molecule can be clearly identified based on their size. Single TPT molecules appear as a triangle with a central depression. This 3-fold symmetry of TPT in the STM contrast agrees with the symmetry of the molecular structure. Furthermore, based on the STM image, undefined structures are physisorbed inside the cavities. This might stem from a transient adsorption of guests (either TMA, TPT, or heptanoic acid molecules) on the STM measurement timescale.

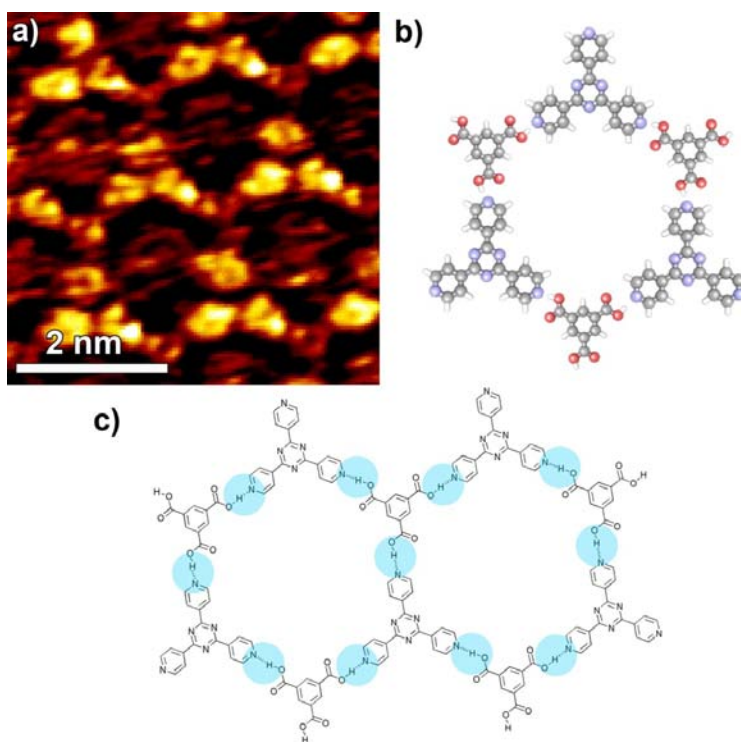


Figure 1.5 (a) STM image of bi-component network of TPT and TMA on HOPG surface; (b) proposed molecular assembly of TPT and TMA molecules; (c) schematic representation of TPT-TMA honeycomb network, intermolecular H-bonds are marked in blue.^[38]

The generation of ordered motifs stabilized by hydrogen bonds on a solid surface requires the fine tuning of the interplay between the interactions among neighboring molecules and the

adsorbate–substrate interactions.^[39] The controlled formation of ordered multicomponent architectures at the solid–liquid interface from a concentrated solution is actually thermodynamically unfavored. In fact, among the various components in the supernatant solution, the component with a greater affinity for the substrate, that is, offering a minimization of the free interface energy per unit area, will assemble on its surface, whereas the others will remain in solution.^[40] To immobilize all the components on the surface, thus to achieve a complete physisorption of all the components at the solid–liquid interface, it is necessary to borrow a strategy commonly employed under UHV, that is, control of the stoichiometry of the molecules absorbed at surfaces.^[28, 41] At the solid–liquid interface, the number of molecules in the solution applied to the surface should be lower than that required to form a monolayer of physisorbed molecules lying flat on the basal plane of the substrate. However, operating under such conditions, that is, at low concentration, can lead to the phase segregation or polymorphism.^[41, 42] Phase segregation, i.e. co-existence of multiple domains of molecules adsorbed on solid surfaces, where each domain consist of different molecules, can be ruled out by proper design of the investigated molecular building blocks and by tuning the intermolecular interactions which might bind the molecules. Adsorption energy of investigated molecules should be nearly equal, which allows all of the molecules to adsorb on the surface at the same time. Ideally intermolecular interactions between the molecules in bi- or multi-component self-assembled structures, have to be energetically higher than the one between the molecules forming monomolecular assembled structures. On the other hand, polymorphism cannot be completely ruled out, but rather controlled be the proper choice of the solvent, and concentration of investigated solutions.^[41, 42]

1.2.2 Carboxylic Acids as Di-hapto Hydrogen-bonding moieties.

The hydrogen-bond form among two adjacent carboxylic acids is the most widely used di-hapto H-bond type for pre-programming 2D networks.^[43] Many groups^[44-47] have reported systems relying on such a di-hapto recognition at the solid-solution interface.^[39, 48-52] Among them, Lackinger and co-workers^[44] showed the formation of linear polymer arrays by the deposition of

an isophthalic acid (1,3-benzene-dicarboxylic acid) solution in heptanoic acid onto HOPG surface. In the STM image (Fig. 1.6a), two types of molecules with different contrasts are identified. Each unit cell contains two molecules differing in their azimuthal orientation and adsorption site. The self-assembly is ruled to a great extent by double H-bonding interactions that are established between consecutive molecules, arranged in *zig-zag* chains within an oblique Bravais lattice, featuring an angle of 108° (Fig. 1.6b and c). Such a deviation from the ideal angle of 120° was explained invoking inter-chain and adsorbate-substrate interactions.

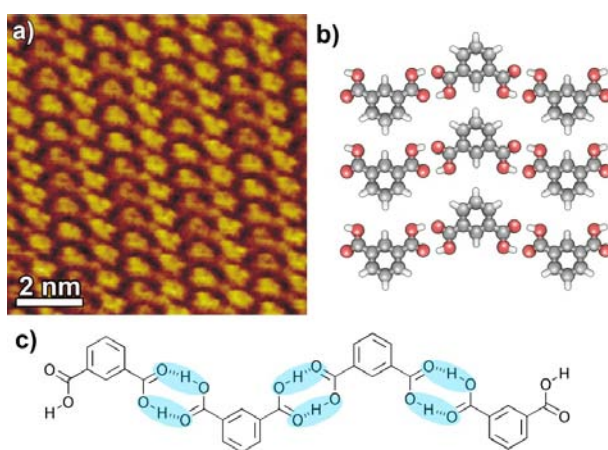


Figure 1.6 (a) STM image of isophthalic acid on HOPG surface; (b) proposed molecular assembly isophthalic acid molecules; (c) schematic representation of *zig-zag* linear polymer, intermolecular H-bonds are marked in blue.^[44]

By using different molecules bearing multiple carboxylic acids, other polymorphs (i.e. other monolayer domain arrangements from the same molecular building-blocks) may be formed.^[46, 47] One among such 2D patterns is the workbench for recent studies on random tiling and topological defects at the solid-liquid interface.^[45, 46] Beton and co-workers have shown that terphenyl-3,5,3',5'-tetracarboxylic acids (TPTC) arrange without translational symmetry but featuring a hexagonal superstructure (Fig. 1.7a and b). The star-shaped structures (highlighted in the square) represent one among five possible arrangements of TPTC molecules.

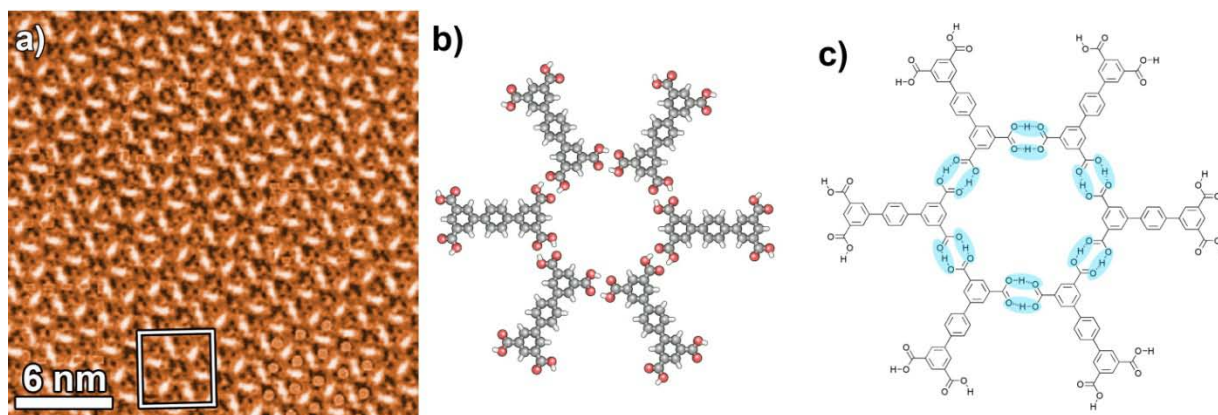


Figure 1.7 (a) STM image of TPTC molecules forming an hexagonal network on HOPG surface; (b) proposed molecular assembly TPTC molecules; (c) schematic representation of TPTC molecules in the star-shaped assembly; intermolecular H-bonds are marked in blue.^[46]

Polymorphism when using carboxylic acids may arise also from the possibility of trimerization of carboxylic acids on surfaces. For instance, pure TMA regions based on trimerization of the carboxyl moieties may form two polymorphs: the chicken-wire and the flower structure (Fig. 1.8). These TMA phases can further host ‘guest’ C_{60} molecules (indicated in red arrows) within their pores whereas the TMA/alcohol bicomponent network does not offer any stable adsorption site for the C_{60} molecules.^[47] Each unit cell contains two molecules differing in their azimuthal orientation and adsorption site. The self-assembly is ruled to a great extent by double H-bonding interactions. In the Figure 1.8b two types of molecular assembly are identified: hexagonal structure (indicated in red), formed by association of six TMA molecules and trimeric structure (indicated in green), formed by association of three TMA molecules.

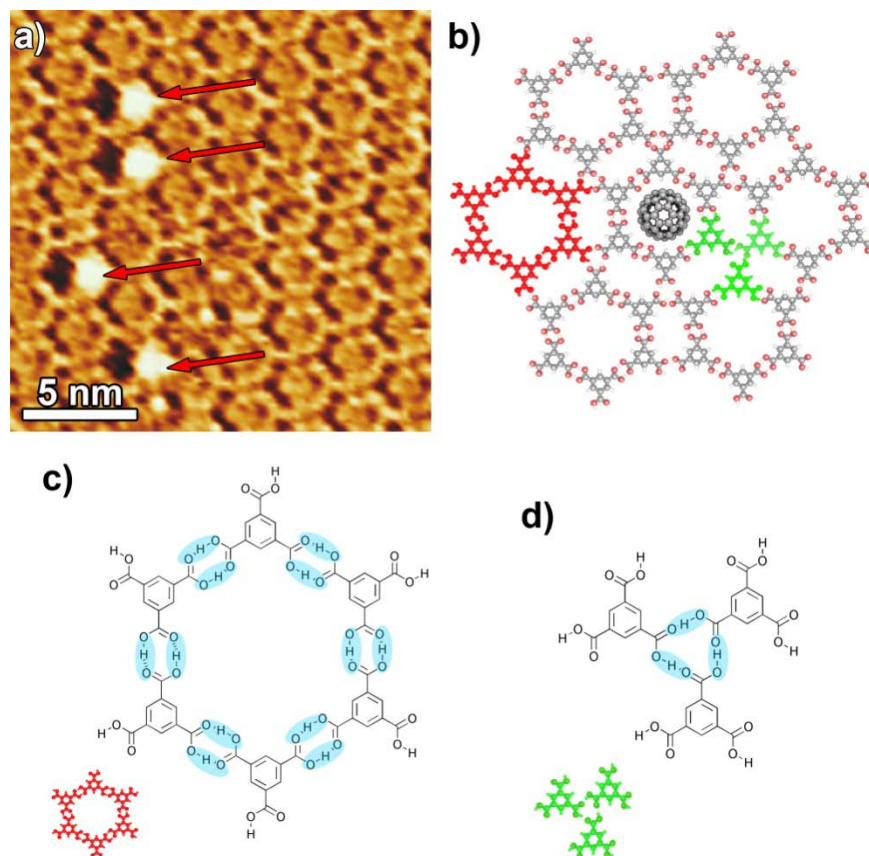


Figure 1.8 (a) STM image of bi-component “host” (TMA) – “guest” (C_{60}) network on HOPG surface; (b) proposed molecular assembly of TMA/ C_{60} molecules; schematic representation of hexagonal (c) and trimeric (d) structures of TMA molecules; intermolecular H-bonds are marked in blue.^[47]

Interestingly, the selective formation of one polymorph among others may be promoted by the choice of the solvent. Lackinger and co-workers provided evidence for such a phenomenon through the 2D pattern formation using 1,3,5-benzenetribenzoic acid (BTB).^[42] The dynamic self-assembly forming different structures by varying the nature of the solvent has been discussed focusing on adsorption rates and stabilization of polar units. In more details, BTB monolayers at the HOPG-saturated solution interface consist of two different non-densely-packed polymorphic architectures. These two structures differ in their H-bonding pattern motif and their packing density. Depending on the ability of the solvent to undergo hydrogen-bonding with the solute molecules, either an oblique or a hexagonal lattice was observed, with the former structure exhibiting rectangular pores and the latter exhibiting circular pores. Nevertheless, in the

STM images a second type of molecule cannot be unambiguously resolved, therefore the authors proposed another explanation for existence of polymorphic structures. For solvents with functional groups being able to hydrogen bond to the solute, a rough dependence of the structure formation on the dielectric constant was found. The more dense and more polar oblique BTB structure was only observed for solvents with a dielectric constant $\epsilon > 3$. Representative STM images of both structures are reported in Figures 1.9b and 1.9c, respectively. The less dense BTB polymorph is a 6-fold chicken-wire structure with circular cavities (approximately 2.8 nm wide), while the other structure exhibits an oblique unit cell and a higher surface density. The remarkably large cavity size of the chicken-wire structure is the result of combination of the hydrogen-bonds between carboxylic groups and the low conformational flexibility of BTB.

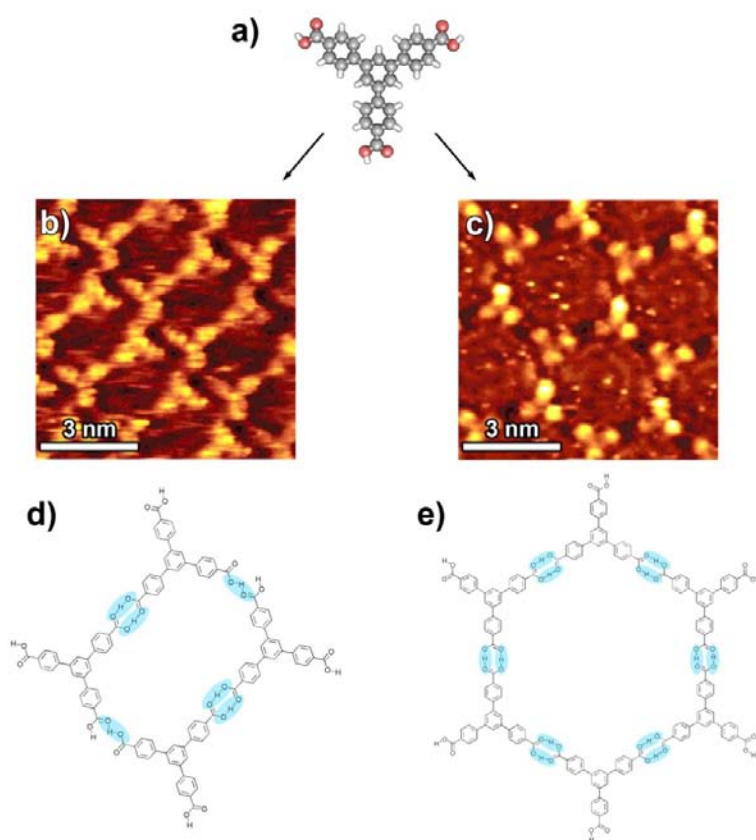


Figure 1.9 (a) 1,3,5-benzenetribenzoic acid (BTP) molecule; (b) STM image of oblique lattice observed upon the use of heptanoic acid, 1-octanol, 1-nonanol, and 1-decanol as a solvent; (c) hexagonal lattice observed upon the use of nonanoic acid and 1-phenyloctane as a solvent of BTP molecules on HOPG surface; Schematic representation of oblique (d) and Hexagonal (e) arrangements of BTP molecules; intermolecular H-bonds are marked in blue.^[42]

In some cases, the solvent can participate actively to the self-assembled pattern, by co-adsorbing to form bi-component networks.^[53] A recent work^[54] has shown that controlled co-deposition of the solvent molecules with melamine can be achieved. Co-adsorption phenomena has been also previously reported in systems consisting on TMA and alcohols.^[47, 55] The process involves the self-assembly of TMA with alcohols of varying length, which co-adsorb on HOPG to form linear patterns. The mixed TMA/alcohol supramolecular structure consists of a hydrogen-bonded network with alternating hydrophobic and hydrophilic regions. The incorporation of the alcohols allows for precise control over the periodicity of the nanostructures.

1.2.3 Combined Di-hapto Hydrogen-bond and van der Waals Interactions.

AD---DA motifs other than carboxylic acids are ideal for pre-programming the formation of networks, due to their vast geometrical diversity. Such double hydrogen-bond forming moieties might be complemented by introducing additional groups undergoing recognition events via van der Waals interactions, which can be obtained through alkyl chain functionalization. For instance, Ziener, Lehn and co-workers,^[56] made use of lactim/lactam moieties with alkoxy-substituted phthalhydrazide molecules, to form an architecture which is simultaneously directed by van der Waals and H-bond interactions. In this case, the self-assembled patterns was found to depend on the solvent employed. The long-chain phthalhydrazide in TCB self-assembles in a stripe-like structure, whereas monolayers formed from 1-chloronaphthalene solutions form trimeric star-like units that arrange in a hexagonal lattice. Figure 1.10a shows an “inverted contrast” STM image, therefore the molecules appears darker than HOPG surface. The origin of the “inversed contrast” phenomenon has not been rigorously explained in the literature, however some intuitive explanations can be found. In 1996, Garcia-Vidal and co-workers^[57] proposed an interesting explanation why such a phenomenon might take place during STM measurements. In some cases of STM experiments, the investigated molecules might adsorb on the metallic tip, changing its electronics and the corrugation of the surface, in those cases the tunneling current might become inverted. The hexagons observed by Ziener and co-workers, are built up from the three-fold symmetric molecular modules, implying that the chirality of a single hexagon emerges

from the self-assembly of achiral (prochiral) molecules (Fig. 1.10b). Each star consists of three molecules of the phthalhydrazide derivative, each trimer giving rise to six hydrogen-bonds (Fig. 1.10c). This arrangement generates voids in the centers of the hexagons, these voids being too small to accommodate an additional trimer. The molecules of 1-chloronaphthalene are able to stabilize the whole assembly by filling the voids, due to the extended conjugation characterizing the system as compared to TCB, thereby compensating the loss of enthalpy per unit area due to the lower surface coverage from TCB and its higher mobility at surface.

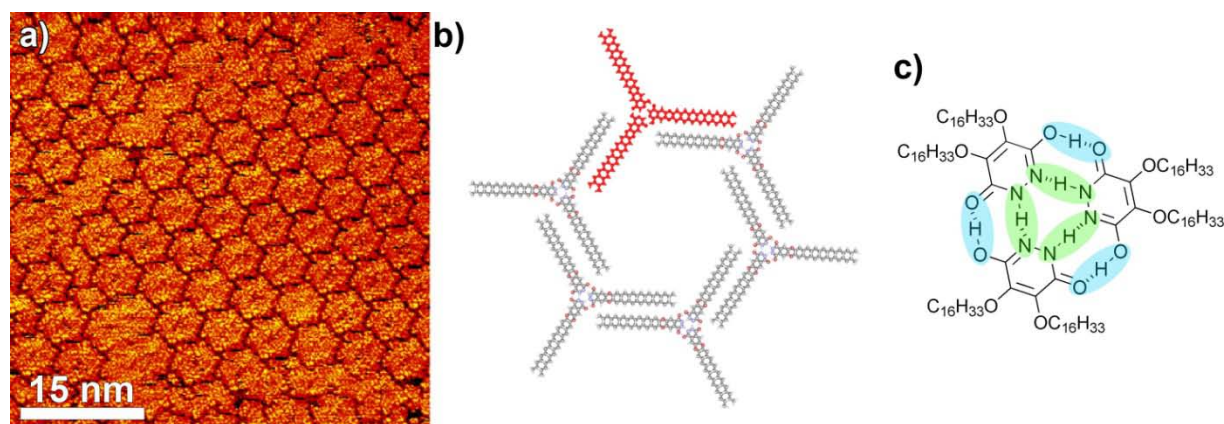


Figure 1.10 (a) Inverted contrast STM image of lactim/lactam architectures formed on HOPG surface; (b) proposed molecular assembly molecules in hexagonal structure; (c) schematic representation trimeric H-bonded structure, intermolecular O-H \cdots O H-bonds are indicated in blue, whereas N-H \cdots N H-bonds are marked in green.^[56]

The two N-H \cdots N hydrogen-bonds between diaminotriazine units have also been extensively used to form hexagonal motifs at the solid-liquid interface. This approach has enabled De Feyter and co-workers to form cyclic hexameric rosette structures, reminiscent of six-bladed windmills, featuring a 2D chiral character.^[58] The rosettes were found to be ordered in rows and form a hexagonal 2D crystal lattice. In Figure 1.11a an STM image of a small area with sub-molecular resolution is reported, showing in details the 2D crystal structure. The blades of the “windmill” appear as bright rods and correspond to the conjugated backbone of OPV, while the alkyl chains are located in the darker areas between the bright blades. Two out of three alkyl chains, which are lying along the direction of one of the main graphite crystallographic axes, can be visualized.

Their interdigitation contributes to the stabilization of the 2D crystal structure. Although the location of the third alkyl chain is not clear as it cannot be viewed, it can be reasonably considered to be back-folded into the supernatant solution.^[59] The diaminotriazine moieties at the opposite end of each molecule are pointing toward the centre of the rosettes, suggesting that their formation occurs through self-complementary hydrogen-bonds between adjacent triazine moieties. Molecular chirality is transferred to the nanostructures, which in turn form chiral 2D crystalline patterns that belong to the P_6 space group. This is the first example of 2D chirality belonging to this space group. Further, not only the 2D pattern is chiral, but the chirality of the 2D crystalline structures is also expressed by the relative orientation of the rosettes with respect to the main crystallographic axes of graphite.

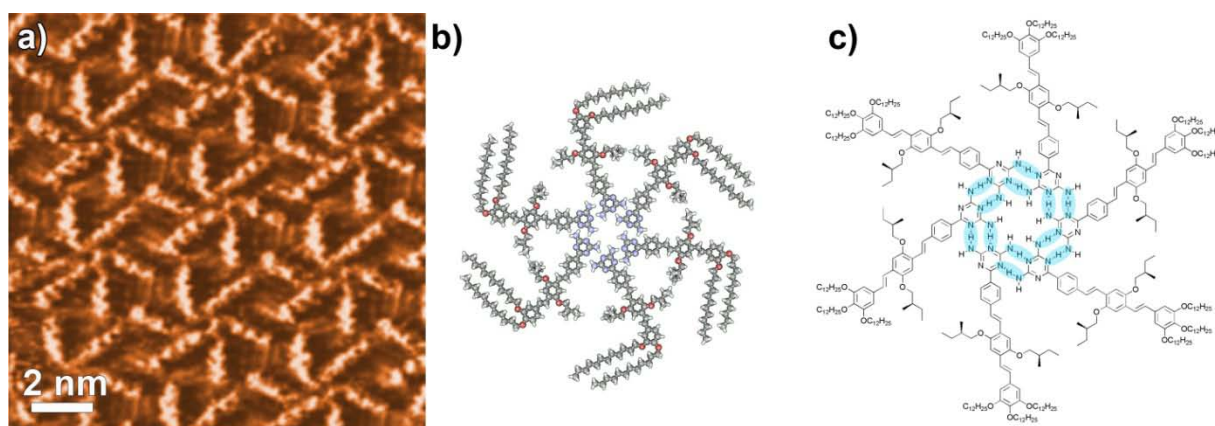


Figure 1.11 (a) STM image of the OPV “windmills” on HOPG surface; (b) proposed molecular assembly of OPV molecules; (c) schematic representation of the self-assembled structure of OPV molecules, intermolecular H-bonds are indicated in blue.^[58]

Harmonizing the functionalities of individual moieties in a supramolecular network represents a versatile approach for developing well-defined polymeric architectures with preprogrammed conformations and tailored properties. In this frame we studied the series of lipophilic guanosines^[60-63] which are very versatile building blocks: depending on the experimental conditions they can undergo different self-assembly pathways, leading to the formation of either H-bonded ribbons or quartet-based columnar structures. Given the possibility to functionalize the guanosines in the side-chains they appear as ideal building blocks for the fabrication of complex

architectures with a controlled high rigidity, thus paving the way towards their future use for scaffolding, that is, to locate functional units in preprogrammed positions. We have shown that guanosine derivatives can form H-bonded ribbon-like or quartet-based supramolecular architectures in solution, depending on the conditions.^[37] STM characterization showed that such molecules can self-assemble from a solution in an apolar solvent into ordered crystalline architectures on surfaces (Fig. 1.12). This self-assembly is governed by the formation of H-bonds between guanosines that dictates the spatial localization of oligothiophenes, ultimately forming 1D conjugated arrays that may be employed as prototypes of supramolecular nanowires.

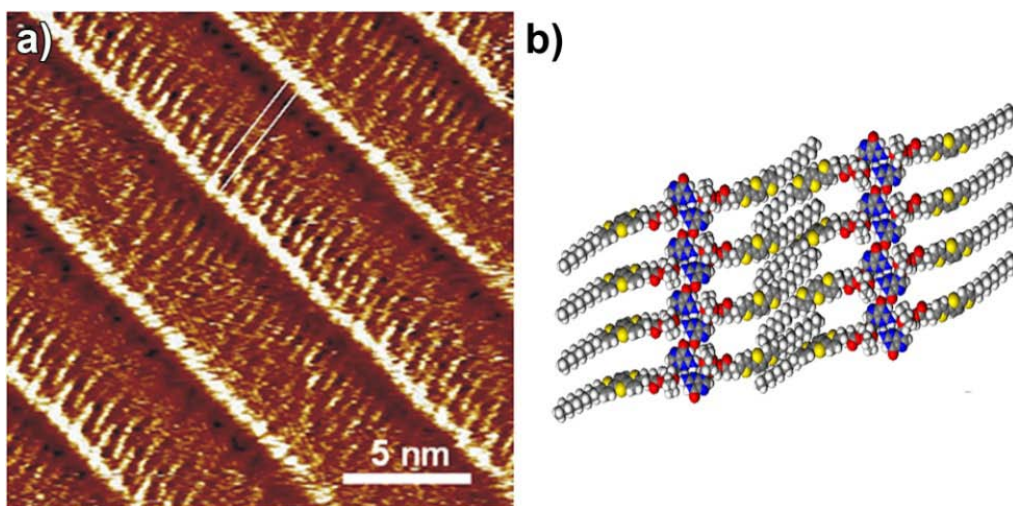


Figure 1.12 (a) STM image of H-bonded ribbons formed by self-assembly of guanosine derivative on HOPG surface; (b) proposed molecular assembly of guanosine derivative.^[37]

1.2.4 Tri-hapto Hydrogen-bonding moieties

Our group has recently demonstrated the controlled formation of bi-component porous networks based upon three consecutive H-bonding.^[20, 28] The hydrogen-bonded networks are formed by modulating the length of di-imide derivative modules, capable of forming three-parallel hydrogen-bonds with complementary modules, like melamine or diacetyl diaminopyridines.^[29, 64] The use of melamine as a cornerstone was pioneered by the Whitesides group^[65] and

demonstrated to self-assemble with perylene-3,4,9,10-tetracarboxylic di-imide (PTCDI) into hexagonal porous networks by Beton and co-workers using UHV conditions.^[66] Our group has extended this approach to a wide variety of di-imide modules at the solution-HOPG interface, using TCB as a solvent (Fig. 1.13).^[29, 67] The porous network forms favourably at low concentrations in the solution (1-10 μM), whereas co-existence of the phases formed by the pure components takes place at concentrations from 20-50 μM . It is interesting to note that, when using flexible linkers, a wide polygon distribution is found. Figure 1.13a shows a pentagon bridging two of the ideal hexagonal structures.

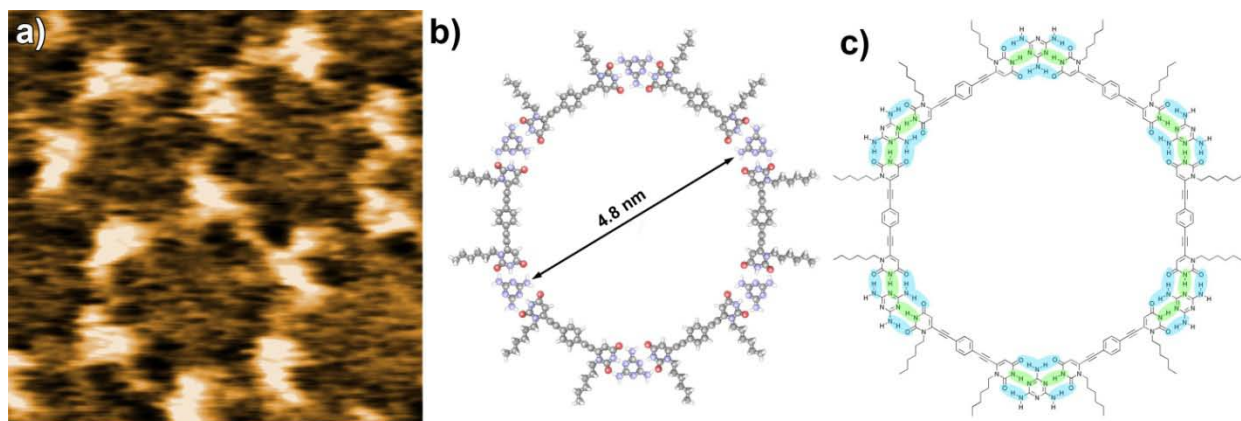


Figure 1.13 (a) STM image of bi-component network of melamine and uracyl derivative on HOPG surface; (b) proposed molecular assembly and schematic representation of hexagonal architecture (c), intermolecular N-H...O H-bonds are marked in blue, whereas N-H...N H-bonds are marked in green.^[28]

Such robust porous networks may also be combined with chemisorbed self-assembled monolayers (SAMs) to functionalize substrates. This approach offers considerable design flexibility, with the network providing an effective pathway to pattern the substrate and the SAM allowing the surface functionalization with sub-molecular resolution. The assembly of melamine and PTCDI in dimethylformamide (DMF) allows for the formation of a bi-component supramolecular network (Fig. 1.14).^[68] Upon addition of adamantine thiol on top of melamine/PTCDI network, the generation of hybrid structures was achieved. Figures 1.14a and b, demonstrates that the supramolecular network serves as a general template for a range of thiolated molecules. This approach, offers a great flexibility in the surface patterning. By proper

design of molecular building blocks the size of the cavities of porous networks can be tuned. Another great advantage of such an approach is the fact that the adsorbed 2D H-bonded network can be literally washed away from the surface. In this way only the chemisorbed compounds will remain on the metallic surface, furthermore they can be located on the surface with sub-molecular precision, by proper design of physisorbed porous networks, the size of the domains can be tuned.

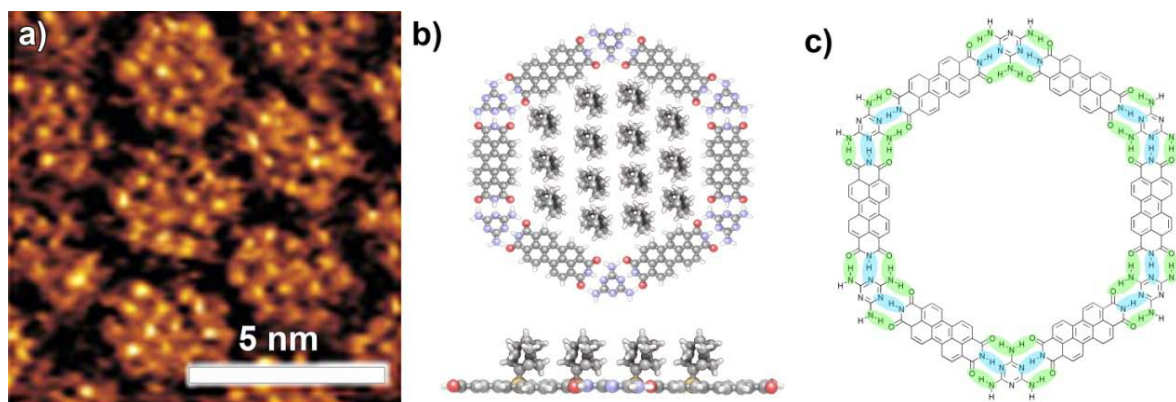


Figure 1.14 (a) STM image of three-component network of melamine, PTCDI and adamantine thiol on gold surface; (b) proposed molecular assembly of a network-SAM hybrid structure; (c) schematic representation of melamine-PTCDI honeycomb network, intermolecular N-H \cdots O H-bonds are marked in green, whereas N-H \cdots N H-bonds are marked in blue.^[68]

1.2.5 Tetra-hapto Hydrogen-bonding moieties

Although no 2D networks connected solely by quadruple hydrogen-bond have been constructed, much work has been adsorbed using these systems to control the two-dimensional pattern formations. A bright example of two-dimensional pattern formation driven by H-bonding has been described by Meijer et al. by the physisorption of chiral phenylenevinylene derivatives at the solid-liquid interface.^[69] Quadruple hydrogen-bonding dominates intermolecular interactions, leading to the formation of dimers on the surface. Figure 1.15a shows an STM height image obtained at the TCB-HOPG interface, where the π -conjugated segments appear as bright regions

and the alkyl tails are located in the dark parts. The long bright rods as observed in Figure 1.15a often appear as two individual bright rods, separated by a dark trough, corresponding to the location of the alkyl chains. The conjugated segments as well as the aliphatic side chains are lying with their long axes parallel to the basal plane of the graphite substrate. The formation of dimer (marked in red) provide evidence for the occurrence of hydrogen-bonding between two OPV molecules which, based upon the ratio between their length and width, the observed features in STM images can be ascribed to all-trans vinylene bonds. The space between two dimers in a lamella is sufficient to accommodate a face-on orientation of the conjugated parts and fully extended chiral (S)-2-methylbutoxy side chains. The face-on orientation allows the overlap between the orbitals of OPV and those of graphite, resulting in a maximum enthalpy gain. At the same time, the inter-molecular interactions between the lateral aliphatic dodecyloxy chains contribute to the stabilization of the lamellar structure of the 2D assembly. Therefore, the orientation of the monomers within the dimers, the orientation of the dimers within the lamellae, and the propagation direction of the lamellae with respect to the symmetry of the substrate are the result of the molecular design, including the chirality of the OPV molecules.

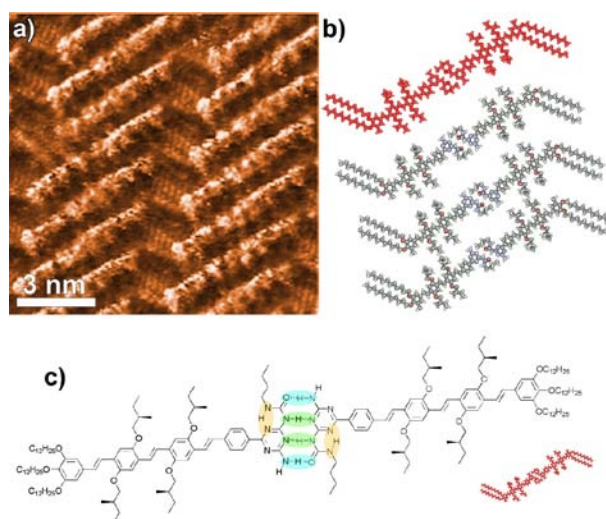


Figure 1.15 (a) STM image of OPV lamellar architecture on HOPG surface; (b) proposed molecular assembly of OPV molecules; (c) schematic representation of OPV dimeric structure, intermolecular N-H...O H-bonds are marked in blue and N-H...N H-bonds in green, whereas intramolecular N-H...N H-bonds are marked in orange.^[69]

1.2.6 Strength of Hydrogen-bond interactions.

A hydrogen bond, $D-H\cdots A$, is an interaction wherein a hydrogen atom is attracted to two atoms, D and A, rather than just one and so acts like a bridge between them. This attraction always increases with increasing electronegativity of D and A, and in the classical view all hydrogen bonds are highly electrostatic and sometimes even partly covalent. A number of hydrogen bonds studied by many groups in the recent literature have been collected and presented in Figure 1.16.^[7] This schematic diagram shows the interplay of effects in many different variations of the interaction. The figure shows H-bond as a borderless interaction that lies between the extremes of a half covalent bond, a pure electrostatic interaction, and a pure van der Waals interaction.

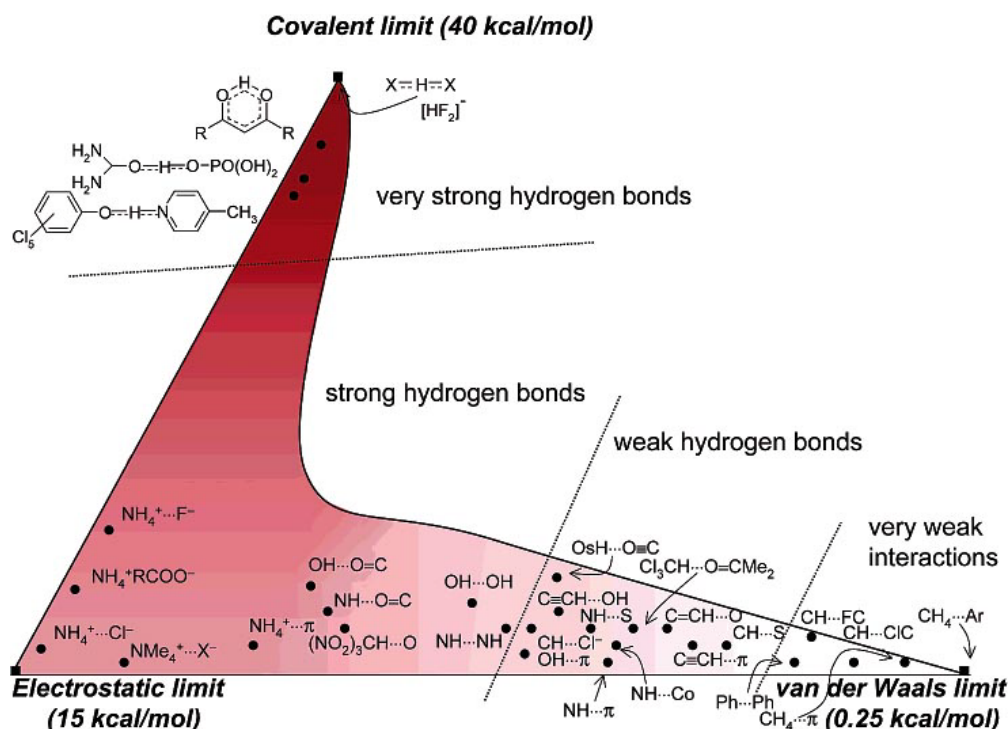


Figure 1.16 The H-bonding interaction energies. The composite nature of the interaction is highlighted by the three extreme situations of widely differing energies. The sketch is not strictly quantitative but the coloring attempts to provide a visual scale of energies. The figure can serve as a rough guide to the balance of electrostatics, van der Waals nature, and covalency in any $D-H\cdots A$ interaction.^[7]

There are, in effect, three axes in this figure radiating out from the “centroid” of the plot and showing the extent of these three main characteristics. The sketch shows all hydrogen bonds as being electrostatic, with variations toward covalency among the so-called very strong hydrogen bonds and toward van der Waals character in the domain of the weak hydrogen bond. The central region corresponds to the classical or conventional hydrogen bond interactions, which are commonly used in the self-assembly of small organic molecules at the solid-liquid interfaces. Figure 1.17 shows, how the strength of intermolecular interactions can be tuned by using single, double,^[15, 70] triple,^[21, 22] quadruple,^[24] and other parallel H-bonds of higher multiplicity, in order to stabilize supramolecular assemblies on solid surfaces.

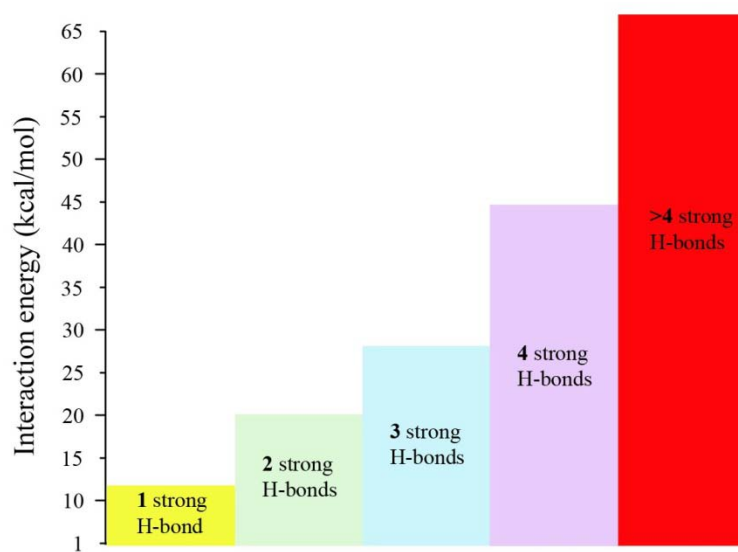


Figure 1.17 Strength of H-bonding interactions vs. their multiplicity.

1.3 Metallo-Ligand Interactions

Supramolecular architectures combining organic moieties with transition metal ions have been widely employed during the last decades.^[71-77] The interest in such assemblies arises both from their robustness and from their electronic features, leading to the development of applications in various research fields.^[78] For instance, monomolecular transistors based on terpyridine-cobalt-terpyridine complexes,^[79] as well as dynamic chemical devices undergoing reversible extension/contraction through a pH-triggered complexation of Pb ions have been reported.^[80] Recently, the use of self-assembly processes to generate hybrid molecular arrays with predefined structures on surfaces has been explored by combining metal centres and organic units.^[81] STM has been used to study various self-assembled systems such as metal-organic 2D coordination networks,^[82, 83] discrete complexes on surfaces^[84-86] or more recently 1D coordination networks based on tectons bridging two coordination poles with different denticities.^[87]

In 2002 De Schryver and co-workers reported an STM investigation of *in-situ* complexation of Pd(OAc)₂ by a monolayer of a bipyridine derivative at the HOPG surface.^[88] The formed monolayer can be then used as a template to build nanostructures. After the successful imaging of the 5,5'-dinonadecyl-2,2'-bipyridine monolayers at the HOPG/1-phenyloctane interface, a drop of Pd(OAc)₂ in 1-phenyloctane was applied. A spontaneous change of the monolayer pattern was observed. Figure 1.18 shows a representative STM image of 5,5'-dinonadecyl-2,2'-bipyridine monolayer physisorbed at the HOPG/air interface after addition of Pd(OAc)₂ in 1-heptanol and drying for two days under ambient conditions.

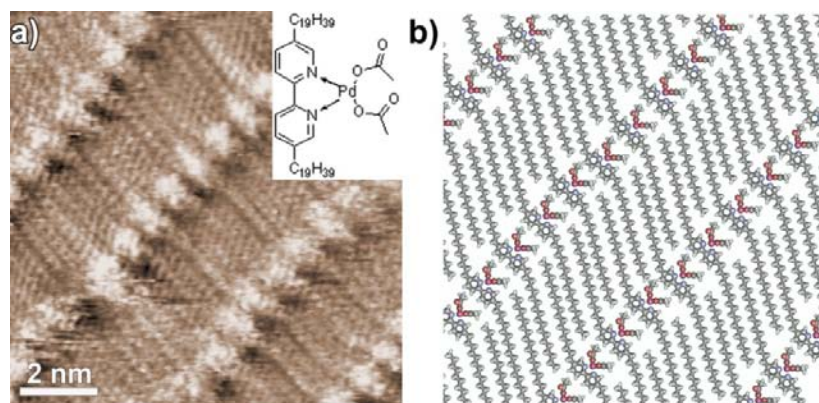


Figure 1.18 (a) STM image of Pd^{II} complexes on HOPG surface; (b) proposed molecular assembly.^[88]

In 2005 Stang and co-workers reported an STM study on the self-assembled supramolecular metallacyclic rectangle cyclobis[(1,8-bis(transPt(PEt₃)₂)anthracene)(1,4'-bis(4-ethynylpyridyl)benzene)](PF₆)₄,^[89] the dimensions of a single rectangle being 3.1 nm by 1.2 nm. The monolayers were studied both on HOPG and Au(111) surfaces to investigate the effect of substrate on their structure. The molecules self-organize into well ordered 2D patterns on both surfaces, and high-resolution STM results clearly reveal a rectangle on both HOPG (Fig. 1.19) and Au(111) surfaces. The symmetry and molecular orientation adopted by the molecules depends on the substrate. The long edge of the rectangles sits on the HOPG surface, while it lays flat on the Au(111) surface, showing that the molecular self-organization of the supramolecular metallacyclic rectangle can be tuned by the appropriate choice of substrate.

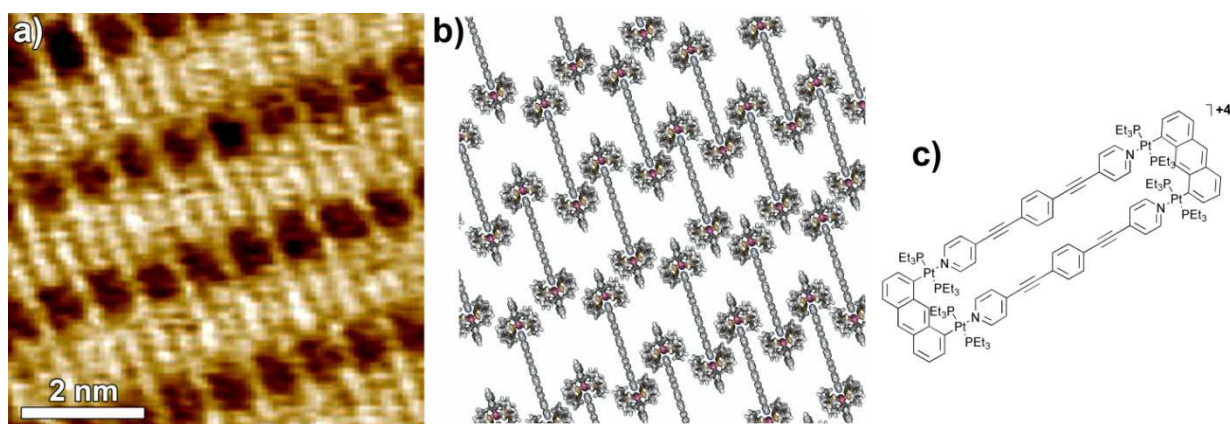


Figure 1.19 (a) STM image of Pt^{II} complex architectures on HOPG surface; (b) proposed molecular assembly; (c) schematic representation of cyclobis[(1,8-bis(transPt(PEt₃)₂)anthracene)(1,4'-bis(4-ethynylpyridyl)benzene)](PF₆)₄.^[89]

STM investigations on a series of neutral salicylaldehyde- and aldemine-derived M^{II} complexes with various positions and lengths of the alkoxy substituents as well as exchangeable functional groups has been recently reported by Ziener and Rieger.^[86] Figure 1.20a shows an STM image of bis(salicylaldehydato)palladium(II) complex at the TCB/HOPG interface. The images allow a detailed analysis of the 2D array, revealing metal–metal distances of 6.7 ± 0.2 Å within the lamellae. The arrangement of the complex cores suggests attractive interactions of the carbonyl

protons with both the phenolate and carbonyl oxygen atoms of adjacent complexes. Applying typical geometric parameters to the 2D structure allows one to evaluate the distance between these atoms to be about $2.6 \pm 0.2 \text{ \AA}$, which is in agreement with the typical length of weak inter- and intra-molecular hydrogen-bonds formed by aldehyde or aldimine protons with adjacent oxygen atoms. On the basis of these findings, the model of the surface structure of Pd^{II} complex was established.

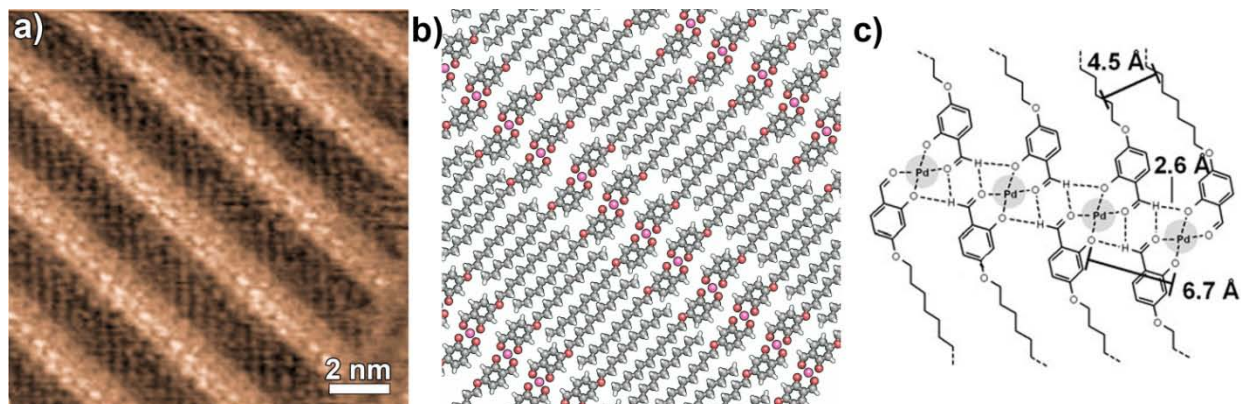


Figure 1.20 (a) STM image of lamellar arrangement of Pt^{II} complexes on HOPG surface; (b) proposed molecular assembly; (c) schematic representation and intermolecular distances on the self-assembled structures observed by STM.^[86]

In 2002, J.-M. Lehn and co-workers reported the synthesis and characterization of bis(terpyridine)-derived ligands which can form $[2 \times 2]$ grid-like complexes.^[90, 91] Additional pyridine substituents on these ligands do not interfere with the complexation process. STM investigations showed that the physisorption of a pure ligand on HOPG took to the formation of highly ordered structures stabilized by additional inter-molecular $\text{C-H} \cdots \text{N}$ hydrogen-bonds, partially through the extra-pyridines. Similar adsorption experiments with one of the corresponding $[2 \times 2]$ Co^{II} grid-type complexes on HOPG led to a well-organized structure with inter-digitation of the extra-pyridine moieties (Fig. 1.21).

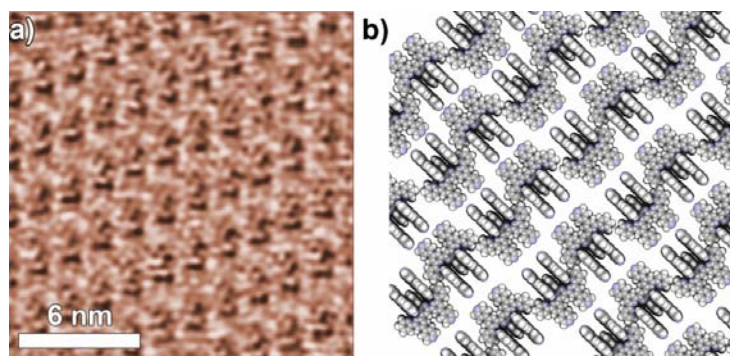


Figure 1.21 (a) STM image of Co^{II} grid-type complexes on HOPG surface; (b) proposed molecular assembly of Co^{II} grids.^[90]

1.4 Van der Waals interactions.

Van der Waals^[92] interactions arise from the polarization of an electron cloud by the proximity of an adjacent nucleus, resulting in a weak electrostatic attraction. They are unspecific and non-directional and hence possess only limited scope in the design of 2D supramolecular architectures. Van der Waals interactions provide a general attractive interaction for polarizable species with an interaction energy proportional to the surface area of contact. Strictly, van der Waals interactions might be divided into dispersion (London forces)^[93] and exchange repulsion terms.^[94] The dispersion interaction is an attractive component that results from the interactions between fluctuating multipoles in adjacent molecules. The energy of dispersion interactions decreases rapidly with distance. The exchange-repulsion defines molecular shape and balances dispersion forces at short range. In case of surface study, especially in STM investigation, very often the molecules are equipped with alkyl or alkoxy chains of various length, which is understandable since the interaction energy between the alkyl chains and a solid substrates increases with the length of the alkyl chain. For instance, the adsorption energy of one methylene group on graphite (HOPG) surface was calculated as $2.6 \text{ kcal mol}^{-1}$ (11 kJmol^{-1} , $\sim 0.1 \text{ eV}$), and was found to be in agreement with temperature-programmed desorption experiments.^[95-98]

De Feyter and co-workers have recently developed a novel class of flexible porous networks, i.e. non-porous networks that adopt porous architectures in a presence of a guest molecules.^[99-101] These flexible networks, are based on hexadecahydrotribenzo[12]annulene (DBA) molecules. DBA molecules with alkoxy substituents form nonporous networks through interdigitation of the alkyl chains and are capable of acting as hosts to template the assembly of guest molecules (Fig. 1.22). The size of the hexagon cavities was tuned by adjusting the length of the alkoxy substituents. Upon addition of large nanographenes (Fig. 1.22a) as guest molecules, honeycomb DBA networks with alkoxy chains reaching $\text{OC}_{20}\text{H}_{41}$ are stabilized (Fig. 1.22b-d), resulting in a large repeating period of 6.3 nm and cavities reaching 5.4 nm in diameter. The number of guest molecules in each cavity is exclusively related to the size of the cavity. Up to six nanographene molecules can be hosted in the same cavity for the DBA derivative with the longest alkoxy chains. DBA host networks show remarkable flexibility: the size, shape, and symmetry of the pores changes in response to the inclusion of guest molecules.

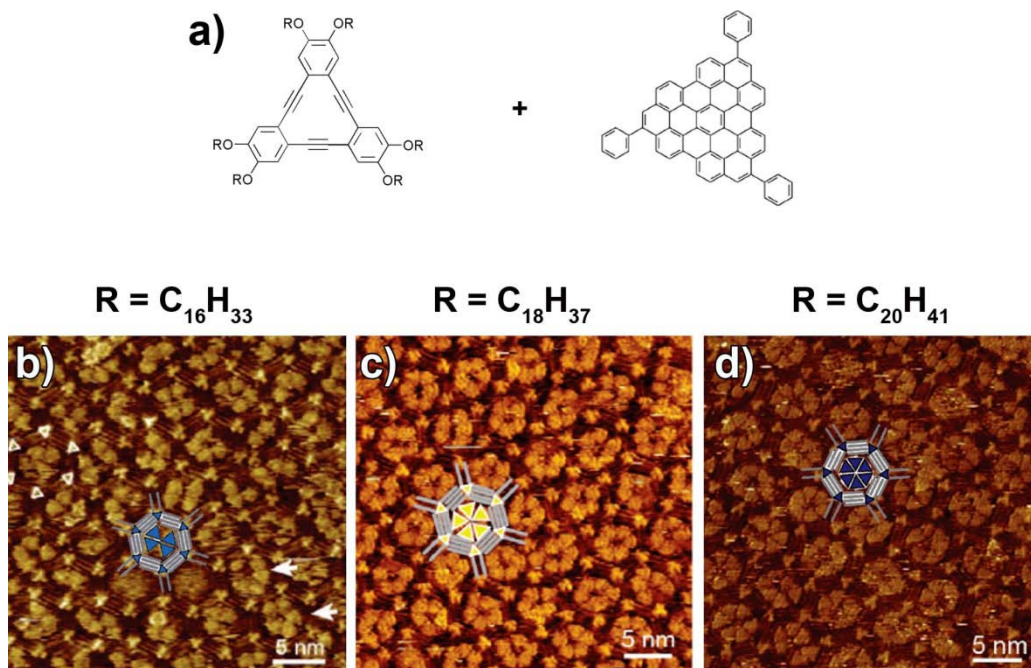


Figure 1.22 (a) Chemical formulas of DBA core and nanographene used as a “host-guest” system; STM image of DBA molecules possessing $OC_{16}H_{33}$ (b), $OC_{18}H_{37}$ (c) and $OC_{20}H_{41}$ (d) alkoxy chains, hosting 4, 5 and 6 nanographene molecules respectively.^[101]

Another example of flexible networks are 2D molecular sieves, obtained using a star-shape stilbenoid compound (1,3,5-tris[(*E*)-2-(3,5-didecyloxyphenyl)-ethenyl]benzene (TSB), whose structure is shown in Figure 1.23. Such a molecules are known self-assemble on HOPG surface leaving empty cavities.^[102] Self-assembly of TSB molecules on HOPG from 1-phenyloctane solution led to the formation of honeycomb cavities with diameter of ca. 1.3 nm (Fig. 1.23a and b). The cavities were able to host coronene (Fig. 1.23c and d), benzo[*rst*]pentaphene (BPP) (Fig. 1.23e and f), or hexabenzocoronene (HBC) molecules (Fig. 1.23g and 1.23h). As one can see on STM images (Fig. 1.23c, e and f), after addition of coronene, BPP and HBC molecules a bright spot appears in the centre of cavities of the TSB network.

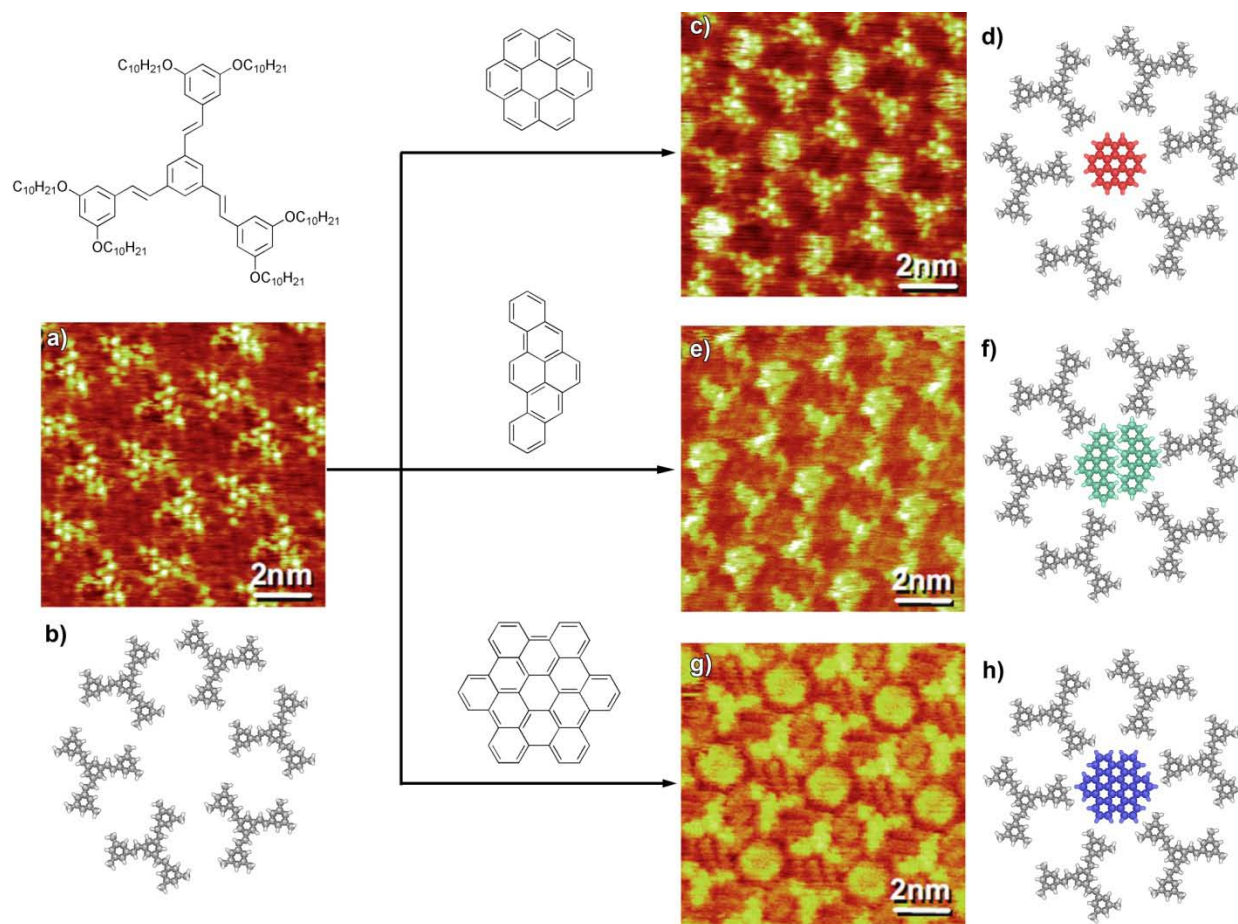


Figure 1.23 STM image and corresponding schematic representation of TSB honeycomb network (a,b) TSB-coronene (b,c), TSB-BPP (e,f) and TSB-HBC (g,f) “host-guest” systems.^[102]

The general “host-guest” complexation is a common strategy in the supramolecular chemist’s toolbox. In this context, complexation of the well-known donor-acceptor thiophene and fullerene (C_{60}) pair^[103] have been characterized at the solid-liquid interface by Freyland and co-workers.^[104] By using a macrocycle decorated with di-thiophene units, C_{60} can undergo preferential adsorption onto the dithiophene “host” sites. Figure 1.24a shows an STM image of ordered macrocycle monolayer, while Figure 1.24b shows where C_{60} molecules are adsorbed after deposition. One could expect the C_{60} molecules adsorbing in the cavities, however in this case they adsorb on top of the bithiophene moieties, which suggest a relatively strong π -donor/ π -acceptor interactions between the thiophene moieties and C_{60} molecules. Such a phenomenon was also observed in the independent study of π -donor/ π -acceptor system, including C_{60}

molecules.^[105] Thanks to the relatively large size of the host macrocycles (and the size of the unit cell area), two C₆₀ molecules can adsorb per macrocycle molecule.

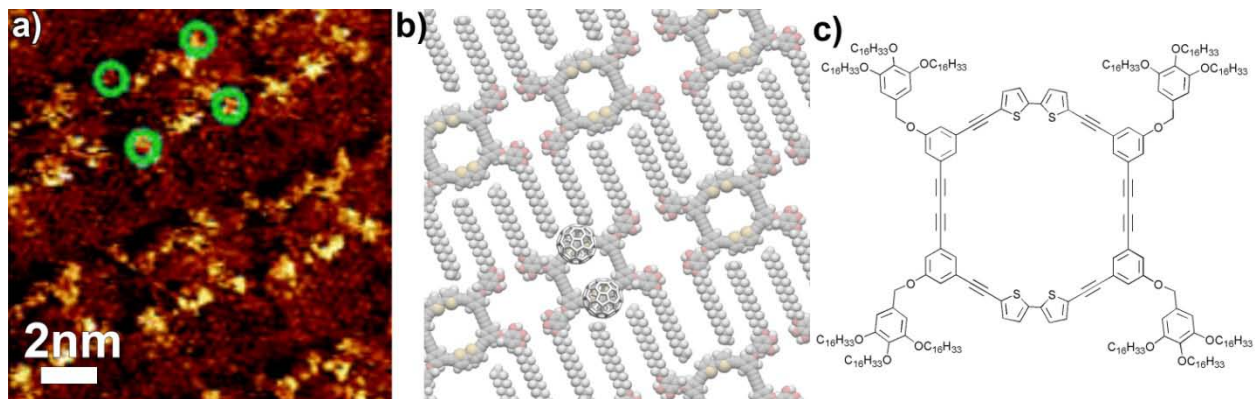


Figure 1.24 (a) STM image of thiophene monolayer on HOPG surface; (b) proposed molecular packing motif; (c) schematic representation of thiophene molecule.^[104]

In 2008 Charra^[106] and co-workers reported the synthesis and characterization of multilayered [2.2]paracyclophane (PCP) moieties. More precisely, they synthesized a series of compounds bearing two functional “clips” that end-cap a central benzene ring (Fig 1.25a) or lower deck of two- and three-layered PCP units (Fig 1.25c and e, respectively). All molecules, were found to form self-assembled lamellar structures at the solid-liquid interface. Figure 1.25b shows the monolayer of the compound bearing benzene as a central ring on HOPG surface. The bright four-branched patterns can be assigned to the rigid conjugated cores of the molecules. The STM images of two- and three-layered PCP-based compounds are shown in Figure 1.25d and f, respectively. Although the images of conjugated cores are strongly modified compared to one-layered molecule, careful interpretation of STM images shows that the conjugated cores are still visible. However, the image contrast is now affected by the bright spots, which might be attributed to the central PCP moieties.

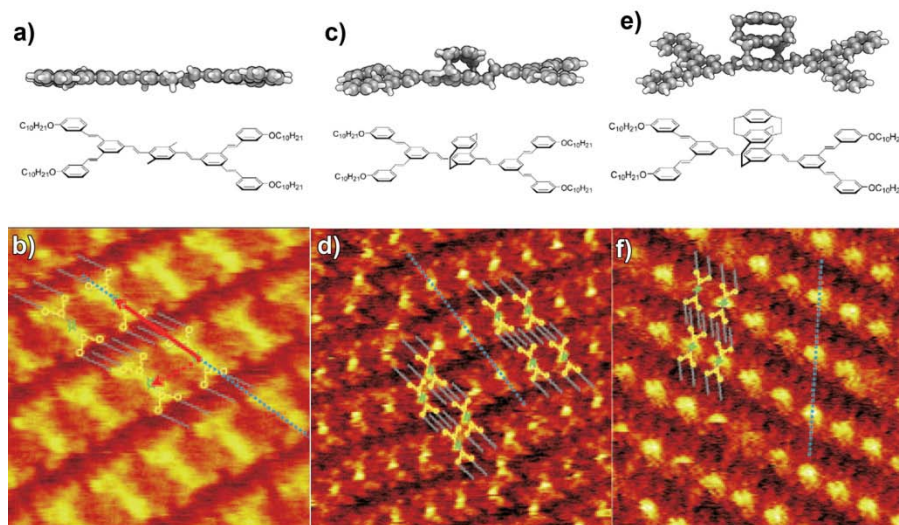


Figure 1.25 (a, c, e) Schematic representation of multilayered PCP derivatives (b, d, f) STM images of one-, two- and three-layered PCP derivative respectively.^[106]

Recently, Mena-Osteritz^[107] and co-workers reported STM study, on particularly designed cyclo [12]thiophene (C[12]T) molecules (Fig. 1.26), cyclic π -conjugated oligomers, which were found to form well-ordered 2D nanostructures, and may host the C_{60} guest molecules.^[108] The fully conjugated cycles C[12]T perfectly ordered in one persistent domain at the HOPG-liquid interface forming hexagonal pattern. 2D hexagonal pattern is stabilized by the weak van der Waals interaction of alkyl side chains between adjacent molecules.

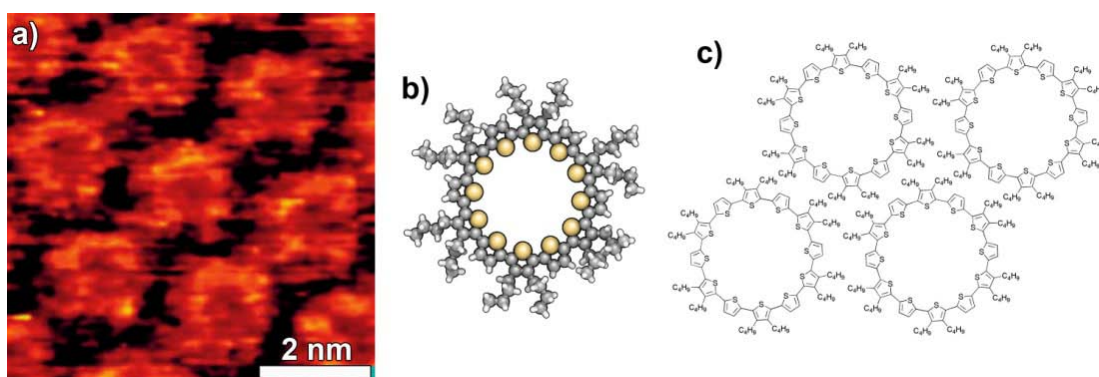


Figure 1.26 (a) STM image of hexagonal network formed by self-assembly of c[12]T molecules on HOPG surface; (b) schematic representation of C[12]T molecules; (c) proposed molecular packing of C[12]T molecules.^[107]

The self-assembly of OBOCMC8, a calyx [8]arene derivative, and of the “host-guest” system OBOCMC8/C₆₀ (Fig. 1.27) supported on the gold (Au(111)) surface was investigated by electrochemical STM,^[109] leading to sub-molecular resolution of the self-assembly of calixarenes molecules. Calixarenes were found to be suitable for fabrication of nanoscale electronic devices because of their ability to host fullerene molecules. OBOCMC8 molecules adsorb on Au(111) surface by carboxyl-, phenyl-, and *tert*-butyl-gold interactions.^[110] OBOCMC8 molecules appear in the STM image (Fig. 1.27a) as ordered arrays of bright objects, i.e. calixes. After addition of C₆₀ molecules, STM image (Fig. 1.27c) shows an ordered array of bright spots surrounded by circular protrusions, corresponding to the OBOCMC8/C₆₀ assembly.

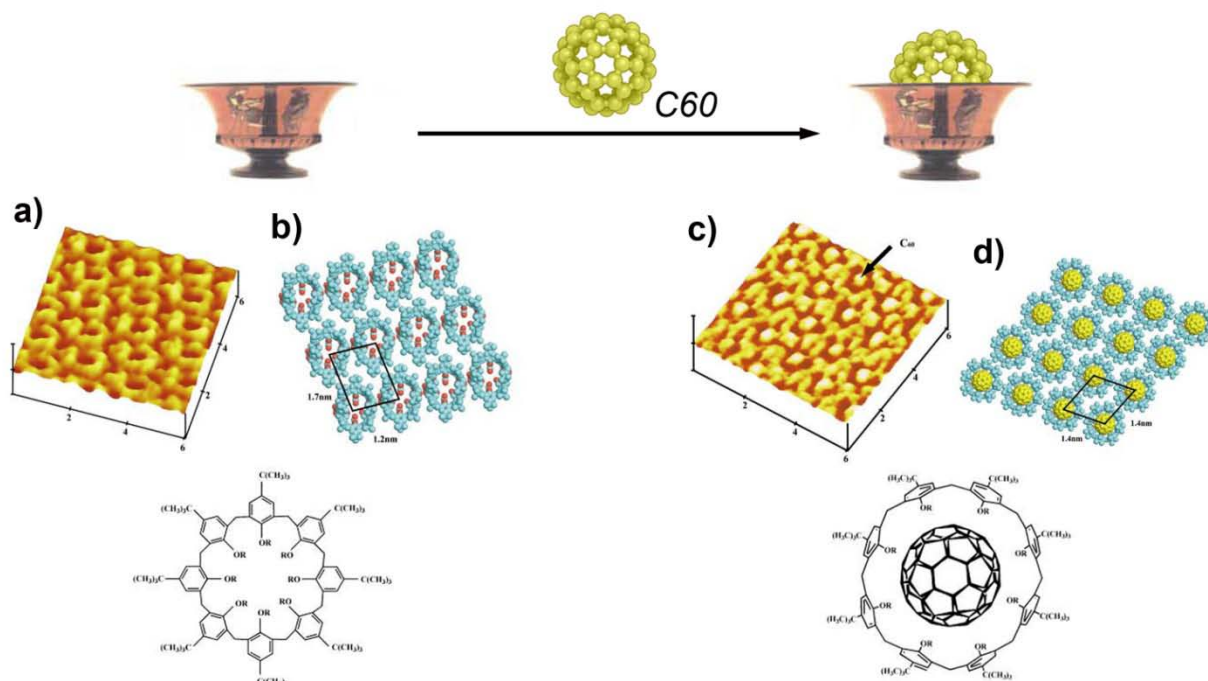


Figure 1.27 (a) STM image of OBOCMC8 monolayer on Au(111) surface; (b) proposed molecular packing motif of OBOCMC8 (c) (a) STM image of OBOCMC8/C₆₀ monolayer on Au(111) surface; (d) proposed molecular packing motif of OBOCMC8/C₆₀ “host-guest” system.^[109]

References

- [1] A. Werner, *Zeitschr. Anorg. Chem.* **1893**, 3, 267.
- [2] E. Fisher, *Ber. Deutsch. Chem. Ges.* **1894**, 27, 2985.
- [3] K. L. Wolf, H. Frahm, H. Harms, *Z. Phys. Chem. (B)* **1937**, 36, 237.

- [4] J.-M. Lehn, *Pure Appl. Chem.* **1979**, *51*, 979.
- [5] J. M. Lehn, *Science* **1993**, *260*, 1762.
- [6] J. M. Lehn, *Proc. Natl. Acad. Sci. U.S.A.* **2002**, *99*, 4763.
- [7] G. R. Desiraju, *Acc. Chem. Res.* **2002**, *35*, 565.
- [8] M. W. Hosseini, *CrystEngComm* **2004**, *6*, 318.
- [9] G. Binnig, H. Rohrer, C. Gerber, E. Weibel, *Phys. Rev. Lett.* **1982**, *49*, 57.
- [10] H. Rohrer, *PNAS* **1987**, *84*, 4666.
- [11] T. F. A. Greef, E. W. Meijer, *Nature* **2008**, *453*, 171.
- [12] D. C. Sherrington, K. A. Taskinen, *Chem. Soc. Rev.* **2001**, *30*, 83.
- [13] A. Ciesielski, G. Schaeffer, A. Petitjean, J. M. Lehn, P. Samorì, *Angew. Chem. Int. Ed.* **2009**, *48*, 2039.
- [14] J.-M. Lehn, *Supramolecular chemistry: concepts and perspectives*, VCH New York, **1995**.
- [15] C. Fouquey, J.-M. Lehn, A.-M. Levelut, *Adv. Mater.* **1990**, *2*, 254.
- [16] J. C. Macdonald, G. M. Whitesides, *Chem. Rev.* **1994**, *94*, 2383.
- [17] E. Fan, C. Vicent, S. J. Geib, A. D. Hamilton, *Chem. Mater.* **1994**, *6*, 1113.
- [18] S. Subramanian, M. J. Zaworotko, *Coord. Chem. Rev.* **1994**, *137*, 357.
- [19] G. A. Jeffrey, *An Introduction to Hydrogen Bonding*, Oxford University Press, **1997**.
- [20] C.-A. Palma, J. Bjork, M. Bonini, M. S. Dyer, A. Llanes-Pallas, D. Bonifazi, M. Persson, P. Samorì, *J. Am. Chem. Soc.* **2009**, *131*, 13062.
- [21] S. Djurdjevic, D. A. Leigh, H. McNab, S. Parsons, G. Teobaldi, F. Zerbetto, *J. Am. Chem. Soc.* **2007**, *129*, 476.
- [22] T. J. Murray, S. C. Zimmerman, *J. Am. Chem. Soc.* **1992**, *114*, 4010.
- [23] O. Lukin, J. Leszczynski, *J. Phys. Chem. A* **2002**, *106*, 6775.
- [24] S. H. M. Söntjens, R. P. Sijbesma, M. H. P. van Genderen, E. W. Meijer, *J. Am. Chem. Soc.* **2000**, *122*, 7487.
- [25] A. M. Mebel, K. Morokuma, M. C. Lin, *J. Chem. Phys.* **1995**, *103*, 7414.
- [26] J. D. Gu, J. Leszczynski, *J. Phys. Chem. A* **2000**, *104*, 6308.
- [27] J. D. Gu, J. Leszczynski, *J. Phys. Chem. A* **2000**, *104*, 7353.
- [28] C.-A. Palma, M. Bonini, A. Llanes-Pallas, T. Breiner, M. Prato, D. Bonifazi, P. Samorì, *Chem. Commun.* **2008**, 5289.

- [29] L. Piot, C.-A. Palma, A. Llanes-Pallas, M. Prato, Z. Szekrényes, K. Kamarás, D. Bonifazi, P. Samorì, *Adv. Funct. Mater.* **2009**, *19*, 1207.
- [30] Z. Mu, L. Shu, H. Fuchs, M. Mayor, L. Chi, *J. Am. Chem. Soc.* **2008**, *130*, 10840.
- [31] C. Meier, U. Ziener, K. Landfester, P. Wehrich, *J. Phys. Chem. B* **2005**, *109*, 21015.
- [32] S. De Feyter, P. C. M. Grim, J. van Esch, R. M. Kellogg, B. L. Feringa, F. C. De Schryver, *J. Phys. Chem. B* **1998**, *102*, 8981.
- [33] R. Matmour, I. De Cat, S. J. George, W. Adriaens, P. Leclère, P. H. H. Bomans, N. A. J. M. Sommerdijk, J. C. Gielen, P. C. M. Christianen, J. T. Heldens, J. C. M. van Hest, D. W. P. M. Löwik, S. De Feyter, E. W. Meijer, A. P. H. J. Schenning, *J. Am. Chem. Soc.* **2008**, *130*, 14576.
- [34] S. Lei, J. Puigmarti-Luis, A. Minoia, M. Van der Auweraer, C. Rovira, R. Lazzaroni, D. B. Amabilino, S. De Feyter, *Chem. Commun.* **2008**, 703.
- [35] A. Gesquiere, S. De Feyter, F. C. De Schryver, F. Schoonbeek, J. van Esch, R. M. Kellogg, B. L. Feringa, *Nano Lett.* **2001**, *1*, 201.
- [36] A. Gesquiere, M. M. S. Abdel-Mottaleb, S. De Feyter, F. C. De Schryver, F. Schoonbeek, J. van Esch, R. M. Kellogg, B. L. Feringa, A. Calderone, R. Lazzaroni, J. L. Brédas, *Langmuir* **2000**, *16*, 10385.
- [37] G. P. Spada, S. Lena, S. Masiero, S. Pieraccini, M. Surin, P. Samorì, *Adv. Mater.* **2008**, *20*, 2433.
- [38] L. Kampschulte, T. L. Werblowsky, R. S. K. Kishore, M. Schmittel, W. M. Heckl, M. Lackinger, *J. Am. Chem. Soc.* **2008**, *130*, 8502.
- [39] J. P. Rabe, S. Buchholz, *Science* **1991**, *253*, 424.
- [40] C. A. Palma, M. Bonini, T. Breiner, P. Samorì, *Adv. Mater.* **2009**, *21*, 1383.
- [41] S. B. Lei, K. Tahara, F. C. De Schryver, M. Van der Auweraer, Y. Tobe, S. De Feyter, *Ang. Chem. Int. Ed.* **2008**, *47*, 2964.
- [42] L. Kampschulte, M. Lackinger, A. K. Maier, R. S. K. Kishore, S. Griessl, M. Schmittel, W. M. Heckl, *J. Phys. Chem. B* **2006**, *110*, 10829.
- [43] M. Lackinger, W. M. Heckl, *Langmuir* **2009**, *25*, 11307.
- [44] M. Lackinger, S. Griessl, T. Markert, F. Jamitzky, W. M. Heckl, *J. Phys. Chem. B* **2004**, *108*, 13652.

- [45] M. Blunt, X. Lin, M. D. Gimenez-Lopez, M. Schroder, N. R. Champness, P. H. Beton, *Chem. Commun.* **2008**, 2304.
- [46] M. O. Blunt, J. C. Russell, M. D. Gimenez-Lopez, J. P. Garrahan, X. Lin, M. Schroder, N. R. Champness, P. H. Beton, *Science* **2008**, 322, 1077.
- [47] J. M. MacLeod, O. Ivasenko, D. F. Perepichka, F. Rosei, *Nanotechnology* **2007**, 18.
- [48] S. Buchholz, J. P. Rabe, *Ang. Chem. Int. Ed.* **1992**, 31, 189.
- [49] K. Eichhorst-Gerner, A. Stabel, G. Moessner, D. Declerq, S. Valiyaveetil, V. Enkelmann, K. Müllen, J. P. Rabe, *Ang. Chem. Int. Ed.* **1996**, 35, 1492.
- [50] S. De Feyter, F. C. De Schryver, *Chem. Soc. Rev.* **2003**, 32, 139.
- [51] S. De Feyter, A. Gesquiere, M. M. Abdel-Mottaleb, P. C. M. Grim, F. C. De Schryver, C. Meiners, M. Sieffert, S. Valiyaveetil, K. Müllen, *Acc. Chem. Res.* **2000**, 33, 520.
- [52] D. M. Cyr, B. Venkataraman, G. W. Flynn, *Chem. Mater.* **1996**, 8, 1600.
- [53] S. De Feyter, P. C. M. Grim, M. Rücker, P. Vanoppen, C. Meiners, M. Sieffert, S. Valiyaveetil, K. Müllen, F. C. De Schryver, *Ang. Chem. Int. Ed.* **1998**, 37, 1223.
- [54] H. Walch, A. K. Maier, W. M. Heckl, M. Lackinger, *J. Phys. Chem. C* **2009**, 113, 1014.
- [55] K. G. Nath, O. Ivasenko, J. A. Miwa, H. Dang, J. D. Wuest, A. Nanci, D. F. Perepichka, F. Rosei, *J. Am. Chem. Soc.* **2006**, 128, 4212.
- [56] A. Mourran, U. Ziener, M. Moller, M. Suarez, J. M. Lehn, *Langmuir* **2006**, 22, 7579.
- [57] N. Mingo, L. Jurczyszyn, F. J. GarciaVidal, R. SaizPardo, P. L. deAndres, F. Flores, S. Y. Wu, W. More, *Phys. Rev. B* **1996**, 54, 2225.
- [58] A. Miura, P. Jonkheijm, S. De Feyter, A. P. H. J. Schenning, E. W. Meijer, F. C. De Schryver, *Small* **2005**, 1, 131.
- [59] J. A. A. W. Elemans, R. Van Hameren, R. J. M. Nolte, A. E. Rowan, *Adv. Mater.* **2006**, 18, 1251.
- [60] G. Gottarelli, S. Masiero, E. Mezzina, S. Pieraccini, J. P. Rabe, P. Samorì, G. P. Spada, *Chem. Eur. J.* **2000**, 6, 3242.
- [61] T. Giorgi, S. Lena, P. Mariani, M. A. Cremonini, S. Masiero, S. Pieraccini, J. P. Rabe, P. Samorì, G. P. Spada, G. Gottarelli, *J. Am. Chem. Soc.* **2003**, 125, 14741.
- [62] S. Pieraccini, S. Masiero, O. Pandoli, P. Samorì, G. P. Spada, *Org. Lett.* **2006**, 8, 3125.
- [63] S. Lena, G. Brancolini, G. Gottarelli, P. Mariani, S. Masiero, A. Venturini, V. Palermo, O. Pandoli, S. Pieraccini, P. Samorì, G. P. Spada, *Chem. Eur. J.* **2007**, 13, 3757.

- [64] D. Bonifazi, S. Mohnani, A. Llanes-Pallas, *Chem. Eur. J.* **2009**, *15*, 7004.
- [65] C. T. Seto, G. M. Whitesides, *J. Am. Chem. Soc.* **1990**, *112*, 6409.
- [66] J. A. Theobald, N. S. Oxtoby, M. A. Phillips, N. R. Champness, P. H. Beton, *Nature* **2003**, *424*, 1029.
- [67] A. Llanes-Pallas, C. A. Palma, L. Piot, A. Belbakra, A. Listorti, M. Prato, P. Samorì, N. Armaroli, D. Bonifazi, *J. Am. Chem. Soc.* **2009**, *131*, 509.
- [68] R. Madueno, M. T. Raisanen, C. Silien, M. Buck, *Nature* **2008**, *454*, 618.
- [69] A. Gesquiere, P. Jonkheijm, F. J. M. Hoeben, A. P. H. J. Schenning, S. De Feyter, F. C. De Schryver, E. W. Meijer, *Nano Lett.* **2004**, *4*, 1175.
- [70] Y. Ducharme, J. D. Wuest, *J. Org. Chem.* **1988**, *53*, 5787.
- [71] S. R. Batten, R. Robson, *Angew. Chem. Int. Ed.* **1998**, *37*, 1460.
- [72] A. J. Blake, N. R. Champness, P. Hubberstey, W. S. Li, M. A. Withersby, M. Schroder, *Coord. Chem. Rev.* **1999**, *183*, 117.
- [73] B. Moulton, M. J. Zaworotko, *Chem. Rev.* **2001**, *101*, 1629.
- [74] C. Janiak, *Dalton Trans.* **2003**, 2781.
- [75] S. Kitagawa, R. Kitaura, S. Noro, *Angew. Chem. Int. Ed.* **2004**, *43*, 2334.
- [76] G. Ferey, C. Mellot-Draznieks, C. Serre, F. Millange, *Acc. Chem. Res.* **2005**, *38*, 217.
- [77] D. L. Long, E. Burkholder, L. Cronin, *Chem. Soc. Rev.* **2007**, *36*, 105.
- [78] A. M. W. C. Thompson, *Coord. Chem. Rev.* **1997**, *160*, 1.
- [79] W. J. Liang, M. P. Shores, M. Bockrath, J. R. Long, H. Park, *Nature* **2002**, *417*, 725.
- [80] M. Barboiu, J. M. Lehn, *Proc. Natl. Acad. Sci. U.S.A.* **2002**, *99*, 5201.
- [81] D. G. Kurth, N. Severin, J. P. Rabe, *Angew. Chem. Int. Ed.* **2002**, *41*, 3681.
- [82] S. Stepanow, N. Lin, J. V. Barth, K. Kern, *J. Phys. Chem. B* **2006**, *110*, 23472.
- [83] S. Stepanow, M. Lingenfelder, A. Dmitriev, H. Spillmann, E. Delvigne, N. Lin, X. B. Deng, C. Z. Cai, J. V. Barth, K. Kern, *Nat. Mater.* **2004**, *3*, 229.
- [84] Y. Kikkawa, E. Koyama, S. Tsuzuki, K. Fujiwara, K. Miyake, H. Tokuhisa, M. Kanosato, *Chem. Commun.* **2007**, 1343.
- [85] G. R. Newkome, P. S. Wang, C. N. Moorefield, T. J. Cho, P. P. Mohapatra, S. N. Li, S. H. Hwang, O. Lukoyanova, L. Echegoyen, J. A. Palagallo, V. Iancu, S. W. Hla, *Science* **2006**, *312*, 1782.
- [86] P. Zell, F. Mogege, U. Ziener, B. Rieger, *Chem. Eur. J.* **2006**, *12*, 3847.

- [87] A. Ciesielski, L. Piot, P. Samorì, A. Jouaiti, M. W. Hosseini, *Adv. Mater.* **2009**, *21*, 1131.
- [88] M. M. S. Abdel-Mottaleb, N. Schuurmans, S. De Feyter, J. Van Esch, B. L. Feringa, F. C. De Schryver, *Chem. Commun.* **2002**, 1894.
- [89] J. R. Gong, L. J. Wan, Q. H. Yuan, C. L. Bai, H. Jude, P. J. Stang, *Proc. Natl. Acad. Sci. U.S.A.* **2005**, *102*, 971.
- [90] U. Ziener, J. M. Lehn, A. Mourran, M. Möller, *Chem. Eur. J.* **2002**, *8*, 951.
- [91] G. Pace, A. Stefankiewicz, J. Harrowfield, J. M. Lehn, P. Samorì, *Chemphyschem* **2009**, *10*, 699.
- [92] J. D. van der Waals, *Nobel Lecture* **1910**.
- [93] J. Israelachvili, *Intermolecular & Surface Forces*, Academic Press, London, **1992**.
- [94] H. Margenau, *Rev. Mod. Phys.* **1939**, 1.
- [95] A. J. Gellman, K. R. Paserba, *J. Phys. Chem. B* **2002**, *106*, 13231.
- [96] K. R. Paserba, A. J. Gellman, *J. Chem. Phys.* **2001**, *115*, 6737.
- [97] K. R. Paserba, A. J. Gellman, *Phys. Rev. Lett.* **2001**, *86*, 4338.
- [98] T. Muller, G. W. Flynn, A. T. Mathauser, A. V. Teplyakov, *Langmuir* **2003**, *19*, 2812.
- [99] S. Furukawa, K. Tahara, F. C. De Schryver, M. Van der Auweraer, Y. Tobe, S. De Feyter, *Angew. Chem. Int. Ed.* **2007**, *46*, 2831.
- [100] K. Tahara, S. Furukawa, H. Uji-I, T. Uchino, T. Ichikawa, J. Zhang, W. Mamdouh, M. Sonoda, F. C. De Schryver, S. De Feyter, Y. Tobe, *J. Am. Chem. Soc.* **2006**, *128*, 16613.
- [101] S. Lei, K. Tahara, X. Feng, S. Furukawa, F. C. De Schryver, K. Müllen, Y. Tobe, S. De Feyter, *J. Am. Chem. Soc.* **2008**, *130*, 7119.
- [102] S. D. Xu, Q. D. Zeng, J. Lu, C. Wang, L. J. Wan, C. L. Bai, *Surf. Sci.* **2003**, *538*, L451.
- [103] L. Smilowitz, N. S. Sariciftci, R. Wu, C. Gettinger, A. J. Heeger, F. Wudl, *Phys. Rev. B* **1993**, *47*, 13835.
- [104] G.-B. Pan, X.-H. Cheng, S. Hoyer, W. Freyland, *J. Am. Chem. Soc.* **2006**, *128*, 4218.
- [105] E. Mena-Osteritz, P. Bauerle, *Adv. Mater.* **2006**, *18*, 447.
- [106] D. Bleger, D. Kreher, F. Mathevet, A. J. Attias, I. Arfaoui, G. Metge, L. Douillard, C. Fiorini-Debuisschert, F. Charra, *Angew. Chem. Int. Ed.* **2008**, *47*, 8412.
- [107] E. Mena-Osteritz, *Adv. Mater.* **2002**, *14*, 609.
- [108] J. Krömer, I. Rios-Carreras, G. Fuhrmann, C. Musch, M. Wunderlin, T. Debaerdemaeker, E. Mena-Osteritz, P. Bauerle, *Angew. Chem. Int. Ed.* **2000**, *39*, 3481.

- [109] G. B. Pan, J. M. Liu, H. M. Zhang, L. J. Wan, Q. Y. Zheng, C. L. Bai, *Angew. Chem. Int. Ed.* **2003**, *42*, 2747.
- [110] G. B. Pan, L. J. Wan, Q. Y. Zheng, C. L. Bai, *Chem. Phys. Lett.* **2003**, *367*, 711.

Chapter 2

Scanning Tunneling Microscopy

Since nearly three decades surfaces and interfaces can be mapped with a sub-nanometer spatial resolution making use of Scanning Probe Microscopies. In this frame, the invention of Scanning Tunneling Microscopy (STM) in 1981^[1] and later Atomic Force Microscopy (AFM) in 1986^[2] boosted the scope to nanoscience and nanotechnology. These two techniques, especially STM, made it possible to visualize and manipulate single molecules, therefore study a variety of physico-chemical properties and processes of nanostructured materials. STM can operate under various environmental conditions including ultra-high vacuum (UHV),^[1, 3] gas stream, air and liquid, thus making it possible to investigate structure and reactivity in 2D with a single molecules resolution.^[4, 5] Over the past three decades, numerous examples of STM visualization of molecule and architectures thereof have been reported^[6-9] for various materials type including liquid crystals, conductive molecular crystals, proteins and self-assembled monolayers.

2.1 Introduction to STM

The main working principle of STM is based on the concept of quantum tunneling.^[10, 11] When a conducting tip is brought as close as possible to the substrate surface, a bias applied between the two can allow electrons to tunnel through the vacuum between them. The resulting tunneling current is a function of the tip position, applied voltage, and the local density of states (LDOS) of the sample. Information is acquired by monitoring the current as the tip's position scans across the surface. By scanning of a $N \times N$ pixel array and measuring the current in each individual point, an image is generated.

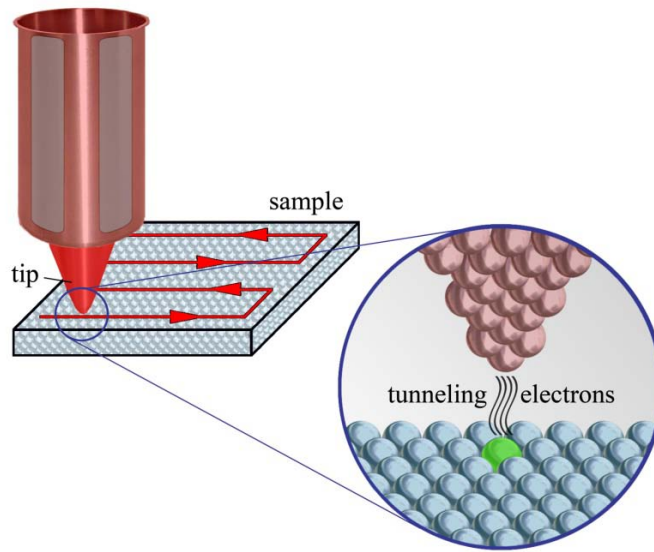


Figure 2.1 Schematic drawing of the STM probe scanning on a sample.

2.2 Working Principle of STM

When a sharp tip is positioned as a local probe above the surface and a voltage is applied, the tunneling of electrons results in a current, which exponentially decays with increasing the distance between the tip and the surface. A tunneling current appears when electrons move through a barrier which classically cannot be overcome (Fig. 2.2). The electrons have to be considered as quantum mechanical objects, possessing the wavelike properties besides their particle like properties. Electrons do not have end abruptly at a wall or barrier, but decay exponentially. If the barrier is thin enough, the probability function may extend through the barrier into the region beyond it and the electrons are thus able to tunnel through the barrier.

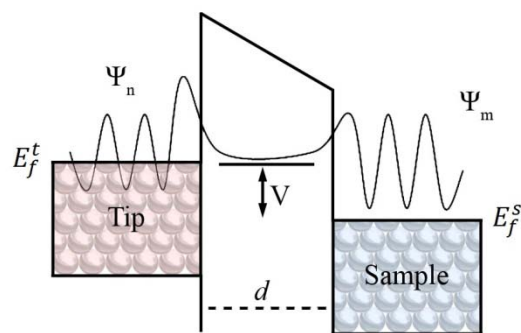


Figure 2.2 Scheme of the tunneling process. Electrons have a non zero probability to be found in the gap, therefore they can only tunnel through the barrier.

When the adsorbate is infinitely far from the substrate surface, its states consist of an occupied electronic molecular orbitals (HOMO state) as well as a series of unoccupied or virtual molecular orbitals (the LUMO state). The most important level on the solid substrate surface, from the standpoint of STM, is the Fermi level, at energy E_f .^[12-14] At zero Kelvin in the case of metals, all electronic states of the solid substrate with $E < E_f$ are fully occupied and those with $E > E_f$ are completely empty. Typically, in STM experiments of conductors performed in a UHV environment, tunneling takes place at energies very near E_f , so electrons are tunneling into substrate states of the surface just above E_f or tunneling out of states just below E_f . A notable modification of this phenomena occurs in the presence of nonconducting physisorbed molecules, especially when studied in ambient air conditions and at the solid-liquid interface, where successful imaging is almost always observed at relatively large bias voltages (typically 0.4–4 V). Thus, the tunneling process in the presence of adsorbates actually can take place over a fairly sizable energy, the “conduction region,” ranging from a few tenths of a volt to a few volts above or below E_f (Fig. 2.3).

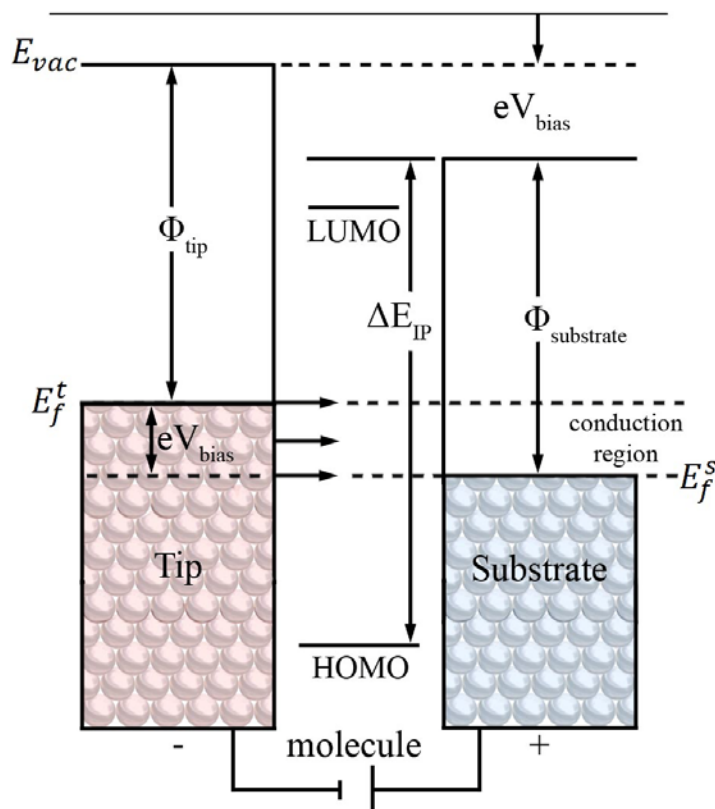


Figure 2.3 Energy level diagram depicting the placement of the HOMO and LUMO levels of a molecular adsorbate relative to the Fermi levels of the substrate (E_f^s) and the tip (E_f^t). Also indicated are the work functions of the substrate ($\Phi_{substrate}$) and the tip (Φ_{tip}). Upon application of a bias to the tip (eV_{bias}), the Fermi level of the tip shifts relative to that of the substrate, giving rise to the “conduction region.”^[12]

When an atom or molecule is weakly physisorbed on the surface, a shift occurs in the energies of both HOMO and LUMO orbitals of the atom or molecule as well as remarkable shift in the energies of the substrate surface. Unfortunately, it is almost impossible to accurately define the energy difference between the substrate surface states and adsorbate states. However, by assuming that the vacuum level of the surface is above the Fermi level by Φ , the work function of the surface, while the energy of the vacuum level of the adsorbate is above its HOMO by IP, the ionization potential of the molecule and the relative spacing between the adsorbate HOMO, LUMO, and vacuum levels is unaffected by adsorption on the surface, the HOMO and LUMO levels of the adsorbate can be located relative to the surface Fermi level.

Different theoretical models with different levels of complexity have been proposed to describe the STM measurements. The quantum mechanical tunneling is based on the wavelike nature of electrons. This property result in a finite probability for electrons to cross a potential barrier V_0 , which is higher than kinetic energy E . For a rectangular barrier, the barrier transmission coefficient T is exponentially dependent on z and the square root of the effective barrier height $(V_0 - E)$.

$$T \propto e^{-2kz} \quad \text{with} \quad k = \frac{[2m(V_0 - E)]^{\frac{1}{2}}}{\hbar} \quad (2.1)$$

Tersoff and Hamman^[11] predict that tunneling current can be expressed as a simple function of the density of states of the tip $\rho_t(E_f)$ and of the Fermi level density of states of the sample $\rho_t(r_0, E_f)$, measured at the position corresponding to the center of curvature of the tip:

$$I \sim V \cdot \rho_t(E_f) \cdot \rho_t(r_0, E_f) \quad (2.2)$$

Therefore, under idealized conditions, the STM image reflects the sample electronic structure. A more realistic quantitative interpretation can be predicted by using the Wentzel-Kramers-Brillouin (WKB) approximation which takes into account that most of the experiments are performed at bias voltages between 1 and 4 V. This method is named after physicists Wentzel, Kramers, and Brillouin, who all developed it in 1926. The WKB theory predicts that the tunneling current is given by:

$$I = \int_0^{eV} \rho_s \cdot \rho_t \cdot T(E, eV) dE \quad (2.3)$$

Where ρ_s and ρ_t are the density of states of the sample and the tip measured with respect to their individual Fermi levels. It is important to point out, that for negative sample bias, $eV < 0$, and for positive bias $eV > 0$. The tunneling transmission probability $T(E, eV, r)$ for electrons with energy E and applied bias voltage V might be also given by

$$T(E, eV) = e^{-\left(\frac{2Z\sqrt{2m}}{\hbar} \sqrt{\frac{\Phi_s + \Phi_t}{2} + \frac{eV}{2} - E}\right)} \quad (2.4)$$

where Z is a distance from sample to tip, and Φ are work functions. At constant tunneling current I , the contour followed by the tip is a function of the density of states of both sample and a tip, together with the tunneling transmission probability.

2.3 Set-Up of Scanning Tunneling Microscope

The tunneling current flowing between the tip and the sample is exponentially dependent on the distance between the two electrodes. In other words, for a given voltage the closer is the tip to the surface the highest is the measured current. The distance between the tip and the sample must typically be held within 0.01 \AA to atomically resolve a metallic or any other conductive surface with STM. Hence it is mandatory to work in a compact and rigid design and to isolate the system from external vibrations, which is technically realized by a damping stage.^[15, 16] Vibrations can be caused by the building itself (15-20 Hz), walking of people (1-4 Hz), vacuum pumps in case of the STM operating in UHV conditions and other apparatus as well as sounds. Silent STM lab – no one walks or speaks, no air-condition – is the best for the imaging process.

While imaging with STM, the scan through the z (vertical), x and y (horizontal) distances is ensured by a piezoelectric element (piezo tube in Fig.2.4). High voltage is applied to the piezo to drive the x and y movements while the z direction is controlled by a feedback loop which compares I to a given current set-point value for each position (x, y) and applies an appropriate voltage to the z -piezo which approaches or retracts the tip in order to keep I constant (case of constant current mode).

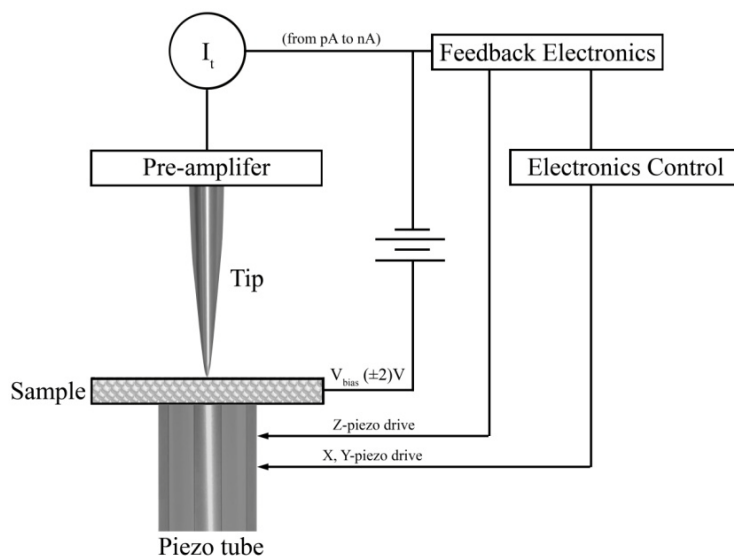


Figure 2.4 Schematic representation of STM set-up.

2.4 Operation Modes of STM

The STM can be operated in either constant current or constant height mode, as shown in Figure 2.5. In the constant current mode of operation, the tip is moving across the surface at pre-set tunneling current, which is maintained at a pre-set value by continuously adjusting the vertical position of the tip with the feedback voltage V_z . In the case, of electronically homogeneous surface, the “topographic” height of the surface features of a sample can be visualized. It is very important to stress the following point: STM does not provide topographic information of adsorbed molecules in a straightforward manner. The broadening of an adsorbate level located far away from E_f results in an extended tail of this resonance which contributes to LDOS. The constant current mode was first the originally employed one, and can be used to track surfaces that are not atomically flat. The height of the surface features might be driven from V_z and the sensitivity of the piezoelectric driver element.

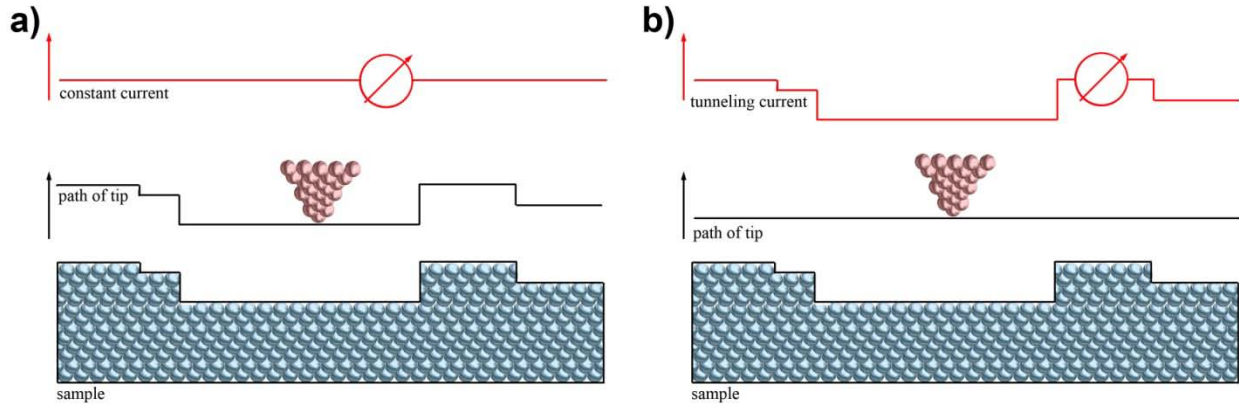


Figure 2.5 (a) constant current imaging mode for obtaining a “topographic” image; (b) constant height imaging mode for measuring current images.

Alternatively, in the constant height mode the tip can scan the sample across the surface at nearly constant height and constant voltage V_z , while the tunneling current is monitored. In this case, the electronic feedback is slowed down to keep the average tunneling current constant. The exponential variations in the tunneling current due to the tip passing over surface features are recorded and plotted as a function of scan position. The constant height mode allows for much faster imaging of atomically flat surfaces compared with the constant current mode, since the feedback loop and piezoelectric driver don't have to re-pinned to the surface features passing under the tip.

2.5 STM Tips

STM tips can be made of e.g. platinum-iridium (Pt/Ir), *tungsten* (W), titanium carbide, gold, silver, etc. A simple preparation method is to cut a thin wire (0.1 mm to 0.3 mm) of the desired material by a cutter or by scissors. Manual cutting of wires is fast, but the success rate for working tips is not too high. Moreover, the shape of the tips is not well defined, making it harder to use them on strongly corrugated samples. The material suited best for this method seems to be Pt/Ir wires. Pt/Ir tips with a very steep geometry can be obtained also by electrochemical etching. Electro-chemically etched tips display characteristics of greater sharpness and of uniformity. They do this more reliably than do tips that have been cut manually. The one big disadvantage with etching techniques similar to this is that the tip is covered with a thin layer of oxide. If this

layer is not removed, tunneling conditions will be unstable and a proper scan simply not possible. The oxide layer can sometimes be removed by performing a controlled tip crash into the sample surface. However such action can greatly affect tip sharpness, and for certain types of sample, any particles picked up from the surface will have undesirable effects.

Tungsten has a step-like density of states with no features and therefore is expected to have the least influence on the tunneling process. However, *tungsten* oxidizes in air quite fast, leading to reduced conductance. For reproducible results, the oxide layer needs to be removed by special treatments in vacuum, i.e. heating, Ar ion sputtering, field emission, electron bombardment or HF bathing. STM tips operated in electrochemistry environments have to be coated with wax or with a solvent resistant polymers, e.g. epoxy, leaving the tip apex uncoated.

Tips used for STM measurements need to be very sharp, the tip radius of curvatures is usually few tens of nm. Nearly 100% of the current in the tunneling junction is transported via tip apex (Fig. 2.6a) allowing the achievement of lateral resolution of ca. 1Å.

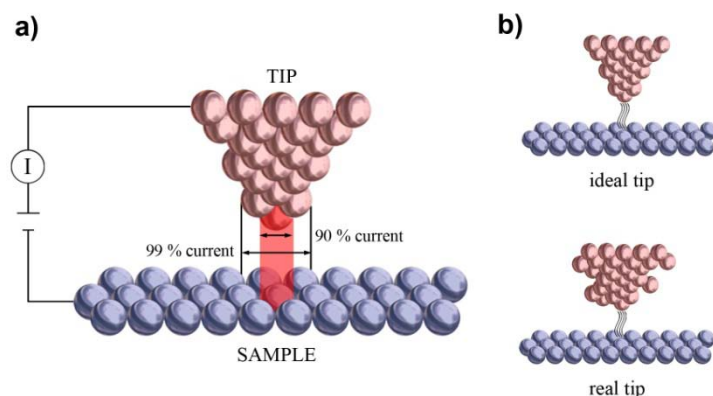


Figure 2.6 (a) Schematic representation of the STM junction current flow; (b) schematic representation of ideal tip and the real one used for STM measurements.

2.6 Concentration of investigated solutions

In most of the studies performed at the solid-liquid interface the STM tip is immersed in an almost saturated solution. However, control over the concentration of investigated solutions is a powerful and general approach for structural selection, also in those cases where multiple patterns may coexist. De Feyter and co-workers^[17] reported STM measurements of a series of alkyl- and alkoxy-substituted rhombic-shaped bis(dehydrobenzo[12]annulene (bisDBA)

derivatives at the 1,2,4-trichlorobenzene (TCB)/graphite interface. By changing the alkyl-chain length and controlling the solute concentrations, bisDBAs were observed to form five structures (Fig. 2.7), three porous structures (porous A, B, and C), and two nonporous structures (nonporous D and E). Interestingly, upon diluting, the nonporous structures were observed to transform into porous structures. Under dilute conditions, partial formation of the Kagome' motif was observed for all compounds.

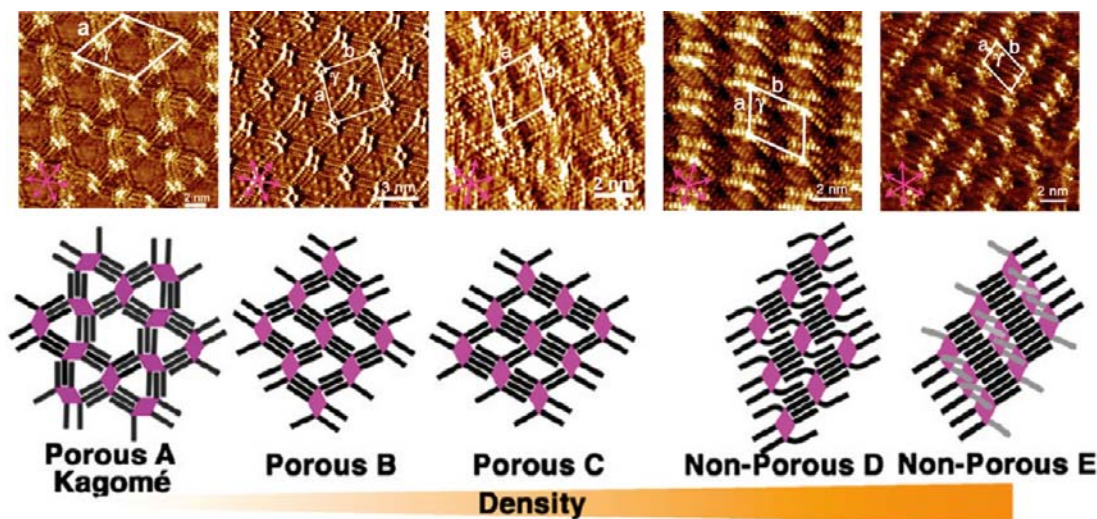


Figure 2.7 Overview of the five structures formed by the bisDBA derivatives: porous A (Kagome), porous B, porous C, nonporous D, and nonporous E.^[17]

The controlled formation of ordered multicomponent architectures at the solid–liquid interface from a concentrated solution is thermodynamically unfavored. In fact, among the various components in the supernatant solution, the component with a greater affinity for the substrate, that is, offering a minimization of the free interface energy per unit area, will assemble on its surface, whereas the others will remain in solution.^[18] To immobilize all the components on the surface, thus to achieve a complete physisorption of all the components at the solid–liquid interface, it is necessary to have a full control over the stoichiometry of the molecules absorbed at surfaces.^[19] At the solid–liquid interface, the number of molecules in the solution applied to the surface should be lower than that required to form a monolayer of physisorbed molecules lying flat on the basal plane of the substrate. However, operating under such conditions, that is, at low concentration, can lead to polymorphism.^[20, 21] Recently a few efforts have been

successful in obtaining uniform monolayers of nanostructures from multiple components leading to well defined patterns different from those of the individual components.^[21, 22]

Phase diagram of bi-component system (Fig. 2.8) was probed at the solid-liquid interface by means of STM by Lackinger and co-workers.^[21] Depending on the concentration of the two solutes, trimesic acid (TMA) and 1,3,5-benzenetribenzoic acid (BTP), six different H-bonded monolayer structures were observed, three of those being mixed TMA+BTP phases. Although both species were always present in solution, the different molecular arrangements on the surface range from pure TMA networks to different hexagonal and rectangular mixed networks (containing BTB and TMA) to arrangements built up from just BTB molecules. Interestingly, in-situ dilution of the samples with pure solvent initiated phase transitions as anticipated from and consistent with the phase diagram, thereby proving that the growth of these mixed networks is thermodynamically controlled.

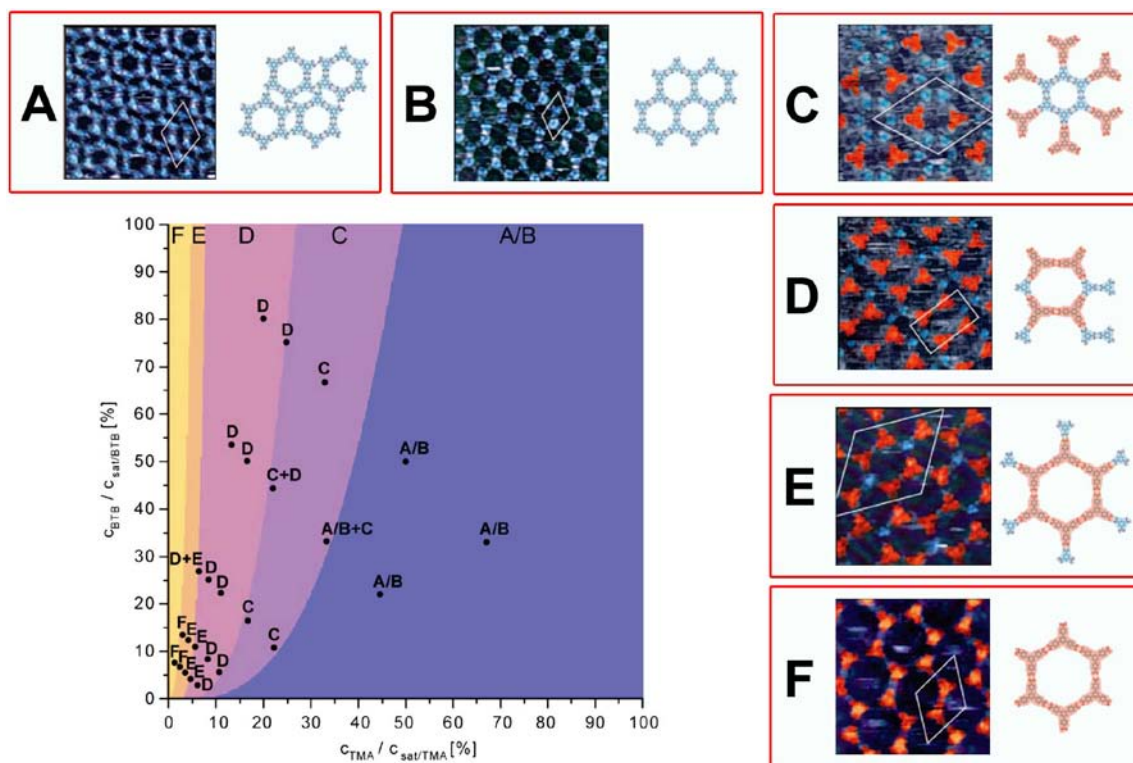


Figure 2.8 Phase diagram of the bimolecular system TMA + BTP in heptanoic acid, and corresponding self-assembled structures of TMA and BTP.

References

- [1] G. Binnig, H. Rohrer, C. Gerber, E. Weibel, *Phys. Rev. Lett.* **1982**, *49*, 57.
- [2] G. Binnig, C. F. Quate, C. Gerber, *Phys. Rev. Lett.* **1986**, *56*, 930.
- [3] H. Rohrer, *PNAS* **1987**, *84*, 4666.
- [4] W. A. Hofer, A. S. Foster, A. L. Shluger, *Reviews of Modern Physics* **2003**, *75*, 1287.
- [5] W. A. Hofer, *Progress in Surface Science* **2003**, *71*, 147.
- [6] S. De Feyter, F. C. De Schryver, *Chem. Soc. Rev.* **2003**, *32*, 139.
- [7] P. Samorì, (ed). *Scanning Probe Microscopy beyond Imaging.*; Wiley-VCH, New York **2006**.
- [8] J. A. Theobald, N. S. Oxtoby, M. A. Phillips, N. R. Champness, P. H. Beton, *Nature* **2003**, *424*, 1029.
- [9] D. F. Perepichka, F. Rosei, *Science* **2009**, *323*, 216.
- [10] J. Tersoff, D. R. Hamann, *Phys. Rev. B* **1985**, *31*, 805.
- [11] J. Tersoff, D. R. Hamann, *Phys. Rev. Lett.* **1983**, *50*, 1998.
- [12] L. C. Giancarlo, G. W. Flynn, *Annu. Rev. Phys. Chem.* **1998**, *49*, 297.
- [13] P. K. Hansma, J. Tersoff, *J. Appl. Phys.* **1987**, *61*, R1.
- [14] N. D. Lang, *Phys. Rev. Lett.* **1985**, *55*, 230.
- [15] J. H. Ferris, J. G. Kushmerick, J. A. Johnson, M. G. Y. Youngquist, R. B. Kessinger, H. F. Kingsbury, P. S. Weiss, *Rev. Sci. Instrum.* **1998**, *69*, 2691.
- [16] S. I. Park, C. F. Quate, *Rev. Sci. Instrum.* **1987**, *58*, 2004.
- [17] K. Tahara, S. Okuhata, J. Adisoejoso, S. B. Lei, T. Fujita, S. De Feyter, Y. Tobe, *J. Am. Chem. Soc.* **2009**, *131*, 17583.
- [18] C. A. Palma, M. Bonini, T. Breiner, P. Samorì, *Adv. Mater.* **2009**, *21*, 1383.
- [19] C. A. Palma, M. Bonini, A. Llanes-Pallas, T. Breiner, M. Prato, D. Bonifazi, P. Samorì, *Chem. Commun.* **2008**, 5289.
- [20] S. B. Lei, K. Tahara, F. C. De Schryver, M. Van der Auweraer, Y. Tobe, S. De Feyter, *Angew. Chem. Int. Ed.* **2008**, *47*, 2964.
- [21] L. Kampschulte, T. L. Werblowsky, R. S. K. Kishore, M. Schmittel, W. M. Heckl, M. Lackinger, *J. Am. Chem. Soc.* **2008**, *130*, 8502.
- [22] S. De Feyter, A. Miura, S. Yao, Z. Chen, F. Wurthner, P. Jonkheijm, A. P. H. J. Schenning, E. W. Meijer, F. C. De Schryver, *Nano Lett.* **2005**, *5*, 77.

Chapter 3

Methods

3.1 STM at the solid-liquid interface

Currently there are several different set-ups in order to study adsorbed molecules on conductive substrates with STM: under ultra high vacuum (UHV), under atmospheric conditions at room temperature by imaging the dry films, at the solid-liquid interface or set-ups which provide electrochemical control of investigated materials. The organic solid-liquid interface provides a particularly interesting environment to carry out the self-assembly experiments and their investigation by scanning tunneling microscopy.^[1] Compared to sample preparation and imaging under UHV conditions, the solid-liquid interface has a number of advantages: 1) the experimental approach is straightforward and does not require a complicated or as expensive infrastructure; 2) the dynamic exchange of molecules adsorbed on the surface and the one in the liquid phase promotes self-healing of defects in the self-assembled layers;^[2, 3] 3) solid-liquid interface provides an excellent environment for *in-situ* chemical modifications of adsorbed molecules. Working under such condition it is possible to trace the changes in the monolayers structure, upon addition of external chemical stimuli, e.g. acidification^[4] or coordination of organic molecules to the metallic centers.^[4, 5]

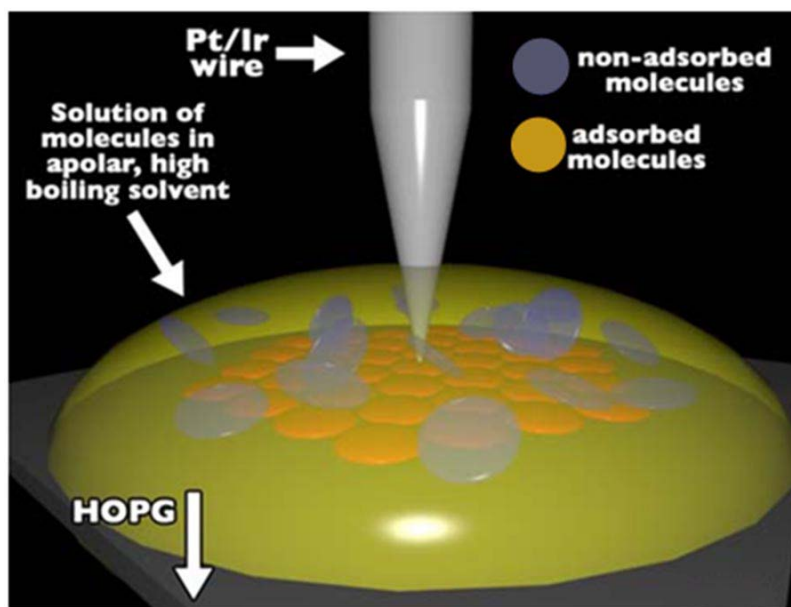


Figure 3.1 Scheme of the STM operating at the solid-liquid interface.

Due to its many advantages, STM at the solid-liquid interface has provided detailed insight into the molecule-substrate and molecule-molecule interactions (e.g. hydrogen bonding, metal complexation or weak van der Waals forces) responsible for the ordering of molecules on the atomically flat surface. In most of the studies performed at the solid-liquid interface the STM tip is immersed in an almost saturated solution in a poorly volatile and apolar solvent.

3.2 Substrate

In order to obtain good resolution during STM imaging, substrates featuring an atomic flatness over several hundred squared nanometers area are required. A typical conductive substrate used for STM investigations is Highly Oriented Pyrolytic Graphite (HOPG) (Fig. 3.2) which is a layered substrate that can be freshly prepared by simple cleaving its surface with an adhesive tape. There are two most important features in the structure and electronic properties of graphite: a 2D layered structure and an amphoteric feature. The basic unit of graphite, i.e. graphene is an extreme state of condensate aromatic hydrocarbons with an infinite in plane-dimension, in which an infinite number of benzene hexagon rings are condensed to form a 2D extended electronic

structure. The trigonal bonding in each graphene sheet involves overlap of carbon sp^2 hybridized orbital in plane, whereas the overlap of carbon p_z orbitals produces delocalized rings of π electrons lying above and below each benzene ring, which makes graphite a good electrical conductor. Graphite thus features a 2D system from both structural and electronic aspect. The stacking of graphene sheets gives graphite (Fig. 3.2), in which the weak intersheet interaction modifies the electronic structure into a semi-metallic one having a quasi-2D nature, as shown in Figure 3.2b. The graphene layers are bonded to each other by weak van der Waals forces, and what is important, they can easily slide over one another, which results in softness and slipperiness of graphite. The amphoteric properties of graphite arise from the fact that graphite can act either as an oxidizer or a reducer in chemical reactions. This characteristic stems from the zero-gap semiconductor type or semi-metallic electronic structure, in which the ionization potential and the electron affinity have the same value of 4.6 eV.^[6-8]

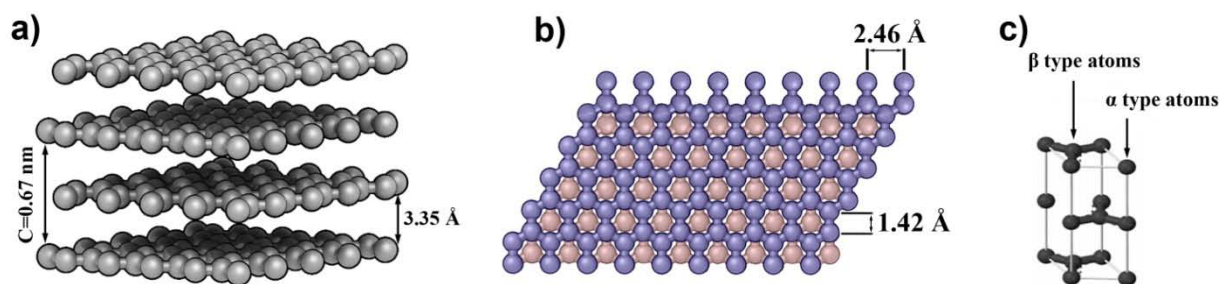


Figure 3.2 X-Ray structure of Highly Oriented Pyrolytic Graphite (HOPG) (a- c) Over-layered graphene sheets; b) α and β atoms type, α type atoms are supposed to be the only atoms visible in STM images of graphite surfaces.

Figure 3.3 displays an STM current images of HOPG with atomic resolution. A periodic hexagonal pattern with lateral spacing of 0.246 nm can be observed on both images. The lateral spacing between carbon atoms in the hexagonally structured graphene sheet however amounts to 0.142 nm only. Thus in the STM images only every second carbon atom or the center of the hexagons in the graphene sheet are effectively resolved. This has been explained by the nonequivalence of the carbon atoms in a graphene layer with respect to their spatial position above the underlying graphene sheet due to the stacking in graphite (see α and β type atoms in

Fig. 3.2c). Alternatively it was suggested that the tunneling probability in the center of the hexagons of the graphene sheets is largest and therefore giving rise to a larger tunneling current.

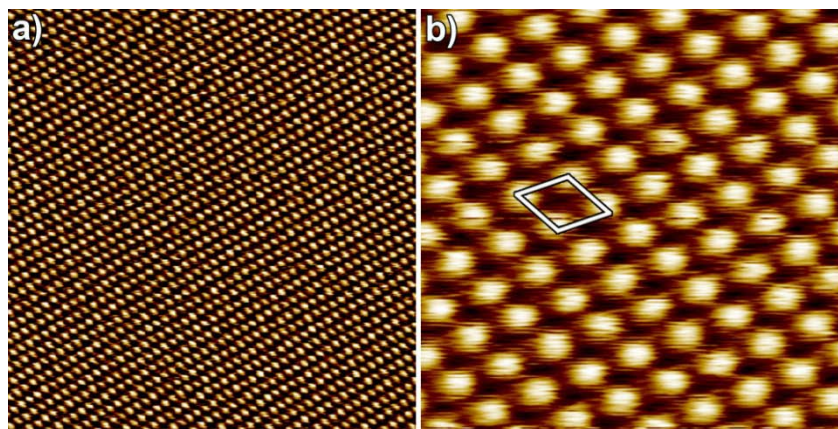


Figure 3.3 STM current images of HOPG (a) 10×10 nm and (b) 3×3 nm. The unit cell is also shown: $a=0.246$ nm. The image has been corrected for thermal drift with SPIP software. ($I_t=65$ pA; $V_t=20$ mV).

Highly oriented pyrolytic graphite (HOPG) is commonly used as solid substrate for STM imaging at the solid-liquid interface, because of its conductive nature and its easy preparation by cleavage to prepare a fresh conductive surface. This flat surface is neutral, hydrophobic and inert to organic solvents. Therefore it should be ideal for the self-assembly of either neutral or ionic adsorbates, since electrostatic interactions can be neglected.

3.3 Solvent

The effect of solvent on the formation of 2D supramolecular architectures at the solid-liquid interface, has been investigated by means of STM by many groups in the past two decades.^[9-17]

The organic solvents used for performance of STM measurements at the solid-liquid interface need to comply with following criteria:

- i) they need to have a low vapor pressure allowing the performance of STM measurements in only a drop of liquid (ca. 5-20 μ L), without the need of use a closed cell,
- ii) they need to be electrochemically inert under experimental conditions,

iii) they should solubilize investigated compounds,

iiii) they should possess the low affinity for adsorption on the substrate used.

Most commonly used solvents have been listed in Table 3.1.

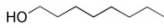


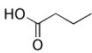
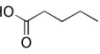
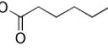
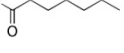
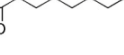

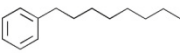
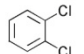
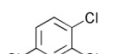
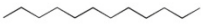
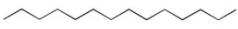
no.	chemical formula	chemical name	chemical structure	functional group	b.p.	ϵ
1	$C_8H_{18}O$	1-octanol		R-OH	195.16	10.30
2	$C_9H_{20}O$	1-nonanol		R-OH	213.37	8.83
3	$C_{10}H_{22}O$	1-decanol		R-OH	231.11	7.93
4	$C_4H_8O_2$	butanoic acid		R-COOH	163.75	2.98
5	$C_5H_{10}O_2$	pentanoic acid		R-COOH	186.12	2.66
6	$C_6H_{12}O_2$	hexanoic acid		R-COOH	205.21	2.61
7	$C_7H_{14}O_2$	heptanoic acid		R-COOH	222.23	3.04
8	$C_8H_{16}O_2$	octanoic acid		R-COOH	239.23	2.85
9	$C_9H_{18}O_2$	nonanoic acid		R-COOH	254.32	2.47
10	$C_{14}H_{22}$	1-phenyloctane		R-(aromatic)	224.61	2.26
11	$C_6H_4Cl_2$	1,2-dichlorobenzene		Cl-(aromatic)	180.03	10.12
12	$C_6H_3Cl_3$	1,2,4-trichlorobenzene (TCB)		Cl-(aromatic)	213.45	2.24
13	$C_{10}H_{22}$	dodecane		R	216.32	2.01
14	$C_{14}H_{30}$	tetradecane		R	253.24	2.03

Table 3.1 List of the solvents commonly used for STM experiments at the solid-liquid interface. Dielectric constant ϵ at ambient temperature (10-30 °C) and boiling point (*b.p.*) temperatures(°C).^[18]

All these solvents are available from Aldrich Chemicals. In this work STM images have been recorded by using 1-phenyloctane, tetradecane or 1,2,4-trichlorobenzene (TCB) as a solvent. The

high boiling temperature and low the dielectric constant of these solvents allowed to measure for several hours having the STM tip immersed in the solution.

References

- [1] J. P. Rabe, S. Buchholz, *Science* **1991**, 253, 424.
- [2] S. Burattini, H. M. Colquhoun, B. W. Greenland, W. Hayes, *Faraday Discuss.* **2009**, 143, 251.
- [3] L. C. Giancarlo, G. W. Flynn, *Annu. Rev. Phys. Chem.* **1998**, 49, 297.
- [4] L. Piot, R. M. Meudtner, T. El Malah, S. Hecht, P. Samorì, *Chem. Eur. J.* **2009**, 15, 4788.
- [5] A. Ciesielski, S. Lena, S. Masiero, G. P. Spada, P. Samorì, *Angew. Chem. Int. Ed.* **2010**, 49, 1963.
- [6] B. T. Kelly, *Applied Surface Publisher, London* **1981**.
- [7] W. T. Pong, J. Bendall, C. Durkan, *Jpn. J. Appl. Phys., Part 1* **2005**, 44, 5443.
- [8] W. T. Pong, C. Durkan, *Jpn. J. Appl. Phys., Part 1* **2005**, 44, 5365.
- [9] W. Mamdouh, H. Uji-i, J. S. Ladislaw, A. E. Dulcey, V. Percec, F. C. De Schryver, S. De Feyter, *J. Am. Chem. Soc.* **2006**, 128, 317.
- [10] L. Kampschulte, M. Lackinger, A. K. Maier, R. S. K. Kishore, S. Griessl, M. Schmittel, W. M. Heckl, *J. Phys. Chem. B* **2006**, 110, 10829.
- [11] M. Lackinger, S. Griessl, W. A. Heckl, M. Hietschold, G. W. Flynn, *Langmuir* **2005**, 21, 4984.
- [12] B. Venkataraman, J. J. Breen, G. W. Flynn, *J. Phys. Chem.* **1995**, 99, 6608.
- [13] M. Lackinger, S. Griessl, T. Markert, F. Jamitzky, W. M. Heckl, *J. Phys. Chem. B* **2004**, 108, 13652.
- [14] K. G. Nath, O. Ivasenko, J. A. Miwa, H. Dang, J. D. Wuest, A. Nanci, D. F. Perepichka, F. Rosei, *J. Am. Chem. Soc.* **2006**, 128, 4212.
- [15] J. M. MacLeod, O. Ivasenko, D. F. Perepichka, F. Rosei, *Nanotechnology* **2007**, 18.
- [16] P. Vanoppen, P. C. M. Grim, M. Rucker, S. De Feyter, G. Moessner, S. Valiyaveetil, K. Mullen, F. C. De Schryver, *J. Phys. Chem.* **1996**, 100, 19636.
- [17] C. J. Li, Q. D. Zeng, C. Wang, L. J. Wan, S. L. Xu, C. R. Wang, C. L. Bai, *J. Phys. Chem. B* **2003**, 107, 747.

[18] *Handbook of Chemistry and Physics*, 87 ed., CRC Press **2007**.

Chapter 4

1D coordination networks at the solid-liquid interface

The nanoscale control over both the geometry and the directionality of supramolecular arrays composed of 1-D coordination networks can be achieved on surface through the design and combination of organic tectons, i.e. building blocks, with metal centers or metal complexes. In this chapter we report on an STM study of combinations of a rigid and flat coordinating tecton bearing both a monodentate and a tridentate coordination poles with either Co^{II} as its chloride complex or Pd^{II} cation in the presence of BF_4^- counter-anions. These combinations lead to the formation of coordination networks which generate long and shape persistent arrays at the graphite – solution interface. Through a subtle modification of the organic tecton consisting in changing the position of nitrogen atom on the pyridine ring from *para* (linear tecton) to *meta* (bent tecton) position, it was possible to modify the geometry of 1-D coordination networks from a linear to *zig-zag* respectively. Furthermore, whereas the linear tecton leads to a centrosymmetric packing of the directional networks on the surface as also observed in the crystalline phase, for the bent tecton, polar arrangements resulting from the *syn*-parallel packing of the consecutive *zig-zag* networks was observed.

All the molecules described in this chapter were synthesized by Dr. Abdelaziz Jouaiti, in the Laboratoire de Chimie de Coordination Organique of Prof. Mir Wais Hosseini, in Strasbourg (France).

4.1 Introduction

The control of molecular organization is of prime importance for exploring collective properties at the nanoscale. Although a large number of studies deals with molecular assemblies in the solid crystalline phase, since a few years different research groups became interested in the design and generation of 2D patterns on surfaces. Such architectures may be observed by exploring random distributions of molecular units bearing no specific interaction sites on the surface or can be constructed using the molecular tectonics approach^[1] in 2 dimensions. The latter approach is a strategy based on the use of active complementary building blocks or tectons incorporating in their structures specific interaction sites and thus capable of self-assembly into extended 1-, 2- or 3D periodic architectures called molecular networks. This approach is general and may be applied to any type of recognition events, in particular recognition processes based on the formation of reversible coordination bonds between organic tectons and metal centres.^[2] Supramolecular architectures combining organic moieties with transition-metal atoms have been widely studied during the last decades. The interest in such assemblies arises from both their robustness and electronic features leading to the development of applications in numerous research fields.^[1-4] For example, monomolecular transistors based on terpyridine-cobalt-terpyridine complexes^[5] as well as dynamic chemical devices undergoing reversible extension/contraction through a pH-triggered complexation of Pb ions^[6] have been reported. Recently, the use of self-assembly processes to generate hybrid molecular arrays with predefined structures on surfaces has been explored by combining metal centres and organic units.^[7] Whereas for crystalline materials, X-ray diffraction techniques, in particular X-ray diffraction on single crystal, are methods of choice, for 2D organisation on surfaces, the scanning tunneling microscopy (STM) has proven to be a powerful technique for the structural characterization of the resulting low dimensional supramolecular systems at the single molecule level.^[8-11] This observation technique has been used to explore various self-assembled systems such as metal-organic 2D coordination networks,^[12-14] discrete complexes on surfaces^[15-20] or more recently 1D coordination networks based on tectons bridging two coordination poles with different denticities.^[21]

In this contribution, we address both the control of geometrical aspects of formation of molecular arrays on surface through the design of the organic tecton and the observation of polar

arrangement of directional 1D hybrid coordination networks with a sub-nanometer resolution at solid-liquid interface by means of scanning tunneling microscopy.

Let us restrict the discussion to 1D single stranded coordination networks (hybrid architectures composed of organic and metallic tectons mutually bridging each other through reversible recognition processes and possessing translational symmetry in one direction of space). For the patterning of surface using this type of assembly, one needs to analyse the intrinsic geometry of the network imposed by the tectons (linear, *zig-zag* or helical) and the packing of consecutive networks on the surface governed both by the lateral network-network and vertical network-surface interactions. Furthermore, for 1D networks, depending on the features of the organic and metallic tectons, either non-directional (centric) or directional (non centric) assemblies may be formed. For crystals composed coordination networks, the vast majority of the cases reported concerns non-directional networks.^[2] However, the design and formation of directional networks is challenging and of interest for exploiting vectorial physical properties. In order to impose the directionality, one must avoid the presence of centres of symmetry. This may be achieved by combining a non centrosymmetric organic tecton of the linear (Tl) or the bent (Tb) type bearing at its extremities one monodentate and one tridentate coordinating poles with metal centres or complexes offering four free coordination sites located in the corners of a square (Fig. 4.1).^[11] The formation of arrays on the surface results from the packing of directional networks. Indeed, the *syn*-parallel packing (Fig. 4.1a and 4.1c) leads to polar domains whereas the *anti*-parallel arrangement generates apolar assemblies (Fig. 4.1b and 4.1d).

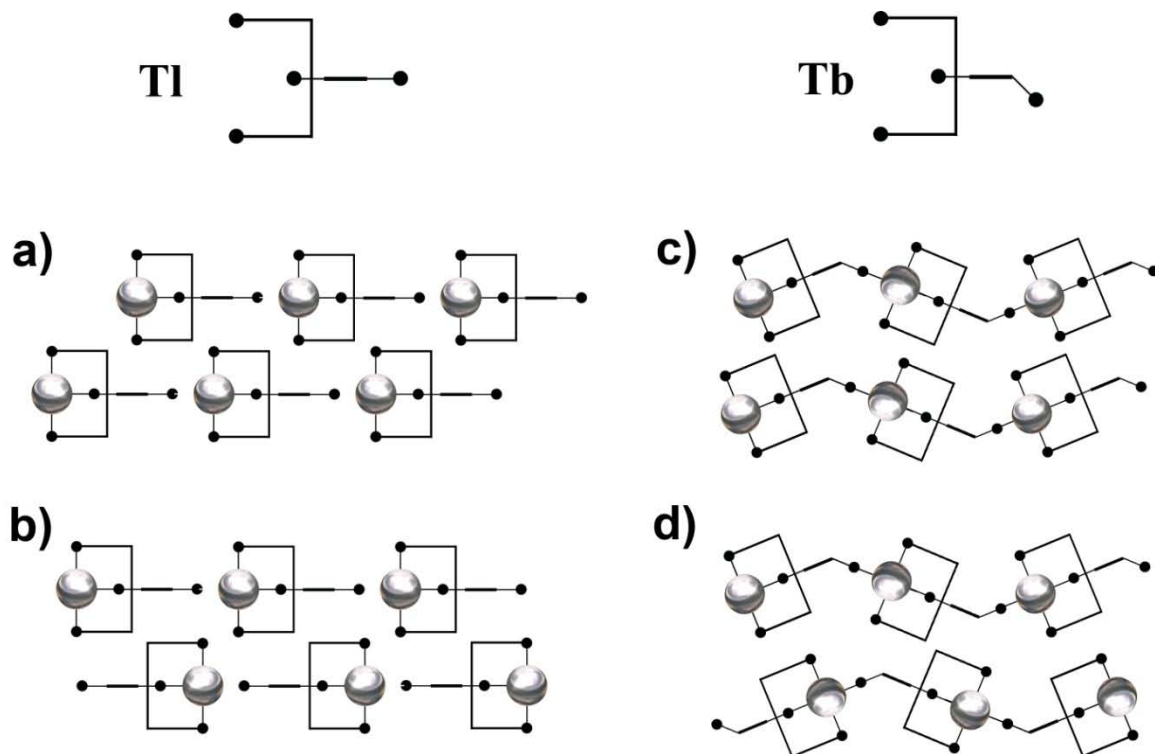


Figure 4.1 Schematic representation of a linear (Tl) and bent (Tb) tectons composed of a monodentate and a tridentate coordinating poles. Their combinations with metal centres offering four free coordination sites occupying the corners of a square leads to the formation of 1D directional coordination networks. Their *syn*-parallel (a and c) or *anti*-parallel (b and d) packing leads to the formation of polar and apolar arrangements respectively.

The design of tectons **1** and **2** was based on an anthracene core bearing two ethynyl groups equipped with a monodentate (pyridine) and a tridentate (terpyridine) poles. Owing to its flat shape and aromatic nature, the electrically/optically active anthracene group was used as a spacer in order to increase the interactions with the graphite surface. The two ethynyl groups behaving as connectors between the anthracene moiety and the two coordination poles were used for maintaining the planarity of the tecton. The two tectons **1** and **2** differ only by the position of the nitrogen atom on the pyridine ring. Indeed, whereas for **1**, the localization of the N atom at the *para* position leads to a linear tecton (Tl, see Fig. 4.1), for the tecton **2**, the positioning of the N atom at the *meta* position affords a bent tecton (Tb, see Fig. 4.1).

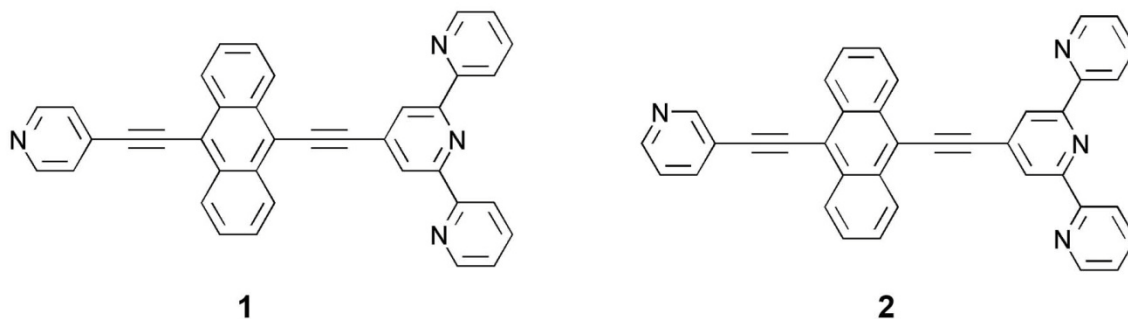


Figure 4.2 Chemical structures of compounds **1** and **2**.

It is worth noting that the combination of neutral tectons such as **1** and **2** with metal cations leads to the formation of 1D directional polycationic coordination networks. The charge balance imposes the presence of anions. When using weakly coordinating anions, the latter usually occupy the empty space between 1D networks and often do not interact with the cationic part of the assembly. For the design principle presented above, the formation of 1D directional coordination networks requires metal centers offering four free coordination sites. This was studied using Pd(II) cations associated with the weakly coordinating BF_4^- anions. A further possibility consisting in combining two coordinating anions such as chloride with a dicationic metal center adopting the octahedral coordination geometry such as Co(II) was also explored. Indeed, in this case the chloride anions occupy the two apical positions leaving thus the square base of the octahedron free for the formation of the network through four M-N coordination bonds.

Recently, in a collaboration with Prof. Hosseini, we have demonstrated, the controlled formation of linear coordination supra-polymers at the solid-liquid interface. The metallo-organic framework were formed by using tecton **1** and palladium(II) or cobalt(II) ions as metal centers. 1D supramolecular arrays were obtained only when using Pd^{II} (Fig.4.3a), whereas 2D arrays were observed when $\text{CoCl}_2 \times \text{H}_2\text{O}$ salt was added (Fig.4.3b). In this chapter will demonstrate, how the small difference between the position of the nitrogen atom in the pyridine ring, can lead to great changes in molecular packing at the solid-liquid interface.

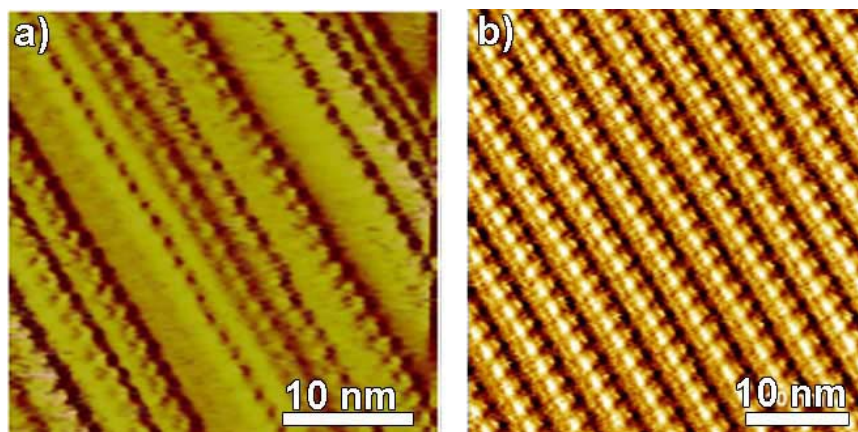


Figure 4.3 STM images of the network generated upon combining tecton **1** with a) CoCl_2 and b) Pd^{II} . Image (a) shows the formation of laterally uncorrelated 1D nanostructures, while (b) displays the parallel packing of 1D networks that leads to the generation of a 2D nanoscale array. a) $V_t=705$ mV; $I_t=13$ pA; b) $V_t=983$ mV; $I_t=13.6$ pA.^[21]

4.2 Results and discussion

The packing of the free tecton **2** on graphite surface was studied by STM by applying a drop of a highly concentrated solution of the neutral tecton **2** in 1-phenyloctane (ca. 1mM). Figure 4.4 shows STM images of a monolayer prepared. The monolayer displays a polycrystalline structure (Fig. 4.4a), which consists of tens of nanometer-wide domains that are stable over several minutes. The assembly can be described by the formation of four parallel lamellae depicted in Figure 4.4c. The bright rods in lamellae **I**, **II** and **III** correspond to the tecton **2**, whereas no ordered structure is visible in lamella **IV**, which might be occupied by solvent molecules of the supernatant solution possessing a high dynamic. Furthermore, as reported by the models presented in Figure 4.4c and d, the molecules between two neighboring lamellae show a “head to tail” motif, i.e. a pyridine unit facing the terpyridine moiety of the adjacent lamella. In the monolayer dipole-dipole energy between the molecules is globally minimized by the orientation of tecton **1** molecules adsorbed on the HOPG surface as shown in Figure 4.4c, whereas in case of model proposed in Figure 4.4d the adjacent rows of molecules should be separated by unoccupied area due to the dipole-dipole repulsions. The angle β between the molecules constitutive of two neighbor lamella is found to be $133 \pm 2^\circ$. It is worth noting that this “head to tail” type arrangement of the tectons leads to the alignment of the permanent dipole moment of the molecular units (calculated value of 2.87 Debye), indicating that dipolar interactions between

molecules within the monolayer play a non negligible role in the molecular self-assembly process as previously reported for organic self-assembled monolayers^[22, 23]. The proposed model of packing, features an overall minimization of the energy due to the dipole-dipole interaction both perpendicularly and along the lamellae (Fig. 4.4c). The unit cell parameters, estimated from small scale image (Fig. 4.4a), amounts to $a = (1.2 \pm 0.2)$ nm, $b = (6.7 \pm 0.1)$ nm, and $\alpha = (93 \pm 2)^\circ$, which lead to an area $A = (8.03 \pm 0.24)$ nm². Each unit cell contains three molecules of tecton **2** and probably two co-adsorbed molecules of solvent since the width of lamella **IV** (1.44 nm) corresponds to the length of a single 1-phenyloctane molecule. It is interesting to notice that the free tectons **2** are arranged on the surface in a preorganised fashion for the binding of metal centres offering the square planar geometry.

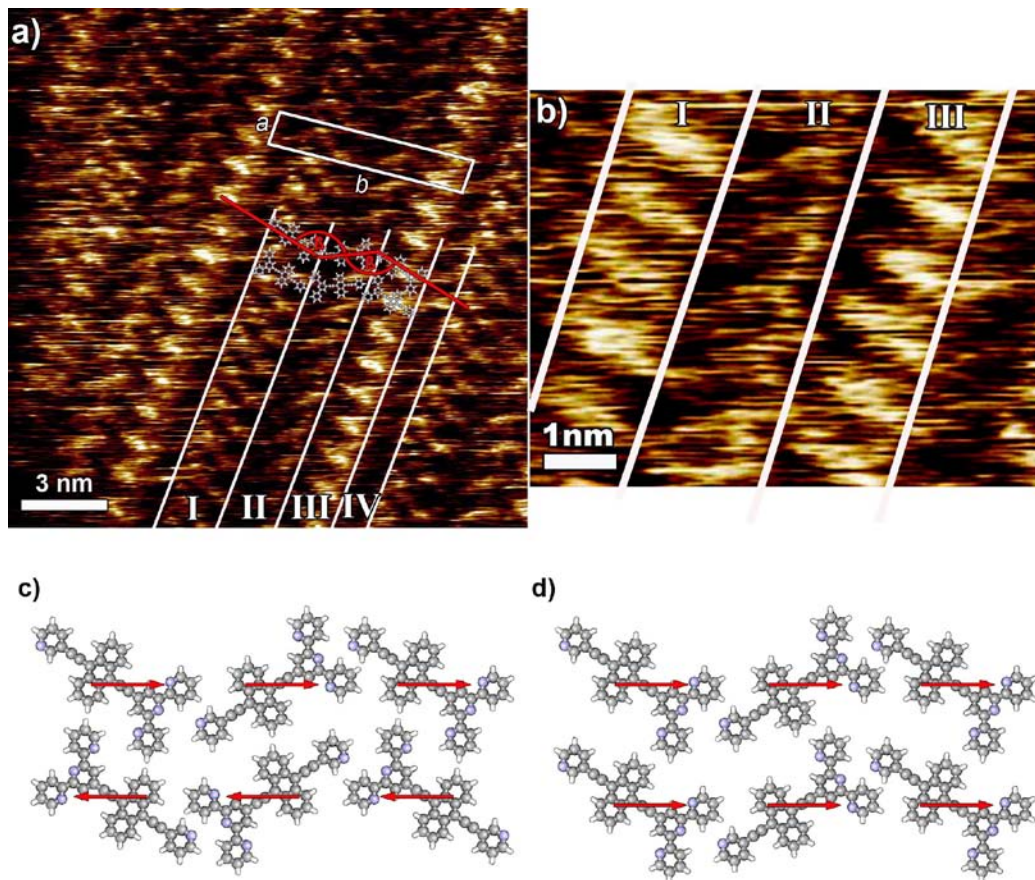


Figure 4.4 (a) Current STM images of a monolayer of the free tecton **2** in prepared by applying on HOPG a drop of a 1mM solution in 1-phenyloctane. Average tunneling parameters: $I_t = 8$ pA, $V_t = 700$ mV. Image (b) STM zoom-in image of (a); (c) and (d) Dipole – Dipole attractive and repulsive interactions respectively.

According to our previous observations on tecton **1** (Fig. 4.3), the combination of the neutral tecton **2** with Pd(II), should lead to the formation of 1D coordination network on a graphite surface^[21]. It is important to note that tecton **2** was visualized at the HOPG–solution interface only upon using 1-phenyloctane as solvent. Study of this system in different solvents like 1,2,4-trichlorobenzene or tetradecane, did not produced any ordered monolayers. For this reason, we continued our study using 1-phenyloctane as a solvent. The large scale STM current image in Figure 4.5a exhibits the bidimensional pattern, i.e. a 2D metal-organic arrays, formed on the HOPG surface upon deposition of a solution (ca. 1 mM) containing the tecton **2** and Pd(II) cation as its tetrafluoroborate salt. The high resolution STM image in Figure 4.5b exhibits brighter spots regularly distributed (marked with white arrow), which can be ascribed to the palladium ions located on the surface. Such a bright contrast is ruled by their high electron density. The distances $l_1=2.07$ nm and $l_2=2.00$ nm between Pd^{II} ions, reported on Figure 4.5b, matches with the contour length of a single molecule **2**. This indicates that 1D polycationic polymers are formed through coordination bonds between palladium cations and neutral ligand **2**, where each coordination square-planar node of the network is composed by a palladium center coordinated to four N atoms of one terpyridine and one pyridine units belonging to consecutive tectons **2**. Within the 1-D network, the angle β between adjacent molecules is $115 \pm 2^\circ$. Interestingly, the consecutive directional *zig-zag* type 1D coordination networks are packed in the parallel fashion (Fig. 4.1c) leading thus to the formation of large bidimensional highly ordered polar domains. The 2D patterns expose some empty areas between networks which are most likely for charge neutralization occupied by BF₄⁻ counter-anions as well as by solvent molecules, leading thus to the formation of a globally neutral monolayer. The packing is characterized by the unit cell $a = (3.6 \pm 0.1)$ nm, $b = (2.0 \pm 0.1)$ nm, and $\alpha = (92 \pm 3)^\circ$, which leads to an area $A = (7.3 \pm 0.2)$ nm² (see the white rectangle in Fig. 4.5a).

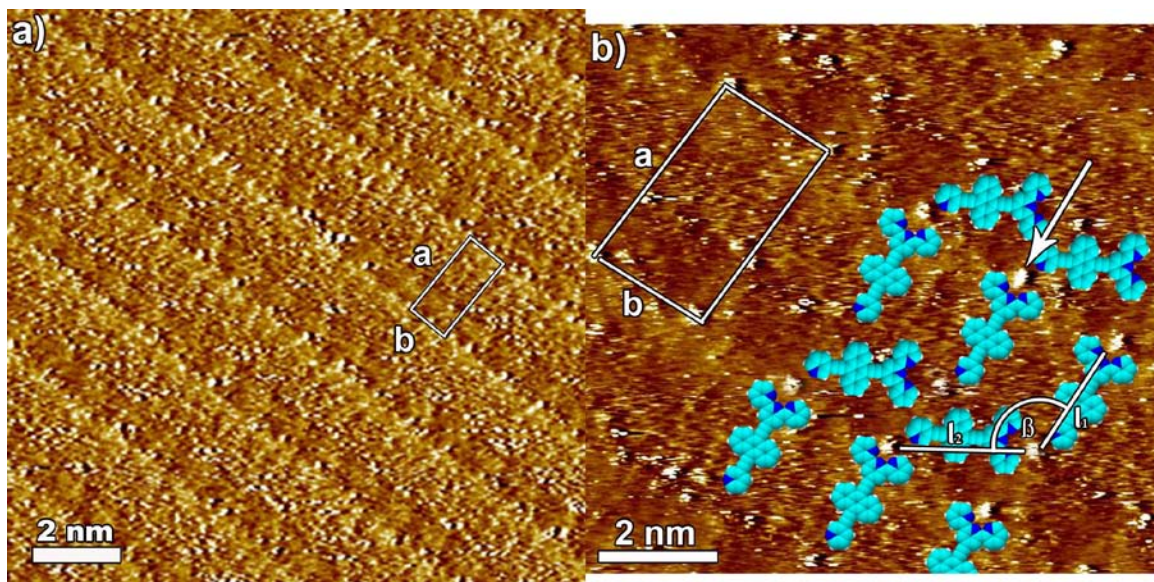


Figure 4.5 STM current images of 2D assembly formed by the tecton **2** and Pd(II) ions on HOPG surface. (a) STM large scale image and (b) small scale STM current image with proposed molecular packing. Average tunneling parameters (a and b): $I_t = 4$ pA, $V_t = 1$ V.

The formation of similar coordination networks using a different metal complex, i.e. CoCl_2 was also studied. Figure 4.6 shows a monolayer of co-crystal formed after the deposition of a solution (ca. 0.5 mM) containing both the neutral tecton **2** and CoCl_2 metal center. As expected, the observation reveals again the formation of 1D *zig-zag* type coordination networks tightly packed in domains which extend over hundreds of nanometers and are stable over several minutes. The bright rods on Figure 4.6 correspond to the tecton **2** making an angle β of $149 \pm 2^\circ$ with their nearest neighbor molecule. Since the constitutive tectons **2** are coordinated to the uncharged CoCl_2 complex, the resulting network is neutral. Finally, the unit cell of the assembly contains two molecules of tecton **2** and two Co^{II} cations and its dimensions, estimated from STM image (Fig. 4.4), are $a = (1.4 \pm 0.1)$ nm, $b = (3.5 \pm 0.1)$ nm, and $\alpha = (89 \pm 2)^\circ$, which lead to an area $A = (4.89 \pm 0.28)$ nm². Again, as in the case of Pd(II) mentioned above, the 1D networks are arranged in *syn-parallel* fashion generating thus polar domains.

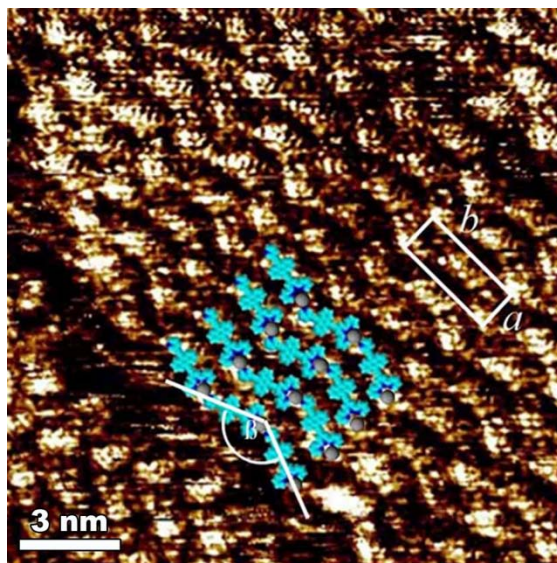


Figure 4.6 STM current image of 1D coordination networks generated upon combining tecton **2** with CoCl_2 complex on HOPG surface, with proposed molecular packing. Average tunneling parameters: $I_t = 25$ pA, $V_t = 500$ mV.

In principle, for combinations of the bent tecton **2** with Pd(II) or Co(II), one would expect either a discrete cyclic motif or an extended *zig-zag* type arrangement. Under the conditions used, in both cases we have only observed the formation of extended architectures on HOPG. This can be ascribed to the thermodynamics governing the physisorption at the solid-liquid interface; for enthalpic reasons, the packing featuring a higher density of molecules adsorbed on the surface is favored^[24]. Finally, during our previous study on the combination of the tecton **1** with CoCl_2 in tetradecane solution, we have observed the formation of directional 1D linear coordination networks leading to 1D physisorbed arrays on HOPG.^[21] In order to investigate the formation of 2D arrays on the surface, we performed the experiment using 1,2,4-trichlorobenzene (TCB) as the solvent. Figure 4.7 shows a monolayer formed upon deposition of a solution containing both the neutral tecton **1** and CoCl_2 metal complex. We do observe the formation of 2D arrays composed of coordination networks adopting, as expected, the linear chain motif. The domains formed are tightly packed and extend over hundreds of nanometers and are stable over several minutes. The bright rods on Figure 4.5 correspond to the tecton **1** making an angle of 180° with their nearest neighbor molecule. Since the constitutive tecton **1** are coordinated with the uncharged CoCl_2 metal complex, the resulting metal-organic arrays are neutral. Finally, the unit

cell of the assembly contains two molecules of tecton **1** and two Co^{II} cations. Its dimensions, estimated from STM image (Fig. 4.7b), are $a = (2.24 \pm 0.1) \text{ nm}$, $b = (2.47 \pm 0.1) \text{ nm}$, and $\alpha = (90.7 \pm 2)^\circ$, which lead to an area $A = (5.53 \pm 0.45) \text{ nm}^2$. In marked contrast with the combination of the tecton **2** with both Pd(II) cation and the CoCl_2 complex for which the directional 1-D networks were packed in *syn*-parallel fashion, for the tecton **1**, the 1-D linear directional networks obtained in the presence of CoCl_2 are packed in an *anti*-parallel fashion on the surface thus leading to apolar domains. This change in packing is interesting, however, for the moment we do not have any explanation for it. Therefore nanoscale control over both the geometry and the directionality of supramolecular arrays composed of 1D coordination networks can be achieved on surface through the design and combination of organic tectons with metal centers or metal complexes.

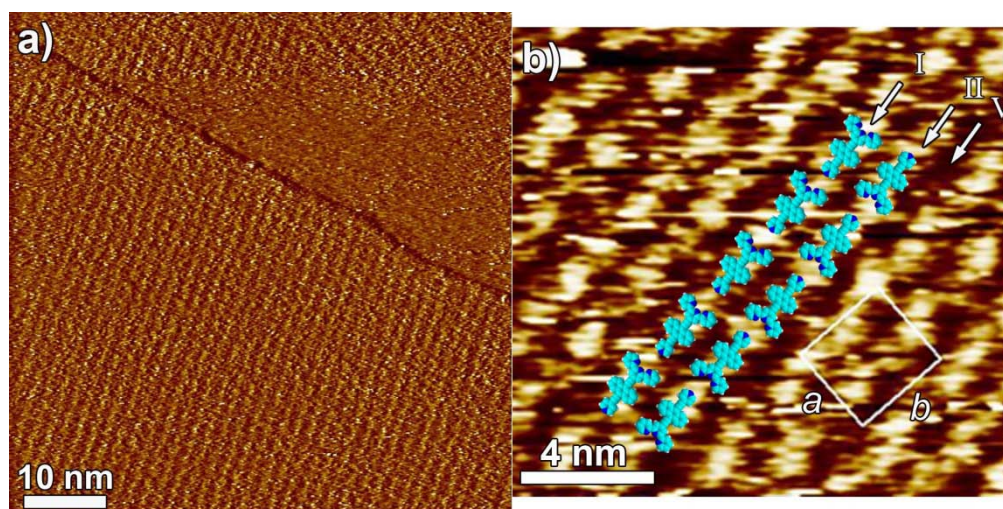


Figure 4.7 (a) STM current images of 2D assembly formed by the tecton **1** and Co^{II} ions on HOPG surface. (b) STM height small scale image of the coordination networks generated upon combining tecton **1** with CoCl_2 complex. Tunneling parameters: $V_t = 700 \text{ mV}$; $I_t = 4 \text{ pA}$

4.3 Conclusions

In conclusion, applying the molecular tectonics approach, using scanning tunneling microscopy observations, we have demonstrated the possibility of controlling at the nanoscale, through the

proper design of the organic tectons and the choice of the metal, both the geometry and the directionality of supramolecular arrays composed of 1D coordination networks on graphite surface. As expected by the design of the two organic tectons **1** and **2** bearing two differentiated coordination poles (pyridine and terpyridine) and differing only by the position of the nitrogen atom on the pyridine ring (*para* or *meta*), we have demonstrated that the geometry of the directional network may be shifted from linear to the zig-zag type. Furthermore, the packing of 1D networks on the graphite surface may be tuned by the choice of the metal center and the nature of the supernatant solvent. Indeed, in the case of Pd(II) cations the packing of cationic networks generates molecular arrays on the surface offering empty spaces for the accommodation of anions (BF_4^-) and solvent molecules. For complex CoCl_2 , the neutral networks densely packed form 2D arrays on the surface. Finally and interestingly, the combination of the bent tecton **2** with either Pd(II) or CoCl_2 leads the polar domains resulting from the *syn*-parallel packing of the directional networks into arrays on the surface. However, when the tecton **1** was combined with CoCl_2 , in marked contrast, *anti*-parallel packing of the linear 1D supramolecular polymers leading to apolar domains was observed. The control on both the geometry of the networks and their polar packing may be of interest to control charge transfer along the 1D architectures.

4.4 Experimental procedures

STM Investigations STM measurements were performed using a Veeco STM (multimode Nanoscope III, Veeco) at the internal interface between HOPG and concentrated solutions of tecton **2**, Pd(II), and Co(II) complexes. For STM measurements, the substrates are glued on a magnetic disk, and an electric contact is made with silver paint (supplied by Aldrich Chemicals). The STM tips were mechanically cut from a Pt–Ir wire (90/10, diameter 0.25 mm). The raw STM data are processed by the application of background flattening, and the drift is corrected using the underlying graphite lattice as a reference. The latter lattice is imaged underneath the molecules by lowering the bias voltage to 20 mV and raising the current to 65 pA. All models were minimized with Chem 3D package at the MM2 level. A drop of the solution was placed on a freshly cleaved HOPG surface, while the surface had already been scanned by STM under the conditions that allowed lattice resolution of the graphite surface. The scan rate was varied

between 0.2 and 0.6 μms^{-1} . Tecton **2** was dissolved in 1-phenyloctane at a concentration 1mM. The Pd(II) complex was also dissolved in 1-phenyloctane at a concentration less than 1mM. The Co(II) complex was dissolved in 1,2,4-trichlorobenzene at a concentration around 500mM (in case of Co(II) complex TCB was used as a solvent, because of its very low solubility in 1-phenyloctane).

Synthesis of Pd(II) Complex A solution of tecton **2** (1 mg, 1.87mmol) in 1-phenyloctane and solution of $[\text{Pd}(\text{CH}_3\text{CN})_4\text{BF}_4]$ (0.83 mg, 1.87mmol) (2 mL) in 1-phenyloctane were mixed and stirred at 60°C for 24 h.

Synthesis of Co(II) Complex A solution of tecton **2** (**1**) (1 mg, 1.87mmol) and $\text{CoCl}_2 \times \text{H}_2\text{O}$ (0.45 mg, 1.87mmol) in 1,2,4-trichlorobenzene (4 mL) was stirred at 60°C for 24 h.

Calculations Calculation of dipole moments were performed using the *Molekel* and *WinGamess* software.

References

- [1] A. M. W. C. Thompson, *Coordination Chemistry Reviews* **1997**, *160*, 1.
- [2] U. S. Schubert, H. Hofmeier, G. R. Newkome, *Modern Terpyridine Chemistry*, Wiley-VCH, Weinheim **2006**.
- [3] M. W. Hosseini, *Chem. Commun.* **2005**, 5825.
- [4] M. W. Hosseini, *Acc. Chem. Res.* **2005**, *38*, 313.
- [5] W. Liang, M. P. Shores, M. Bockrath, J. R. Long, H. Park, *Nature* **2002**, *417*, 725.
- [6] M. Barboiu, J. M. Lehn, *Proc. Natl. Acad. Sci. USA* **2002**, *99*, 5201.
- [7] D. G. Kurth, N. Severin, J. P. Rabe, *Angew. Chem. Int. Ed.* **2002**, *41*, 3681.
- [8] S. De Feyter, F. C. De Schryver, *J. Phys. Chem. B* **2005**, *109*, 4290.
- [9] M. Surin, P. Samorì, *Small* **2007**, *3*, 190.
- [10] K. Müllen, J. P. Rabe, *Acc. Chem. Res.* **2008**, *41*, 511.
- [11] L. J. Wan, *Acc. Chem. Res.* **2006**, *39*, 334.
- [12] S. Stepanow, N. Lin, J. V. Barth, K. Kern, *Vol. 110*, **2006**, pp. 23472.
- [13] S. Stepanow, M. Lingenfelder, A. Dmitriev, H. Spillmann, E. Delvigne, N. Lin, X. Deng, C. Cai, J. V. Barth, K. Kern, *Nat. Mater.* **2004**, *3*, 229.

- [14] U. Schlickum, R. Decker, F. Klappenberger, G. Zoppellaro, S. Klyatskaya, M. Ruben, I. Silanes, A. Arnau, K. Kern, H. Brune, *Nano Lett.* **2007**, 7, 3813.
- [15] G. R. Newkome, P. S. Wang, C. N. Moorefield, T. J. Cho, P. P. Mohapatra, S. N. Li, S. H. Hwang, O. Lukoyanova, L. Echegoyen, J. A. Palagallo, V. Iancu, S. W. Hla, *Science* **2006**, 312, 1782.
- [16] Y. Kikkawa, E. Koyama, S. Tsuzuki, K. Fujiwara, K. Miyake, H. Tokuhisa, M. Kanosato, *Chem. Commun.* **2007**, 1343.
- [17] M. M. S. Abdel-Mottaleb, N. Schuurmans, S. D. Feyter, J. V. Esch, B. L. Feringa, F. C. D. Schryver, *Chem. Commun.* **2002**, 2002, 1894.
- [18] P. Zell, F. Moglele, U. Ziener, B. Rieger, *Chem. Eur. J.* **2006**, 12, 3847.
- [19] S. De Feyter, M. M. S. Abdel-Mottaleb, N. Schuurmans, B. J. V. Verkuijl, J. H. van Esch, B. L. Feringa, F. C. De Schryver, *Chem. Eur. J.* **2004**, 10, 1124.
- [20] B. A. Hermann, L. J. Scherer, C. E. Housecroft, E. C. Constable, *Adv. Funct. Mater.* **2006**, 16, 221.
- [21] M. Surin, P. Samorì, A. Jouaiti, N. Kyritsakas, M. W. Hosseini, *Angew. Chem. Int. Ed.* **2007**, 46, 245.
- [22] Y. Wei, W. Tong, C. Wise, X. Wei, K. Armbrust, M. Zimmt, *Journal of the American Chemical Society* **2006**, 128, 13362.
- [23] Y. Lalatonne, J. Richardi, M. P. Pileni, *Nat. Mater.* **2004**, 3, 121.
- [24] P. Samorì, N. Severin, K. Müllen, J. P. Rabe, *Adv. Mater.* **2000**, 12, 579.

Chapter 5

Self-assembled architectures based on H-bonding

*“Without hydrogen bonds, all wooden structures would collapse,
cement would crumble, oceans would vaporize,
and all living things would disintegrate into inanimate matter”*

G. A. Jeffrey, Wolfram Saenger, 1991

The *hydrogen bond* (H-bond) has such a great influence in gaseous, liquid, and solid-state chemistry that its consequences were observed long before it was identified and given a name. Most of hydrogen bonds are weak attractions with a binding strength about one-tenth of that of covalent bond. The importance of hydrogen bonding in the structure and function of biological molecules had been forecasted by the success of the Watson and Crick base-pairing in interpreting the structure of the nucleic acids in 1953 and by the α -helix and pleated sheet structures in proteins proposed by Pauling, Corey and Branson (1951).

In this chapter we will focus our attention on 2D supramolecular architectures formed by multiple H-bonds at the solid-liquid interface. We will also discuss the role of the H-bonding in abiotic systems, further investigated by means of STM. In some cases reported in this chapter, both *Density Functional Theory* (DFT) and *Molecular Dynamics* (MD) computations have been performed to gain additional information on self-assembly phenomena of investigated molecular systems.

Chapter 5.1

2D supramolecular porous networks

2D supramolecular porous networks, are ordered structures with cavities formed by organic and inorganic molecules on top of a solid substrate. The porous architectures can act as a host for other organic molecules. For this reason, these systems are often called as “host-guest” systems. The molecular building blocks of the pores are held together by non-covalent interactions, such as H-bonding, van der Waals interactions or metal-organic coordination. The pores can be formed by a single or by different species. The size of the pores can be tuned by changing the building blocks. In the collaboration with the group of Prof. Jean-Marie Lehn from Institut de Science et d'Ingénierie Supramoléculaires at University of Strasbourg (ISIS-UdS, Strasbourg, France), we designed and investigated by means of STM, a functionalized molecular modules capable of self-associating, through self-complementary H-bonding patterns comprising twelve strong H-bonds to form 2D porous networks at the solid-liquid interface. The self-association of these hexatopic di(acetamido)pyridine based molecules through directional H-bonding between two lateral recognition sites of neighboring molecules allowed the formation of two-dimensional supramolecular polymers which were self-assembled on graphite.

The molecules described in this chapter has been synthesized by Gaël Schaeffer, in the Laboratoire de Chimie Supramoléculaire of Prof. J.-M. Lehn, whereas all *Molecular Dynamics* calculations were performed by Carlos-Andres Palma in our research group.

5.1.1 Introduction

Supramolecular polymers is a broad term involving the supramolecular recognition of monomers to generate supermolecules.^[1, 2] This literal definition incorporate a wide spectrum of supramolecular architectures, from networks^[3-9] and oligomers^[10] to liquid crystals^[2, 11] and elastomers.^[12] Construction of 2D molecular networks on solid surfaces based on self-assembly of small organic molecules is a subject of intense interest owing to the perspective of various applications in the field of nanoscience and nanotechnology.^[13-16] Supramolecular self-assembly can become an alternative for current lithographic techniques to create surface patterns in the low nanometer regime.^[17] The design and control of the structure and functionality of molecular networks requires insight in the correlation between molecular structural features, i.e. shape, nature, and position of interacting sites, as well as molecular electronic properties and the topology of supramolecular architectures. This strategy is known as crystal engineering and has rapidly developed in 2D systems.^[7, 18, 19] Due to their high directionality, hydrogen bonds play a key role in molecular recognition processes, and formation of supramolecular architectures in solution, in the solid state and for surface patterning.^[20-24] Two-dimensional hydrogen bonded networks on surfaces demonstrate the unique potential of tailoring supramolecular assemblies for nanotechnology applications. Many novel adsorbate-substrate systems are known to exhibit a high degree of order on a large scale, and scanning tunneling microscopy (STM) has proven its capability for investigations of submolecularly resolved structural and electronic properties.^[25-28] We searched for purely organic systems, in which the molecular-recognition-driven polyassociation of monomers would be ensured by a well-defined hydrogen-bonded pattern of self-complementary units. Previous examples have strongly favored this type of supramolecular interaction as it combines simplicity with directionality. The high association constants expected from the formation multiple hydrogen bonds suggested the use of a diaminopyridine-substituted isophthalamide molecule derivatives (Fig. 5.1), which are known to self-associate in solution by formation of H-bonds.^[29, 30]

In this chapter, we will demonstrate how scanning tunneling microscopy (STM) can be used in conjunction with molecular dynamics (MD) to elucidate the fine structure of supramolecular polymers which feature a high degree of conformational freedom within their multivalent H-bonding capability.

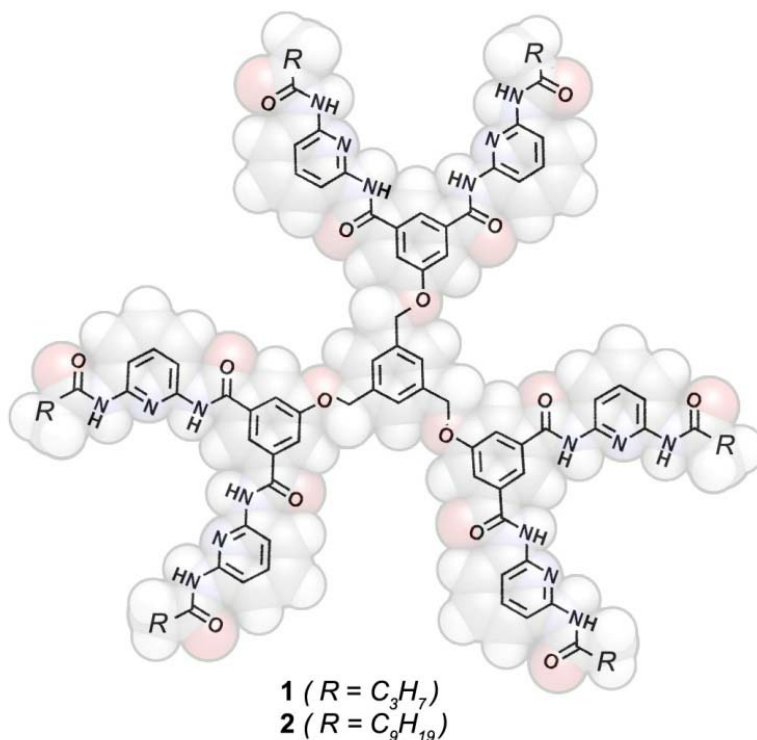


Figure 5.1 Molecular structure of the investigated molecules **1** and **2**.

5.1.2 Results and discussion

Scanning Tunneling Microscopy We started investigating the self-assembled structures by applying a drop of a warm $5 \pm 1 \mu\text{M}$ solution of the molecule **1** in 1,2,4-trichlorobenzene (TCB) on the graphite surface. Monolayer formation can be visualized via STM within a few minutes thereafter. Figure 5.2a depicts the honeycomb 2D porous networks obtained with **1**. The hexagonal lattice features an unit cell $a = (4.9 \pm 0.2) \text{ nm}$ and $\alpha = (61 \pm 3)^\circ$, corresponding to an area $A = (20.99 \pm 1.06) \text{ nm}^2$. Interestingly upon applying a drop of a worm solution of **2**, of exact concentration as in the case of **1** similar honeycomb networks was observed (Fig. 5.2b). Interestingly, both monolayers feature the exact same unit cell and unit cell area, strongly suggesting that substituted alkyl chains do not play any significant role in the self-assembly process at the TCB-HOPG interface.

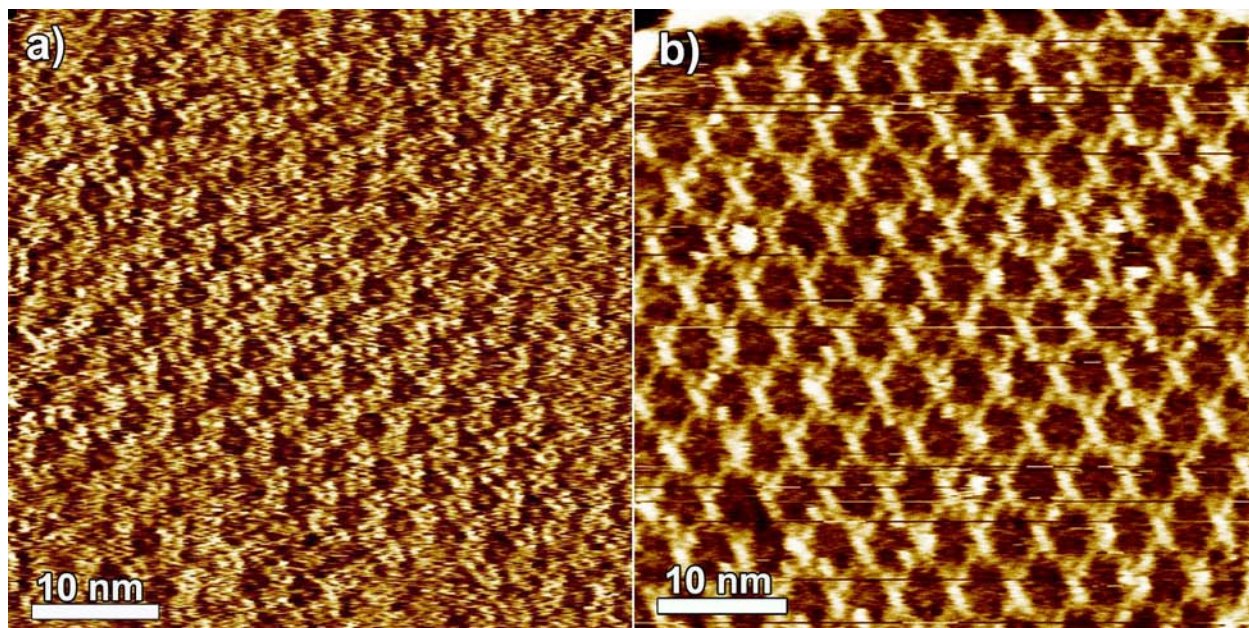


Figure 5.2 Large scale STM height images of the self-assembled 2D porous network of **1** (a) and **2** (b) at the 1,2,4-trichlorobenzene-HOPG interface. Average tunneling parameters: $I_t = 5$ pA, $V_t = 350$ mV.

At this point, we had to address several questions in order to understand the mechanism of polyassociation of molecules **1** and **2** and the formation of porous networks at the solid-liquid interface. First, and probably the most important one was to understand the conformational preferences of investigated molecules. We focused our attention on the bis(acetamido)pyridine functional units of investigated molecular building blocks, which were unambiguously involved in the formation of 2D networks. Bis(acetamido)pyridine are known of their preference to exist in the *trans* conformation^[31] (Fig. 5.3), however several works have been reported, where those molecules were found in their the *cis* conformation.^[32, 33]

Density functional calculations The ability to understand and predict the stability of H-bonded systems is of importance for the rational bottom-up fabrication of complex supramolecular architectures. A number of experimental and theoretical methods have been applied for the analysis of the H-bonded systems to obtain simple and reliable models for interpreting their stabilities. The main target of *ab initio* investigation was to define the energy difference between the two possible conformations of bis(acetamido)pyridine units, i.e. the energy difference between the *trans* and *cis*, isomers. The monomers and their dimers were the subject of recent studies by theoretical DFT- B3LYP/6-311G++(d,p) method. The interaction energies of the dimers counterparts were estimated as the energy difference between the dimer and isolated

ligands. The molecular geometries of hydrogen-bonded dimers have been fully optimized using the density functional theory (DFT) with B3LYP functional^[34, 35]. The standard 6-31G++(d,p) basis set was used in all calculations. Literature analysis^[36-38] shows that the geometries, relative stabilities, and frequencies of the structures calculated at the B3LYP/6-31G++(d,p) level are in a good accordance with experimental data.

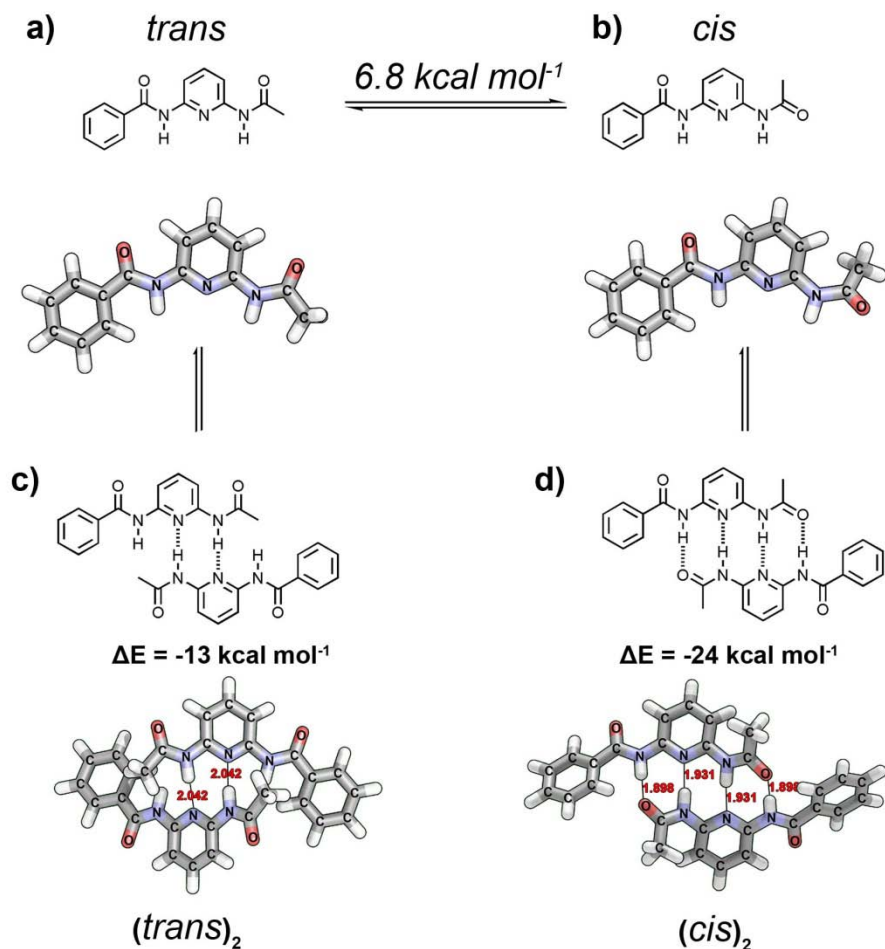


Figure 5.3 Bis(acetamido)pyridine unit of **1** and **2** in its *trans* (a) and *cis* (b) conformation; Self-association of two acetamido terminal groups in the DAD-DAD *trans* (c) and DADA-ADAD *cis* (d) conformation via two and four strong H-bonds respectively.

At the single molecule level isomer *trans* was found to be more stable than *cis* (Fig. 5.3) by $6.8 \text{ kcal mol}^{-1}$, which might be explained by the presence of the two stabilizing intra-molecular hydrogen bonds ((*aromatic*)C-H \cdots N) in the case of *trans* isomer, whereas in the case of isomer

cis, the structure might be destabilized by repulsive interaction between (*aromatic*)C-H and -CH₃ group. Nevertheless, in case of dimeric structures (*cis*)₂ dimer was found to be more stable than the (*trans*)₂ one by 11 kcal mol⁻¹ (Fig. 5.3). The energy difference between those dimers can be explained by comparing the number of H-bonds. Molecules in (*trans*)₂ dimer are held together by two strong (N-H···N) hydrogen-bonds. Such a dimeric structure might be also presented as a DAD-DAD dimer. Interestingly, by changing the conformation to *cis*, molecules can form DADA-ADAD dimers, i.e. (*cis*)₂, where the molecules are held together by 2 strong (N-H···N) and two strong (N-H···O) H-bonds.

It is very important to note once again, that those two monolayers are identical. In fact we performed statistical analysis to define the small length differences between the vectors *l* and *h* (Fig. 5.4a and b), in both monolayers. Different areas of crystalline patterns of **1** and **2** have been measured, which results in the length of vector *l*: 2.29 nm for **1** and 2.31 nm for **2**, whereas the length of vector *h* was estimated as 4.56 nm for **1** and 4.55 nm for **2**.

Based on computational results, we were able to propose molecular packing for the monolayers visualized by STM for **1** and **2**. As stated above both monolayers can be characterized by an unit cell $a = (4.9 \pm 0.2)$ nm and $\alpha = (61 \pm 3)^\circ$, corresponding to an area $A = (20.99 \pm 1.06)$ nm², where each unit cell contain two molecules **1** or **2**. Molecules, being more precise the bis(acetamido)pyridine units adopt *cis* conformation, and are one out of two units from three arms of the molecule is associating with neighboring molecules forming dimers. Each molecule is forming twelve H-bonds with three neighboring molecules (Fig. 5.4c,d,e). However, it was still unclear for us how the rest of bis(acetamido)pyridine units are involved in the formation of 2D H-bonded networks (indicated in blue in Fig. 5.4c) on HOPG surface.

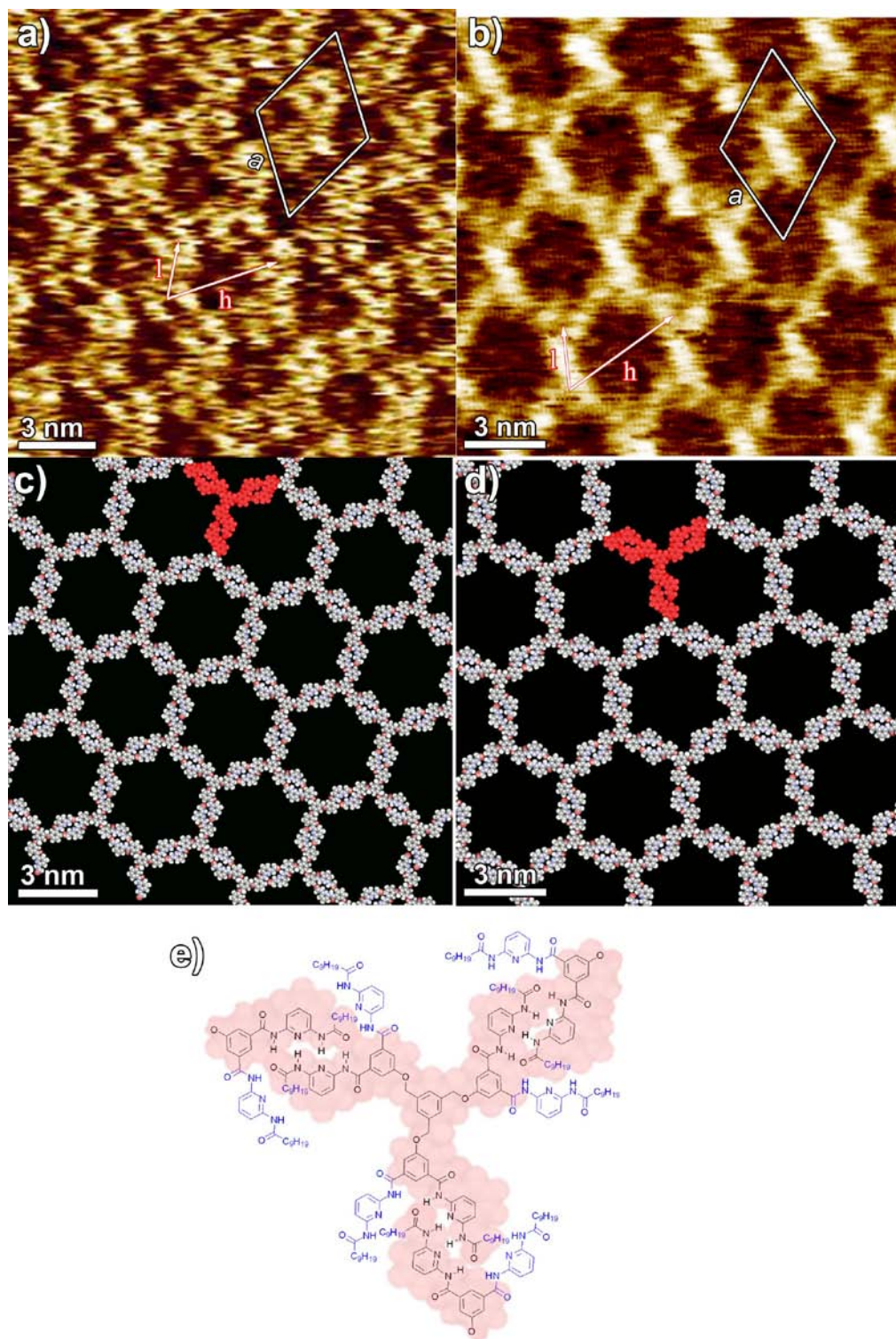


Figure 5.4 STM small scale images of **1** (a) and **2** (b); Tunneling parameters: Average tunneling current (I_t) = 15 pA, tip bias voltage (V_t) = 350 mV; Proposed molecular packing of **1** (c) and **2** (d) compared with theoretical model (e).

Between the concentrations that were investigated for both molecular systems (500, 50, 5 and 0.5 μM), in case of molecule **2** a concentration of $0.5 \pm 0.1 \mu\text{M}$ afforded a polymorphic tight-packed pattern in coexistence with the previously observed honeycomb pattern. Figure 5.5a depicts the second polymorph structure (**B**) alongside the previously investigated crystalline honeycomb domain. The molecules **2** self-assemble in lamellar fashion on HOPG surface. The tight-packed oblique lattice features an unit cell $a = (7.2 \pm 0.2) \text{ nm}$, $b = (2.6 \pm 0.2) \text{ nm}$ and $\alpha = (58 \pm 3)^\circ$, corresponding to an area $A = (15.87 \pm 0.79) \text{ nm}^2$, where each unit cell contains two molecules **2**. Among the entire supramolecular structure in domain **A** some defects (indicated with white arrow in Fig. 5.4a) have been observed.

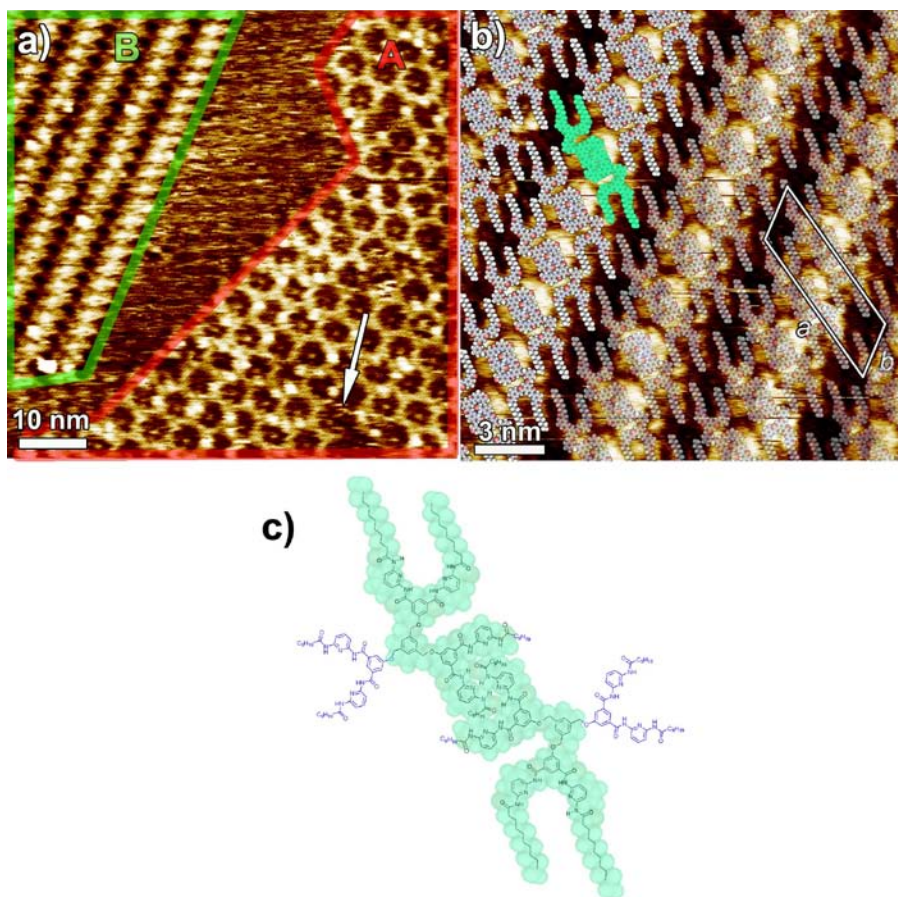


Figure 5.5 (a) STM large scale image displaying two coexisting domains **A** and **B**. (b) STM small scale image of molecules **2** in polymorphic architecture and corresponding proposed molecular packing motif compared with theoretical model(c).

Within the crystalline domain B, the molecules are forming dimers (Fig. 5.5c) via 4 strong H-bonds in DADA-ADAD arrays. Furthermore, entire domain is stabilized by weak van der Waals interactions between the alkyl chains and HOPG surface. Surprisingly, only four out of twelve alkyl chains have been visualized by STM. Presumably, as in case of monolayers obtained by working at higher concentration the alkyl chains are backfolded into supernatant solution.

Molecular Dynamics (MD) All MD simulations were performed with the general force field MMFF as implemented in the package CHARMM 35. Detail information about the MD calculations will be given elsewhere.^[39] Figure 5.6a depicts the main hydrogen-bond interaction between adjacent dimers found during the conformational search. It has been found that bis(acetamido)pyridine units adopt *trans* conformation, which was predicted by DFT analysis to be more stable than the *cis* one. The primary interaction consist of two simultaneous hydrogen-bonds from two bis(acetamido)pyridine units of adjacent molecules N-H's (bright molecule) to a perpendicular carbonyl in a third bis(acetamido)pyridine fragment (right hand side molecule). In this information in our hands, we were able to proposed new packing motif for both molecular systems, i.e. **1** and **2** in their honeycomb networks (Fig. 5.6b).

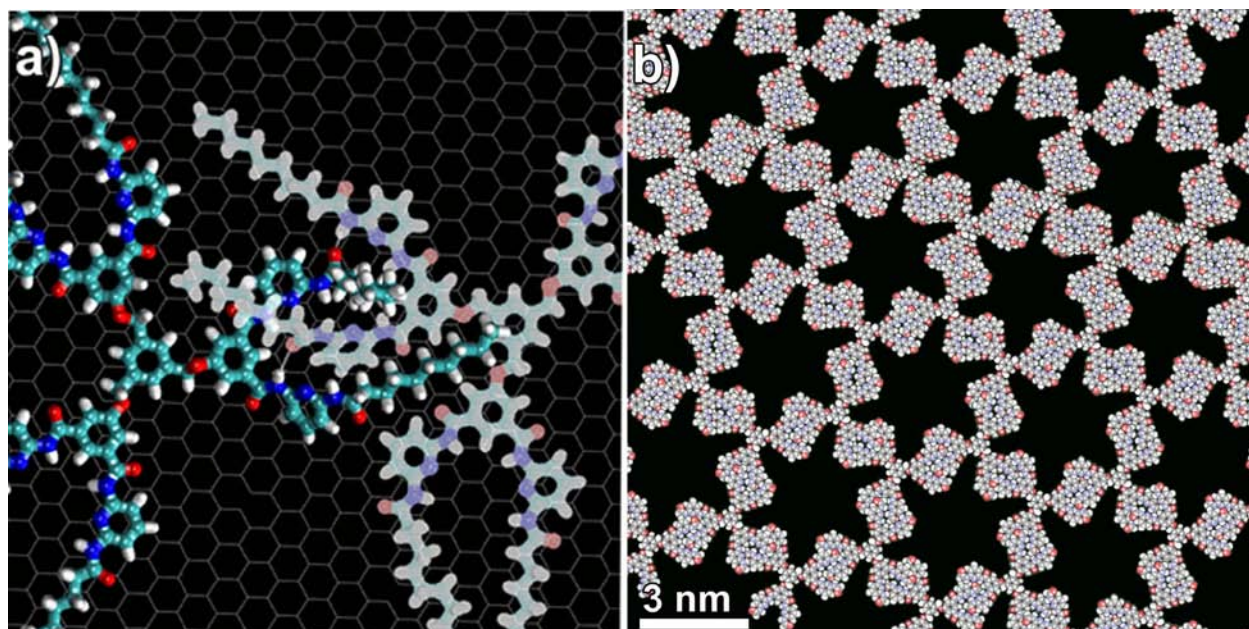


Figure 5.6 (a) Fragment of H-bonded structure predicted by MD calculation; (b) proposed molecular packing motif of the molecules in the honeycomb network, based on the structures computed with MD.

The proposed molecular packing motif differs from the one proposed previously (Fig. 5.4b, c and d). The main difference, i.e. conformational preferences of bis(acetamido)pyridine units, might be explained by the fact that MD computations were based on the system involving six molecules pre-arranged in hexagonal architecture, whereas the DFT calculations were based only on bis(acetamido)pyridine monomers and dimers. It is also important to note at this point, that MD computations predicted that the alkyl chains were not in the same plain as the cores of the molecules. In other words, they should be backfolded into solution, which was observed by the means of STM.

5.1.3 Conclusions

In summary we have demonstrated with the help of an STM a highly dynamic, yet periodic polymer network at the solid-liquid interface, formed by polyassociation of hexatopic di(acetamido)pyridine based molecules through directional H-bonding between two lateral recognition sites of neighboring molecules. Interestingly, di(acetamido)pyridine derivative possessing six long alkyl chains in its structure was found to form polymorphic structures depending on the concentration of investigated solutions. Despite, the results obtained by STM were not straight forward, by simple DFT and more advanced MD calculations, we were able to propose two different molecular packing motifs. Such a approach, i.e. combining experimental procedures like STM measurements with theoretical computations, especially Molecular Dynamics, might give more information on assembly preferences, time and temperature dependant stability of supramolecular architectures.

5.1.4 Experimental procedure

Scanning Tunneling Microscopy STM measurements were performed using a Veeco scanning tunneling microscope (multimode Nanoscope III, Veeco) at the interface between highly oriented pyrolytic graphite (HOPG) and a supernatant solution. Diluted solutions of molecule **1** were applied to the basal plane of the surface. The STM tips were mechanically cut from a Pt/Ir wire (90/10, diameter 0.25 mm). The raw STM data are processed by the application of background flattening and the drift is corrected using the underlying graphite lattice as a reference. The latter lattice is imaged underneath the molecules by lowering the bias voltage to 20 mV and raising the

current to 65 pA. Molecule **1** was dissolved in dimethyl sulfoxide (DMSO) and diluted with 1,2,4-trichlorobenzene (TCB) to give 500 ± 1 μM , 50 ± 1 μM , 5 ± 1 μM and 0.5 ± 1 μM solutions respectively. Monolayer pattern formation was achieved by applying 4 μL of a warm (30-40°C) solution onto freshly cleaved HOPG. The same protocol was applied to molecule **2**.

Density functional calculations DFT calculations were done in vacuum at room temperature by using the GAUSSIAN 03^[40] program, running on an SGI Altix 350 Linux server^[41].

References

- [1] J.-M. Lehn, *Supramolecular chemistry: concepts and perspectives*, VCH New York, **1995**.
- [2] L. Brunsveld, B. J. B. Folmer, E. W. Meijer, R. P. Sijbesma, *Chem. Rev.* **2001**, *101*, 4071.
- [3] C. A. Palma, M. Bonini, A. Llanes-Pallas, T. Breiner, M. Prato, D. Bonifazi, P. Samorì, *Chem. Commun.* **2008**, 5289.
- [4] L. Kampschulte, T. L. Werblowsky, R. S. K. Kishore, M. Schmittel, W. M. Heckl, M. Lackinger, *J. Am. Chem. Soc.* **2008**, *130*, 8502.
- [5] M. Lackinger, S. Griessl, W. A. Heckl, M. Hietschold, G. W. Flynn, *Langmuir* **2005**, *21*, 4984.
- [6] M. Lackinger, S. Griessl, T. Markert, F. Jamitzky, W. M. Heckl, *J. Phys. Chem. B* **2004**, *108*, 13652.
- [7] K. Tahara, S. Okuhata, J. Adisojoso, S. B. Lei, T. Fujita, S. De Feyter, Y. Tobe, *J. Am. Chem. Soc.* **2009**, *131*, 17583.
- [8] L. Kampschulte, M. Lackinger, A. K. Maier, R. S. K. Kishore, S. Griessl, M. Schmittel, W. M. Heckl, *J. Phys. Chem. B* **2006**, *110*, 10829.
- [9] J. M. MacLeod, O. Ivasenko, D. F. Perepichka, F. Rosei, *Nanotechnology* **2007**, *18*.
- [10] A. Llanes-Pallas, M. Matena, T. Jung, M. Prato, M. Stohr, D. Bonifazi, *Angew. Chem. Int. Ed.* **2008**, *47*, 7726.
- [11] T. Kato, *Science* **2002**, *295*, 2414.
- [12] E. Wisse, A. J. H. Spiering, F. Pfeifer, G. Portale, H. W. Siesler, E. W. Meijer, *Macromol.* **2008**, *42*, 524.
- [13] J. V. Barth, G. Costantini, K. Kern, *Nature* **2005**, *437*, 671.

- [14] J. Frommer, *Angew. Chem. Int. Ed.* **1992**, *31*, 1298.
- [15] J. A. Theobald, N. S. Oxtoby, M. A. Phillips, N. R. Champness, P. H. Beton, *Nature* **2003**, *424*, 1029.
- [16] M. Surin, P. Samorì, *Small* **2007**, *3*, 190.
- [17] J. R. Sheats, B. W. Smith, *Microlithographic Science and Technology*, Marcel Drakker, *1st ed.*; New York 1998.
- [18] S. Furukawa, S. De Feyter, *Top. Curr. Chem.* **2008**, *287*, 87.
- [19] F. Cicoira, C. Santano, F. Rosei, *Top. Curr. Chem.* **2008**, *285*, 203.
- [20] R. Matmour, I. De Cat, S. J. George, W. Adriaens, P. Leclère, P. H. H. Bomans, N. A. J. M. Sommerdijk, J. C. Gielen, P. C. M. Christianen, J. T. Heldens, J. C. M. van Hest, D. W. P. M. Löwik, S. De Feyter, E. W. Meijer, A. P. H. J. Schenning, *J. Am. Chem. Soc.* **2008**, *130*, 14576.
- [21] A. Gesquiere, S. De Feyter, F. C. De Schryver, F. Schoonbeek, J. van Esch, R. M. Kellogg, B. L. Feringa, *Nano Lett.* **2001**, *1*, 201.
- [22] A. Gesquiere, P. Jonkheijm, F. J. M. Hoeben, A. P. H. J. Schenning, S. De Feyter, F. C. De Schryver, E. W. Meijer, *Nano Lett.* **2004**, *4*, 1175.
- [23] A. Llanes-Pallas, C. A. Palma, L. Piot, A. Belbakra, A. Listorti, M. Prato, P. Samorì, N. Armaroli, D. Bonifazi, *J. Am. Chem. Soc.* **2009**, *131*, 509.
- [24] C. A. Palma, J. Bjork, M. Bonini, M. S. Dyer, A. Llanes-Pallas, D. Bonifazi, M. Persson, P. Samorì, *J. Am. Chem. Soc.* **2009**, *131*, 13062.
- [25] K. W. Hipps, X. Lu, X. D. Wang, U. Mazur, *J. Phys. Chem.* **1996**, *100*, 11207.
- [26] J. K. Gimzewski, C. Joachim, *Science* **1999**, *283*, 1683.
- [27] K. W. Hipps, D. E. Barlow, U. Mazur, *J. Phys. Chem. B* **2000**, *104*, 2444.
- [28] M. Lackinger, M. Hietschold, *Surf. Sci.* **2002**, *520*, L619.
- [29] V. Berl, M. Schmutz, M. J. Krische, R. G. Khoury, J. M. Lehn, *Chem. Eur. J.* **2002**, *8*, 1227.
- [30] A. Ciesielski, G. Schaeffer, A. Petitjean, J. M. Lehn, P. Samorì, *Angew. Chem. Int. Ed.* **2009**, *48*, 2039.
- [31] F. H. Beijer, R. P. Sijbesma, J. A. J. M. Vekemans, E. W. Meijer, H. Kooijman, A. L. Spek, *J. Org. Chem.* **1996**, *61*, 6371.
- [32] C. M. Drain, X. X. Shi, T. Milic, F. Nifiatis, *Chem. Commun.* **2001**, 287.

- [33] M. Matena, A. Llanes-Pallas, M. Enache, T. Jung, J. Wouters, B. Champagne, M. Stohr, D. Bonifazi, *Chem. Commun.* **2009**, 3525.
- [34] R. M. Dickson, A. D. Becke, *J. Chem. Phys.* **1993**, *99*, 3898.
- [35] C. Lee, W. Yang, R. G. Parr, *Phys. Rev. B* **1988**, *37*, 785.
- [36] A. M. Mebel, K. Morokuma, M. C. Lin, *J. Chem. Phys.* **1995**, *103*, 7414.
- [37] J. D. Gu, J. Leszczynski, *J. Phys. Chem. A* **2000**, *104*, 6308.
- [38] J. D. Gu, J. Leszczynski, *J. Phys. Chem. A* **2000**, *104*, 7353.
- [39] C.-A. Palma, *PhD Thesis* **2010**.
- [40] M. J. Frisch, G. W. Trucks, H. B. Schlegel, G. E. Scuseria, M. A. Robb, J. R. Cheeseman, J. Montgomery, T. J. A.; Vreven, K. N. Kudin, J. C. Burant, J. M. Millam, S. S. Iyengar, J. Tomasi, V. Barone, B. Mennucci, M. Cossi, G. Scalmani, N. Rega, G. A. Petersson, H. Nakatsuji, M. Hada, M. Ehara, K. Toyota, R. Fukuda, J. Hasegawa, M. Ishida, T. Nakajima, Y. Honda, O. Kitao, H. Nakai, M. Klene, X. Li, J. E. Knox, H. P. Hratchian, J. B. Cross, V. Bakken, C. Adamo, J. Jaramillo, R. Gomperts, R. E. Stratmann, O. Yazyev, A. J. Austin, R. Cammi, C. Pomelli, J. W. Ochterski, P. Y. Ayala, K. Morokuma, G. A. Voth, P. Salvador, J. J. Dannenberg, V. G. Zakrzewski, S. Dapprich, A. D. Daniels, M. C. Strain, O. Farkas, D. K. Malick, A. D. Rabuck, K. Raghavachari, J. B. Foresman, J. V. Ortiz, Q. Cui, A. G. Baboul, S. Clifford, J. Cioslowski, B. B. Stefanov, G. Liu, A. Liashenko, P. Piskorz, I. Komaromi, R. L. Martin, D. J. Fox, T. Keith, M. A. Al-Laham, C. Y. Peng, A. Nanayakkara, M. Challacombe, P. M. W. Gill, B. Johnson, W. Chen, M. W. Wong, C. Gonzalez, J. A. Pople, *Gaussian 03, Revision C.02*, Gaussian, Inc., Wallingford CT, 2004.
- [41] http://www-curri.u-strasbg.fr/calcul_intensif_scalaire/environnement.php.

Chapter 5.2

1D supramolecular helical polymers

The greatest control over the geometry in H-bond supramolecular architectures, especially in H-bonded supramolecular polymers, can be achieved by using conformationally rigid molecular modules self-assembled through strong H-bonds. Their magnitude depends of their multiplicity, nature of donor/acceptor pairs and their secondary attractive/repulsive interactions. In the collaboration with the groups of Prof. Jean-Marie Lehn from Institut de Science et d'Ingénierie Supramoléculaires (ISIS, Strasbourg, France) and Prof. Mats Persson from Surface Science Research Centre at University of Liverpool (United Kingdom) we designed and synthesized a functionalized molecular module capable of self-associating, through self-complementary H-bonding patterns comprising four strong and two medium strength H-bonds to form dimers. The self-association of these phenylpyrimidine based dimers through directional H-bonding between two lateral pyridin-2(1H)-one units of neighboring molecules allowed the formation of highly compact one-dimensional supramolecular polymers which were self-assembled on graphite. The concentration dependent study by Scanning Tunneling Microscopy (STM) at the solid-liquid interface revealed the controlled generation of either linear supramolecular 2D arrays, or long helical supramolecular polymers with a high shape persistence.

The molecule described in this chapter has been synthesized by Artur Stefankiewicz, in the Laboratoire de Chimie Supramoléculaire of Prof. J.-M. Lehn, whereas all *ab initio* calculations were performed by Dr. Felix Hanke in the group of Prof. Mats Persson.

5.2.1 Introduction

Supramolecular polymers combine pre-programmed geometries, stabilities and peculiar mechanical properties as direct results of the joint effect of non-covalent primary and their related secondary interactions holding together functionalized molecular modules.^[1-8] Taking advantage of the high selectivity and strength as well as the reversible nature and exceptional directionality of these interactions, materials featuring simultaneously tunable properties,^[9-11] self-healing and easy solution processability can be tailored.^[12, 13] Macroscopically long and linear non-covalent polymer arrays can be obtained by self-assembly from low molecular weight molecules exposing complementary H-bond forming moieties^[14-19] connected by a spacer.^[20-24] Upon thermal activation of molecular building blocks non-covalent architectures might be used to form covalent polymers.^[25, 26] Through the simultaneous use of multiple and interdigitated H-bonds bridging conformationally rigid molecular modules, it is possible to increase the strength of these interactions and to achieve a full control over the geometry of the supramolecular architecture.^[27, 28]

Self-assembly phenomena have been used to design and synthesize molecular units capable of organizing into helical superstructures.^[29-36] Besides the multiplicity, the magnitude of the interaction holding together the molecular units depends on the nature of donor/acceptor pairs and their secondary attractive/repulsive interactions. In the last few decades supramolecular discrete or macroscopically long architectures have been developed by using double,^[37, 38] triple,^[39-41] quadruple,^[42-47] quintuple,^[48] and sextuple^[49] parallel H-bonds. Despite the increasing synthetic effort, the number of supramolecular polymers based on very strong and multiple H-bond connected modules is still relatively small. Thus far the highest value of the association equilibrium constant for the self-assembly of dimers, was estimated to exceed 10^8 M^{-1} , and was obtained for a discrete H-bonded dimer with quadruple bonds among ureidopyrimidone derivatives.^[42, 47] Despite a loss in conformational control on the overall architecture, most of the known supramolecular linear polymers based on H-bonding interactions incorporate aliphatic spacers, as they grant improved solubility in organic media.^[42, 46, 50] Moreover no helical supramolecular polymers have so far been visualized by STM at the solid-liquid interface.

In this chapter we describe a functionalized molecular module **1** capable of self-associating through self-complementary H-bonding patterns comprising interdigitated four strong and two medium strength H-bonds to form strongly bound dimers. The self-association of these

conformationally rigid phenylpyrimidine based dimers through directional H-bonding between two lateral pyridin-2(1H)-one units of neighboring molecules (Fig. 5.7) allowed the formation of two differently ordered supramolecular polymers as computationally described by dispersion-corrected density functional studies. In particular, a concentration dependent study by Scanning Tunneling Microscopy (STM) at the solid-liquid interface revealed the controlled molecular self-assembly on graphite forming either highly compact linear supramolecular arrays laterally interacting via van der Waals forces to generate micrometer-sized 2D nanopatterns, or hundreds of nanometers long helical supramolecular polymers featuring a high shape persistence.

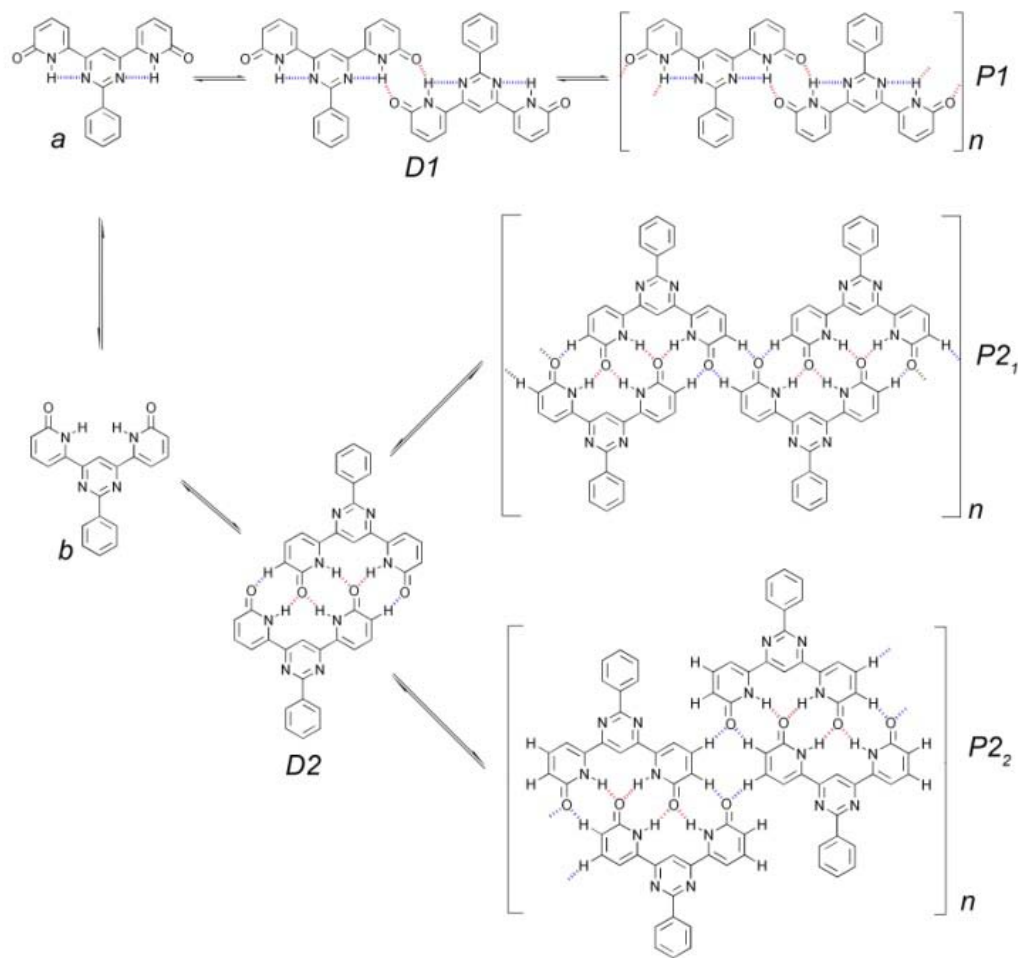


Figure 5.7 Molecular structure of the investigated molecule **1** in two possible isomers (*a* and *b*) and corresponding dimers (*D1* and *D2*) as well as related supramolecular polymers (*P1*, *P2₁* and *P2₂*) formed via hydrogen bonds between the dimeric units.

5.2.2 Results and discussion

Solution studies The C_2 symmetric isomer of the molecule **1** consists of two 2-pyridone units bridged by a phenylpyrimidine spacer. Although molecules bearing 2-pyridone moieties are known to form rigid dimers in the solid-state, the crystal structure of 2-pyridone incorporating systems can also display a second type of arrangement being a virtually infinitely long H-bonded linear polymer, i.e. featuring a catemer motif.^[51] Because of the very low solubility of **1** in both organic and inorganic media, NMR experiments were carried out using solutions in a polar organic solvent such as dimethyl sulfoxide (DMSO). Both ^1H NMR and 2D NMR studies revealed that the thermodynamically stable structure of molecule **1** is isomer **b** (Fig. 5.7 and 5.8).

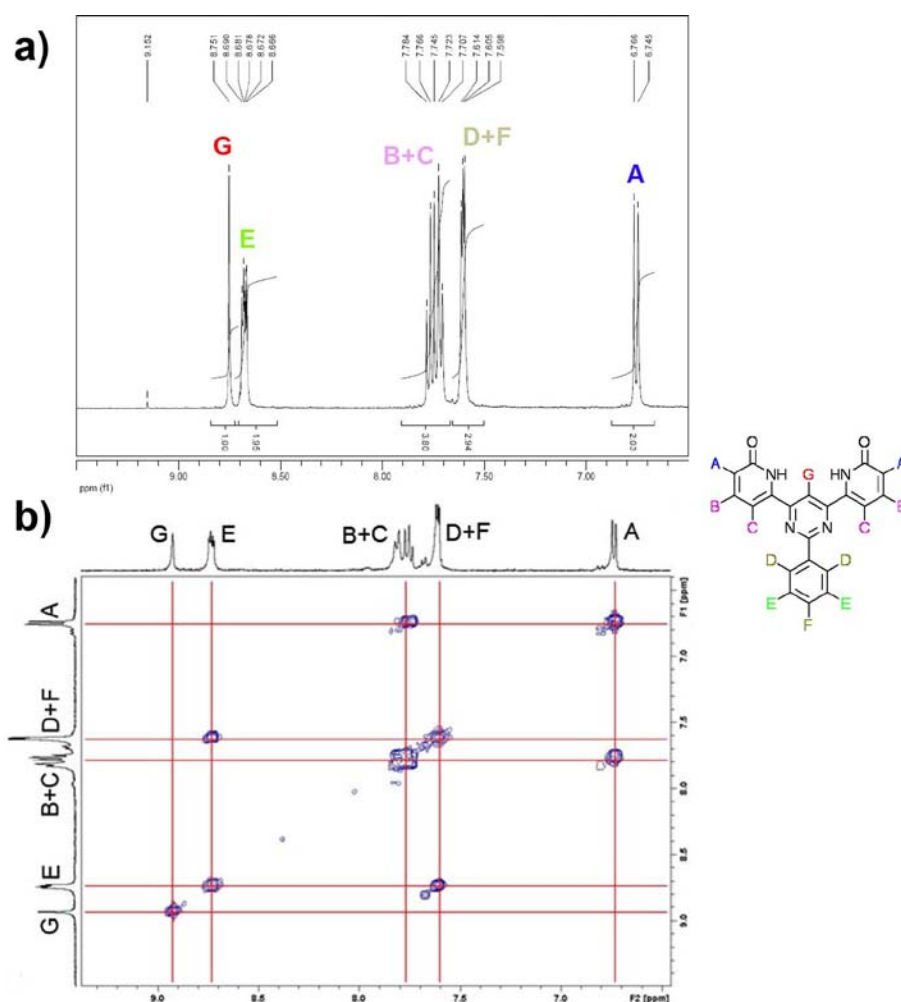


Figure 5.8 (a) Proposed pick assignment of **1** on the ^1H NMR spectra recorded at 95°C ; (b) 2D COSY spectrum ($[\text{D}_6]\text{DMSO}$, 25°C).

Since all NMR experiments were performed in DMSO, it is highly possible, that intramolecular N-H \cdots N H-bonds in isomer **a**, have been broken and DMSO molecules are now bounded with the molecule **1**. Under this hypothesis, the pyridone units can rotate through C-C (pyridone-pyrimidine) bond, resulting in the structure of **b** isomer of **1**. High resolution mass spectroscopy (HR-MS) provided further evidence for the presence, in DMSO solutions, of the supramolecular H-bonded species including dimers (Fig. 5.9a) and longer oligomeric species, observed over a wider spectrum range (Fig. 5.9b). Dimers **D2** (obtained from dimerisation of isomer **b** in Fig. 5.7) self-associate through additional hydrogen bonds between C-H \cdots O to form two types of supramolecular linear polymers. Both of them feature a greater number of co-existing H-bonds between dimers compared to the polymer **PI** that would be obtained by the assembly of the monomer adopting a different conformation (**a** in Fig. 5.7).

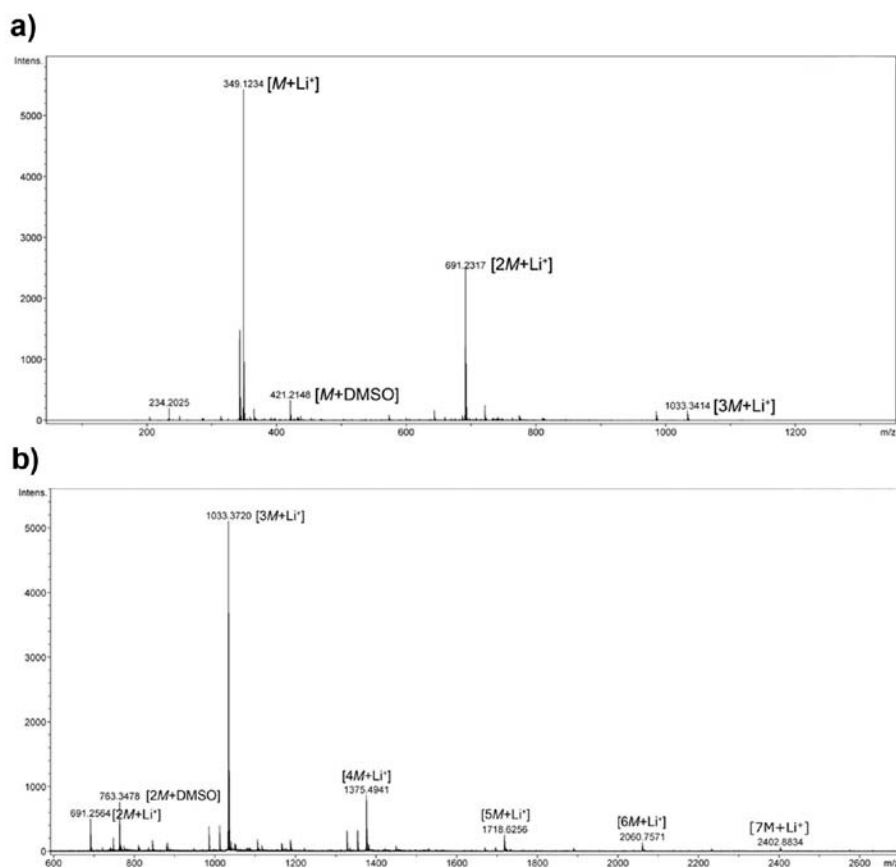


Figure 5.9 HR-MS (ES) spectrum of molecule **1** in DMSO in (a) medium and (b) large scale mass range.

Density functional calculations The conformations of isomers **a** and **b** were obtained by starting from planar conformations which were allowed to relax perpendicularly to the plane. This leads to a favored *non-planar* monomer conformation in the case of **b**, while **a** was found to be stable only in a *planar* conformation. At the single molecule level isomer **a** was found to be more stable than **b** (see Table 5.1) because of the two stabilizing intra-molecular hydrogen bonds (N-H...N). In the case of isomer **b**, the *non-planar* conformation was found to be slightly more stable than the *planar* one by 0.36 kcal/mol. The *non-planarity* of isomer **b**, comes from the tilting of pyridone units with respect to the central pyrimidine unit (Fig. 5.10).

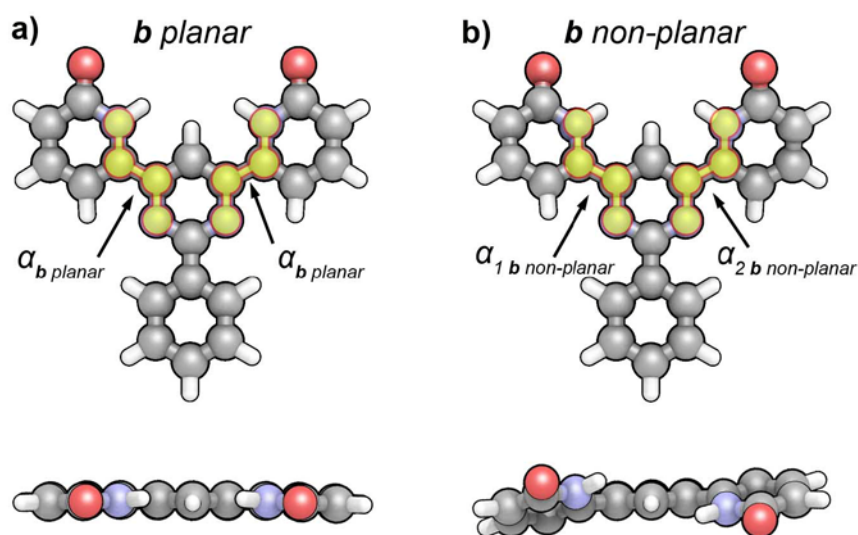


Figure 5.10 Final structures of investigated monomer **b** structure in its *planar* (a) and *non-planar* (b) conformation and indicated torsion angles.

Relative energies reported in the Table 5.1 are given with respect to the structure of isomer **b** in its *non-planar* conformation.

Monomer structure	Relative Energy (kcal/mol)	Pyridone-pyrimidine angle tilt (°)
<i>a planar</i>	-7.78	180
<i>a non-planar</i>	Not stable	N.A.
<i>b planar</i>	0.39	180
<i>b non-planar</i>	0	161

Table 5.1 Relative stability of all monomer structures derived from Figure 5.7. The energy of the *non-planar* conformation of monomer **b** will serve as reference throughout the paper.

We computed two possible dimer configurations **D1** and **D2** (Fig. 5.7) and estimated the strength of the hydrogen bonds, to gain insight into the experimental self-assembly behavior of many molecular units forming supramolecular H-bonded polymers. Their computed energies of formation are given in Table 5.2. Even though monomer **b** is predicted to be less stable than **a**, the data in Table 5.2 show that dimer **D2** is much more stable than **D1**. This can be explained by the number of H-bonds (six in **D2** vs. two in **D1**), it is further confirmed by the NMR data showing only presence of isomer **b**. Therefore we focused our attention on the structures derived from **D2**.

Interaction	E_{bind} (kcal/mol)
<i>D1 planar</i>	29.15
<i>D1 non-planar</i>	32.10
<i>D2 planar</i>	40.69
<i>D2 non-planar</i>	41.05
<i>D2-D2 planar(in T2₁)</i>	5.22
<i>D2-D2 helical(in T2₁)</i>	6.09
<i>D2-D2 planar(in T2₂)</i>	9.05
<i>D2-D2 helical(in T2₂)</i>	11.94

Table 5.2 Binding energy of two dimers (**D1**, **D2**) and interaction energies between the dimers in the corresponding polymeric structures. Intra-dimer energies are defined as $E = -(E_{\text{dimer}} - 2E_{b,\text{helical}})$; inter-dimer binding energies are $E = -(E_{\text{tetramer}} - 2E_{\text{dimer}})$.

The self-association of the *non-planar* dimers **D2** can lead to the formation of supramolecular polymers **P2₁** and **P2₂** (Fig. 5.7), which can eventually exhibit a helical conformation. To explore this conformational behavior we have computed tetramers **T2₁** and **T2₂** being segments of polymers **P2₁** and **P2₂**, respectively. Each tetramer was relaxed in its *planar* and *non-planar* conformation. The latter turned out to have a *helical* character.

Consistent with the previous results, the helical tetramers were found to be more stable than the planar conformations by 0.87 (**T2₁**) and 2.89 (**T2₂**) kcal/mol, with total binding energies per tetramer $E_{\text{bind}} = -(E_{\text{tot}} - 4E_{b,\text{helical}})$ calculated as 88.2 and 94.1 kcal/mol, respectively. To estimate the stability of longer polymer chains, we have also calculated the binding energies

corresponding to the dimer-dimer interaction within the polymeric structures, as given in Table 5.2. The total binding energies as well as the inter-dimer energies suggest that polymer $P2_2$ is slightly more stable than $P2_1$ in vacuum. From simple geometric arguments, it is possible to estimate the helical tilt angle between successive dimers from the relaxed helical tetramer structures. These values are found to be 26.8° ($T2_1$) and 3.6° ($T2_2$). The model of the helical supramolecular polymers $P2_2$ and $P2_2$ are portrayed in Figure 5.11.

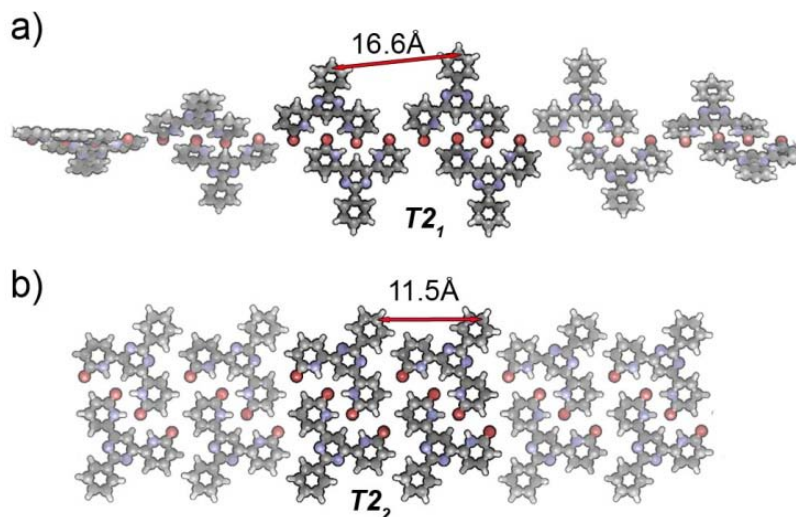


Figure 5.11 Relaxed structure of the 1D *helical* polymers based on tetramers (a) $T2_1$ and (b) $T2_2$. In the latter the *helical* character is barely visible because of the very small tilt angle of 3.6° .

One theoretical question remains about the formation and motif of extended planar 2D nanostructures. Figure 5.12 shows the $P2_1$ and $P2_2$ motif forming a monolayer of molecules which are laterally held together by two (C-H \cdots O) H-bonds and dispersive interactions. Both structures are made out of $D2$ dimers. The energies of formation, shown in Table 5.3, demonstrate clearly that $P2_2$ is more stable than $P2_1$. Such a greater stability is determined by a significantly higher packing density of the H-bond network, as proved by the smaller unit cell area per molecule.

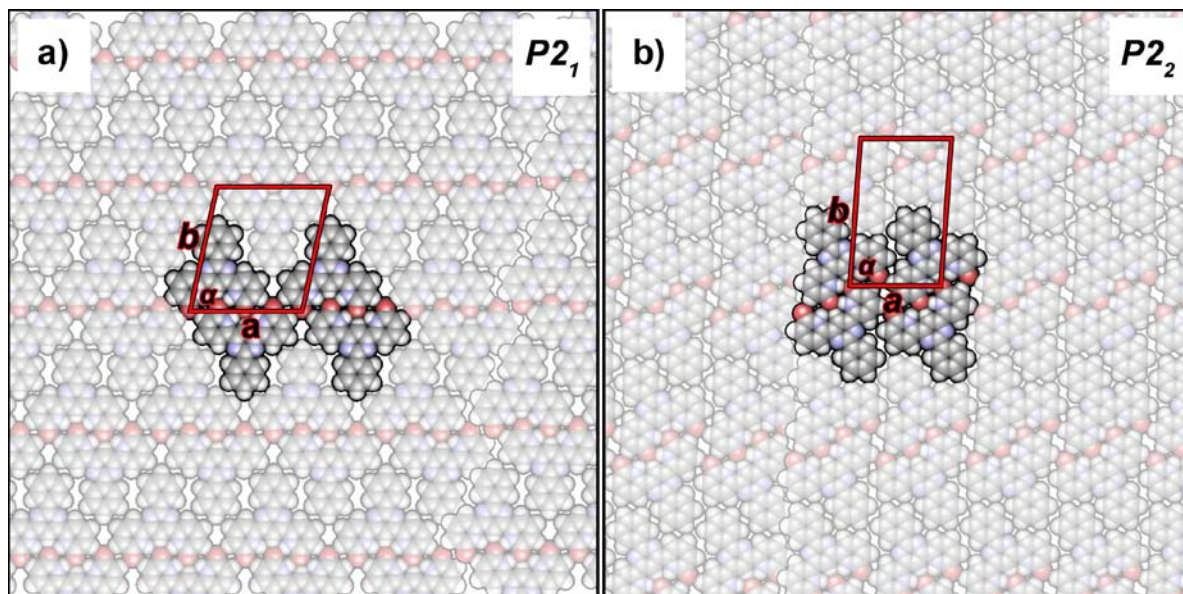


Figure 5.12 Relaxed structure of the 1D *planar* polymers (a) $P2_1$ and (b) $P2_2$ further stabilized by lateral van der Waals interactions to form planar 2D patterns. The optimized cell parameters and energetics are given in Table 5.3.

Structure	Binding energy E_{bind}	Cell parameters (a, b, α)	Cell area A (nm ²)
$P2_1$	52.28	(1.51, 1.71, 77.1°)	2.51
$P2_2$	54.27	(1.23, 2.01, 86.6°)	2.47

Table 5.3 Binding energy per dimer $E_{\text{bind}} = -(E_{\text{tot}} - 2E_{b,\text{helical}})$ (in kcal/mol) and unit cell parameters (a, b in nm) for the structures shown in Fig. 5.11.

STM Characterization Scanning tunneling microscopy (STM) was used to probe the self-assembly behavior of the molecule **1** at the solution-graphite interface. In light of the limited choice in the solvent as a result of the very poor solubility of **1**, a drop of a $60 \pm 1 \mu\text{M}$ solution in 1,2,4-trichlorobenzene (TCB) was applied to the graphite surface. Figure 5.13 shows STM height images of the obtained physisorbed monolayer featuring a polycrystalline structure, which consists of hundreds of square nanometers large crystalline domains that are stable over several minutes. These domains exhibit a unit cell: $a = (1.15 \pm 0.2)$ nm, $b = (1.91 \pm 0.2)$ nm, $\alpha = (87 \pm 2)^\circ$, leading to an area $A = (2.19 \pm 0.22)$ nm², where each unit cell contains two molecules **1**, i.e.

a dimer **D2** (indicated in red on Fig. 5.13c). This cell assignment for a layer of dimers **D2** is in accordance with the computed structure of $P2_2$ (Fig. 5.12b and 5.13c). The supramolecular hydrogen bonded polymer built from molecule **1** can be described as a sum of dimers **D2**, held together by four weak H-bonds $C=O\cdots H-C$, i.e. the bond holding together the **D2**. Within a dimer the two molecules **1** are interacting via four strong (N-H \cdots O) and two of medium strength (C-H \cdots O) H-bonds (Fig. 5.7). Furthermore, the entire supramolecular architecture is stabilized by lateral dispersion interactions between the phenyl rings of **1**, along with out-of-plane dispersion interactions that couple the 2D layer to the HOPG.

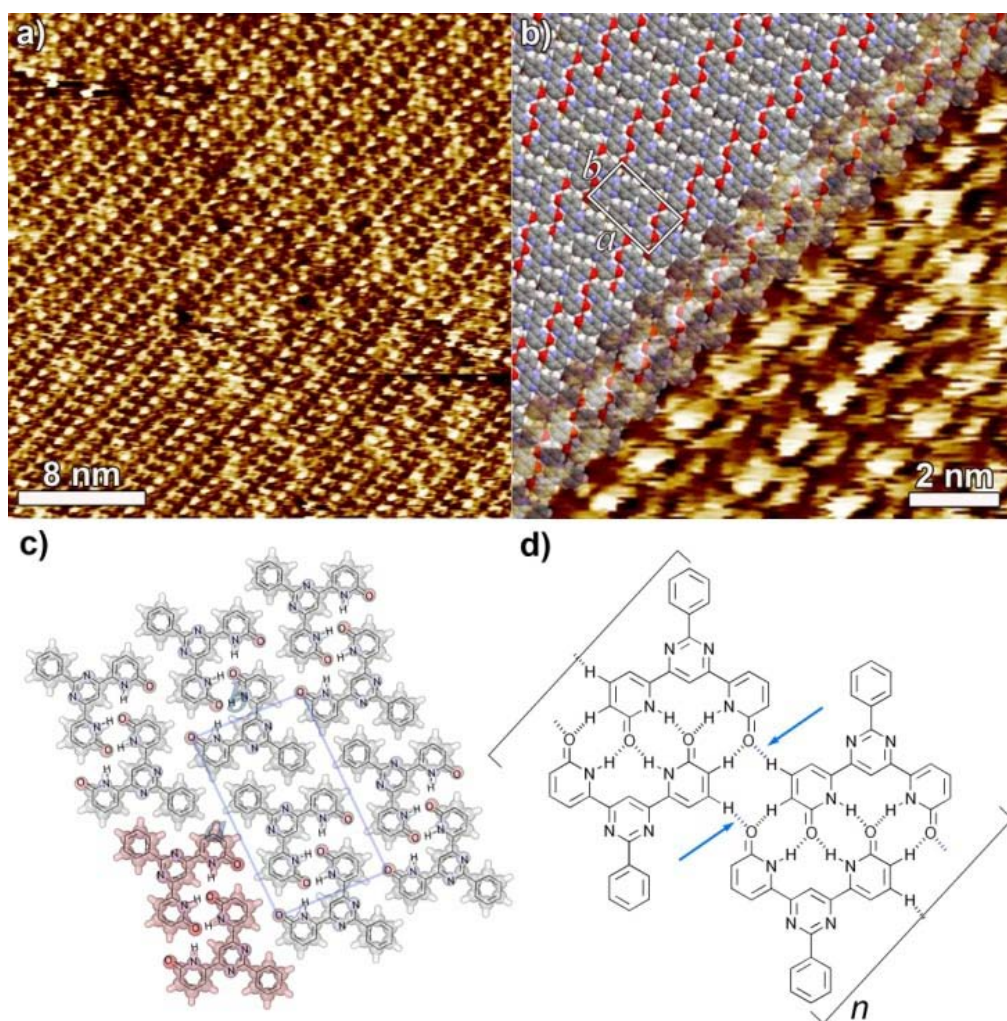


Figure 5.13 (a) and (b) STM height images of a film of linear supramolecular H-bonded polymer at the liquid-graphite interface self-assembled from solution in TCB forming the 2D nanopattern. Tunneling parameters: Average tunneling current (I_t) = 15 pA, tip bias voltage (V_t) = 300 mV; (c) Partial structure of computed layer consisting of **D2**, (d) Chemical structure of the H-bonded polymer.

Films prepared from less concentrated solutions ($5\pm 1\ \mu\text{M}$) reveal the first example of a helical supramolecular polymer at the solid-liquid interface, as displayed in the STM images in Figures 5.14a and 5.14b. Such an arrangement is dictated by the non co-planar nature of **D2** and the **D2-D2** bonds, which was already predicted by our calculations. Along a linear array in Figure 5.14b a reproducible periodicity in the height contrast was found. This periodic contrast can be assigned to a half-pitch of ca. 15 molecules. Under this hypothesis the tilt angle between two adjacent **D2** amounts to 12° . It is worth noticing that the structure of **P2** visualized with STM is slightly different than those predicted by DFT calculations, the latter showing tilt angles of either 27° or 3.6° , for **P2₁** or **P2₂**, respectively.

Based on this consideration, it is not yet possible to determine whether the *helical* polymers observed are of the form **P2₁** or **P2₂**. Given that the calculations were performed in vacuum, it is not surprising that the theoretically estimated tilt angles differ from the experimental values of 12° . In fact, due to the limited computational resources even on a state-of-the-art super-computer, our all-electron calculations could not consider both the non-covalent interactions between adsorbate - substrate and 1D supramolecular polymers forming 2D patterns. The latter leads to a partial overlap between adjacent supramolecular polymer chains as marked with red and blue circles in Figure 5.14b, corresponding to the phenyl substituents of neighboring molecules. Significantly, the intra-arrow distance between the circles (white arrow in Fig. 5.14b) amounts to $1.6\pm 0.2\ \text{nm}$, indicating that the previously calculated structure of **P2₁** (Fig. 5.11) is observed on the surface.

This observation excludes the alternative scenario, i.e. the helical **P2₂** configuration, which is somewhat surprising given the energetics presented in Table 5.2; such a behavior can be attributed to both adsorbate-substrate and/or solvent-molecule interactions. Molecules in the **P2₁** configuration are physisorbed on HOPG to form helical 2D patterns in order to maximize the interactions with the graphite surface.

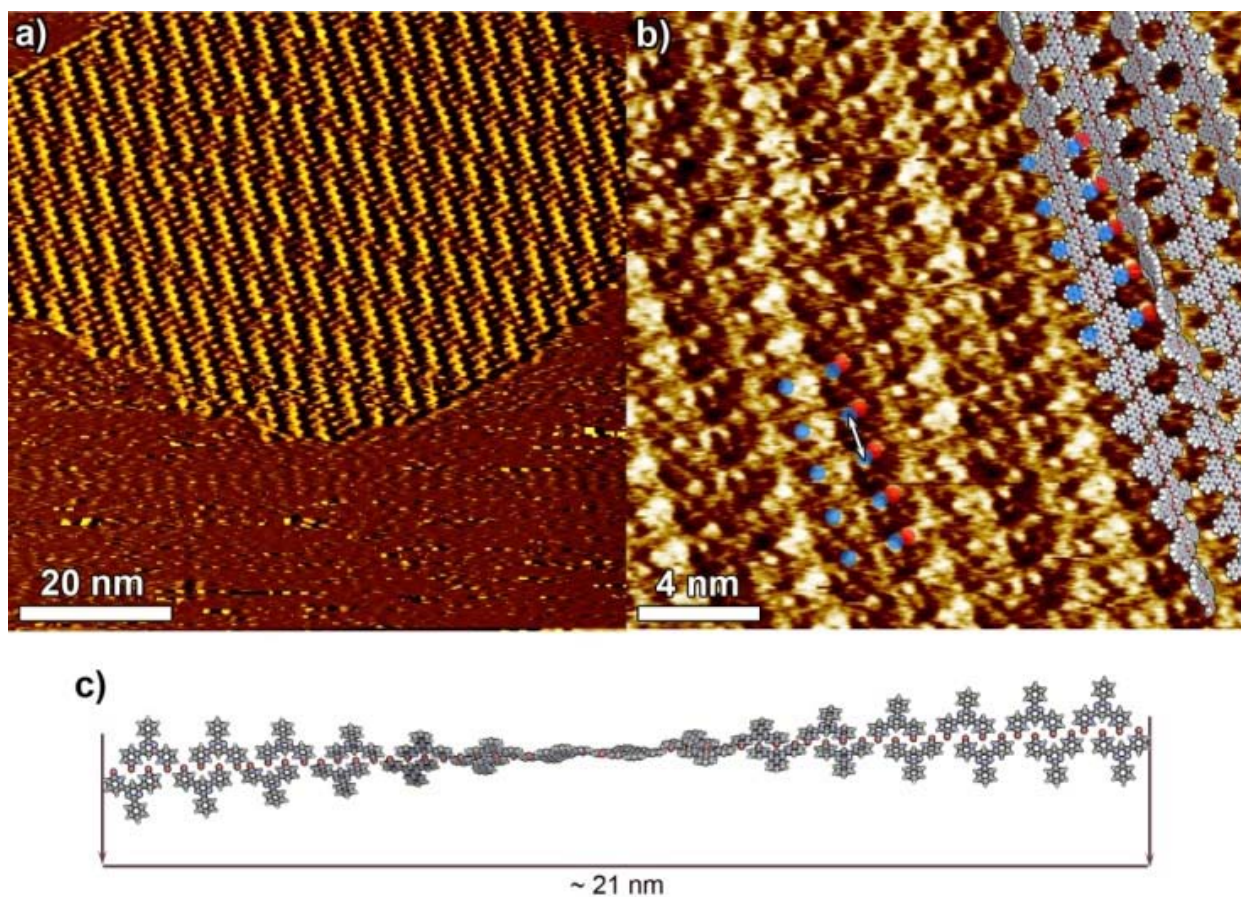


Figure 5.14 (a) and (b) STM height images of a film of linear supramolecular H-bonded polymer at the liquid-graphite interface self-assembled from solution in TCB. The helical architecture is evident in both the (a) large scale and (b) small scale image; (c) Schematic representation of the polymeric helical architecture having a half pitch of 21 nm. Tunneling parameters $I_t = 15\text{pA}$, $V_t = 300\text{ mV}$ in a) and b).

5.2.3 Conclusions

We described the bottom-up fabrication of highly compact supramolecular polymers ($P2_1$ and $P2_2$) composed of 6,6'-(2-phenylpyrimidine-4,6-diyl)dipyridin-2(1H)-one molecules based on the generation of four strong (N-H \cdots O) H-bonds which are further reinforced by two (C-H \cdots O) H-bonds of medium strengths. Scanning Tunneling Microscopy studies at the solid-liquid interface revealed that upon use of highly concentrated solutions, i.e. solutions between $2\pm 0.2\text{ mM}$ and $60\pm 1\text{ }\mu\text{M}$, the adsorption of the molecules adopting a nearly planar conformation on the HOPG surface and formation of $P2_2$ is promoted. Conversely, upon use of low concentrated solutions, i.e. from $60\pm 1\text{ }\mu\text{M}$ to $6\pm 0.5\text{ }\mu\text{M}$ the supramolecular arrays consisting of $P2_1$ whose

helical conformation is observed at the solid-liquid interface. The unambiguous assignment of the two structures was possible by using dispersion-corrected density functional calculations to relax the two-dimensional surface structure of both the planar and helical configurations. The possibility to develop helical supramolecular polymers at the solid-liquid interface is of potential interest for the fabrication of chiral surfaces from small achiral molecules. The present strategy relies on a design of supramolecular system that combines a rigid molecular module with multiple interdigitated H-bonds between donor/acceptor pairs. This strategy is of general applicability to the development of highly stable and compact supramolecular scaffolds and provides an enhanced control over the superstructure, leading to improved properties of the supramolecular material. The incorporation of functional units in the molecule may allow for the fabrication of a new generation of multifunctional yet responsive nanomaterials for electronics, catalysis and medicine.

5.2.4 Experimental procedure

Instrumentation ^1H NMR spectra were recorded using a Bruker Avance 400 spectrometer at 400 MHz. Chemical shifts are given in ppm. The residual solvent peak was used as reference for calibration (CDCl_3 : 7.26 ppm, $[\text{D}_6]\text{DMSO}$: 2.50 ppm). ^{13}C NMR spectra were recorded using a Bruker Avance 400 spectrometer at 100 MHz. All spectra were measured in broadband decoupled conditions. Chemical shifts are given in ppm. The residual solvent peak were taken as reference (CDCl_3 : 77.0 ppm, $[\text{D}_6]\text{DMSO}$: 39.43). Unless otherwise noted, spectra were recorded at 25°C. 2D NMR (COSY, NOESY) were recorded using a Bruker Avance 400 spectrometer. High Resolution Mass Spectrometry (HR-MS) analyses were performed on a Bruker Micro TOF mass spectrometer at the Service de Spectrométrie de Masse, Université de Strasbourg. The observed pattern was always compared to the theoretical pattern. For the grid-type complex analysis, the concentration was adjusted for approximately 5×10^{-3} mol/L in acetonitrile solution. At concentrations below 1×10^{-4} mol/L fragmentation products of the supramolecular polymer were observed. Elemental analyses were performed on a home built apparatus of the “Service d’Analyses du CNRS” (Lyon) and at the Service de Microanalyse, Université de Strasbourg. Data are given in percentage. Fast atom bombardment (FAB) mass spectra were recorded with a ZAB-HF VG spectrometer with m-nitrobenzyl alcohol as the matrix.

Scanning Tunneling Microscopy Current STM measurements were performed using a Veeco scanning tunneling microscope (multimode Nanoscope III, Veeco) at the interface between highly oriented pyrolytic graphite (HOPG) and a supernatant solution. Diluted solutions of **1** were applied to the basal plane of the surface. For STM measurements the substrates were glued on a magnetic disk and an electric contact is made with silver paint (Aldrich Chemicals). The STM tips were mechanically cut from a Pt/Ir wire (90/10, diameter 0.25 mm). The raw STM data were processed through the application of background flattening and the drift was corrected using the underlying graphite lattice as a reference. The latter lattice was visualized by lowering the bias voltage to 20 mV and raising the current to 65 pA. Mother solution of 6-6'-(2-phenylpyrimidine-4,6-diyl)dipyridin-2(1H)-one (**1**) was dissolved in DMSO at 95°C and diluted with 1,2,4-trichlorobenzene (TCB) to give 5 ± 1 μM and 60 ± 1 μM solutions. Monolayer pattern formation was achieved by applying 4 μL of a warm (60-70°C) solution onto freshly cleaved HOPG. Then STM images were recorded only after achieving a negligible thermal drift.

Density functional Calculations The relative stability of monomers, dimers, tetramers, and extended periodic structures obtained from **1**, was calculated using all-electron PBE-GGA^[52] density functional calculations with a numeric atomic orbital basis as implemented in the FHI-aims package.^[53] Dispersion interactions were accounted for by using a first-principles based "sum over C_6/R^6 "-scheme that has been shown to properly describe both hydrogen-bonded systems and purely dispersive interactions.^[54] The FHI-aims *tight* basis set and integration grids used throughout this study are converged to within 10^{-3} kcal/mol per dimer. All forces have been converged to within 5×10^{-3} eV/Å. This very tight criterion was required to reliably quantify the small energy differences between the various conformations. Vibrational modes and frequencies for the monomer and dimer structures were obtained using a finite-difference determination of the Hessian matrix, with displacements of $\pm 5\times 10^{-3}$ Å for each atomic coordinate. The unit cell geometry was relaxed for several different periodic dimer motifs, using a script based on the Atomic Simulation Environment.^[55]

References

- [1] T. F. A. Greef, E. W. Meijer, *Nature* **2008**, *453*, 171.

- [2] Q. W. Li, W. Y. Zhang, O. S. Miljanic, C. H. Sue, Y. L. Zhao, L. H. Liu, C. B. Knobler, J. F. Stoddart, O. M. Yaghi, *Science* **2009**, 325, 855.
- [3] G. A. Breault, C. A. Hunter, P. C. Mayers, *Tetrahedron* **1999**, 55, 5265.
- [4] L. C. Palmer, S. I. Stupp, *Acc. Chem. Res.* **2008**, 41, 1674.
- [5] J. A. A. W. Elemans, A. E. Rowan, R. J. M. Nolte, *J. Mater. Chem.* **2003**, 13, 2661.
- [6] P. Leclère, E. Hennebicq, A. Calderone, P. Brocorens, A. C. Grimsdale, K. Müllen, J. L. Brédas, R. Lazzaroni, *Prog. Polym. Sci.* **2003**, 28, 55.
- [7] H. Fenniri, B. L. Deng, A. E. Ribbe, *J. Am. Chem. Soc.* **2002**, 124, 11064.
- [8] J. H. van Esch, B. L. Feringa, *Angew. Chem. Int. Ed.* **2000**, 39, 2263.
- [9] A. Cnossen, D. Pijper, T. Kudernac, M. M. Pollard, N. Katsonis, B. L. Feringa, *Chem. Eur. J.* **2009**, 15, 2768.
- [10] A. Miura, Z. J. Chen, H. Uji-i, S. De Feyter, M. Zdanowska, P. Jonkheijm, A. P. H. J. Schenning, E. W. Meijer, F. Wurthner, F. C. De Schryver, *J. Am. Chem. Soc.* **2003**, 125, 14968.
- [11] M. Sofos, J. Goldberger, D. A. Stone, J. E. Allen, Q. Ma, D. J. Herman, W. W. Tsai, L. J. Lauhon, S. I. Stupp, *Nat. Mater.* **2009**, 8, 68.
- [12] L. Brunsveld, B. J. B. Folmer, E. W. Meijer, R. P. Sijbesma, *Chem. Rev.* **2001**, 101, 4071.
- [13] J. M. Lehn, *Polym. Int.* **2002**, 51, 825.
- [14] G. P. Spada, S. Lena, S. Masiero, S. Pieraccini, M. Surin, P. Samorì, *Adv. Mater.* **2008**, 20, 2433.
- [15] G. Gottarelli, S. Masiero, E. Mezzina, S. Pieraccini, J. P. Rabe, P. Samorì, G. P. Spada, *Chem. Eur. J.* **2000**, 6, 3242.
- [16] S. Lena, G. Brancolini, G. Gottarelli, P. Mariani, S. Masiero, A. Venturini, V. Palermo, O. Pandoli, S. Pieraccini, P. Samorì, G. P. Spada, *Chem. Eur. J.* **2007**, 13, 3757.
- [17] A. Gesquière, M. M. S. Abdel-Mottaleb, S. De Feyter, F. C. De Schryver, F. Schoonbeek, J. van Esch, R. M. Kellogg, B. L. Feringa, A. Calderone, R. Lazzaroni, J. L. Brédas, *Langmuir* **2000**, 16, 10385.
- [18] U. Ziener, E. Breuning, J. M. Lehn, E. Wegelius, K. Rissanen, G. Baum, D. Fenske, G. Vaughan, *Chem. Eur. J.* **2000**, 6, 4132.
- [19] A. Ajayaghosh, S. J. George, *J. Am. Chem. Soc.* **2001**, 123, 5148.

- [20] T. Gulik-Krzywicki, C. Fouquey, J. M. Lehn, *Proc. Nat. Acad. Sci. U.S.A.* **1993**, *90*, 163.
- [21] A. Llanes-Pallas, M. Matena, T. Jung, M. Prato, M. Stohr, D. Bonifazi, *Angew. Chem. Int. Ed.* **2008**, *47*, 7726.
- [22] J. V. Barth, J. Weckesser, C. Z. Cai, P. Günter, L. Bürgi, O. Jeandupeux, K. Kern, *Angew. Chem. Int. Ed.* **2000**, *39*, 1230.
- [23] S. B. Lei, C. Wang, S. X. Yin, H. N. Wang, F. Xi, H. W. Liu, B. Xu, L. J. Wan, C. L. Bai, *J. Phys. Chem. B* **2001**, *105*, 10838.
- [24] R. van Hameren, A. M. van Buul, M. A. Castriciano, V. Villari, N. Micali, P. Schon, S. Speller, L. M. Scolaro, A. E. Rowan, J. A. A. W. Elemans, R. J. M. Nolte, *Nano Lett.* **2008**, *8*, 253.
- [25] D. F. Perepichka, F. Rosei, *Science* **2009**, *323*, 216.
- [26] L. Grill, M. Dyer, L. Lafferentz, M. Persson, M. V. Peters, S. Hecht, *Nat. Nanotechnol.* **2007**, *2*, 687.
- [27] J. M. MacLeod, O. Ivasenko, D. F. Perepichka, F. Rosei, *Nanotechnology* **2007**, *18*, 424031.
- [28] J. Adisojoso, K. Tahara, S. Okuhata, S. Lei, Y. Tobe, S. De Feyter, *Angew. Chem. Int. Ed.* **2009**, *48*, 7353.
- [29] A. E. Rowan, R. J. M. Nolte, *Angew. Chem. Int. Ed.* **1998**, *37*, 63.
- [30] A. P. H. J. Schenning, A. F. M. Kilbinger, F. Biscarini, M. Cavallini, H. J. Cooper, P. J. Derrick, W. J. Feast, R. Lazzaroni, P. Leclere, L. A. McDonell, E. W. Meijer, S. C. J. Meskers, *J. Am. Chem. Soc.* **2002**, *124*, 1269.
- [31] R. Jaeger, H. Schönherr, G. J. Vancso, *Macromolecules* **1996**, *29*, 7634.
- [32] J. J. L. M. Cornelissen, M. Fischer, N. A. J. M. Sommerdijk, R. J. M. Nolte, *Science* **1998**, *280*, 1427.
- [33] R. B. Prince, L. Brunsveld, E. W. Meijer, J. S. Moore, *Angew. Chem. Int. Ed.* **2000**, *39*, 228.
- [34] L. Brunsveld, B. G. G. Lohmeijer, J. A. J. M. Vekemans, E. W. Meijer, *PCCP* **2000**, *2*, 2305.
- [35] D. B. Amabilino, E. Ramos, J. L. Serrano, T. Sierra, J. Veciana, *J. Am. Chem. Soc.* **1998**, *120*, 9126.
- [36] D. B. Amabilino, E. Ramos, J. L. Serrano, J. Veciana, *Adv. Mater.* **1998**, *10*, 1001.

- [37] Y. Ducharme, J. D. Wuest, *J. Org. Chem.* **1988**, *53*, 5787.
- [38] C. Fouquey, J. M. Lehn, A. M. Levelut, *Adv. Mater.* **1990**, *2*, 254.
- [39] S. Djurdjevic, D. A. Leigh, H. McNab, S. Parsons, G. Teobaldi, F. Zerbetto, *J. Am. Chem. Soc.* **2007**, *129*, 476.
- [40] M. Kotera, J. M. Lehn, J. P. Vigneron, *Chem. Commun.* **1994**, 197.
- [41] T. J. Murray, S. C. Zimmerman, *J. Am. Chem. Soc.* **1992**, *114*, 4010.
- [42] F. H. Beijer, R. P. Sijbesma, H. Kooijman, A. L. Spek, E. W. Meijer, *J. Am. Chem. Soc.* **1998**, *120*, 6761.
- [43] L. Brunsveld, J. A. J. M. Vekemans, J. H. K. K. Hirschberg, R. P. Sijbesma, E. W. Meijer, *Proc. Nat. Acad. Sci. U.S.A.* **2002**, *99*, 4977.
- [44] B. J. B. Folmer, R. P. Sijbesma, H. Kooijman, A. L. Spek, E. W. Meijer, *J. Am. Chem. Soc.* **1999**, *121*, 9001.
- [45] J. H. K. K. Hirschberg, L. Brunsveld, A. Ramzi, J. A. J. M. Vekemans, R. P. Sijbesma, E. W. Meijer, *Nature* **2000**, *407*, 167.
- [46] R. P. Sijbesma, F. H. Beijer, L. Brunsveld, B. J. B. Folmer, J. H. K. K. Hirschberg, R. F. M. Lange, J. K. L. Lowe, E. W. Meijer, *Science* **1997**, *278*, 1601.
- [47] S. H. M. Söntjens, R. P. Sijbesma, M. H. P. van Genderen, E. W. Meijer, *J. Am. Chem. Soc.* **2000**, *122*, 7487.
- [48] W. Jaunky, M. W. Hosseini, J. M. Planeix, A. De Cian, N. Kyritsakas, J. Fischer, *Chem. Commun.* **1999**, 2313.
- [49] A. Ciesielski, G. Schaeffer, A. Petitjean, J. M. Lehn, P. Samorì, *Angew. Chem. Int. Ed.* **2009**, *48*, 2039.
- [50] D. C. Sherrington, K. A. Taskinen, *Chem. Soc. Rev.* **2001**, *30*, 83.
- [51] C. B. Aakeröy, A. M. Beatty, M. Nieuwenhuyzen, M. Zou, *Tetrahedron* **2000**, *56*, 6693.
- [52] J. P. Perdew, K. Burke, M. Ernzerhof, *Phys. Rev. Lett.* **1996**, *77*, 3865.
- [53] V. Blum, R. Gehrke, F. Hanke, P. Havu, V. Havu, X. Ren, K. Reuter, M. Scheffler, *Comp. Phys. Comm.* **2009**, *180*, 2175.
- [54] A. Tkatchenko, M. Scheffler, *Phys. Rev. Lett.* **2009**, *102*, 073005.
- [55] S. R. Bahn, K. W. Jacobsen, *Computing in Science & Engineering* **2002**, *4*, 56.

Chapter 5.3

H-bonded bi-component supramolecular 1D polymers

The visualization of supramolecular bi-component polymers at liquid-solid interface paves the way towards the understanding of the mechanism of their formation at the surface. Systems based on six hydrogen bonds in a linear or *zig-zag* array can be obtained by mixing a Janus type of cyanuric wedge and a corresponding Hamilton receptor as ditopic complementary monomers. By using two different types of the wedges molecules featuring a different conformational rigidity we were able to control the geometry of linear supramolecular polymer. In the collaboration with the group of Prof. Jean-Marie Lehn from Institut de Science et d'Ingénierie Supramoléculaires (ISIS, Strasbourg, France) we designed bi-component supramolecular polymers, which were investigated by means of STM at the solid-liquid interface. The architecture consists of two alternating molecules bridged through six parallel H-bonds at each node using complementary ADA-ADA type of donor wedge and a corresponding (DAD-DAD array) receptor. A controlled geometry of the virtually infinite 1D architecture, i.e. a linear or a *zig-zag* motif, was obtained by using two different types of the wedges molecules featuring a different conformational rigidity.

The molecule described in this chapter has been synthesized by Gaël Schaeffer and Dr. Anne Petitjean, in the Laboratoire de Chimie Supramoléculaire of Prof. J.-M. Lehn.

5.3.1 Introduction

Self-assembly of molecular species into well-defined multi-component supramolecular architectures^[1] can be obtained by selective association of complementary building-blocks undergoing molecular recognition events. Among weak interactions, hydrogen bonds offer high control over the process of molecular self-assembly: due to its unique nature it combines reversibility, directionality, specificity and cooperativity. They have in particular been implemented for the generation of supramolecular polymers through the polyassociation of molecular components bearing complementary recognition groups.^[2-6] Supramolecular polymers can simultaneously display good material properties with low-viscosity melts.^[7] Their mechanical features result especially from secondary interactions, in particular the strength, reversibility and directionality of those interactions. Hitherto H-bonded supramolecular architectures have been self-assembled on solid surfaces into highly ordered motifs, both under ultra-high vacuum (UHV)^[8-10] and at the solid-liquid interface.^[11] While for the former case the formation of multi-component one-dimensional (1D) H-bonded polymers was recently reported,^[12, 13] for the latter so far the effort has been primarily devoted to H-bonded architectures consisting of multi-component discrete assemblies^[14-19] or to mono-component 1D polymers.^[20-23] The generation of ordered motifs stabilized by hydrogen bonds on a solid surface requires the fine tuning of the interplay between the interactions among neighboring molecules and the adsorbate-substrate interactions.^[24] The controlled formation of ordered multi-component architectures at the solid-liquid interface from a concentrated solution is thermodynamically unfavoured. In fact, among the various components in the supernatant solution, the one featuring a greater affinity for the substrate, i.e. offering a minimization of the free interface energy per unit area, will pack on its surface, whereas the others will remain solvated in the solution.^[25] To immobilize all the components on the surface, thus to achieve a complete physisorption of all the components at the solid-liquid interface, it is necessary to borrow a strategy commonly employed under UHV, i.e. mastering a control over the stoichiometry of the molecules absorbed at surfaces.^[26] At the solid-liquid interface the number of molecules in the solution applied to the surface should be lower than that required to form a monolayer of physisorbed molecules lying flat on the basal plane of the substrate. However, operating under such conditions, i.e. at low concentration, can lead to polymorphism.^[27, 28] Although the use of H-bonds to form bi-component linear supramolecular polymers was introduced over 15 years ago,^[4-6] to date the

STM visualization has not been explored at the liquid-solid interface for supramolecular polymers, composed of two components interacting via multiple hydrogen bonds, leading to an architecture with a controlled geometry and in principle an infinite length. Scanning tunneling microscopy (STM) at the solid-liquid interface has been proven to be the method of choice for the visualization of monolayers as it offers detailed sub-molecular scale insight into self-assembly of organic molecules on surfaces and its evolution with time with a millisecond resolution.

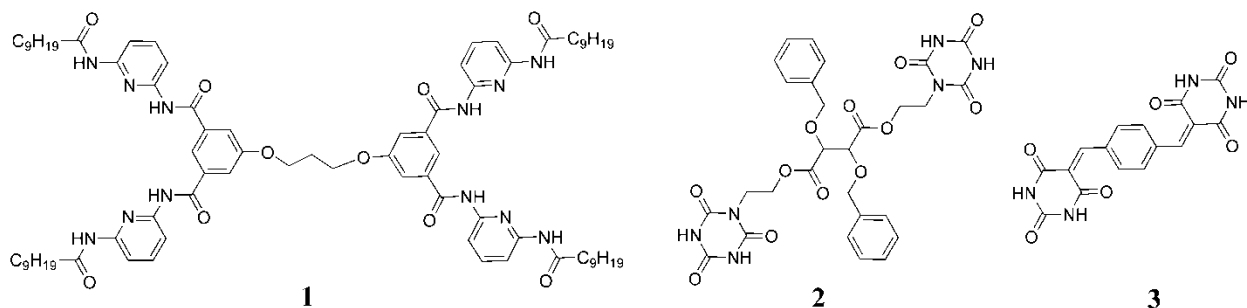


Figure 5.15 Ditopic molecular components bearing hydrogen bonding recognition groups.

In this chapter we present the STM visualization at liquid-solid interface at room temperature of the formation of supramolecular hydrogen-bonded polymers with either a linear or a *zig-zag* geometry on highly oriented pyrolytic graphite (HOPG) surfaces. To this end we used the ditopic molecular components **1-3** (Fig. 5.15) bearing complementary hydrogen bonding recognition groups: either a Janus type cyanuric wedge **2** or barbituric wedge **3** (ADA-ADA-array) and a corresponding (DAD-DAD-array) receptor unit **1**.^[29, 30] These molecules were selected because they are known to form 1D supramolecular polymeric strands in solution by polyassociation through sextuple hydrogen bonding between their respective recognition sites (Fig. 5.16).^[31]

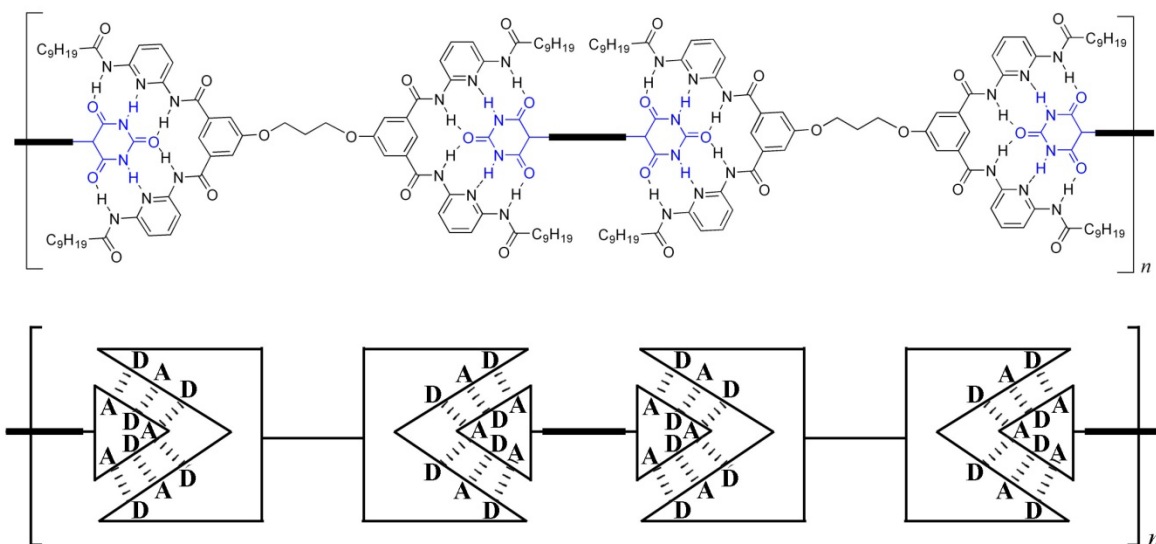


Figure 5.16 Formation of a main-chain supramolecular polymer by polyassociation of molecular monomers of type **1** and **2, 3** through sextuple hydrogen bonding between their complementary recognition units.

5.3.2 Results and discussion

We started by investigating the homo-molecular self-assembled structures obtained by applying a drop of a $6 \pm 1 \mu\text{M}$ solution of the molecule **1**^[32] in 1,2,4-trichlorobenzene (TCB) on the graphite surface. Figure 5.17 shows STM images of the obtained monolayer featuring a polycrystalline structure: two different domains **I** and **II** coexist for a few minutes (Fig. 5.17).

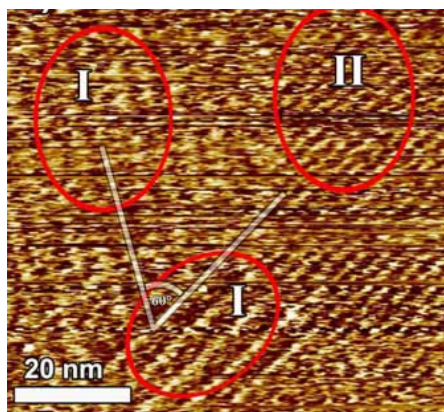


Figure 5.17 Survey STM image showing two polymorphous domains of molecule **1**, $I_t = 0.5 \text{ pA}$, $V_t = 150 \text{ mV}$.

The two crystals are characterized by a different packing motif. The assembly in domain **I** presents parallel lamellae (Fig. 5.18a) and has a unit cell $a = (1.78 \pm 0.2)$ nm, $b = (5.62 \pm 0.2)$ nm, and $\alpha = (90 \pm 2)^\circ$, corresponding to an area $A = (10.0 \pm 1.2)$ nm², given that each unit cell contains one molecule **1**. Given its size there is space enough to accommodate all the aliphatic side groups on the surface, although since we have not resolved them, we do not have unambiguous confirmation of this aspect. It is interesting to point out that the life time of domain **I** was very short, i.e. it disappeared after a few minutes, proving its metastable nature. The poor stability of domain **I** was also evidenced by its high molecular dynamics on a time scale comparable to that of the tip scanning. For this reason we have not been able to achieve a high sub-molecular resolution. Such a poor stability is not surprising: for enthalpy reasons, the system is prone to form a densely packed assembly, thus minimizing the size of the unit cell. The more stable domain **II** features the unit cell: $a = (4.42 \pm 0.2)$ nm, $b = (5.65 \pm 0.2)$ nm, $\alpha = (90 \pm 2)^\circ$, leading to an area $A = (24.9 \pm 1.4)$ nm², where each unit cell contains four molecules **1** (Fig. 5.18b). Among them, one molecule (marked with white arrow) seems to be partially desorbed. Given the area of the darker spots in the STM image $A_{S1} = (11 \pm 2)$ nm² (Fig. 5.19), and by comparing it with the area occupied by a 2D projected C_9H_{19} chain $A_{C_9H_{19}} = (0.33 \pm 0.02)$ nm², it is likely that all fourteen nonyl side chains are physisorbed on the HOPG surface, although, due to their high dynamics, we are unable to resolve them.

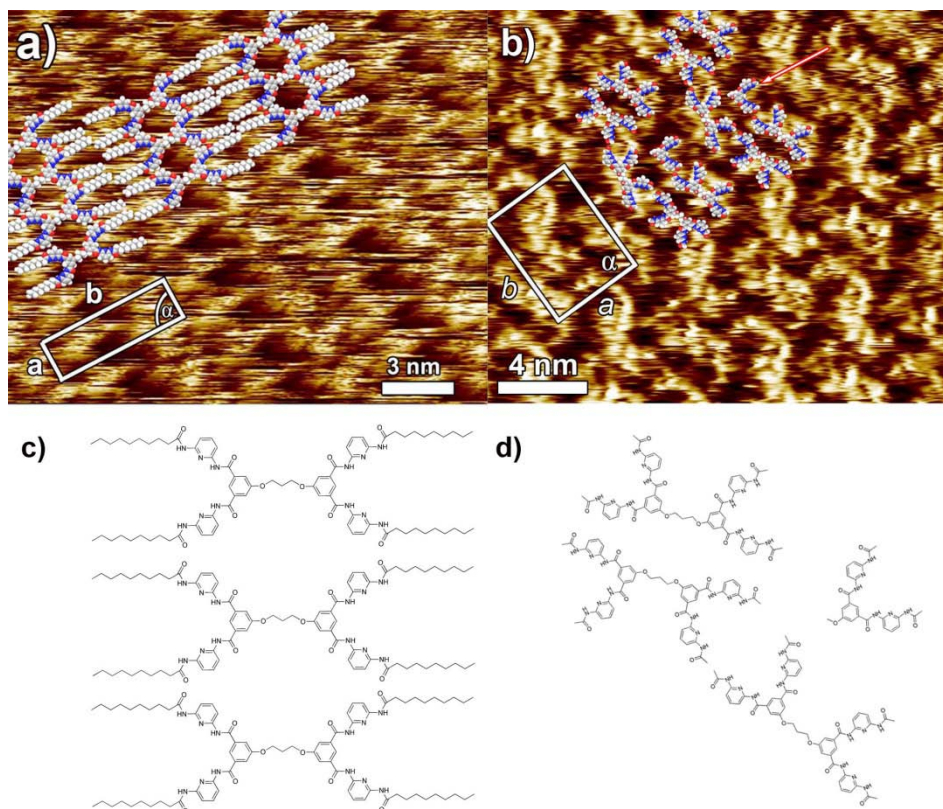


Figure 5.18 STM height images of a monolayer of molecule **1** at the liquid-graphite interface self-assembled from a solution 1,2,4-trichlorobenzene. (a) Zoom-in image of domain **I**; $I_t = 0.5$ pA, $V_t = 100$ mV, (b) Zoom-in of domain **II**; $I_t = 15$ pA, $V_t = 300$ mV, (c) molecular model of the molecular crystallites in domain **I**; (d) molecular model of the molecular crystallites in domain **II**.

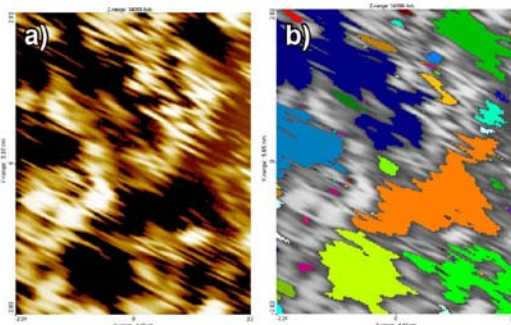


Figure 5.19 Empty areas computed using SPIP software; (a) as an example we show a zoom into the STM image of 2D crystal of molecule **1** on HOPG; (b) the colored domains are those whose area have been estimated through an automatic procedure of pixel counting.

We have then extended our studies to hetero-molecular non-covalently engineered main-chain supramolecular polymers resulting from the self-assembly on graphite from a bi-component

solution including molecule **1** and either molecule **2** or **3**.^[33, 34] It is important to note that molecule **1** was visualized at the HOPG – solution interface only upon using TCB as solvent. Study of this system in different solvents, i.e. 1-phenyloctane and tetradecane, did not produced any ordered monolayers. Because of this reason we continued our study using TCB as a solvent. It is worth pointing out that both molecules **2** and **3** were not found to form ordered structures in single-component films at the liquid-solid interface, highlighting a low affinity for the graphite surface. The hetero-molecular monolayer was formed by applying to the surface a 4 μL drop of the solution in TCB. The two bi-component solutions have been obtained by mixing 5-10 mM solutions of **1+2** or **1+3** in DMSO and subsequently diluting them with TCB to yield concentrations of $4\pm 1 \mu\text{M}$ and $3\pm 1 \mu\text{M}$ for **1+2** and **1+3**, respectively. The procedure for the deposition of the two components on the surface is critical for the formation of the mixed polymer: it was indeed found that if one partner molecule is already physisorbed on the surface, its partial desorption is energetically unfavorable, thereby hindering the emergence of molecular recognition leading to homogeneous intermixing on the substrate surface. Therefore both **1+2** and **1+3** solutions were prepared *ex situ*. It is important to note that the formation of bi-component polymers was visualized only when the ratio of the concentrations of the molecules was $30\pm 5 \%$ of molecule **1** to $70\pm 5 \%$ of molecule **2** and **3**.

By decreasing the concentration of molecules **2** and **3** or increasing the concentration of molecule **1**, only patterns of molecule **1** were seen on the HOPG surface. This observation confirms the greater affinity of molecule **1** for the graphite surface.

Figure 5.20a shows a STM height image of the linear hetero-molecular polymer resulting from deposition of a mixture of molecules **1** and **2**. The monolayer displays a polycrystalline structure, which consists of tens of nanometer-wide domains that are stable over several minutes. The proposed packing motif is in excellent agreement with that suggested by modeling (Fig. 5.16): the symmetric molecule **1** is forming six hydrogen bonds with each neighboring molecule **2**. The formation of a linear architecture is made possible especially taking advantage of the conformational flexibility of the cyanuric wedge **2**. All the cores of the molecules are physisorbed flat on the surface. The unit cell parameters amounts to $a = (2.72 \pm 0.2) \text{ nm}$, $b = (3.45 \pm 0.2) \text{ nm}$, and $\alpha = (35.8 \pm 2)^\circ$, leading to an area $A = (5.5 \pm 0.6) \text{ nm}^2/\text{dimer}$, where each unit cell contains one molecule **1** and one molecule **2** (Fig. 5.19a). Figure 5.20c displays the proposed supramolecular motif featuring a bi-component linear association **1+2**, which matches

the pattern observed in the STM image, ruling out the presence of the energetically equivalent armchair based motif. Deposition of a small amount (around 4 μL) of molecule **1** and of the bridging molecule **3** in a stoichiometry 3:7 results also in the formation of a 1D hetero-molecular polymer. However, differently from the linear motif observed for **1+2**, the bi-component supramolecular polymer displays an intra-lamellar *zig-zag* geometry. The angle β between the two adjacent molecular units in the 1D supramolecular polymer amounts to $90 \pm 2^\circ$. This change in packing can be ascribed to the greater rigidity of molecule **3** compared to **2**. In order to enable hetero-molecular association of two edges of molecule **1**, the latter system needs to adopt a bent-conformation, which is possible thanks to its central flexible moiety i.e. the $-\text{OC}_3\text{H}_6\text{O}-$ unit. The distance between the two parallel lamellae, i.e. between two bright adjacent structures in the STM image, corresponds to the length of C_9H_{19} -chains indicating that in this case all the C_9H_{19} -chains of molecule **1** are physisorbed on the HOPG surface. However, given the dynamics on a time scale faster than the tip scanning, we were not able to resolve them (Fig. 5.20b). The darker areas in the STM current images have been estimated in both Figures, i.e. 5.20a and 5.20b and compared with the space that should be occupied by the nonyl chains physisorbed on the graphite. They were found to be $A_{s1+2} = 0.85 \text{ nm}^2$ and $A_{s1+3} = 2.45 \text{ nm}^2$ for **1+2** and **1+3** respectively, whereas the modeled area occupied by each C_9H_{19} chain amounts to $A_{\text{C}_9\text{H}_{19}} = (0.33 \pm 0.02) \text{ nm}^2$. This suggests that for the monolayer of **1+2** (most of) the chains are backfolded in the supernatant solution, whereas for **1+3** they are packed on the surface. The unit cell parameters amount to $a = (3.93 \pm 0.2) \text{ nm}$, $b = (4.27 \pm 0.2) \text{ nm}$, $\alpha = (75 \pm 2)^\circ$, $A = (16.2 \pm 1.2) \text{ nm}^2/\text{dimer}$, where each unit cell contains two molecules **1** and two molecules **3** (Fig. 5.20a). Figure 5.20d depicts the proposed packing model of a fragment of the bi-component linear polymer **1+3**. Also in this case each molecule **1** is forming six hydrogen bonds with each neighboring molecules **3**.

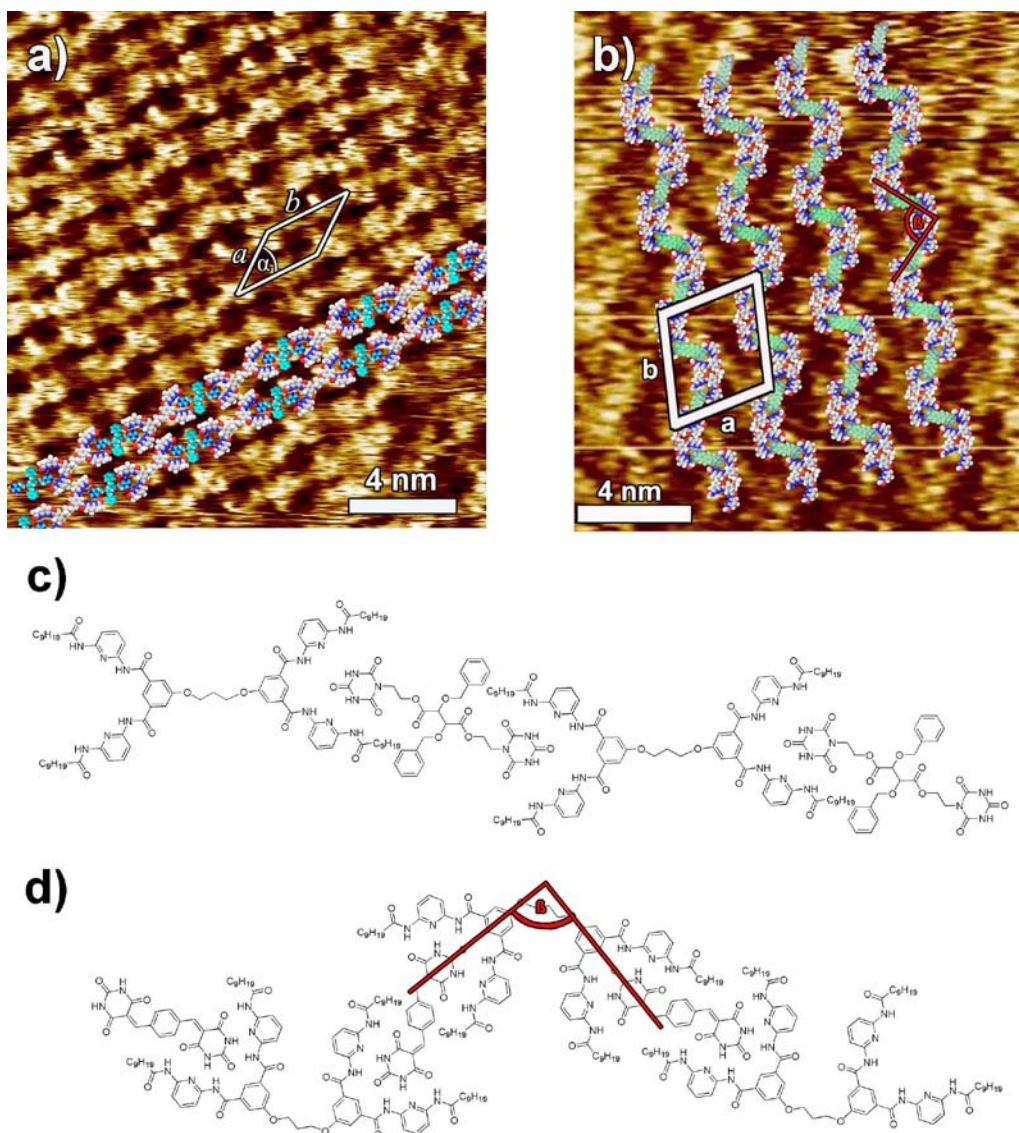


Figure 5.20 (a) and (b) STM height images of a monolayer of linear bi-component supramolecular H-bonded polymer at the liquid-graphite interface self-assembled from TCB solution; (a) small scale image displays linear structure of polymer **1+2**; $I_t = 20$ pA, $V_t = 300$ mV; the area of the darker spots $A_s = 1.3 \pm 2$ nm²; (b) zoomed image of domain contains self-assembled bi-component polymer **1+3**; $I_t = 20$ pA, $V_t = 300$ mV; the area of the darker spots $A_s = 4 \pm 1$ nm²; (c) molecular model of the linear polymer **1+2**; (d) molecular model of the linear polymer **1+3**.

5.3.3 Conclusions

In summary, by working in a low concentration regime, that is in experimental conditions not susceptible to thermodynamically driven phase segregation between two components on the

solid-liquid interface, we have been able for the first time to visualize by STM on the molecular scale the physisorption of 1D main-chain bi-component H-bonded supramolecular polymers at surfaces. This was possible by proper design of complementary building blocks linked by the formation of six H-bonds at each node. By using two different wedge molecules **2** and **3** featuring a different conformational rigidity, we were able to control the geometry of the linear supramolecular polymer. When a flexible component was used to bridge molecules **1**, a linear structure was obtained, whereas when the bridging molecule was rigid, a *zig-zag* motif was observed. The visualization of bi-component supramolecular polymers at liquid-solid interface paves the way towards the understanding of the mechanism of their formation on surfaces.^[7] It also adds further weight to the initial concept of supramolecular polymers and supramolecular polymer chemistry,^[35] that has by now been widely implemented, in particular in the bulk. Furthermore, the generation of rigid bi-component supramolecular polymers (supramolecular polymer **1+3**) presenting a controlled curvature at the liquid-solid interface represents the first important step towards the nanopatterning of surfaces with multi-component functional architectures for exploitation of vectorial properties. The introduction of cross-linking components^[31] may allow extension into 2D supramolecular assemblies.

5.3.4 Experimental procedure

Scanning Tunneling Microscopy STM measurements were performed using a Veeco scanning tunneling microscope (multimode Nanoscope III, Veeco) at the interface between highly oriented pyrolytic graphite (HOPG) and a supernatant solution. Diluted solutions of molecule **1** or bi-component polymers **1+2** and **1+3** were applied to the basal plane of the surface. For STM measurements the substrates were glued on a magnetic disk and an electric contact is made with silver paint (Aldrich Chemicals). The STM tips were mechanically cut from a Pt/Ir wire (90/10, diameter 0.25 mm). The raw STM data are processed by the application of background flattening and the drift is corrected using the underlying graphite lattice as a reference. Measurements of the area of the dark zones between molecular crystallites in the STM images, were computed by using SPIPTM software (Fig. 5.17). The latter lattice is imaged underneath the molecules by lowering the bias voltage to 20 mV and raising the current to 65 pA. All of the models were minimized with Chem3D at the MM2 level. Mother solution of 1,3-Bis(3,5-bis(6-decanoylamino)pyridin-2-ylcarbamoyl)phenoxy)propane (**1**) was dissolved in DMSO and diluted

with 1,2,4-trichlorobenzene (TCB) to give 6 ± 1 μM solution. Preparation of molecule **1** has been described elsewhere. Monolayer pattern formation was achieved by applying $4\mu\text{L}$ of a warm (30 – 40°C) solution onto freshly cleaved HOPG. Supramolecular polymers were obtained by mixing 5 – 10mM solutions of **1** with 5 – 10mM solutions of **2** or **3** in DMSO and diluting the mixture with TCB to yield concentrations of 4 ± 1 μM and 3 ± 1 μM for **1+2** and **1+3**, respectively.

References

- [1] J.-M. Lehn, *Supramolecular chemistry: concepts and perspectives*, VCH New York, **1995**.
- [2] C. Fouquey, J.-M. Lehn, A.-M. Levelut, *Advanced Materials* **1990**, *2*, 254.
- [3] L. Brunsveld, B. J. B. Folmer, E. W. Meijer, R. P. Sijbesma, *Chem. Rev.* **2001**, *101*, 4071.
- [4] J. M. Lehn, *Polym. Int.* **2002**, *51*, 825.
- [5] J. M. Lehn, *Prog. Polym. Sci.* **2005**, *30*, 814.
- [6] T. Gulik-Krzywicki, C. Fouquey, J. M. Lehn, *Proc. Natl. Acad. Sci. USA* **1993**, *90*, 163.
- [7] T. F. A. Greef, E. W. Meijer, *Nature* **2008**, *453*, 171.
- [8] J. V. Barth, *Annu. Rev. Phys. Chem.* **2007**, *58*, 375.
- [9] J. V. Barth, G. Costantini, K. Kern, *Nature* **2005**, *437*, 671.
- [10] F. Rosei, M. Schunack, Y. Naitoh, P. Jiang, A. Gourdon, E. Laegsgaard, I. Stensgaard, C. Joachim, F. Besenbacher, *Prog. Surf. Sci.* **2003**, *71*, 95.
- [11] S. De Feyter, F. C. De Schryver, *Chem. Soc. Rev.* **2003**, *32*, 139.
- [12] M. E. Cañas-Ventura, W. Xiao, D. Wasserfallen, K. Müllen, H. Brune, J. V. Barth, R. Fasel, *Angew. Chem. Int. Ed* **2007**, *46*, 1814.
- [13] A. Llanes-Pallas, M. Matena, T. Jung, M. Prato, M. Stöhr, D. Bonifazi, *Angew. Chem. Int. Ed.* **2008**, *47*, 7726.
- [14] K. G. Nath, O. Ivasenko, J. A. Miwa, H. Dang, J. D. Wuest, A. Nanci, D. F. Perepichka, F. Rosei, *J. Am. Chem. Soc.* **2006**, *128*, 4212.
- [15] S. De Feyter, M. Larsson, A. Gesquiere, H. Verheyen, F. Louwet, B. Groenendaal, J. van Esch, B. L. Feringa, F. De Schryver, *Chemphyschem* **2002**, *3*, 966.

- [16] W. Mamdouh, R. E. A. Kelly, M. D. Dong, L. N. Kantorovich, F. Besenbacher, *J. Am. Chem. Soc.* **2008**, *130*, 695.
- [17] A. Miura, Z. J. Chen, H. Uji-i, S. De Feyter, M. Zdanowska, P. Jonkheijm, A. P. H. J. Schenning, E. W. Meijer, F. Wurthner, F. C. De Schryver, *J. Am. Chem. Soc.* **2003**, *125*, 14968.
- [18] K. Eichhorst-Gerner, A. Stabel, G. Moessner, D. Declerq, S. Valiyaveetil, V. Enkelmann, K. Müllen, J. P. Rabe, *Angew. Chem. Int. Ed.* **1996**, *35*, 1492.
- [19] S. De Feyter, A. Miura, S. Yao, Z. Chen, F. Wurthner, P. Jonkheijm, A. P. H. J. Schenning, E. W. Meijer, F. C. De Schryver, *Nano Lett.* **2005**, *5*, 77.
- [20] G. P. Spada, S. Lena, S. Masiero, S. Pieraccini, M. Surin, P. Samorì, *Adv. Mater.* **2008**, *20*, 2433.
- [21] H. Zhou, H. Dang, J. H. Yi, A. Nanci, A. Rochefort, J. D. Wuest, *J. Am. Chem. Soc.* **2007**, *129*, 13774.
- [22] S. De Feyter, A. Gesquiere, F. De Schryver, C. Meiners, M. Sieffert, K. Müllen, *Langmuir* **2000**, *16*, 9887.
- [23] G. Gottarelli, S. Masiero, E. Mezzina, S. Pieraccini, J. P. Rabe, P. Samorì, G. P. Spada, *Chem. Eur. J.* **2000**, *6*, 3242.
- [24] J. P. Rabe, S. Buchholz, *Science* **1991**, *253*, 424.
- [25] C. A. Palma, M. Bonini, T. Breiner, P. Samorì, *Adv. Mater.* **2009**, *21*, 1383.
- [26] C. A. Palma, M. Bonini, A. Llanes-Pallas, T. Breiner, M. Prato, D. Bonifazi, P. Samorì, *Chem. Commun.* **2008**, 5289.
- [27] S. B. Lei, K. Tahara, F. C. De Schryver, M. Van der Auweraer, Y. Tobe, S. De Feyter, *Angew. Chem. Int. Ed.* **2008**, *47*, 2964.
- [28] L. Kampschulte, T. L. Werblowsky, R. S. K. Kishore, M. Schmittel, W. M. Heckl, M. Lackinger, *J. Am. Chem. Soc.* **2008**, *130*, 8502.
- [29] S. K. Chang, A. D. Hamilton, *J. Am. Chem. Soc.* **1988**, *110*, 1318.
- [30] S. K. Chang, D. Van Engen, E. Fan, A. D. Hamilton, *J. Am. Chem. Soc.* **1991**, *113*, 7640.
- [31] V. Berl, M. Schmutz, M. J. Krische, R. G. Khoury, J. M. Lehn, *Chem. Eur. J.* **2002**, *8*, 1227.
- [32] E. Kolomiets, E. Buhler, S. J. Candau, J. M. Lehn, *Macromolecules* **2006**, *39*, 1173.

- [33] Z. Q. Wang, L. Y. Wang, X. Zhang, J. C. Shen, S. Denzinger, H. Ringsdorf, *Macromol. Chem. Phys.* **1997**, *198*, 573.
- [34] B. S. Jursic, E. D. Stevens, *Tetrahedron Lett.* **2003**, *44*, 2203.
- [35] J. M. Lehn, *Macromol. Symp.* **1993**, *69*, 1.

Chapter 5.4

Self-assembly of N^9 -alkylguanines at the solid-liquid interface

Molecular self-assembly is central to many processes in both biology and supramolecular chemistry. The G-quartet, a hydrogen-bonded macrocycle formed by cation-templated assembly of guanosine, was first identified in 1962 as the basis for the aggregation of 5'-guanosine monophosphate. Nowadays it is well known that many nucleosides, oligonucleotides, and synthetic derivatives form a rich array of functional G-quartets. The G-quartet, a hydrogen-bonded complex that binds cations, fits particularly well with contemporary studies in molecular self-assembly and non-covalent synthesis. However, to understand better the formation of complicated structures like double-helix of DNA, we have to understand first the self-assembly of its building blocks, i.e. nucleic acids. In the collaboration with the group of Prof. Gian Piero Spada from Bologna University (Italy), we designed and investigated by means of STM, a series of N^9 -substituted alkylguanines molecular modules capable of self-associating, through self-complementary H-bonding patterns .

The molecules described in this chapter has been synthesized by Rosaria Perone, in the group of Prof. Gian Piero Spada from Bologna University (Italy).

5.4.1 Introduction

The self-assembly of small molecular modules into non-covalently linked polymeric nanostructures is a subject of continuous interest.^[1-4] In particular, supramolecular structures with high degree of order can be obtained through the self-association of organic molecules on flat solid surfaces.^[5-8] Such structures can be used as scaffolds to position electrically/ optically active groups in pre-determined locations in 2D,^[9, 10] thereby paving the way towards a wide range of applications, e.g. in electronic and optical devices.^[11] Unique character of H-bonding, which offer high control over the process of molecular self-assembly, is on the basis of sophisticated programs for self-assembly such as those based the Watson-Crick base pairing^[12] which direct the formation of the helical structure of DNA. Among nucleobases, guanine is very versatile.^[13-15] depending on the experimental conditions it can undergo different self-assembly pathways. In the presence of certain metal ions, guanines can form G-quartet based architectures (Fig. 5.21b) such as octamers or columnar polymeric aggregates.^[13, 16-20] In the absence of metal templates, guanines without C(8) sterically demanding substituent^[21] can self-assemble, both in solution and in the solid state, into ribbonlike architectures.^[14, 22-26] For guanosine derivatives physisorbed at surfaces the thermodynamically stable ribbons were found to be characterized by cyclic NH(2)-O(6) and NH(1)-N(7) hydrogen bonds (Fig. 5.21c). In the solid state, the ribbons, by bridging gold electrodes, were found to be photoconductive.^[27] More interestingly, these ribbons also exhibit rectifying properties.^[28] A field-effect transistor based on this supramolecular structures, was described.^[29] Hitherto guanine based H-bonded supramolecular architectures were self-assembled on surfaces into highly ordered motifs and studied with scanning tunneling microscopy (STM) under ultra-high vacuum (UHV).^[30, 31] Conversely at the solid-liquid interface the effort was mainly addressed towards the study of lipophilic guanosine monolayers.^[14, 32, 33] We decided to study at the solid-liquid interface physisorbed monolayers of N^9 -alkylguanines because the absence of the sugar when compared to the previously studied guanosines and the presence of an aliphatic side-group can be foreseen to favor the molecular adsorption on graphite.^[3] In general, the formation of ordered motifs stabilized by hydrogen bonds on a solid surface requires the fine tuning of the interplay between the interactions among adjacent molecules and the adsorbate-substrate interactions.^[34] To achieve a full understanding over the self-assembly of guanine at the solid-liquid interface, here we performed a sub-molecularly resolved STM study of physisorbed monolayers on graphite of a series of N^9 -

alkylguanines with linear alkyl side-chains from $-C_2H_5$ up to $-C_{18}H_{37}$ (Fig. 5.21). This comparative study was carried out by applying a drop of a 1.0 ± 0.1 mM solution of the chosen guanine molecule in 1,2,4-trichlorobenzene (TCB) on freshly cleaved highly oriented pyrolytic graphite (HOPG).

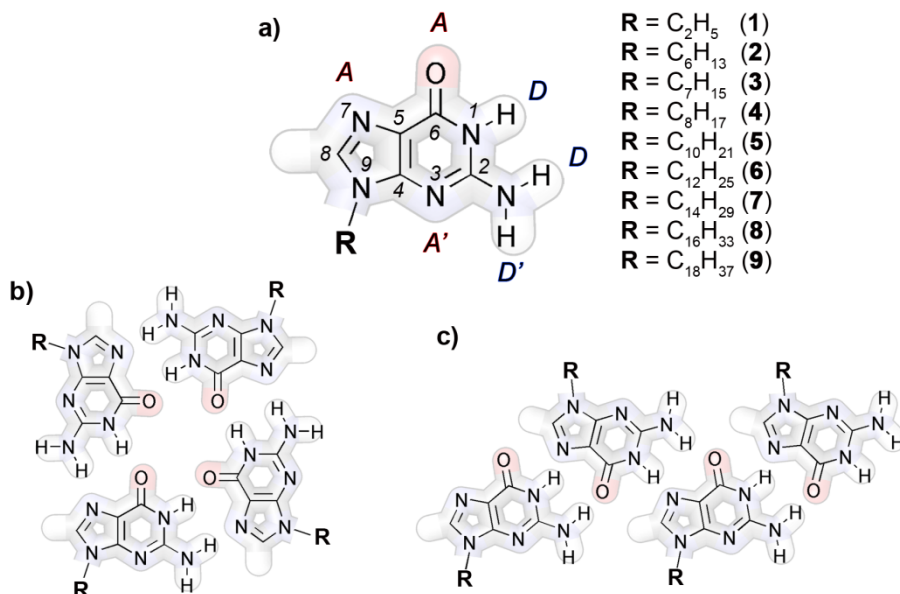


Figure 5.21 (a) Chemical formula of the different investigated guanines; H-bonded motifs of self-assembled guanines: (b) quartet based (involved pairing NH(2)-N(7) and NH(1)-O(6)) and (c) ribbon based (involved pairing: NH(2)-O(6) and NH(1)-N(7)) architectures.

5.4.2 Results and discussion

For the crystalline pattern obtained from each guanine self-assembled on HOPG the unit cell parameters, i.e. length of vectors a and b , α (angle between the vectors), unit cell area (A), number of molecules in the unit cell (N_{mol}), area occupied by a single molecule in the unit cell (A_{mol} , with $A_{mol} = A/N_{mol}$) and estimated projection of the molecular van der Waals volume onto surface (A_{vdW}) are given in Table 5.4. All proposed packing motifs for molecules **1-9**, have been compared with theoretical models (Fig. 5.22-5.26).

Guanine derivative	Side chain	Unit cell parameters ^a						
		<i>a</i> [nm]	<i>b</i> [nm]	α	<i>A</i> [nm ²]	<i>N_{mol}</i>	<i>A_{mol}</i> [nm ²]	<i>A_{vdW}</i> [nm ²]
1	C ₂ H ₅	1.00 ± 0.2	1.51 ± 0.2	(92±3)°	1.51 ± 0.21	2	0.75 ± 0.1	0.55 ± 0.02
2	C ₆ H ₁₃	0.98 ± 0.2	1.63 ± 0.2	(84±3)°	1.58 ± 0.20	1	1.58 ± 0.2	0.75 ± 0.02
3	C ₇ H ₁₅	0.97 ± 0.2	1.85 ± 0.2	(81±3)°	1.77 ± 0.19	2	0.88 ± 0.1	0.80 ± 0.02
4	C ₈ H ₁₇	1.27 ± 0.2	2.01 ± 0.2	(58±3)°	2.15 ± 0.22	2	1.07 ± 0.1	0.85 ± 0.02
5	C ₁₀ H ₂₁	1.19 ± 0.2	1.46 ± 0.2	(96±3)°	1.72 ± 0.21	1	1.72 ± 0.2	0.90 ± 0.02
6	C ₁₂ H ₂₅	1.00 ± 0.2	4.19 ± 0.2	(68±3)°	3.76 ± 0.21	4	0.94 ± 0.1	1.00 ± 0.02
7	C ₁₄ H ₂₉	1.00 ± 0.2	4.73 ± 0.2	(68±3)°	4.25 ± 0.21	4	1.06 ± 0.1	1.10 ± 0.02
8	C ₁₆ H ₃₃	1.00 ± 0.2	5.27 ± 0.2	(68±3)°	4.73 ± 0.21	4	1.18 ± 0.1	1.20 ± 0.02
9	C ₁₈ H ₃₇	1.00 ± 0.2	5.81 ± 0.2	(68±3)°	5.22 ± 0.21	4	1.31 ± 0.1	1.30 ± 0.02

Table 5.4 Unit cell parameters of all guanine derivatives at the solid-liquid interface *a* and *b* are the vector lengths and α the angle between those vectors; *A* is the unit cell area, *N_{mol}* the number of molecules in the unit cell and *A_{mol}* (= *A*/*N_{mol}*) is the area occupied by single molecules within the unit cell; *A_{vdW}* is the estimated van der Waals area.

Figure 5.22 shows STM image of the monolayer obtained from molecule **1**: it reveals a crystalline ribbon-like architecture. In this 2D crystal the ethyl side chains are most likely physisorbed flat on the surface, although due to their high conformational dynamics they could not be resolved. The area occupied by a single molecule **1** corresponds to 0.75±0.1 nm², being in the good agreement with the van der Waals area of **1**.

The supramolecular motif, can be well-described by the formation of a one dimensional H-bonded ribbon involving the following pairing: NH(2)-O(6) and NH(1)-N(7) (model in Fig. 5.21c), in good accordance with previous observations on guanosine^[33] derivatives.

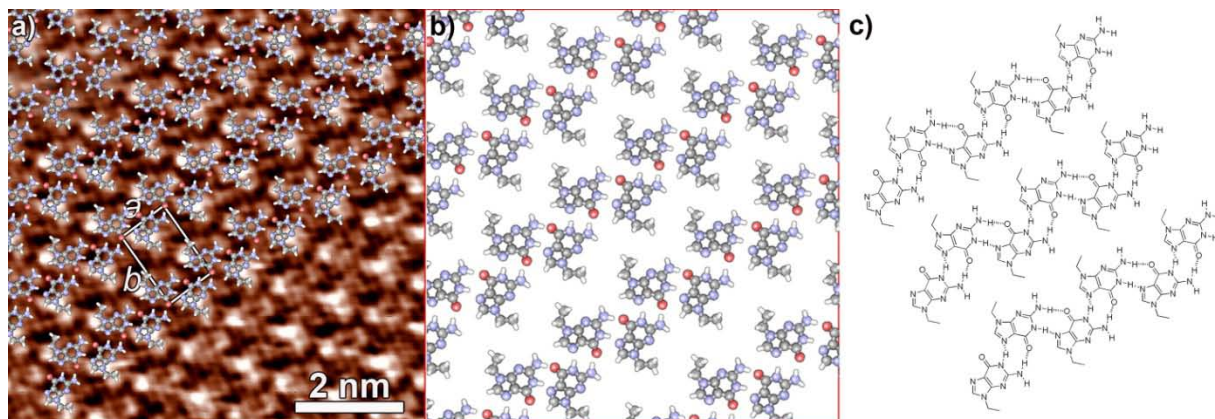


Figure 5.22 (a) STM images of monolayers of ribbon-like structure of **1**. Tunneling parameters: average tunneling current (I_t) = 15 pA, bias voltage (V_t) = 350 mV.; Comparison of the proposed molecular packing of **1** (b) with theoretical model (c).

Self-assembled structures of molecule **2** exhibit a 2D crystal with the hexyl side-chains physisorbed flat on the surface (Fig. 5.23). Differently from the monolayer of **1**, self-assembly of **2** is not dictated by the formation of H-bonding between adjacent molecules, but rather unspecific van der Waals interactions between molecules and the substrate rule the generation of an ordered monolayer.

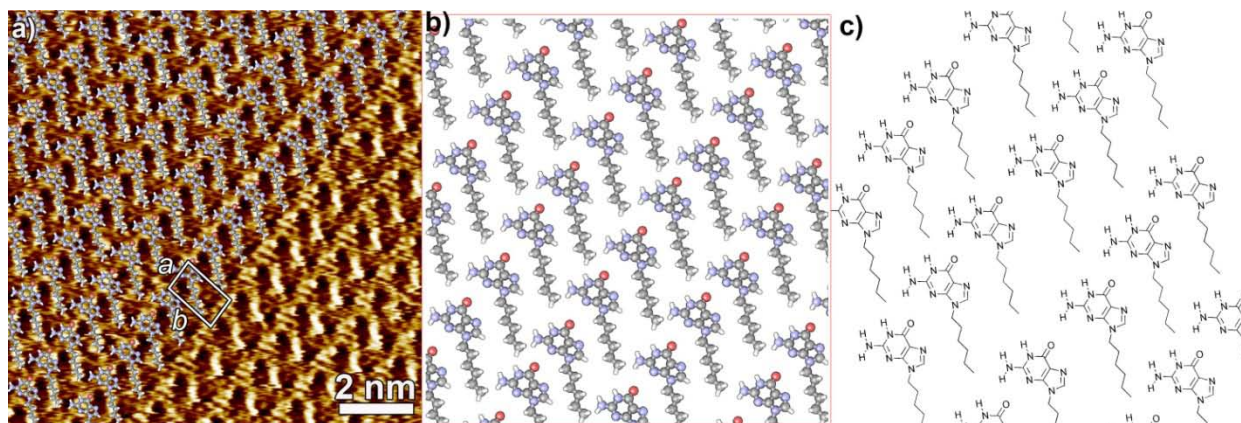


Figure 5.23 (a) STM images of monolayers of **2**. Tunneling parameters: average tunneling current (I_t) = 15 pA, bias voltage (V_t) = 350 mV.; Comparison of the proposed molecular packing of **2** (b) with theoretical model (c).

Similar motif was observed in a monolayer of **5** (Fig. 5.24). The packing is very loose as proved by the large discrepancy between A_{mol} and A_{vdW} . Despite such large voids which could host a

second ad-molecule, we observed only one molecule per unit cell as probably ruled by the registry with the substrate.

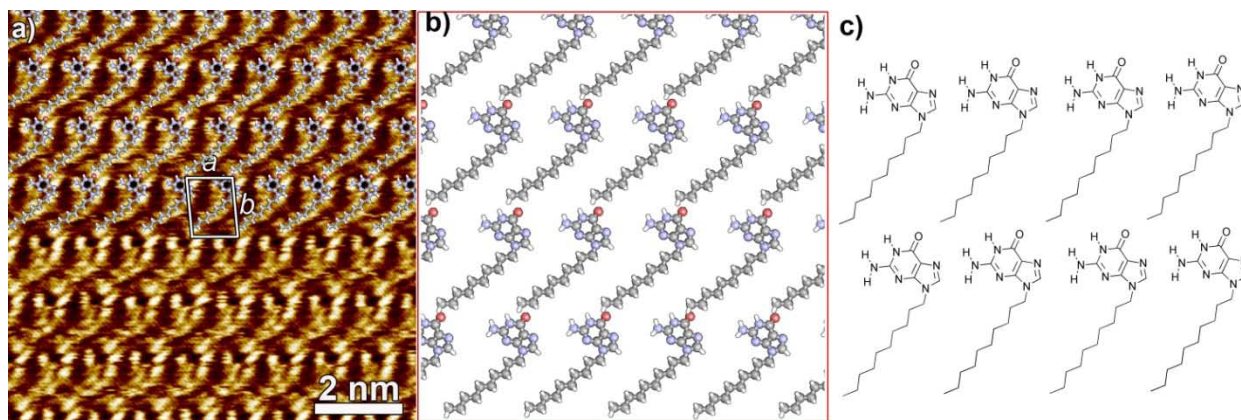


Figure 5.24 (a) STM images of monolayers of **5**. Tunneling parameters: average tunneling current (I_t)= 15 pA, bias voltage (V_t) = 350 mV.; Comparison of the proposed molecular packing of **5** (b) with theoretical model (c).

Figure 5.25 portrays the STM image recorded on a monolayer of molecule **3**. It reveals large ordered lamelle featuring a dimer packing motif involving the following pairing: NH(2)-N(7) and NH(1)-O(6). The comparison of the area occupied by a single molecule, i.e. $0.88 \pm 0.1 \text{ nm}^2$, with the van der Waals molecule's size of $0.80 \pm 0.02 \text{ nm}^2$, suggests that the heptyl side chains are physisorbed at surface, though due to their high conformational dynamics they could not be resolved.

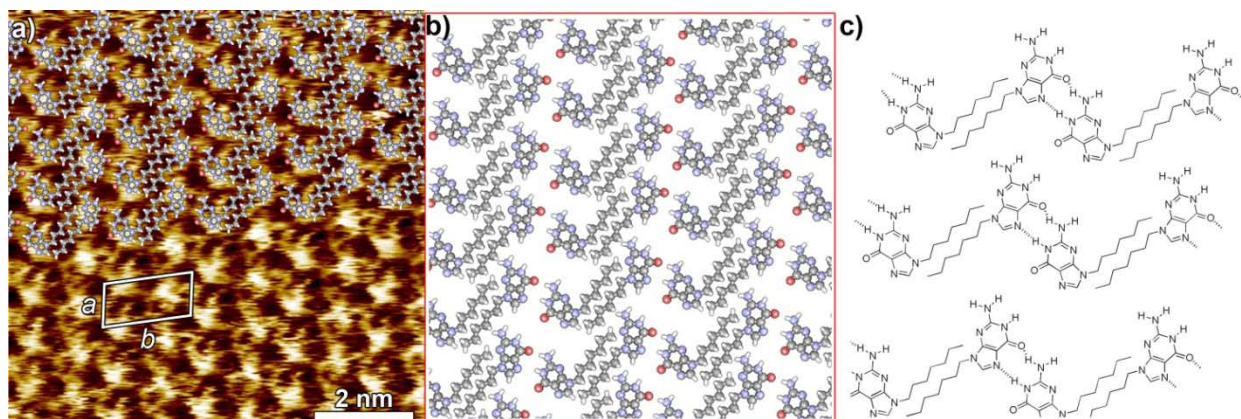


Figure 5.25 (a) STM images of monolayers of **3**. Tunneling parameters: average tunneling current (I_t)= 17 pA, bias voltage (V_t) = 360 mV.; Comparison of the proposed molecular packing of **3** (b) with theoretical model (c).

Figure 5.26 shows a monolayer of **4** at the HOPG-solution interface. As in case of **3**, the packing can be described by the formation of a dimer involving the pairing NH(2)-N(7) and NH(1)-O(6). The octyl side chains are supposedly physisorbed on the graphite surface. However, differently from the case of pattern formed through self-assembly of **3**, within the dimers only one alkyl chain is physisorbed on the HOPG surface.

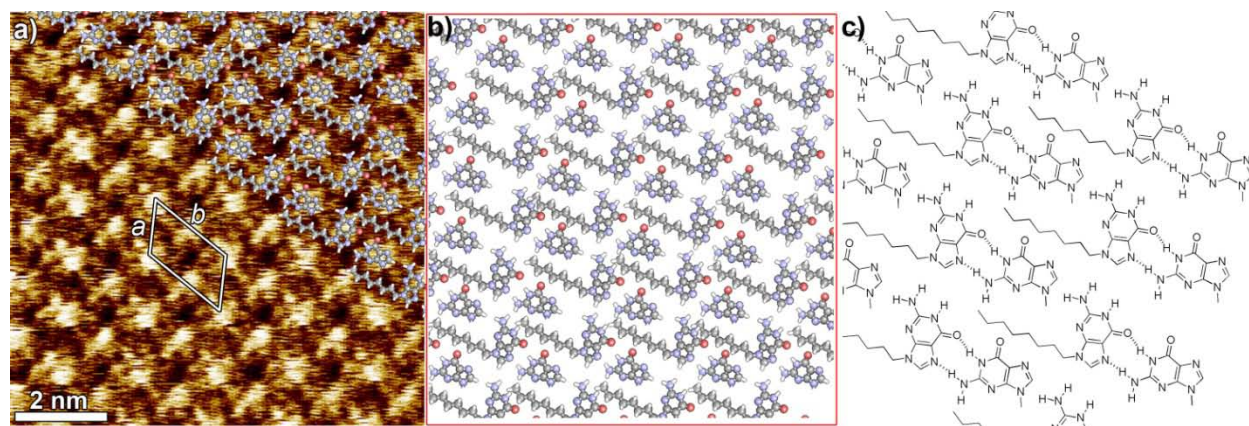


Figure 5.26 (a) STM images of monolayers of **4**. Tunneling parameters: average tunneling current (I_t) = 17 pA, bias voltage (V_t) = 360 mV.; Comparison of the proposed molecular packing of **4** (b) with theoretical model (c).

Following, we have focused our attention to the self-assembly of guanines exposing longer alkyl side chains. Interestingly, regardless the length of the side chain ($C_{12}H_{25}$ for **6**, $C_{14}H_{29}$ for **7**, $C_{16}H_{33}$ for **8** and $C_{18}H_{37}$ for **9**) the observed monolayers exhibit a similar motif consisting of H-bonded ribbons, involving the pairing NH(2)-O(6) and NH(1)-N(7) (Fig. 5.27). In the 2D crystals the long side chains are clearly visible: they are physisorbed flat on the surface and are interdigitated between adjacent supramolecular ribbons, thereby stabilizing the entire monolayer. Further, the comparison of the unit cell parameters of monolayers of **6-9** self-assembled at the HOPG-solution interface (Table 5.4) reveals that the only difference between those structures is the value of b vector, thus affecting also the area occupied by a single guanine molecule (A_{mol}). Interestingly, the difference between A_{mol6} and A_{mol7} matches the difference between A_{mol7} and A_{mol8} , i.e. 0.11 nm^2 , being in good agreement with the area occupied by an ethylene group, i.e. $0.12 \pm 0.01 \text{ nm}^2$. Difference between A_{mol8} and A_{mol9} amounts to $0.13 \pm 0.01 \text{ nm}^2$. For monolayers of **6-9** the packing is extremely tight as revealed by the very similar values of A_{mol} and A_{vdW} for each system.

The thermodynamic characteristics of guanine association, obtained from the gas phase experiments,^[35, 36] revealed that the energy of supramolecular polymerization in motifs like those visualized by STM, amounts to 32-36 kcal/mol per molecule. In comparison the adsorption energy of alkyl chains on the HOPG surface, determined by temperature-programmed desorption experiments,^[37, 38] increases linearly with the chain length and are on the same energy range (Table 5.5).

Guanine derivative	Side chain	Adsorption energy in kcal/mol*
1	C ₂ H ₅	5.2
2	C ₆ H ₁₃	15.6
3	C ₇ H ₁₅	18.2
4	C ₈ H ₁₇	20.8
5	C ₁₀ H ₂₁	26
6	C ₁₂ H ₂₅	31.2
7	C ₁₄ H ₂₉	36.4
8	C ₁₆ H ₃₃	41.6
9	C ₁₈ H ₃₇	46.8

Table 5.5 Energy of physisorption of alkyl chains with increasing length on HOPG surface. Note that the adsorption energy of one methylene group on graphite is around 2.6 kcal/mol (11 kJ/mol, ~0.1 eV). Therefore, the adsorption energy of guanine derivatives **1-9** was estimated by multiplying this value by the number of methylene units in the alkyl chains of adjacent guanine derivatives.

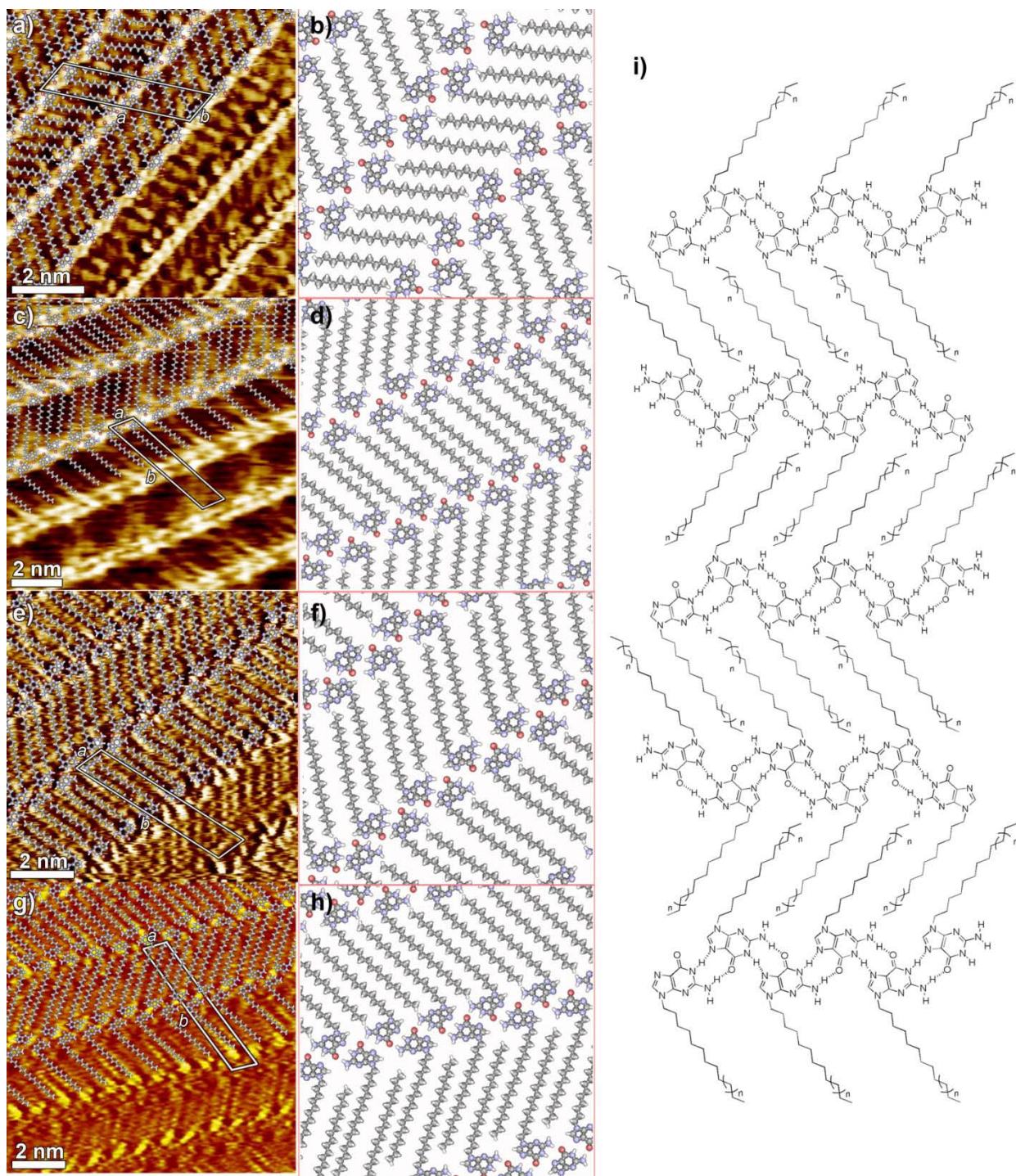


Figure 5.27 STM images and proposed molecular packing of H-bonded ribbons obtained from (a, b) **6**, (c, d) **7**, (e, f) **8**, and (g, h) **9**. Tunneling parameters: $I_t=17\text{pA}$, $V_t=360\text{ mV}$; (i) theoretical model of H-bonded ribbon formed by self-assembly of guanine derivatives **6-9**.

5.4.3 Conclusions

In summary, we have performed a comparative STM study on the self-assembly at the HOPG-solution interface of substituted guanines exposing in the N⁹-position alkyl side chains with different length. Molecules **1-9** were found to form monomorphic 2D crystals, which are stable on the several tens of min time scale and exceed various hundreds of nm². Subtle changes in the length of the alkyl side-chains dramatically influenced the 2D patterns on graphite. Derivatives with alkyl tails longer than C₁₂ (**6-9**) self-assembled into linear H-bonded ribbons through the NH(2)-O(6) and NH(1)-N(7) pairing with 4 molecules in the unit cell. The same H-bonding pattern was observed for N⁹-ethylguanine **1**, but the packing shows only 2 molecules in the unit cell (the adjacent H-bonded non-centrosymmetric ribbons run indeed in parallel way while for **6-9** they are anti-parallel). For derivatives with tails of intermediate length (from C₆ to C₁₀) no H-bonded supramolecular polymers were formed at surface: ordered monolayers of single (non-H-bonded) molecules (**2** and **5**) or H-bonded dimers (**3** and **4**) were observed. In light of the dynamic self-assembly characteristics of guanines, our results can be of interest for the generation of responsive nanopatterned surfaces featuring pre-programmed structural motifs at the supramolecular level.

5.4.4 Experimental procedure

Scanning Tunneling Microscopy STM measurements were performed using a Veeco scanning tunneling microscope (multimode Nanoscope III, Veeco) in constant current mode at the interface between highly oriented pyrolytic graphite (HOPG) and a supernatant solution. All guanine derivatives were dissolved in DMSO at 95°C and diluted with 1,2,4-trichlorobenzene (TCB) to give 1±0.1 mM solutions. Diluted solutions of all guanine derivatives were applied to the basal plane of the surface. For STM measurements the substrates were glued on a magnetic disk and an electric contact is made with silver paint (Aldrich Chemicals). The STM tips were mechanically cut from a Pt/Ir wire (90/10, diameter 0.25 mm). The raw STM data were processed through the application of background flattening and the drift was corrected using the underlying graphite lattice as a reference. The latter lattice was visualized by lowering the bias voltage to 20 mV and raising the current to 65 pA. All of the models were minimized with Chem3D at the MM2 level, which includes potentials for H-bonds and torsion potentials for

describing rotations around single bonds. We decided to use MM2 force field since it is a rather inexpensive method from the computational time viewpoint which has been proven to be successfully employed to describe poly-atomic structures based on H-bonding. Mother solution of alkylated guanine derivatives were dissolved in DMSO at 95°C and diluted with 1,2,4-trichlorobenzene (TCB) to give 1mM solutions. Monolayer pattern formation was achieved by applying 4 μ L of solution onto freshly cleaved HOPG. Then STM images were recorded only after achieving a negligible thermal drift.

References

- [1] J. M. Lehn, *Science* **2002**, 295, 2400.
- [2] T. F. A. Greef, E. W. Meijer, *Nature* **2008**, 453, 171.
- [3] A. Ciesielski, S. Lena, S. Masiero, G. P. Spada, P. Samorì, *Angew. Chem. Int. Ed.* **2010**, 49, 1963.
- [4] O. Ivasenko, J. M. MacLeod, K. Y. Chernichenko, E. S. Balenkova, R. V. Shpanchenko, V. G. Nenajdenko, F. Rosei, D. F. Perepichka, *Chem. Commun.* **2009**, 1192.
- [5] J. V. Barth, G. Costantini, K. Kern, *Nature* **2005**, 437, 671.
- [6] T. Kudernac, S. B. Lei, J. A. A. W. Elemans, S. De Feyter, *Chem. Soc. Rev.* **2009**, 38, 402.
- [7] M. Surin, P. Samorì, *Small* **2007**, 3, 190.
- [8] J. A. Theobald, N. S. Oxtoby, M. A. Phillips, N. R. Champness, P. H. Beton, *Nature* **2003**, 424, 1029.
- [9] A. Ciesielski, L. Piot, P. Samorì, A. Jouaiti, M. W. Hosseini, *Adv. Mater.* **2009**, 21, 1131.
- [10] G. P. Spada, S. Lena, S. Masiero, S. Pieraccini, M. Surin, P. Samorì, *Adv. Mater.* **2008**, 20, 2433.
- [11] A. P. H. J. Schenning, E. W. Meijer, *Chem. Commun.* **2005**, 3245.
- [12] J. D. Watson, F. H. C. Crick, *Nature* **1953**, 171, 737.
- [13] J. T. Davis, G. P. Spada, *Chem. Soc. Rev.* **2007**, 36, 296.
- [14] S. Lena, G. Brancolini, G. Gottarelli, P. Mariani, S. Masiero, A. Venturini, V. Palermo, O. Pandoli, S. Pieraccini, P. Samorì, G. P. Spada, *Chem. Eur. J.* **2007**, 13, 3757.
- [15] S. Sivakova, S. J. Rowan, *Chem. Soc. Rev.* **2005**, 34, 9.
- [16] J. T. Davis, *Angew. Chem. Int. Ed.* **2004**, 43, 668.

- [17] D. Gonzalez-Rodriguez, P. G. A. Janssen, R. Martin-Rapun, I. De Cat, S. De Feyter, A. P. H. J. Schenning, E. W. Meijer, *J. Am. Chem. Soc.* **2010**, DOI: 10.1021/ja908537k.
- [18] S. Pieraccini, S. Masiero, O. Pandoli, P. Samorì, G. P. Spada, *Org. Lett.* **2006**, 8, 3125.
- [19] L. Ma, M. Melegari, M. Colombini, J. T. Davis, *J. Am. Chem. Soc.* **2008**, 130, 2938.
- [20] M. Nikan, J. C. Sherman, *Angew. Chem. Int. Ed.* **2008**, 47, 4900.
- [21] J. L. Sessler, M. Sathiosatham, K. Doerr, V. Lynch, K. A. Abboud, *Angew. Chem. Int. Ed.* **2000**, 39, 1300.
- [22] H. Liddar, J. Li, A. Neogi, P. B. Neogi, A. Sarkar, S. Cho, H. Morkoc, *Appl. Phys. Lett.* **2008**, 92.
- [23] A. M. S. Kumar, J. D. Fox, L. E. Buerkle, R. E. Marchant, S. J. Rowan, *Langmuir* **2009**, 25, 653.
- [24] S. Mihai, A. Cazacu, C. Arnal-Herault, G. Nasr, A. Meffre, A. van der Lee, M. Barboiu, *New J. Chem.* **2009**, 33, 2335.
- [25] W. Mamdouh, R. E. A. Kelly, M. D. Dong, L. N. Kantorovich, F. Besenbacher, *J. Am. Chem. Soc.* **2008**, 130, 695.
- [26] W. M. Heckl, D. P. E. Smith, G. Binnig, H. Klagges, T. W. Hansch, J. Maddocks, *Proc. Nat. Acad. Sci. U.S.A.* **1991**, 88, 8003.
- [27] R. Rinaldi, E. Branca, R. Cingolani, S. Masiero, G. P. Spada, G. Gottarelli, *Appl. Phys. Lett.* **2001**, 78, 3541.
- [28] R. Rinaldi, G. Maruccio, A. Biasco, V. Arima, R. Cingolani, T. Giorgi, S. Masiero, G. P. Spada, G. Gottarelli, *Nanotechnology* **2002**, 13, 398.
- [29] G. Maruccio, P. Visconti, V. Arima, S. D'Amico, A. Biasco, E. D'Amone, R. Cingolani, R. Rinaldi, S. Masiero, T. Giorgi, G. Gottarelli, *Nano Lett.* **2003**, 3, 479.
- [30] R. Otero, M. Schock, L. M. Molina, E. Laegsgaard, I. Stensgaard, B. Hammer, F. Besenbacher, *Angew. Chem. Int. Ed.* **2005**, 44, 2270.
- [31] R. Otero, W. Xu, M. Lukas, R. E. A. Kelly, E. Laegsgaard, I. Stensgaard, J. Kjems, L. N. Kantorovich, F. Besenbacher, *Angew. Chem. Int. Ed.* **2008**, 47, 9673.
- [32] T. Giorgi, S. Lena, P. Mariani, M. A. Cremonini, S. Masiero, S. Pieraccini, J. P. Rabe, P. Samorì, G. P. Spada, G. Gottarelli, *J. Am. Chem. Soc.* **2003**, 125, 14741.
- [33] G. Gottarelli, S. Masiero, E. Mezzina, S. Pieraccini, J. P. Rabe, P. Samorì, G. P. Spada, *Chem. Eur. J.* **2000**, 6, 3242.

- [34] S. De Feyter, F. C. De Schryver, *Chem. Soc. Rev.* **2003**, 32, 139.
- [35] J. Sponer, J. Leszczynski, P. Hobza, *J. Phys. Chem.* **1996**, 100, 5590.
- [36] J. Sponer, J. Leszczynski, P. Hobza, *J. Phys. Chem.* **1996**, 100, 1965.
- [37] K. R. Paserba, A. J. Gellman, *J. Phys. Chem. B* **2001**, 105, 12105.
- [38] T. Muller, G. W. Flynn, A. T. Mathauser, A. V. Teplyakov, *Langmuir* **2003**, 19, 2812.

Chapter 6

Dynamers at the solid-liquid interface

“I can hardly doubt that when we have some control of the arrangement, of the things on molecular scale, we will get an enormously greater range of possible properties that substances can have and of different things we can do.”

Richard P. Feynman, Eng. Sci. 1960, 23, 22-36

Since R. P. Feynman gave his famous lecture in 1959, rapid advances in the chemical, physical and biological science have shed an enormous amount of light on natural and biological machines, enabling the scientist to comprehend them down to the molecular level. Being amongst the most accomplished imitators of *Nature*, scientist have devoted a lot of effort to the development of artificial molecular machines, trying to mimic functions which are reminiscent of those in biological world. Nanoscale control over mechanical movement of molecules has been intensely investigated in the last two decades, aiming at the development of molecular machines that can be implemented in miniaturized systems based on single or few molecules. In this chapter we will discuss molecular systems able to undergo conformational changes, as a result of external stimuli such as a light irradiation, metal complexation or change in pH.

Chapter 6.1

Reversible assembly/re-assembly process between two highly ordered supramolecular guanine motifs

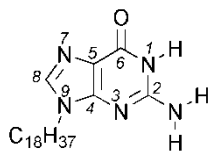
The Watson–Crick base pairing underlying DNA’s helical structure is very well known, but nucleobases can form a variety of other hydrogen-bonded motifs. Guanines, in particular, can assemble into dimers, ribbons or macrocyclic G-quartets that are relevant to fields as diverse as organic electronics or drug design. Guanine-based assemblies on surfaces have been widely investigated by STM, but under ultra-high vacuum (UHV). In the collaboration with the group of Prof. Gian Piero Spada from University of Bologna (Italy), we investigated by the means of STM operating at the solid-liquid interface, the solutions of guanines bearing a long alkyl side chain that were so dilute they could all be adsorbed on the surface. The molecules first assembled into extended ribbons on the highly oriented pyrolytic graphite surface. The addition of potassium ions to the solution triggered the formation of macrocyclic G-quartets centred around the cations. When the potassium ions were subsequently captured by addition of a cryptand [2.2.2] molecules, the ribbons re-assembled on HOPG surface. On acidification of the solution, the protonated cryptands released the potassium ions, inducing the re-formation of the G-quartets. Finally, the formation of ribbons could be triggered again by further addition of cryptands. The surface areas covered by either the ribbons or the quartets were found to be very similar, suggesting that the conversions occur on the surface without involving desorption and re-adsorption steps.

The molecules described in this chapter has been synthesized by Dr. Stefano Lena, in the group of Prof. Gian Piero Spada from University of Bologna (Italy).

6.1.1 Introduction

Reversible non-covalent interactions are ruling complex systems and phenomena in nature. Nucleobases, which are essential components of the genetic material in all living organisms, encode sophisticated programs for self-assembly into highly ordered and complex architectures, such as the fascinating double-helix of DNA.^[1] Alongside Watson-Crick base pairing,^[1] directing the formation of the helical structure of DNA, nucleobases can interact through other H-bonded motifs to form various complex supramolecular architectures,^[2] such as guanine (G) quadruplexes.^[3] The G-quartet (G_4), a H-bonded macrocycle typically formed by cation-templated assembly, was first identified in 1962 as the basis for the aggregation of 5'-guanosine monophosphate (5'-GMP),^[4] and fits particularly well with contemporary studies in molecular self-assembly and non-covalent synthesis.^[5-10] Guanine is an extremely versatile building block: depending on the environment it is able to self-assemble into various discrete architectures including dimers, ribbons and macrocycles.^[11, 12] In the presence of certain cations, they can form G_4 -based octamers or columnar aggregates (supramolecular polymers) depending on the concentration of the cation and nucleobase. The guanine-based structures are interesting for applications in organic electronics,^[13] and synthesis of supramolecular hydrogels,^[14] whereas G-quartets are well-known to hold potential in several biological processes^[15] and in anticancer drug design as they can act as enzyme telomerase inhibitors, being therefore of importance for controlling tumor immortalization.^[16, 17]

While the self-assembly of guanines into G_4 -based architectures (not templated by a metal center) on solid surfaces has been studied by Scanning Tunneling Microscopy (STM) under ultrahigh vacuum (UHV),^[18, 19] STM explorations at the solid-liquid interface have been primarily carried out on guanosine derivatives.^[20-24] Although the structure of guanine quadruplex templated by a metal center was introduced over 40 years ago, to date, its visualization by STM once assembled at the solid-liquid interface has been reported only by our group.^[25]



1

Figure 6.1 Chemical formula of the investigated guanine derivative 1.

In this chapter we present a sub-molecularly resolved STM study at the solid-liquid interface of the metal templated reversible assembly/re-assembly process of a N^9 -alkylguanine into highly ordered G quartets and G ribbons on highly oriented pyrolytic graphite (HOPG) surfaces, which represents a continuation of the work presented in Chapter 5.4. We focused our attention on the octadecyl guanine derivative **1** (Fig. 6.1), which was found to form extremely stable domains among all guanine derivatives reported in Chapter 5.4. The presence of a long aliphatic side-chain and the absence of the sugar when compared to the previously studied guanosines are expected to promote the molecular physisorption on HOPG. The self-assembly of **1** on HOPG has been studied as neat component and upon sub-sequent addition of cryptand [2.2.2] molecules, potassium picrate and trifluoromethanesulfonic acid to trigger the reversible interconversion between two different highly ordered supramolecular motifs (Fig. 6.2), which was previously indirectly monitored by $^1\text{H-NMR}$ and circular dichroism to occur in solution.^[26]

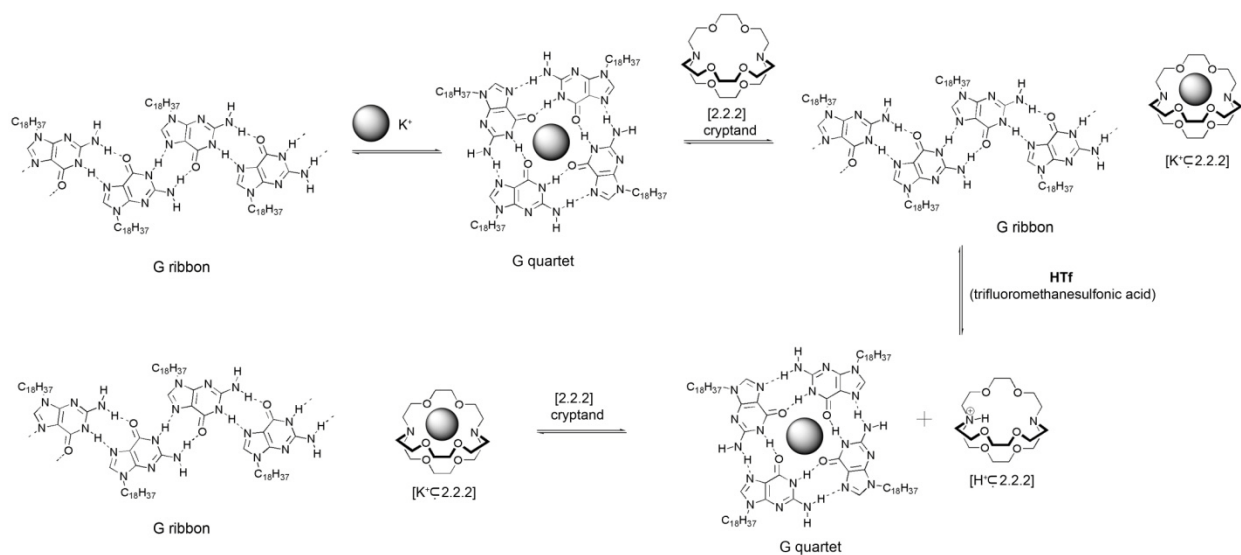


Figure 6.2 The stepwise reversible interconversion between the G ribbon (**1_n**) and the G quartet **K(1₄)**. The gray sphere represents the K^+ ions.

In general, the generation of ordered motifs stabilized by hydrogen bonds at the solid-liquid interface requires the fine tuning of the interplay between interactions involving solvent molecules, solute molecules and substrate.^[27] The STM observation of a conformational or assembly switching process occurring at the solid-liquid interface cannot be obtained by operating with concentrated solutions. This is because, as ruled by the thermodynamics of the

physisorption at the solid-liquid interface, given a solution containing a large number of identical molecules possessing two or more conformations, the component with a greater affinity for the substrate, i.e. offering a minimization of the free interface energy per unit area, will assemble on its surface, whereas the others will remain in the supernatant solution.^[28, 29] To have a full control on the switching process and immobilize all the components on the surface, thus to achieve a complete physisorption of all different components at the solid-liquid interface, it is mandatory to tune the stoichiometry of the molecules absorbed at surface.^[30, 31] At the solid-liquid interface, the number of molecules in the solution applied to the surface should be lower than that required to form a monolayer of physisorbed molecules lying flat on the substrate.

6.1.2 Results and discussion

Initially we investigated the self-assembly of **1** by applying a drop of a (100 ± 2) μM solution in 1,2,4-trichlorobenzene (TCB) on the graphite surface. STM image of the obtained monolayer (Fig. 6.3a) showed a crystalline structure consisting of ribbon-like architectures. In this 2D crystal the octadecyl side chains are physisorbed flat on the surface and are interdigitated between adjacent supramolecular ribbons. The unit cell parameters, $a = (5.81 \pm 0.2)$ nm, $b = (1.0 \pm 0.2)$ nm, and $\alpha = (68 \pm 3)^\circ$, lead to an area $A = (5.22 \pm 0.21)$ nm², where each unit cell contains four molecules. Thus, the area occupied by a single molecule **1** corresponds to (1.3 ± 0.1) nm². The supramolecular motif, can be well described by the formation of a one dimensional H-bonded ribbon involving the following pairing: NH(2)-O(6) and NH(1)-N(7) (Fig. 6.3b). This self-assembly behavior is in good accordance with previous observations on guanosine derivatives.^[21]

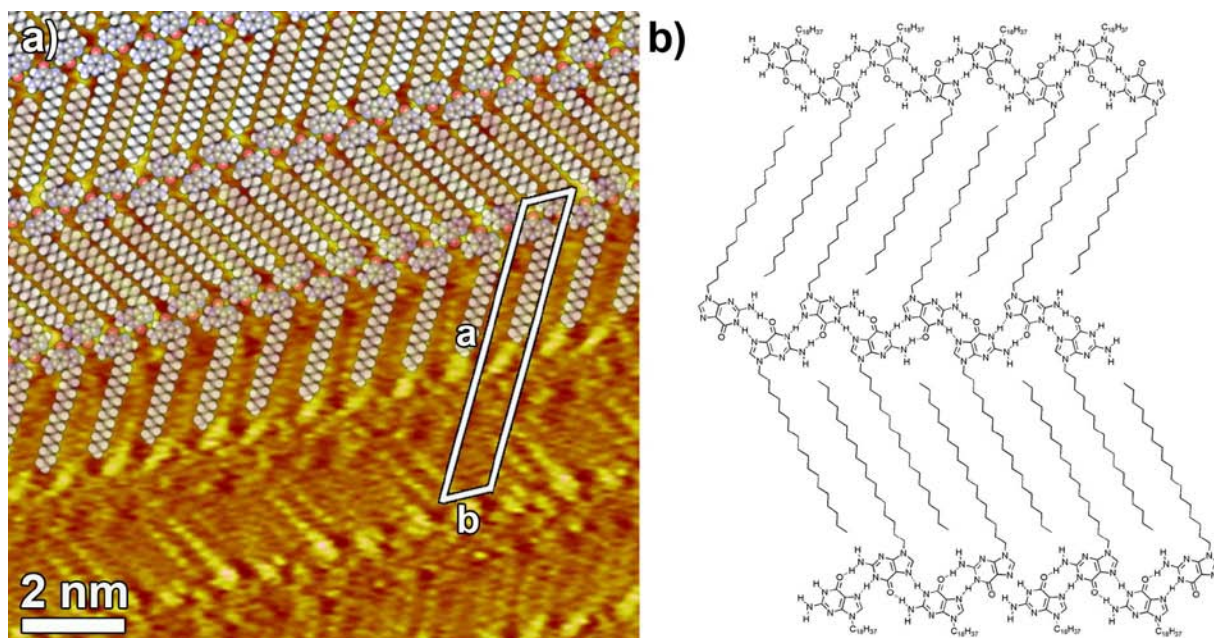


Figure 6.3 (a) STM image of the monolayer of supramolecular ribbon-like architectures of **1**. Tunneling parameters: average tunneling current (I_t) = 15 pA, bias voltage (V_t) = 350 mV; (b) theoretical packing motif of G ribbon of **1**.

Although in general STM investigation of sub-monolayer thick films obtained from low concentrated solutions may lead to polymorphism, such a behavior was ruled out in our case: concentration dependent experiments revealed that by applying a drop of $(10 \pm 2) \mu\text{M}$ or $(500 \pm 2) \mu\text{M}$ solutions in TCB onto the graphite surface only the ribbons shown in Fig. 6.3a were monitored even on survey images on the hundreds of nanometers scale (Fig. 6.4).

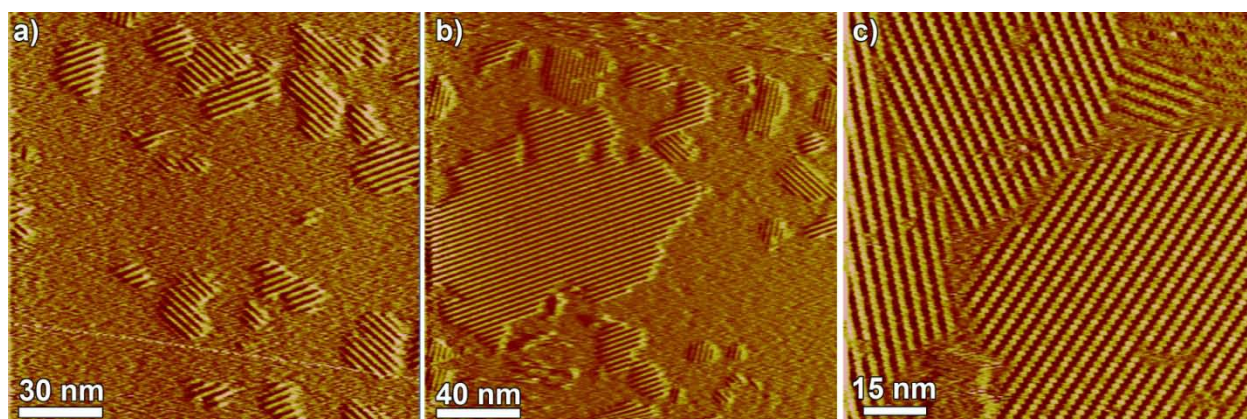


Figure 6.4 STM images of monolayers of supramolecular architectures of **1** at the graphite-TCB interface self-assembled from: (a) $10 \pm 2 \mu\text{M}$, (b) $100 \pm 2 \mu\text{M}$ and (c) $500 \pm 2 \mu\text{M}$ solutions. Tunneling parameters (a)-(c): average tunneling current (I_t) = 15 pA, bias voltage (V_t) = 350 mV

The STM study of a monolayer of guanine **1** solution containing 100 equiv of potassium picrate revealed the formation of a G₄-based architecture at surface (Fig. 6.5a). The unit cell parameters, $a = (1.6 \pm 0.2)$ nm and $\alpha = (90 \pm 3)^\circ$, lead to an area $A = (2.77 \pm 0.28)$ nm², where each unit cell contains four molecules **1** and one potassium ion. The area occupied by single molecule **1** amounts to (0.7 ± 0.1) nm². Figure 6.5b shows the proposed molecular packing motif, can be well described by the formation of a H-bonded macrocyclic structure involving the following pairing: NH(2)-O(6) and NH(1)-N(7). The circular feature exhibiting a high contrast in Figure 6.5a can be ascribed to the potassium ions, located in the center of G₄-based structure. It is most likely, that the coordinated potassium ions are not in the same plane as four molecules **1** forming quartet, as also known in solution.^[32] To enable formation of NH(2)-N(7) hydrogen bonds between adjacent G₄ (Figure 1d), stabilizing the entire supramolecular arrangement, the alkyl chains of **1** are back folded into the supernatant solution. The G₄ packing motif in Figure 6.5b differs from that observed in UHV on quartets formed in absence of templating ions.^[18] The presence of C₁₈H₃₇ alkyl side chains attached to the N(9) position of the guanine prevents the formation of the NH(9)-N(3) bond. Therefore, to stabilize the entire supramolecular structure into G₄-based architecture, another well-defined intra-quartet H-bond, i.e. NH(2)-N(7) bonding, is formed.

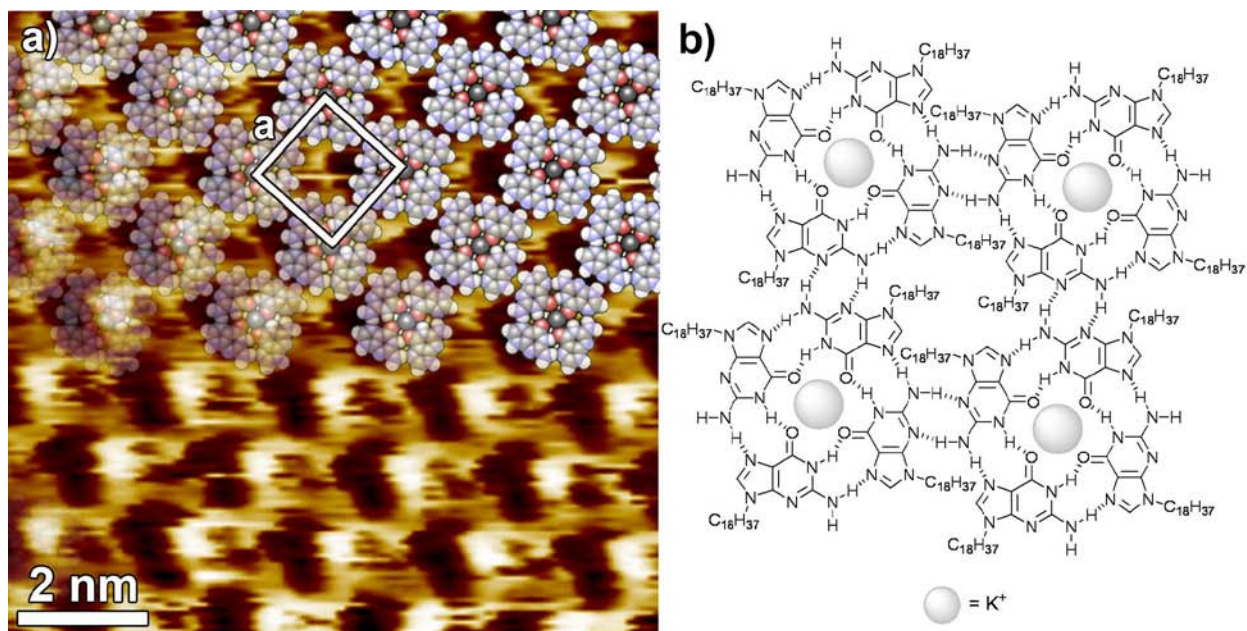


Figure 6.5 (a) STM image of the monolayer of the G₄-based architectures of **1**. Tunneling parameters: $I_t = 5$ pA, $V_t = 200$ mV; (b) theoretical packing motif of G₄-based architecture of **1**.

It is well known that an isolated tetramer of guanine complexed with the metal center is not thermodynamically stable in solution, thus octameric or larger G_4 -based stacks intercalated by cations are typically formed. In STM imaging at the solid-liquid interface, it is very difficult to perform a “tomography” of a molecular assembly in order to unambiguously determine, in our case, if the observed packing in Figure 6.5a corresponds to a single layer or double-decker (i.e., octamer) architecture.

To gain deeper insight into the two structures, and into their interconversion, in-situ successive assembly/re-assembly cycles from ribbon to G_4 -based architectures was accomplished. To the initial ribbon-like motif of Figure 6.6a, upon in-situ addition of 10 mM potassium picrate solution in TCB, the G_4 -based supramolecular motif was obtained (Fig. 6.6b). To sequester the ions from the G_4 , we opted to use a cryptand [2.2.2] since it offers an efficient complexation of K^+ to yield the cryptate $[K^+ \subset 2.2.2]$. Upon subsequent in-situ addition of 10 mM [2.2.2] cryptand solution to the G_4 supramolecular architectures, the guanine re-assembled on HOPG into the original ribbon (Fig. 6.6c). The difference in the orientation of the molecules **1** was observed. Such phenomenon was not surprising since the backfolded alkyl chains may re-adsorb on the HOPG surface along one out of three possible directions, leading to orientation changes of entire supramolecular architecture. By adding 10 mM solution of trifluoromethanesulfonic acid (HTf) in TCB, the potassium ions were released from the cryptate and the G_4 -based assembly was regenerated (Fig. 6.6d). In order to complete the switching process, i.e. to deprotonate nitrogen atoms of the cryptand and to form again the ribbon structures, alkaline solution was applied to the surface. Unfortunately, even in presence of a great excess of triethylamine it was not possible to trigger the formation of ribbons at surfaces. In fact we observed only disordered structures, which couldn't be resolved by the means of STM. However, upon further addition of a [2.2.2] cryptand solution, the ribbon structure was regenerated (Fig. 2d).

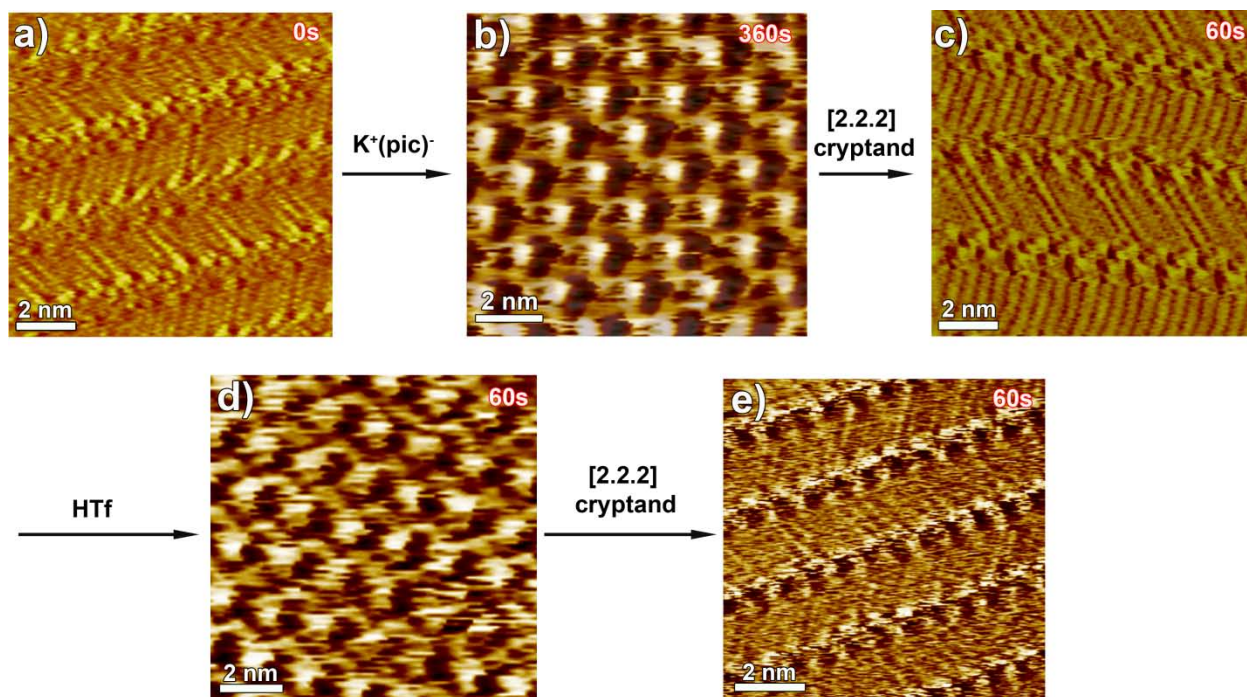


Figure 6.6 Consecutive STM images showing the structural evolution of a monolayer of **1** over 9 min time scale (time range displays in the right-upper part of the images correspond to the time which was needed to reach the equilibrium after addition of reacting agents). (a), (c) and (e) show ribbon-like structure, whereas (b) and (d) exhibit G_4 -based architectures. Tunneling parameters: $V_t=200$ mV - 400 mV, $I_t = 5$ pA - 15 pA.

The similar area occupied by single molecule **1** in the ribbon structure and in the G_4 -based architecture quartet on surface (see Experimental Procedures below) indicate that the switching process may have occurred on the HOPG surface, i.e. without subsequent desorption and re-adsorption although conclusive direct evidences could not be obtained. If different areas are occupied by single molecules of the reactant and product that self-assemble at the solid-liquid interface in a reaction or switching process, the total number of molecules at the surface will be changed, thus requiring the occurrence of a desorption and/or re-adsorption process. However, STM imaging at the solid-liquid interface cannot offer real-time monitoring of the reaction process in its intermediate states, thus the occurrence of the reaction at the surface or through a desorption/re-adsorption process cannot be unambiguously determined. The reproducibility of the sub-molecularly resolved STM imaging of the interconversion of **1** from ribbons to G_4 requires stringent experimental conditions characterized by an extremely low thermal gradient (below 3°C) and a high control over the concentration of the employed solutions (HTf

concentration could not exceed that needed to protonate only the nitrogen atoms of cryptand, otherwise only disordered monolayers were obtained).

6.1.3 Conclusions

In summary, we provided the first direct evidence on the sub-nm scale of a dyanmer operating at surfaces by means of STM. The versatile guanine **1** molecule was reversibly interconverted at the solid-liquid interface between two highly ordered supramolecular motifs, i.e. H-bonded ribbon and G₄-based architectures, upon sub-sequent addition of cryptand [2.2.2] molecules, potassium picrate and trifluoromethanesulfonic acid. The visualization of such supramolecular interconversion at the solid-liquid interface opens new avenues towards understanding the mechanism of formation and functioning of complex nucleobase architectures like DNA or RNA. Furthermore, the in-situ reversible assembly and re-assembly between two highly ordered supramolecular structures at the surfaces represents the first step towards the generation of nanopatterned responsive architectures.

6.1.4 Experimental procedure

Scanning Tunneling Microscopy STM measurements were performed using a Veeco scanning tunneling microscope (multimode Nanoscope III, Veeco) at the interface between highly oriented pyrolytic graphite (HOPG) and a supernatant solution. Diluted solutions of **1** were applied to the basal plane of the surface. For STM measurements the substrates were glued on a magnetic disk and an electric contact is made with silver paint (Aldrich Chemicals). The STM tips were mechanically cut from a Pt/Ir wire (90/10, diameter 0.25 mm). The raw STM data were processed through the application of background flattening and the drift was corrected using the underlying graphite lattice as a reference. The latter lattice was visualized by lowering the bias voltage to 20 mV and raising the current to 65 pA. All of the models were minimized with Chem3D at the MM2 level. Mother solution of octadecylguanine (**1**) was dissolved in DMSO at 95°C and diluted with 1,2,4-trichlorobenzene (TCB) to give 10±2 μM, 100±2 μM and 500±2 μM solutions. Monolayer pattern formation was achieved by applying 4μL of solution onto freshly cleaved HOPG. Then STM images were recorded only after achieving a negligible thermal drift.

Theoretical calculations For comparison of the area occupied by a single molecule in the ribbon-like structure and G₄ architecture, to determine whether the interconversion may have occurred on the surface, we have added to the experimentally determined area occupied by a single molecule in a G₄ structure (amounting to $0.7 \pm 0.1 \text{ nm}^2$) the area potentially occupied by the octadecyl side chain adsorbed fully flat on surface. This was computed using the following equation:

$$A_{C_{18}H_{37}} = \frac{3\sqrt{3}}{2} \times (0.142)^2 \times 18 = 0.6 \text{ nm}^2 \quad (6.1)$$

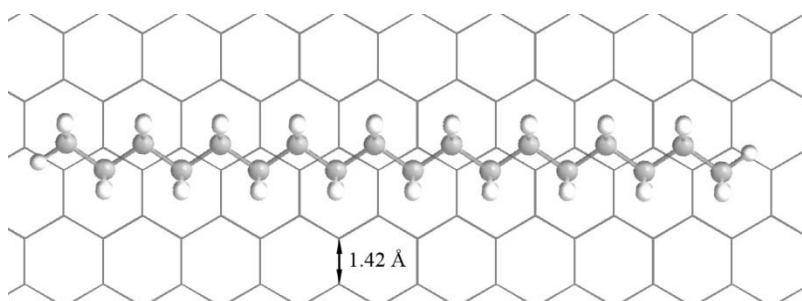


Figure 6.7 Single C₁₈H₃₇ chain adsorbed at HOPG surface

Thus the sum amounts to ca. 1.3 nm^2 , matching therefore well the experimentally estimated area occupied by a single molecule in a ribbon like structure, i.e. $(1.3 \pm 0.1) \text{ nm}^2$.

References

- [1] J. D. Watson, F. H. C. Crick, *Nature* **1953**, 171, 737.
- [2] S. Sivakova, S. J. Rowan, *Chem. Soc. Rev.* **2005**, 34, 9.
- [3] J. T. Davis, *Angew. Chem. Int. Ed.* **2004**, 43, 668.
- [4] M. Gellert, M. N. Lipsett, D. R. Davies, *Proc. Nat. Acad. Sci. U.S.A.* **1962**, 48, 2013.

- [5] J.-M. Lehn, *Supramolecular chemistry: concepts and perspectives*, VCH New York, **1995**.
- [6] J. S. Lindsey, *New J. Chem.* **1991**, *15*, 153.
- [7] J. F. Stoddart, H. R. Tseng, *Proc. Nat. Acad. Sci. U.S.A.* **2002**, *99*, 4797.
- [8] D. Philp, J. F. Stoddart, *Angew. Chem. Int. Ed.* **1996**, *35*, 1155.
- [9] G. M. Whitesides, E. E. Simanek, J. P. Mathias, C. T. Seto, D. N. Chin, M. Mammen, D. M. Gordon, *Acc. Chem. Res.* **1995**, *28*, 37.
- [10] D. N. Reinhoudt, M. Crego-Calama, *Science* **2002**, *295*, 2403.
- [11] J. T. Davis, G. P. Spada, *Chem. Soc. Rev.* **2007**, *36*, 296.
- [12] S. Lena, S. Masiero, S. Pieraccini, G. P. Spada, *Chem. Eur. J.* **2009**, *15*, 7792.
- [13] R. Rinaldi, G. Maruccio, A. Biasco, V. Arima, R. Cingolani, T. Giorgi, S. Masiero, G. P. Spada, G. Gottarelli, *Nanotechnology* **2002**, *13*, 398.
- [14] N. Sreenivasachary, J. M. Lehn, *Proc. Nat. Acad. Sci. U.S.A.* **2005**, *102*, 5938.
- [15] S. Neidle, S. Balasubramanian, *Quadruplex nucleic acids*, Royal Society of Chemistry, **2006**.
- [16] E. S. Baker, J. T. Lee, J. L. Sessler, M. T. Bowers, *J. Am. Chem. Soc.* **2006**, *128*, 2641.
- [17] T. de Lange, *Science* **1998**, *279*, 334.
- [18] R. Otero, M. Schock, L. M. Molina, E. Laegsgaard, I. Stensgaard, B. Hammer, F. Besenbacher, *Angew. Chem. Int. Ed.* **2005**, *44*, 2270.
- [19] R. Otero, W. Xu, M. Lukas, R. E. A. Kelly, E. Laegsgaard, I. Stensgaard, J. Kjems, L. N. Kantorovich, F. Besenbacher, *Angew. Chem. Int. Ed.* **2008**, *47*, 9673.
- [20] T. Giorgi, S. Lena, P. Mariani, M. A. Cremonini, S. Masiero, S. Pieraccini, J. P. Rabe, P. Samorì, G. P. Spada, G. Gottarelli, *J. Am. Chem. Soc.* **2003**, *125*, 14741.
- [21] G. Gottarelli, S. Masiero, E. Mezzina, S. Pieraccini, J. P. Rabe, P. Samorì, G. P. Spada, *Chem. Eur. J.* **2000**, *6*, 3242.
- [22] S. Lena, G. Brancolini, G. Gottarelli, P. Mariani, S. Masiero, A. Venturini, V. Palermo, O. Pandoli, S. Pieraccini, P. Samorì, G. P. Spada, *Chem. Eur. J.* **2007**, *13*, 3757.
- [23] G. P. Spada, S. Lena, S. Masiero, S. Pieraccini, M. Surin, P. Samorì, *Adv. Mater.* **2008**, *20*, 2433.
- [24] D. González-Rodríguez, P. G. A. Janssen, R. Martín-Rapun, I. De Cat, S. De Feyter, A. P. H. J. Schenning, E. W. Meijer, *J. Am. Chem. Soc.* **2009**, *132*, 4710.

- [25] A. Ciesielski, S. Lena, S. Masiero, G. P. Spada, P. Samorì, *Angew. Chem. Int. Ed.* **2010**, *49*, 1963.
- [26] S. Pieraccini, S. Masiero, O. Pandoli, P. Samorì, G. P. Spada, *Org. Lett.* **2006**, *8*, 3125.
- [27] S. De Feyter, F. C. De Schryver, *Chem. Soc. Rev.* **2003**, *32*, 139.
- [28] C. A. Palma, M. Bonini, T. Breiner, P. Samorì, *Adv. Mater.* **2009**, *21*, 1383.
- [29] C.-A. Palma, J. Bjork, M. Bonini, M. S. Dyer, A. Llanes-Pallas, D. Bonifazi, M. Persson, P. Samorì, *J. Am. Chem. Soc.* **2009**, *131*, 13062.
- [30] A. Ciesielski, G. Schaeffer, A. Petitjean, J. M. Lehn, P. Samorì, *Angew. Chem. Int. Ed.* **2009**, *48*, 2039.
- [31] C. A. Palma, M. Bonini, A. Llanes-Pallas, T. Breiner, M. Prato, D. Bonifazi, P. Samorì, *Chem. Commun.* **2008**, 5289.
- [32] A. L. Marlow, E. Mezzina, G. P. Spada, S. Masiero, J. T. Davis, G. Gottarelli, *J. Org. Chem.* **1999**, *64*, 5116.

Chapter 6.2

Modulating the self-assembly at the solid-liquid interface by pH-mediated conformational switching

The design of functional chemical devices is a hallmark of supramolecular chemistry. It is based on the structural organization and functional integration within a molecular or supramolecular architecture of components presenting features such as photo-, electro- or iono-activity. In the collaboration with the group of Prof. Stefan Hecht from Humboldt University in Berlin (Germany), we designed and investigated by the means of STM two-dimensional ordering of molecules adsorbed on the surface at the solid-liquid interface, that are capable to undergo large conformational changes upon the application of an external chemical stimulus, i.e. change of pH. As a model system we have chosen BTP derivative, which incorporates three tridentate coordination sites of two triazole moieties bridged by a central pyridine ring.

The molecules described in this chapter has been synthesized by Tamer El Malah, in the group of Prof. Stefan Hecht at Humboldt University in Berlin (Germany).

6.2.1 Introduction

Nanoscale control over the mechanical movement of molecules has been intensely investigated in the recent past, aiming at the development of molecular machines^[1-4] that can be implemented in miniaturized systems based on the self-assembly of small molecules.^[5-7] Molecular movement in such systems can be used directly to create nano-porous materials or nanotweezers that can capture or release host molecules^[8-10] or indirectly in order to alter the electronic or optical properties of the systems, for example the nanoswitches^[11] or fluorescence sensors.^[12, 13] In this context it is crucial to design molecular systems able to undergo large conformational changes as a result of external stimuli such as light irradiation,^[14-17] metal complexation^[18-20] or change in pH.^[19] Among them, pH represents a prototypical biological stimulus and is ideally suited for studies performed in solution or at the solid-liquid interface. A related approach has been already used to trigger conformational switching of molecular grippers^[21, 22] that can open or close, or in dynamic chemical devices,^[18] where the change of pH can preferentially lead to the complexation or release of metal ions by the system, enabling the reversible contraction/extension of the molecule. However, to exploit such molecular motions the individual building blocks have to be organized into larger functional arrays on meso- and macroscopic length scales at interfaces. This can be accomplished by making use of self-assembly, which is a reliable bottom-up approach for the fabrication of functional surfaces.^[23, 24] We have recently engaged in a program to utilize click chemistry to construct (macro)molecules of defined shape, thereby using the 2,6-bis(1-phenyl-1,2,3-triazol-4-yl)pyridines (BTP) motif as the key structural feature.^[19, 25, 26] Due to lone pair repulsion, the extended (*syn,syn*)₃ conformation of the BTP scaffold is strongly destabilized and hence the BTP prefers to adopt the thermodynamically favored, kinked (*anti,anti*)₃ conformation (Fig. 6.8), in analogy to bipyridines or terpyridines. Due to favorable electrostatic interactions, the “kinked” *anti,anti* conformation of the BTP core dominates in solution at neutral pH, whereas the repulsive interactions between the lone pair of the nitrogen atoms destabilize the alternative “extended” *syn,syn* conformation. This repulsive interaction can be switched into an attractive one by the addition of acids or metal ions to the solution, causing either protonation or metalation of the BTP core followed by a large structural change from the “kinked” to its corresponding “extended” conformation. As evident from several crystal structures,^[25, 26] the BTP core structure is highly conserved and resembles a flat heteroaromatic entity, able to stack very efficiently as

reflected in the low solubility of unsubstituted derivatives. Based on these observations, we were interested in exploring the self-assembly of properly substituted BTP derivatives at the liquid-solid interface (2D), i.e. their monolayer formation.

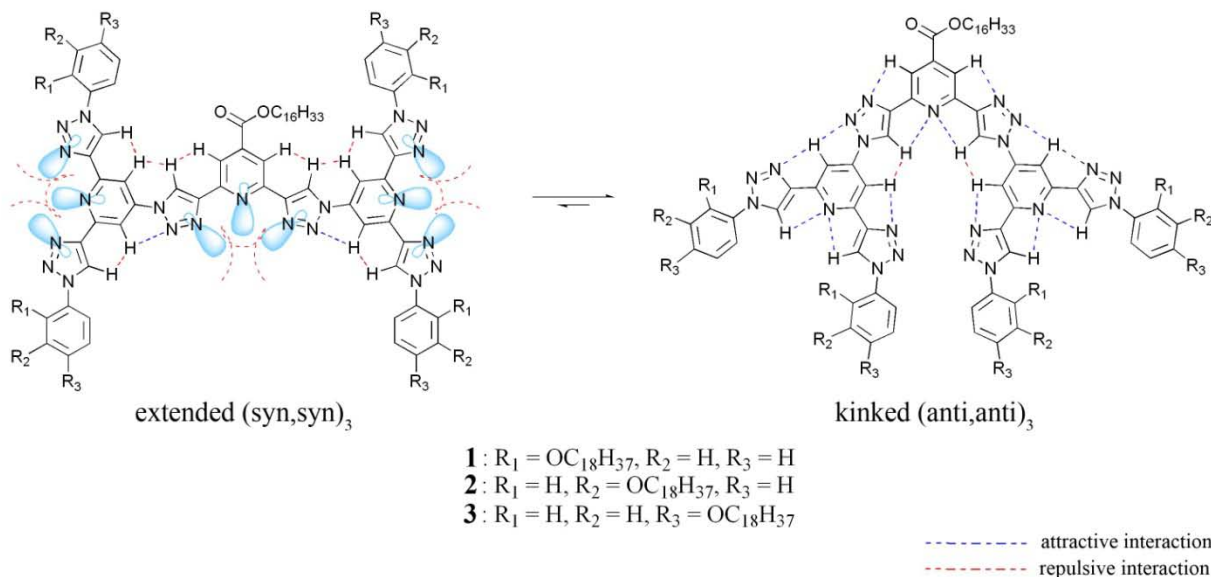


Figure 6.8 Conformational preference of the BTP scaffolds **1-3** to adopt a kinked $(anti,anti)_3$ conformation mainly due to electrostatic and steric repulsion in the $(syn,syn)_3$ conformation.

6.2.2 Results and discussion

Figure 6.9a-c displays STM images of the monolayers of the molecules **1-3**, prepared by applying a drop of a 1 mM solution in 1,2,4-trichlorobenzene (TCB) onto HOPG surface. Interestingly only in case of **1** derivative well ordered monolayer was observed (Fig. 6.9a), whereas in case of **2** (Fig. 6.9b) and **3** (Fig. 6.9c) derivatives only disordered structures were formed at the graphite surface. To gain further insight into the self-assembly of BTP derivatives, we extended our studies to more diluted solutions, i.e. 100 μ M and 10 μ M. Unfortunately, the molecules were not found (by the means of STM), to form any ordered structures. We also extended our study to different solvents, i.e. 1-phenyloctane, tetradecane and 1-heptanoic acid, however once again the obtained results were meaningless.

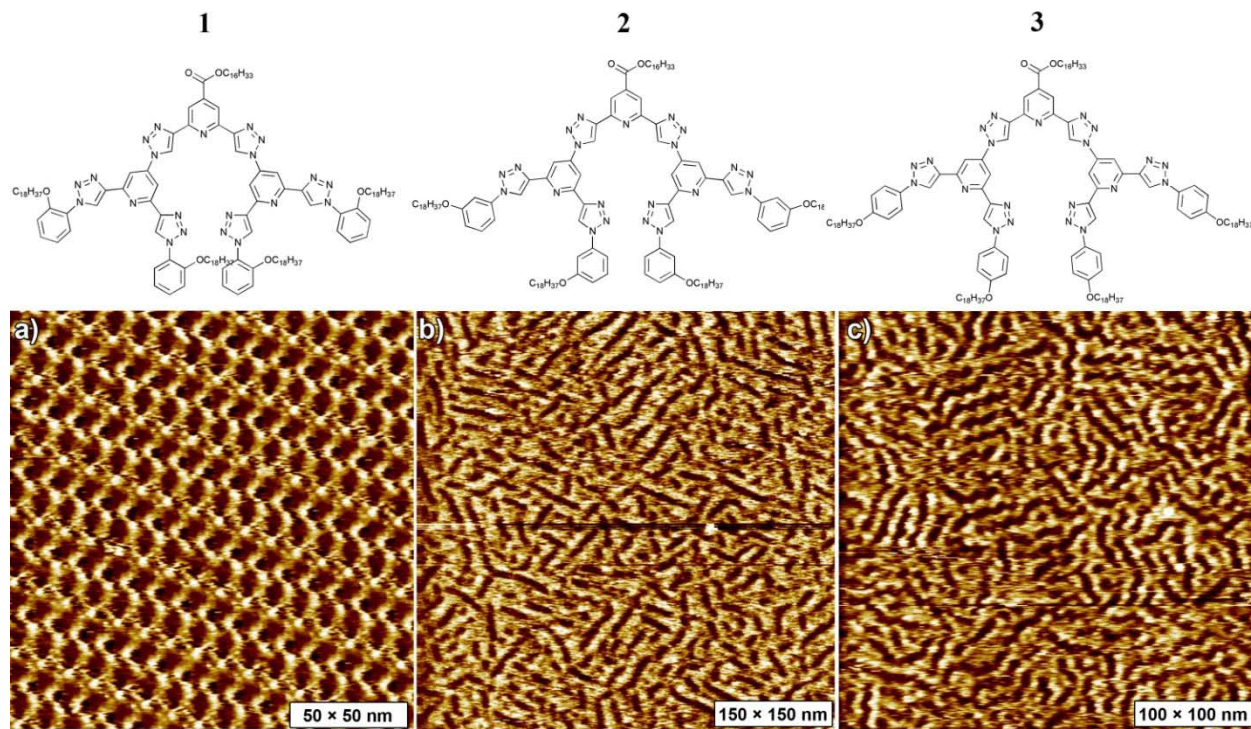


Figure 6.9 Large scale STM images of the **1** (a), **2** (b) and **3** (c) derivatives self-assembled at the solid-liquid interface. Tunneling parameters (a-c): average tunneling current (I_t) = 5 pA, bias voltage (V_t) = 500 mV.

As described above, only molecules **1** was found to form ordered monolayer at the solid-liquid interface. Figure 6.10a displays a small scale STM image of molecules **1** self-assemble on HOPG surface from 1 mM solution in TCB. The unit cell parameters, $a = (7.91 \pm 0.2)$ nm, $b = (3.11 \pm 0.2)$ nm, and $\alpha = (68 \pm 2)^\circ$, lead to an area $A = (22.7 \pm 1.51)$ nm² as well as the proposed packing model in Figure 6.10b suggest that each unit cell is composed by four molecules **1** in their “kinked” conformation, which are probably interacting via van der Waals forces. It is likely that all *ortho*-substituted side chains are physisorbed on the HOPG surface, although, owing to their highly dynamic nature, we are unable to resolve them. It is important to note that molecules **1** were visualized only at the solution – HOPG interface using TCB as solvent.

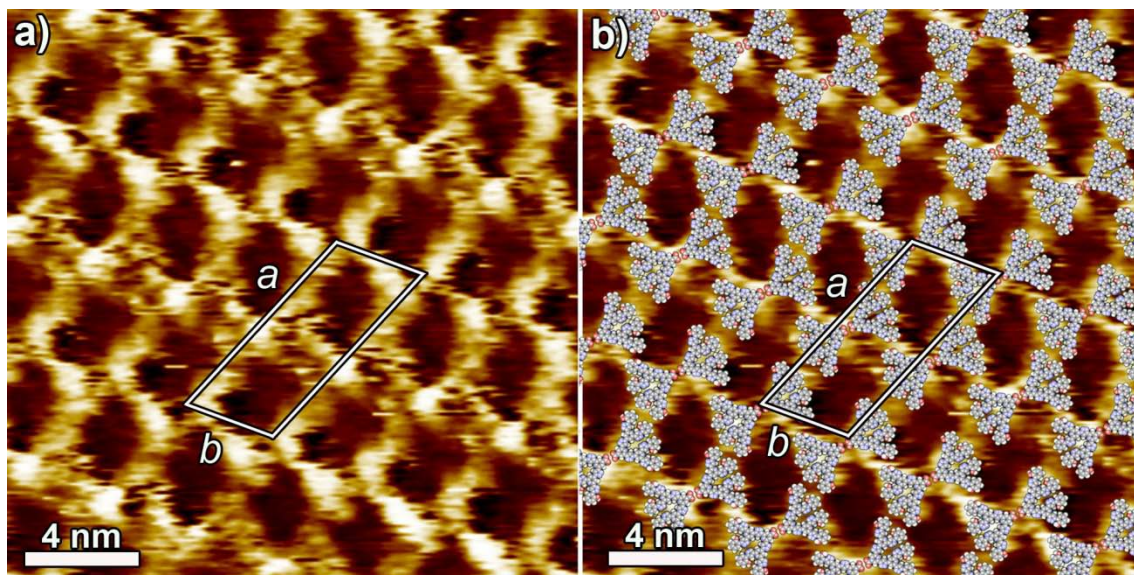


Figure 6.10 (a) STM image of the lamellar assembly of molecules **1** physisorbed on HOPG; (b) proposed molecular packing model showing the molecules **1** in their “kinked” conformation. Tunneling parameters: $I_t = 5$ pA, $V_t = 500$ mV.

In order to trigger the switching of the molecules **1-3** from the “kinked” to the “extended” conformation, a small amount of trifluoroacetic acid (1 mM TFA in TCB) was added on top of the solution covering the already formed monolayers on the surface. Surprisingly, only one out of three molecules was found to undergo conformational changes upon addition of acid. Figure 6.11 shows the resulting physisorbed monolayer of **2** obtained after applying the acidified solution to the surface. In this acidified environment the resulting structure of **2** (Fig. 6.11b) displays 2D architecture consisting of a lamellar-like motif, which appeared on the surface 60 seconds after the deposition of the acidified solution, and can be characterized by the unit cell parameters, $a = (3.21 \pm 0.2)$ nm, $b = (2.61 \pm 0.2)$ nm, and $\alpha = (93 \pm 2)^\circ$, lead to an area $A = (7.7 \pm 0.6)$ nm², where each unit cell contains one molecule **2**. The lamellar domains extend over tens of nanometers and no part of the substrate surface was found to be occupied by molecules adsorbed in the previously described “disordered” packing. The high resolution image (Fig. 6.11a) reveals that the adsorbed molecules adopt an “extended” conformation, thereby unequivocally confirming the occurrence of protonation. It is likely that all *meta*-substituted side chains are backfolded into supernatant solution. The proposed packing model (Fig. 6.11b), extrapolated from high resolution STM measurements, shows unambiguously that the cores of molecule **2** adopt an “extended” conformation, in line with protonation. Significantly, virtually

identical protonation-driven transformations were observed both for ex situ and in situ acidifications of **2**.

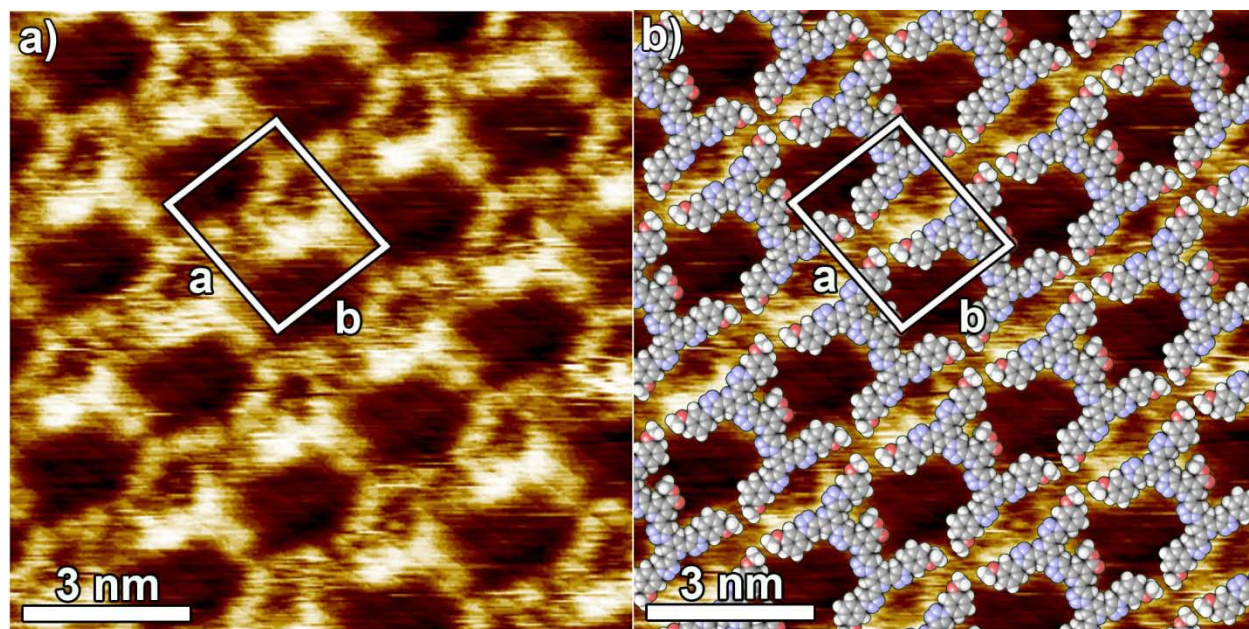


Figure 6.11 (a) small scale STM current image of the lamellar assembly of **2** physisorbed on HOPG; (b) proposed molecular packing model showing the molecules **2** in their “extended” conformation. Tunneling parameters: $I_t = 5$ pA, $V_t = 500$ mV.

The real-time conformational switch, and related reorganization of the self-assembled pattern, occurring at the solid–liquid interface have been monitored *in-situ* on the scale of several tens of nanometers. The transformation from the disordered layer to the “lamellar” motif for **2** based monolayers could be monitored in real-time on the timescale of several tens of seconds, taking advantage of the slow nature of the process. The observed slow switching kinetics are caused by the long alkoxy chains of **2**, providing an increased desorption energy on graphite and hence a partial hindrance towards reorganization of the self-assembled motif. Figure 6.12 shows a set of measurements where the “disordered” layer is gradually converted into “lamellar” over a time scale of 60 seconds, the latter “lamellar” packing becoming the more favorable over the time. The total coverage of the surface by the “lamellae” assembly is completed a few minutes after the deposition of the droplet of the acidified solution. The fuzzy parts on the STM images

correspond to areas where the considerable mobility of the molecules, triggered by the protonation process, hinders high resolution STM imaging.

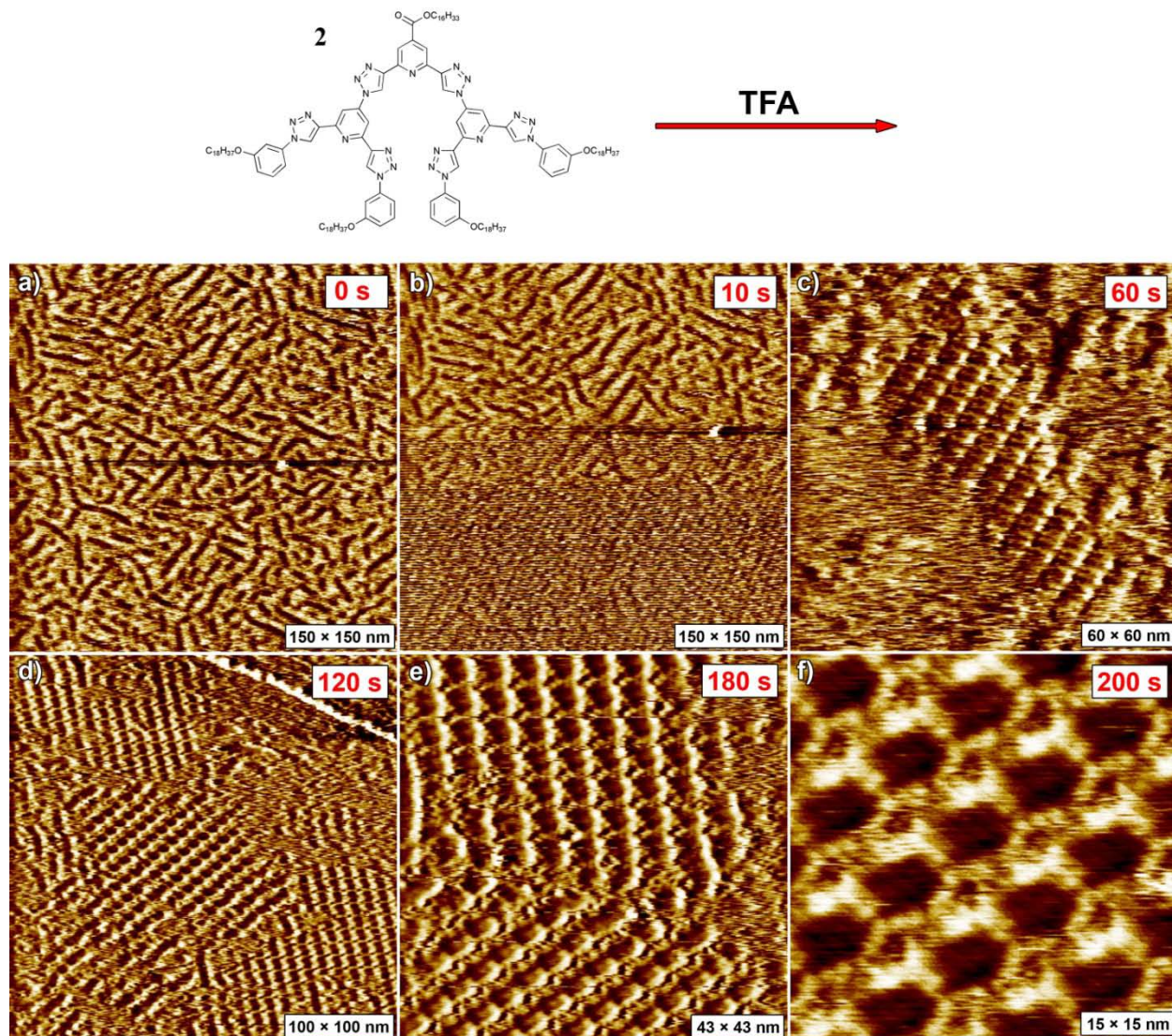


Figure 6.12 Consecutive STM images showing the structural evolution of a monolayer of **2** over 3 min after the addition of ca. 5 μ L of 1mM solution of TFA in TCB. (a) Image taken right before the addition of TFA (b) After 10 seconds (c) After 1 minute (d) After 2 minutes (e) after 3 minutes and (f) after 200 seconds. Tunneling parameters: $I_t = 5$ pA, $V_t = 500$ mV.

6.2.3 Conclusions

In summary, we have utilized STM to visualize large conformational changes of a responsive molecular building block resulting in its dramatically altered self-assembly behavior at the solid–

liquid interface. Protonation can successfully be used to overcome the repulsive interaction between the adjacent N atoms present in the neutral “kinked” heteroaromatic BTP molecule and result in the formation of an “extended” conformation on a HOPG surface. This represents the first yet crucial step towards the development of reversible pH triggered switches at the solid-liquid interface. Unfortunately, it is still unclear for us why only one out of three molecules, was found to undergo such conformational changes. However, the fact that we observed well ordered monolayers of *ortho* substituted BTP derivative, i.e. molecule **1**, is consistent with our previous experiments on BTP derivatives, where only *ortho* substituted molecules were found to form well ordered supramolecular architectures at the solid-liquid interface.^[19] It is evident that the alkoxy-substitution plays a crucial role in the stabilization of self-assembled monolayers at the solid-liquid interface, their interaction with HOPG surface increases linearly with the length of the C_n chains. It is most likely, that in case of molecules **2** (*meta*) and **3** (*para*) in their “kinked” (*anti, anti*)₃ conformation, all of the alkoxy chains cannot physisorbed at the same time on HOPG surface, therefore the molecules adopt another conformation, which was visualized at the solid-liquid interface. Furthermore, more sophisticated, functionalized (macro)molecules are being synthesized in order to control the adsorption conformation of extended foldamers on solid substrate surfaces^[27] and to switch relevant physico-chemical properties within the monolayer, in particular fluorescence and conductivity.

6.2.4 Experimental procedure

Scanning Tunneling Microscopy STM measurements were performed using a Veeco scanning tunneling microscope (multimode Nanoscope III, Veeco) at the interface between highly oriented pyrolytic graphite (HOPG) and a supernatant solution. Diluted solutions of molecules **1-3** were applied to the basal plane of the surface. For STM measurements the substrates were glued on a magnetic disk and an electric contact is made with silver paint (Aldrich Chemicals). The STM tips were mechanically cut from a Pt/Ir wire (90/10, diameter 0.25 mm). The raw STM data were processed through the application of background flattening and the drift was corrected using the underlying graphite lattice as a reference. The latter lattice was visualized by lowering the bias voltage to 20 mV and raising the current to 65 pA. All of the models were minimized with Chem3D at the MM2 level. The molecules were dissolved in 1,2,4-trichlorobenzene with an approximate concentration of 1 mM, and diluted to the concentrations 100 μM and 10 μM

respectively. The protonation of the molecules was performed *ex situ*, by addition of trifluoroacetic acid (TFA) to the solution containing the molecules before the deposition, and *in situ*, that is, when an acidified solution of 1,2,4-trichlorobenzene was deposited on top of the already formed monolayers, under the STM tip. It is important to note that the *ex situ* and *in situ* protonation of the molecule **2** led to the same effects on the monolayers, whereas the *ex situ* and *in situ* protonation of **1** and **3** solutions did not result in any meaningful results.

References

- [1] B. L. Feringa, *Nature Chemistry* **2010**, *2*, 429.
- [2] V. Balzani, M. Gomez-Lopez, J. F. Stoddart, *Acc. Chem. Res.* **1998**, *31*, 405.
- [3] E. R. Kay, D. A. Leigh, F. Zerbetto, *Angew. Chem. Int. Ed.* **2007**, *46*, 72.
- [4] K. Kinbara, T. Aida, *Chem. Rev.* **2005**, *105*, 1377.
- [5] V. Balzani, A. Credi, F. M. Raymo, J. F. Stoddart, *Angew. Chem. Int. Ed.* **2000**, *39*, 3349.
- [6] F. M. Raymo, *Adv. Mater.* **2002**, *14*, 401.
- [7] W. R. Browne, B. L. Feringa, *Nature Nanotech.* **2006**, *1*, 25.
- [8] T. Muraoka, K. Kinbara, T. Aida, *J. Am. Chem. Soc.* **2006**, *128*, 11600.
- [9] T. Muraoka, K. Kinbara, T. Aida, *Nature* **2006**, *440*, 512.
- [10] A. Khan, C. Kaiser, S. Hecht, *Angew. Chem. Int. Ed.* **2006**, *45*, 1878.
- [11] J. E. Green, J. W. Choi, A. Boukai, Y. Bunimovich, E. Johnston-Halperin, E. DeIonno, Y. Luo, B. A. Sheriff, K. Xu, Y. S. Shin, H. R. Tseng, J. F. Stoddart, J. R. Heath, *Nature* **2007**, *445*, 414.
- [12] V. A. Azov, A. Schlegel, F. Diederich, *Angew. Chem. Int. Ed.* **2005**, *44*, 4635.
- [13] A. Archut, G. C. Azzellini, V. Balzani, L. De Cola, F. Vogtle, *J. Am. Chem. Soc.* **1998**, *120*, 12187.
- [14] J. M. Mativetsky, G. Pace, M. Elbing, M. A. Rampi, M. Mayor, P. Samorì, *J. Am. Chem. Soc.* **2008**, *130*, 9192.
- [15] G. Pace, V. Ferri, C. Grave, M. Elbing, C. von Hanisch, M. Zharnikov, M. Mayor, M. A. Rampi, P. Samorì, *Proc. Nat. Acad. Sci. USA* **2007**, *104*, 9937.
- [16] J. Henzl, M. Mehlhorn, H. Gawronski, K. H. Rieder, K. Morgenstern, *Angew. Chem. Int. Ed.* **2006**, *45*, 603.
- [17] C. Dri, M. V. Peters, J. Schwarz, S. Hecht, L. Grill, *Nature Nanotech.* **2008**, *3*, 649.

- [18] M. Barboiu, J. M. Lehn, *Proc. Nat. Acad. Sci. USA* **2002**, *99*, 5201.
- [19] L. Piot, R. M. Meudtner, T. El Malah, S. Hecht, P. Samorì, *Chem. Eur. J.* **2009**, *15*, 4788.
- [20] A. Ciesielski, S. Lena, S. Masiero, G. P. Spada, P. Samorì, *Angew. Chem. Int. Ed.* **2010**, *49*, 1963.
- [21] Y. Yamakoshi, R. R. Schlittler, J. K. Gimzewski, F. Diederich, *J. Mater. Chem.* **2001**, *11*, 2895.
- [22] V. A. Azov, A. Beeby, M. Cacciarini, A. G. Cheetham, F. Diederich, M. Frei, J. K. Gimzewski, V. Gramlich, B. Hecht, B. Jaun, T. Latychevskaia, A. Lieb, Y. Lill, F. Marotti, A. Schlegel, R. R. Schlittler, P. J. Skinner, P. Seiler, Y. Yamakoshi, *Adv. Funct. Mater.* **2006**, *16*, 147.
- [23] J. P. Rabe, S. Buchholz, *Science* **1991**, *253*, 424.
- [24] S. De Feyter, F. C. De Schryver, *Chem. Soc. Rev.* **2003**, *32*, 139.
- [25] R. M. Meudtner, S. Hecht, *Angew. Chem. Int. Ed.* **2008**, *47*, 4926.
- [26] R. M. Meudtner, S. Hecht, *Macromol. Rapid Commun.* **2008**, *29*, 347.
- [27] J. van Esch, H. Valkeiner, S. Hartwig, S. Hecht, *Foldamers: Structure, Properties, and Applications (Eds.: S. Hecht, I. Huc)*, Wiley-VCH, Weinheim **2007**, 403.

Chapter 6.3

3D responsive self-assembled monolayers: positioning molecular functions onto surfaces

So far, several examples of chemically controlled switching of small molecules physisorbed flat at the solid-liquid interface have been presented. The final section of this thesis will be dedicated to illustrating how such molecular switches, when designed ingeniously, can also be powered by nature's most abundant and powerful energy source, i.e. light. In the collaboration with the group of Prof. Stefan Hecht from Humboldt University in Berlin (Germany), we designed and characterized by the means of STM three-dimensional (3D) responsive monolayers adsorbed on the surface at the solid-liquid interface, that are capable to undergo conformational changes upon the light irradiation. As a model system we have chosen oligofluorene derivative, equipped with two carboxylic acid groups, long alkyl chains and photo-switchable azobenzene unit. Oligofluorene platform acts as a pedestal that enforces a controlled orientation of the functional groups, i.e. azobenzene units, relative to the surface and determines their size spacing between these groups, resulting in arrays of functional 3D molecular switches operating at the solid-liquid interface.

The molecule described in this chapter has been synthesized by Dr. David Bléger, in the group of Prof. Stefan Hecht.

6.3.1 Introduction

Small organic molecules, capable of undergoing efficient and reversible photochemical reactions between two stable isomers featuring markedly different properties, continue to impact the materials world. It has been widely accepted that supramolecular assemblies of well-defined π -conjugated oligomers will play a crucial role in the advancement of molecular electronic devices, since their precise chemical structure and physical properties are able to define functional properties and facilitate enhanced control over their supramolecular architecture.^[1, 2] Among conjugated oligomers, oligofluorenes (OFs) often act as high performance blue emitters for application in organic light-emitting diodes (OLEDs). Moreover, OFs possessing a ternary symmetry confer very promising properties for nonlinear optics and electronic or optoelectronic devices.^[3, 4] Attaching reversibly switchable molecular functions, such as molecules that can undergo photo-, redox-, or electric field-induced isomerization, to the surface is a topic of major interest for the preparation of advanced nanosystems.^[5-10] Among photochromic molecules, azobenzenes have been extensively studied for their unique photoisomerization.^[11] The transition from the thermodynamically more stable *trans* to the *cis* conformation can be induced by irradiation with UV light and reversed upon heating or irradiation with visible light.^[12] The isomerization occurs at the N=N double bond yielding two different states, identified by the *trans*(E)- and the *cis*(Z)-isomer. Such photochemical reversible *trans-cis* isomerization of azobenzene was first described by Krollpfeiffer and co-workers,^[13] and it has been thoroughly studied in the last decades.^[14, 15]

The mechanism of the photoisomerization of azobenzene molecules has been a fundamental subject for many years not only for its potential applications in industry^[15-18] but also for its longstanding debate on the isomerization process occurring along either the inversional or the rotational pathway (Fig. 6.13).^[15, 19] In solutions, the UV-visible spectra of the molecule are featured with two major absorption bands corresponding to the $S_0 \rightarrow S_1$ and the $S_0 \rightarrow S_2$ transitions. The former transition relates to a symmetry-forbidden $n-\pi^*$ transition with the maximum intensity near 440 nm whereas the latter transition corresponds to a symmetry-allowed $\pi-\pi^*$ transition with the maximum intensity near 320 nm.^[20, 21] Early steady-state measurements show that the quantum yields of the *trans*-to-*cis* isomerization are wavelength-dependent: The yield measured in hexane solvent is 0.20-0.27 upon excitation to the $S_1(n-\pi^*)$ state but it drops dramatically to 0.09-0.12 for the $S_2(\pi-\pi^*)$ excitation.^[20, 21] However, the quantum yields become

almost wavelength-independent when rotation about the N-N double bond is restricted by blocking the rotation with a bulky group.^[22, 23] According to the recent theoretical study,^[19] the inversion channel is energetically less favored, however from the other hand rotation channel can be favored out in case of restricted azobenzenes such as azobenzenophanes.^[22]

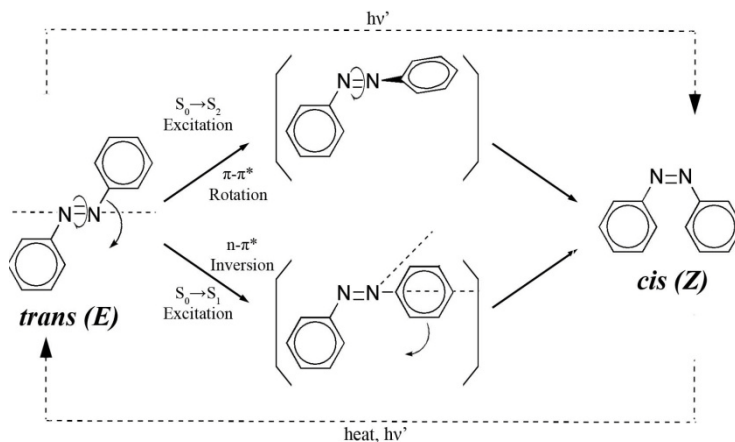


Figure 6.13 Reaction mechanism of photoisomerization of *trans*-azobenzene.^[15]

While the solution properties are well-established, a poor investigation on densely packed molecular assembly at surfaces of isomerizable molecules has been performed. A key requirement for preserving such functions in an adsorbed monolayer film is sufficient free volume availability for the functional group as well as an adsorption geometry that avoids direct contact of this group with the surface. In particular on metal substrates the latter can result in a strong degradation or even complete quenching of the desired function.^[24] The reversible switching of azobenzene derivatives has already been investigated at room temperature on the single molecule level by Scanning Tunneling Microscopy (STM) experiments in ultra-high vacuum (UHV) studies on isolated molecules packed parallel to the basal plane of the substrate,^[25-27] in physisorbed monolayers at the solid-liquid interface,^[28, 29] on SAMs chemisorbed on Au surface,^[5, 7] on Au nanoparticles^[30, 31] and as co-adsorbate in a chemisorbed alkyl thiolated SAM on solid flat substrates.^[32] To date, STM visualization at the solid-liquid interface of monolayers consist only from the azobenzene molecules in their *cis* form was not reported. Monolayers consist of azobenzene derivatives in their *cis* conformation, can be characterized by low stability and dynamic nature, i.e. the tendency to *cis*→*trans* isomerization.

Therefore, it is a great challenge to design molecular systems which can allow to visualize, by the means of STM the photoisomerisation process at the single molecule level.

In this chapter we introduce a novel concept where the azobenzene functional units can be precisely located on the surface and separate with the given distance. The molecules are physisorbed on highly oriented pyrolytic graphite (HOPG) surface via rigid platform based on terfluorene unit **1**, equipped with two carboxyl group at each end and lateral dodecyl chains. We decided to use fluorene based platform, since they are known to form well ordered monolayers at the solid-liquid interface.

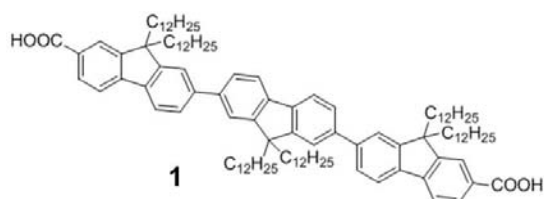


Figure 6.14 Molecular structure of fluorene based molecular platform **1**.

A recent work^[33] has shown that controlled formation of the H-bonded networks on the HOPG surface can be achieved by using star-shaped oligofluorenes end-capped with carboxylic groups (Fig. 6.14). Those molecules have been found to form, H-bonded honeycomb networks at the solid-liquid interface.

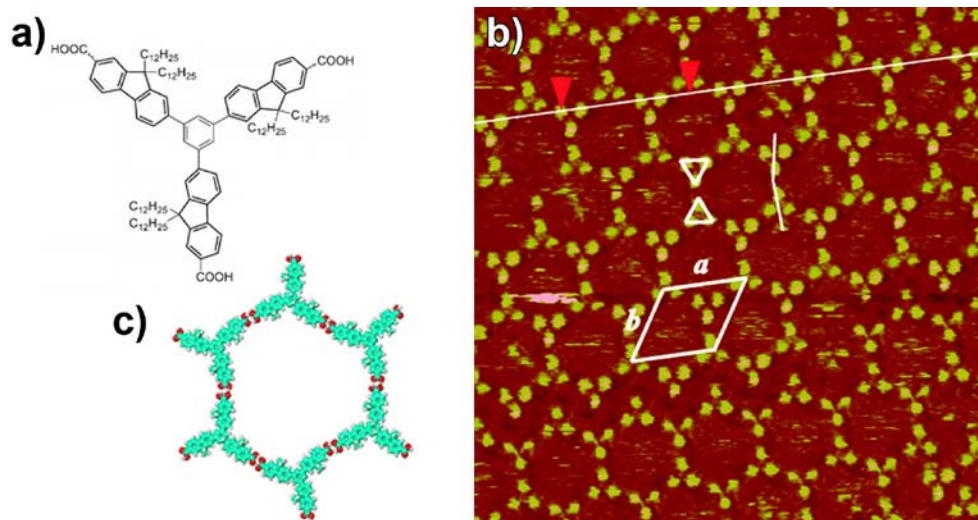


Figure 6.14 (a) Molecular structure star-shaped oligofluorene derivative; (b) STM image of physisorbed monolayer and proposed molecular packing motif (c).^[33]

Knowing, that oligofluorene-based molecules, especially the ones equipped with carboxylic groups, are forming well ordered monolayers, we decided to use them as a platforms in our molecular systems. These platforms, can also act as pedestals that enforce a controlled orientation of the functional azobenzene groups relative to the surface, and determine the by their size the spacing between photochemically switchable azobenzene groups, resulting in arrays of 3D responsive molecular motors (Fig. 6.15). Functional molecules **2** and **3**, can be expected to self-assemble into 2D supramolecular arrays (see molecule **2** in Fig. 6.15) or into 1D linear H-bonded supramolecular polymers (see molecule **3** in Fig. 6.15), thanks to the presence of two carboxylic groups, and they can also act as pedestals that enforce a controlled orientation of the photochemically switchable azobenzene groups, resulting in arrays of 3D responsive molecular motors (Fig. 6.15). Furthermore, our scaffold, by offering the possibility to control switching of azobenzenes when placed at tunable distance one another, can be a viable approach to explore fundamental photochemical properties of non-interacting azobenzenes at surfaces such as the contribution of $\pi-\pi^*$ vs $n-\pi^*$ in the isomerization paving the way towards the development of azobenzene based unirotational switches (in $\pi-\pi^*$ process).^[22, 23]

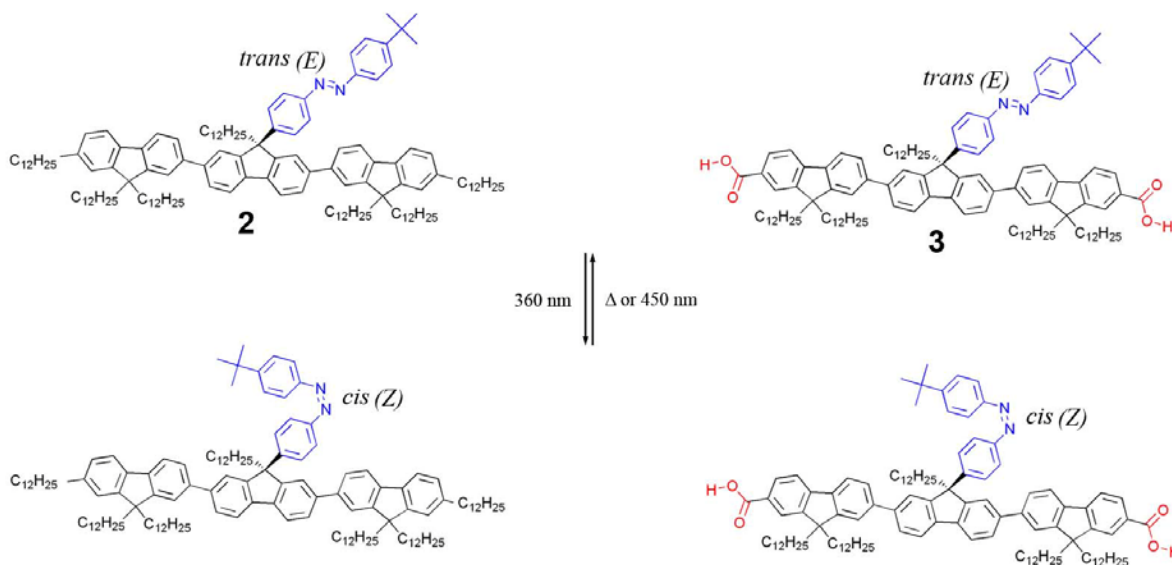


Figure 6.15 Schematic representation of functionalized platforms **1** and **2**, capable to undergo controlled reversible photochemical reaction upon the light irradiation.

6.3.2 Results and discussion

Scanning tunneling microscopy (STM) was used to probe the self-assembly behavior of the molecules **1-3** at the solution-graphite interface. Initially we investigated the self-assembled structures obtained by applying a drop of a supernatant solution of molecules **1** in 1-phenyloctane. Figure 6.16a shows large scale STM current image of physisorbed monolayer which consists of hundreds of square nanometers large polycrystalline curved structures that are stable over several hours. Molecules **1** form H-bonded linear supramolecular polymers, thanks to the presence of two carboxylic acid groups at extremis. Furthermore the entire crystalline structure is stabilized by interdigitated alkyl chains. Domains observed with STM exhibit a unit cell: $a = (3.06 \pm 0.2)$ nm, $b = (2.75 \pm 0.2)$ nm, $\alpha = (40 \pm 2)^\circ$ leading to an area $A = (5.4 \pm 0.47)$ nm², where each unit cell contains one molecule **1** (Fig. 6.16c).

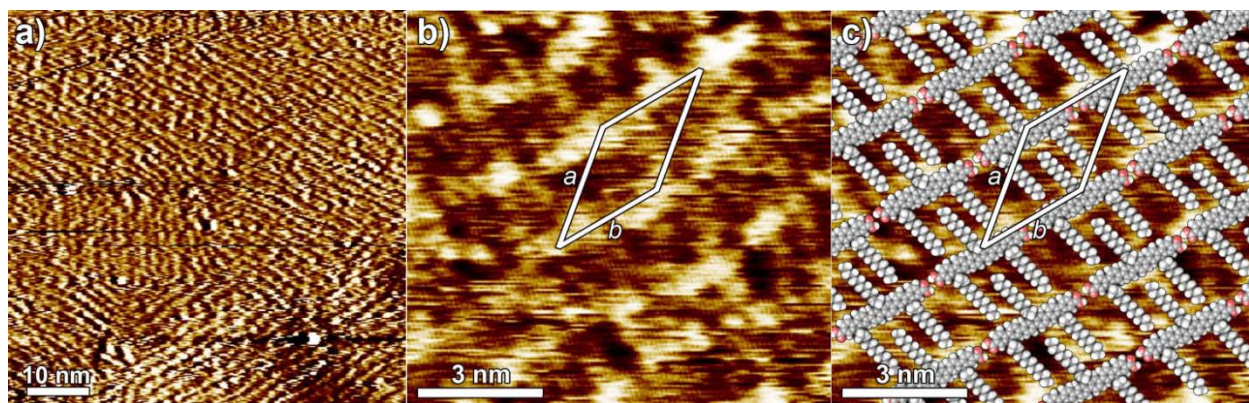


Figure 6.16 (a) Large scale STM height image of **1** at the solid-liquid interface; (b) Small scale STM height image of **1** at the solid-liquid interface; (c) proposed CPK packing model of the self-assembly of **1**. Tunneling parameters: Average tunneling current (I_t) = 5 pA, tip bias voltage (V_t) = 1.5 V.

We extended our study to the solution of the molecule **2**. Unfortunately, the molecules **2** were found to form disordered structures at the solid-liquid interface. Self-assembly study of **2** in different solvents like 1,2,4-trichlorobenzene (TCB), tetradecane, heptanoic acid and nonanoic acid, as well as concentration dependency experiments did not produced any significant results. We then extended our study to the solution of the molecule **3**. A drop (4 μ L) of a 1 mM solution of *trans*-**3** in 1-phenyloctane. Figure 6.17a shows an STM height image of the physisorbed monolayer. It reveals a monocrystalline domain obtained from a hundreds of square nanometers

large polycrystalline structure (Fig. 6.18a) which is stable over several minutes. Within the crystal it is possible to identify self-assembled 1D H-bonded supramolecular polymers, as a result of the formation of hydrogen bonds between the carboxylic acid groups attached to the terfluorene pedestal. The crystalline structure is further stabilized by interdigitation of the alkyl chains between adjacent polymer rows. Only three out of the five dodecyl chains attached to building block **3** are physisorbed on the HOPG surface, owing to the tetrahedral geometry of sp^3 -hybridized 9-carbon atoms of the fluorenes; the two other dodecyl chains point toward the supernatant solution.^[33] Interestingly, periodic brighter spots are observed within the monolayer. In view of their spacing through molecular modeling it is possible to assign them to the upright oriented azobenzene parts of the molecules (marked in yellow in Fig. 6.17a) emerging as pillars from the flat 2D structure. Taking into account the adsorption energy of two different functional units of central fluorene moiety (position 9, sp^3 carbon), i.e. azobenzene unit and $-C_{12}H_{25}$ alkyl chain, and the presence of heteroatoms in the azobenzene moiety together with the bulky *tert*-butyl end-group, it is most likely that the affinity for HOPG is higher for $-C_{12}H_{25}$ substituent. Note that the adsorption energy of one methylene group on graphite is around 2.6 kcal/mol (11 kJ/mol, ~ 0.1 eV).^[34, 35] The size of observed bright features (0.81 nm^2) is 80% larger than the van der Waals cross-section of the azobenzene moiety of molecule **3** packed edge-on on the basal plane of HOPG (0.45 nm^2). However, such a discrepancy can be explained in view of the moiety's dynamic nature, i.e. possible rotation among fluorene-azobenzene C-C bond, and the scanning speed of the STM tip. Indeed rotation among single C-C bond can be as fast as 10^{-12} sec,^[36] whereas the speed of STM imaging is on the 10^{-4} sec time scale. The observed crystalline domains exhibit a unit cell: $a = (2.9 \pm 0.2) \text{ nm}$, $b = (2.2 \pm 0.2) \text{ nm}$, $\alpha = (50 \pm 2)^\circ$ leading to an area $A = (4.88 \pm 0.47) \text{ nm}^2$, where each unit cell contains one molecule **3** (Fig. 6.17a).

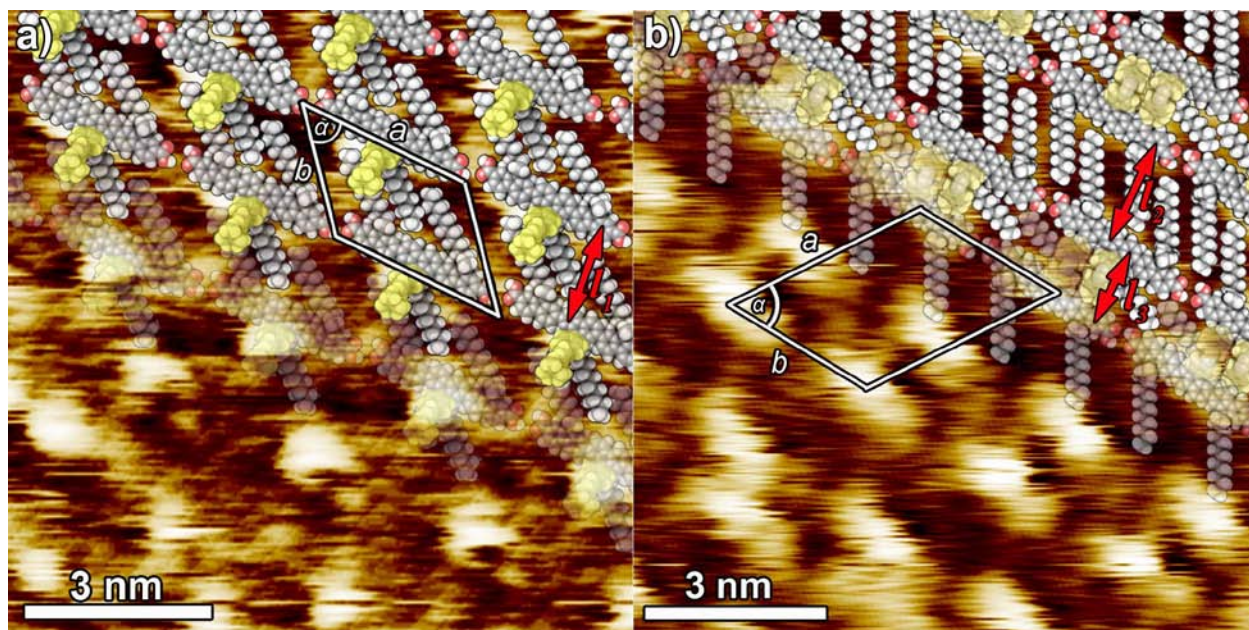


Figure 6.17 STM height image of **3** at the HOPG-1-phenyloctane interface in its *trans* isomer (a), and *cis* form (b) obtained upon UV irradiation of the *trans* monolayer for ca. 1h. Tunneling parameters: average tunneling current $I_t = 5\text{ pA}$ and tip bias voltage $V_t = 2\text{ V}$.

It is noteworthy that molecules **3** were found to form an ordered physisorbed monolayer at the HOPG–solution interface only upon using 1-phenyloctane as solvent. Study of this system in different solvents like 1,2,4-trichlorobenzene (TCB), tetradecane, heptanoic acid and nonanoic acid did not produce any ordered 2D structures. Also the choice of the concentration of the investigated solutions was stringent. Crystalline domains (Fig. 6.18a) were observed only upon the use of 1mM solutions of **3**. STM investigation of diluted solutions of **3** in 1-phenyloctane, i.e. 100 and 10 μM , did not produce any meaningful results.

The STM image of the interface after *in-situ* irradiation of the monolayer of **3** with UV light (UV-Pen Type Lamp, 354 nm, 1 mW) is displayed in Figures 6.17b and 6.18d. The domains, which feature a different structure if compared to that in Figure 6.17b, exhibit linear supramolecular architectures that can be ascribed to H-bonded supramolecular polymers of *cis*-**3**, as revealed by the following observations. First, the spacing between two adjacent 1D arrays is in this case is not always identical, as found in physisorbed monolayers of *trans*-**3** ($l_1 = 1.6\text{ nm}$). Two different spacing values between alternating polymer rows can be extracted from the STM

image, i.e. l_2 (1.7) and l_3 (1.2 nm) as marked with red arrows on Figure 6.17b. In the *cis*-domains, the H-bonded 1D architectures are laterally spaced according to a “dimeric” motif, where two building blocks of adjacent rows are held in close proximity. These more compact packing features a different tilt of the aliphatic side chains as well as azobenzene units likely interacting through Van der Waals forces. Despite we cannot provide an unambiguous and detailed insight into the conformation adopted by the azobenzene units, the bright features in the STM image are clearly different compared to *trans*-**3** domains. When a bright protrusion emerged at the center of *trans*-**3** molecules, in *cis*-**3** the bright features extend over the whole platform, most likely indicative of a decrease of the molecular height. Domains observed with STM exhibit a unit cell: $a = (3.6 \pm 0.2)$ nm, $b = (2.9 \pm 0.2)$ nm, $\alpha = (57 \pm 2)^\circ$ leading to an area $A = (8.75 \pm 0.63)$ nm², where each unit cell contains two molecules **3** (Fig. 6.17b). Importantly, such a dimeric motif was visualized only upon illumination of the monolayer with UV light. Finally, such observations, together with the non-photoresponsive character of **1**, i.e. the bare platform bearing no azobenzene (Fig. 6.16), strongly support that the monolayer observed after UV light irradiation is based on *cis*-**3** molecules.

The reversible structural reorganization of the monolayer of **3** from *trans* to *cis* motif was monitored in real-time over several tens of minutes, taking advantage of the slow nature of the process. Figure 6.18 shows a set of measurements where the *trans* domains are gradually converted into *cis* ones over a time scale of 55 min (Fig. 6.18a-d), the latter *cis* packing becoming the more favorable over time. The total coverage of the surface by the *cis* assembly is completed in 55 min after the irradiation (Fig. 6.18d). The fuzzy parts on the STM images correspond to areas where the considerably high mobility of the molecules, triggered by the irradiation process, hinders high resolution STM imaging.

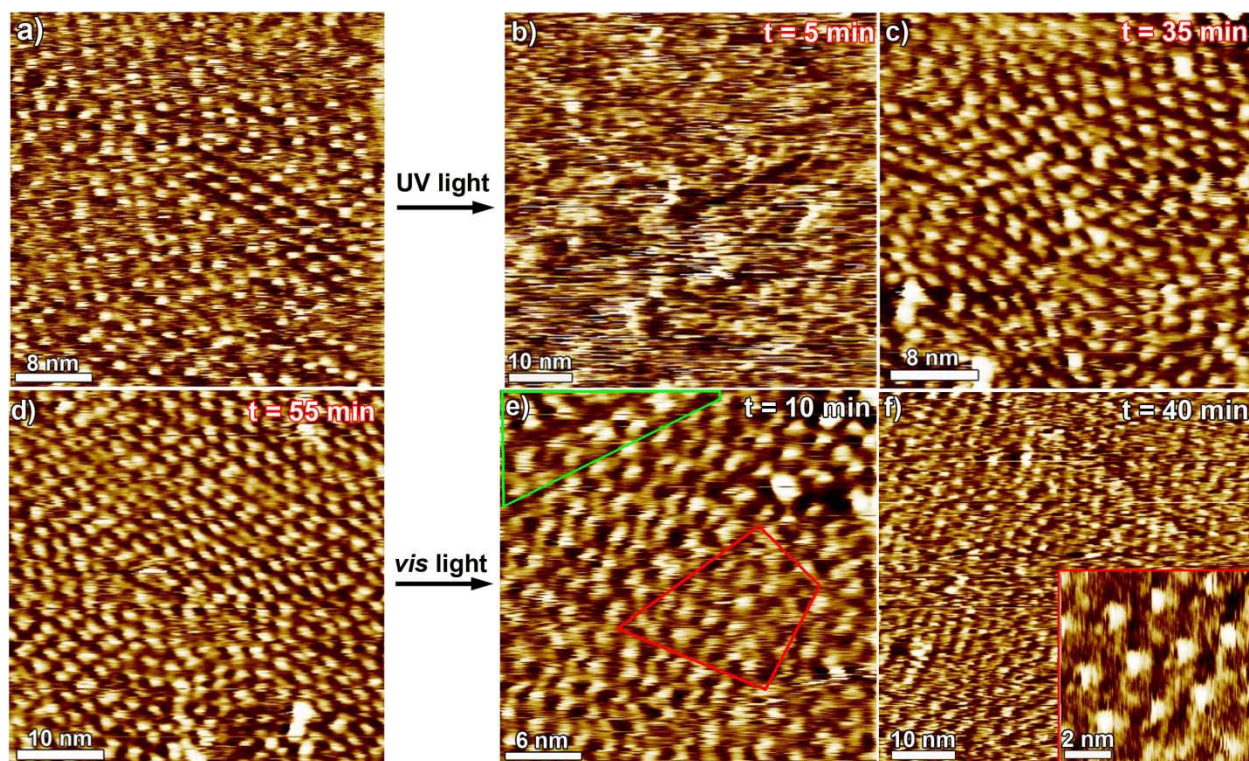


Figure 6.18 Structural reorganization of a monolayer of *trans*-**3** (a) to a monolayer of *cis*-**3** (d) upon UV light irradiation, and back process leading to the recovery of a monolayer of *trans*-**3** (f) upon visible light irradiation. (a-d) Large scale STM height images of **3** at the solid-liquid interface after different irradiation time with the UV light starting from a monolayer of *trans*-**3** (a); (e, f) Large scale STM height images of **3** at the solid-liquid interface recorded after 10 min (e) and 40 min (f) of visible light irradiation starting from a monolayer of *cis*-**3** (d). On figure (e), where the two isomers are co-adsorbed, the red lines encircle a *trans*-**1** domain, the green lines encircle a *cis*-**3** domain. Tunneling parameters: $I_t = 5\text{ pA}$ and $V_t = 2\text{ V}$.

The area occupied by single molecule in the *trans* and *cis* form amount to $(4.88 \pm 0.47)\text{ nm}^2$ and $(4.35 \pm 0.34)\text{ nm}^2$, respectively. Such a difference indicates that the switching process has occurred by desorption of *trans*-**3** and subsequent readsorption of *cis*-**3** molecules present in the supernatant solution (as established by solution studies, after one hour irradiation at 357 nm the supernatant solution contains 34 % of *cis*-**3** molecules). Upon irradiation of the *cis*-**3** monolayer with visible light the *trans* monolayer 2D motif is formed again (Fig. 6.18e,f). A short illumination (Fig. 6.18e) leads to monolayers exposing the two coexisting isomers, i.e. *trans* (marked in red) and *cis* (marked in green). Further irradiation resulted in desorption of the molecules, which after some time (ca. 40 min) re-adsorb in *trans* type of assembly (Fig. 6.18f), proving the reversible nature of the process.

Solution study: **3** does not exhibit the typical behavior of azobenzene derivatives in solution since, upon irradiation at the maximum of the π - π^* transition absorbance (360 nm) in phenyloctane (solvent used for the STM investigations), only *ca.* 34 % of the *trans* form is isomerized into the *cis* form, thus leading to a relatively *cis*-poor photostationary state (PSS) (estimated by NMR spectroscopy, see Fig. 6.19). The partial quenching of the *trans* to *cis* isomerization results most likely from energy and electron transfers between the azobenzene unit and the terfluorene platform, a highly fluorescent chromophore. Note that also the terfluorene fluorescence is quenched in **3**. Nevertheless, complete quenching of the *trans* to *cis* isomerization was very likely avoided by connecting the azobenzene to the terfluorene *via* a non-conjugated linker that is, the sp^3 -hybridized 9-carbon atom of the central fluorene.

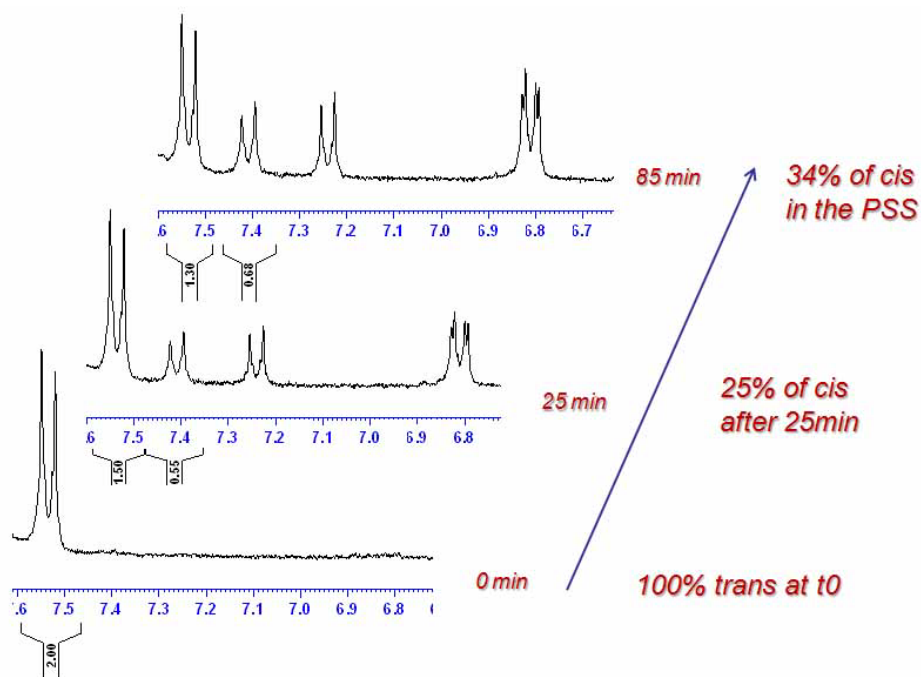


Figure 6.19 ^1H NMR spectra of **3** and the evolution of proton signals during the irradiation of a 10^{-3} M solution of **3** in CD_2Cl_2 at 357nm.

Interestingly, the choice of the used solvent has no visible influence on the composition in the PSS, as noticed by UV-Vis spectrometry. Indeed, the UV-vis spectra of **3** (before and after irradiation) in dichloromethane and in 1-phenyloctane can be superimposed (Fig. 6.20).

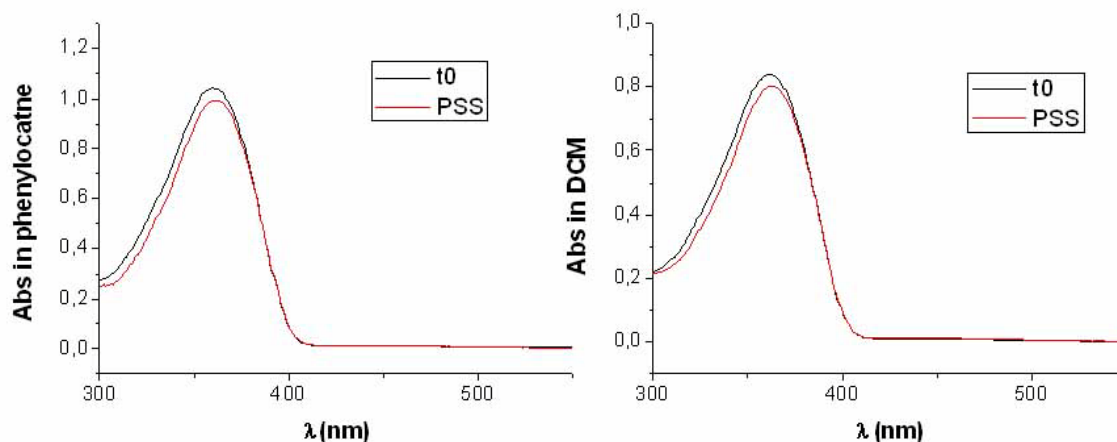


Figure 6.20 UV-Vis spectra of **3** in 1-phenyloctane and dichloromethane.

6.3.3 Conclusions

In summary, we have shown that properly designed fluorene platform **1**, can self-assemble into 1D H-bonded supramolecular polymers at the solid-liquid interface. Properly designed 3D building block (**3**) exposing a vertically oriented azobenzene when physisorbed on HOPG in its *trans* form has been investigated by STM. The switching of the monolayer consisting of upright oriented *trans*-azobenzene to the corresponding monolayer based on *cis*-azobenzenes has been triggered by light, leading to a significant structural change of the self-assemblies in the 3D (decrease of height) as well as in the plane of the substrate (different packing). The present results provide the first example of sub-molecularly resolved vertically oriented switchable chromophores in physisorbed monolayers as well as physisorbed azobenzene switch monitored in the two states at surfaces. We are currently investigating the possibility to nail this type of building blocks on carbon based surfaces *via* a two-step process involving first the physisorption of the molecules with controllable spacing on the surface followed by their chemisorption *via* chemical groups suitable to react with HOPG and graphene. These chemical groups can be attached to the C9 positions of the fluorene units using well-established nucleophilic substitution strategies, or at the end of the alkyl chains. Our scaffold, by offering the possibility to control switching of azobenzenes when placed at tunable distance one another, can be a viable approach to explore fundamental photochemical properties of non-interacting azobenzenes at surfaces such as the contribution of $\pi\text{-}\pi^*$ vs $n\text{-}\pi^*$ in the isomerization paving the way towards the development

of azobenzene based unirotational switches (in π - π^* process) by performing the isomerization inside a chiral medium.

6.3.4 Experimental procedure

Scanning Tunneling Microscopy STM measurements were performed using a Veeco scanning tunneling microscope (multimode Nanoscope III, Veeco) at the interface between highly oriented pyrolytic graphite (HOPG) and a supernatant solution. Solutions of molecules **1-3** were applied to the basal plane of the surface. For STM measurements the substrates were glued on a magnetic disk and an electric contact is made with silver paint (Aldrich Chemicals). The STM tips were mechanically cut from a Pt/Ir wire (90/10, diameter 0.25 mm). The raw STM data were processed through the application of background flattening and the drift was corrected using the underlying graphite lattice as a reference. The latter lattice was visualized by lowering the bias voltage to 20 mV and raising the current to 65 pA. All of the models were minimized with Chem3D at the MM2 level. The molecules were dissolved in 1-phenyloctane with an approximate concentration of 1 mM, and diluted to the concentrations 100 μ M and 10 μ M respectively. The irradiation of the molecules was performed *ex situ*, and *in situ*, i.e. before and after depositing the solutions of **3** on top of HOPG surface, by using UV-Pen Type Lamp (354 nm, 1mW). It is important to note that the *ex situ* irradiation of the molecules **3** did not produced any significant results. This peculiar experiment, i.e. *in situ* irradiation of the sample which is scanned by STM tip, couldn't be performed using the Faraday cage, which is used for STM measurements to shield the setup from electromagnetic fields, and without the glass bell (shielding from acoustic noise) since we had to investigate the samples in an open set-up to avoid warming up the sample.

References

- [1] A. Miura, P. Jonkheijm, S. De Feyter, A. P. H. J. Schenning, E. W. Meijer, F. C. De Schryver, *Small* **2005**, *1*, 131.
- [2] J. M. Tour, *Chem. Rev.* **1996**, *96*, 537.
- [3] K. Okumoto, Y. Shirota, *Chem. Mater.* **2003**, *15*, 699.

- [4] Y. Shirota, *J. Mater. Chem.* **2000**, *10*, 1.
- [5] B. Baisch, D. Raffa, U. Jung, O. M. Magnussen, C. Nicolas, J. Lacour, J. Kubitschke, R. Herges, *J. Am. Chem.Soc.* **2009**, *131*, 442.
- [6] J. M. Mativetsky, G. Pace, M. Elbing, M. A. Rampi, M. Mayor, P. Samorì, *J. Am. Chem.Soc.* **2008**, *130*, 9192.
- [7] G. Pace, V. Ferri, C. Grave, M. Elbing, C. von Hanisch, M. Zharnikov, M. Mayor, M. A. Rampi, P. Samorì, *Proc. Nat. Acad. Sci. USA* **2007**, *104*, 9937.
- [8] A. N. Shipway, I. Willner, *Acc. Chem. Res.* **2001**, *34*, 421.
- [9] V. Balzani, A. Credi, M. Venturi, *ChemPhysChem* **2008**, *9*, 202.
- [10] T. Kondo, K. Uosaki, *J. Photochem. Photobiol. C* **2007**, *8*, 1.
- [11] C. Dugave, L. Demange, *Chem. Rev.* **2003**, *103*, 2475.
- [12] T. Nagele, R. Hoche, W. Zinth, J. Wachtveitl, *Chem. Phys. Lett.* **1997**, *272*, 489.
- [13] F. Krollpfeiffer, C. Muhlhausen, G. Wolf, *Annalen* **1934**, *508*, 39.
- [14] J. Griffiths, *Chem. Soc. Rev.* **1972**, *1*, 481.
- [15] N. Tamai, H. Miyasaka, *Chem. Rev.* **2000**, *100*, 1875.
- [16] R. H. Berg, S. Hvilsted, P. S. Ramanujam, *Nature* **1996**, *383*, 505.
- [17] T. Ikeda, O. Tsutsumi, *Science* **1995**, *268*, 1873.
- [18] I. Willner, S. Rubin, T. Zor, *J. Am. Chem.Soc.* **1991**, *113*, 4013.
- [19] E. W. G. Diau, *J. Phys. Chem. A* **2004**, *108*, 950.
- [20] H. Rau, *In Photochromism: Molecules and Systems; Durr, H., Bouas-Laurent, H., Eds.; Elsevier: Amsterdam and references therein* **1990**, 165.
- [21] G. Zimmerman, L.-Y. Chow, U.-J. Paik, *J. Chem. Phys.* **1958**, *80*, 3528.
- [22] H. Rau, E. Lüddecke, *J. Am. Chem. Soc.* **1982**, *104*, 1616.
- [23] H. Rau, *J. Photochem.* **1984**, *26*, 221.
- [24] L. A. Bumm, J. J. Arnold, M. T. Cygan, T. D. Dunbar, T. P. Burgin, L. Jones, D. L. Allara, J. M. Tour, P. S. Weiss, *Science* **1996**, *271*, 1705.
- [25] J. Henzl, M. Mehlhorn, H. Gawronski, K. H. Rieder, K. Morgenstern, *Angew. Chem. Int. Ed.* **2006**, *45*, 603.
- [26] B. Y. Choi, S. J. Kahng, S. Kim, H. Kim, H. W. Kim, Y. J. Song, J. Ihm, Y. Kuk, *Phys. Rev. Lett.* **2006**, *96*.

- [27] M. Alemani, M. V. Peters, S. Hecht, K. H. Rieder, F. Moresco, L. Grill, *J. Am. Chem. Soc.* **2006**, *128*, 14446.
- [28] S. De Feyter, A. Gesquiere, M. M. Abdel-Mottaleb, P. C. M. Grim, F. C. De Schryver, C. Meiners, M. Sieffert, S. Valiyaveetil, K. Mullen, *Acc. Chem. Res.* **2000**, *33*, 520.
- [29] C. L. Feng, Y. J. Zhang, J. Jin, Y. L. Song, L. Y. Xie, G. R. Qu, L. Jiang, D. B. Zhu, *Surf. Sci.* **2002**, *513*, 111.
- [30] C. Raimondo, F. Reinders, U. Soydaner, M. Mayor, P. Samorì, *Chem. Commun.* **2010**, *46*, 1147.
- [31] J. Zhang, J. K. Whitesell, M. A. Fox, *Chem. Mater.* **2001**, *13*, 2323.
- [32] S. Yasuda, T. Nakamura, M. Matsumoto, H. Shigekawa, *J. Am. Chem. Soc.* **2003**, *125*, 16430.
- [33] Z. Ma, Y.-Y. Wang, P. Wang, W. Huang, Y.-B. Li, S.-B. Lei, Y.-L. Yang, X.-L. Fan, C. Wang, *ACS Nano* **2007**, *1*, 160.
- [34] K. R. Paserba, A. J. Gellman, *Phys. Rev. Lett.* **2001**, *86*, 4338.
- [35] A. J. Gellman, K. R. Paserba, *J. Phys. Chem. B* **2002**, *106*, 13231.
- [36] J. R. Zheng, K. W. Kwak, J. Xie, M. D. Fayer, *Science* **2006**, *313*, 1951.

Conclusions and Perspectives

We have studied the self-assembly on surfaces of different molecular systems into supramolecular nanostructures, as obtained by balancing the interplay of intramolecular, intermolecular, and interfacial interactions. At the solid-liquid interface supramolecular structures, formed by non-covalent interactions like metallo-ligand, hydrogen-bonding and van der Waals interactions have been studied by using Scanning Tunnelling Microscopy (STM).

In this thesis we proved that the combination of supramolecular chemistry at surfaces and interfaces and scanning probe microscopies can offer highest level of control over the bottom-up nanofabrication of functional materials. The use of supramolecular approach made it possible to locate functional groups in the 2D with a high degree of precision, thus to nanopattern the surface at will. STM investigations at the solid-liquid interface enabled the exploration of these structures and dynamic processes with a sub-molecular resolution based on various materials type. In this way we were able to fabricate for the first time a dynamers operating on a surface.

We have demonstrated the possibility of control at the nanoscale of both the geometry and the directionality of supramolecular arrays composed of 1D coordination networks on the graphite surface. Furthermore, the packing of 1D networks on graphite surfaces may be tuned by the proper design of the organic molecules, the choice of metal center and the nature of the supernatant solvent. In the case of Pd(II) cations, the packing of cationic networks generates molecular arrays on the surface, offering empty spaces for the accommodation of anions (BF_4^-) and solvent molecules. For CoCl_2 complexes, the densely packed neutral networks form 2D arrays on the surface. The control on both the geometry of the networks and their polar packing may be of interest to control charge transfer along the 1-D architectures.

We have also given extensive details on how single molecules, decorated with molecular recognition units, are able to self-organize into 2D supramolecular porous networks at the solid-liquid interface. In the collaboration with a group of Prof. Jean-Marie Lehn from Université de Strasbourg (France), we have identified a highly crystalline 2D porous network which only exhibits a limited amount of polymorphism at (sub-) monolayer concentrations. The network was formed by hexatopic diacetylamino-pyridine molecules which can adopt a three-fold symmetry and form multiple strong H-bonds, leading to the formation of supramolecular 2D networks.

We described the bottom-up fabrication of highly compact supramolecular polymeric arrays composed of 6,6'-(2-phenylpyrimidine-4,6-diyl)dipyridin-2(1H)-one molecules based on the generation of four strong (N-H \cdots O) H-bonds which are further reinforced by two (C-H \cdots O) H-bonds of medium strengths. STM studies at the solid-liquid interface revealed that upon use of concentrated solutions, the adsorption of the molecules adopting a nearly planar conformation on the HOPG surface and formation of 2D supramolecular arrays was promoted. Conversely, upon use of solutions at low concentration, the 1D supramolecular arrays, whose helical conformation was observed at the solid-liquid interface. The unambiguous assignment of the two structures was possible by using dispersion-corrected density functional calculations to relax the two-dimensional surface structure of both the planar and helical configurations.

We have demonstrated, that by working at a low concentration, in experimental conditions not susceptible to thermodynamically driven phase segregation between two components on the solid-liquid interface, we have been able for the first time to visualize, by STM on the molecular scale, the physisorption of 1D main-chain bicomponent H-bonded supramolecular polymers at surfaces, owing to appropriate design of complementary building blocks linked by the formation of six H-bonds at each node. By using two different connecting molecules, featuring different conformational rigidity, we were able to control the geometry of the linear supramolecular polymers self-assembled at the solid-liquid interface.

We performed a sub-molecularly resolved STM study of physisorbed monolayers on graphite of a series of N^9 -alkylguanines with linear alkyl side-chains from $-C_2H_5$ up to $-C_{18}H_{37}$. All guanine derivatives were found to form monomorphic 2D crystals, which are stable on the several tens of min time scale and exceed various hundreds of nm². Subtle changes in the length of the alkyl side-chains dramatically influenced the 2D patterns on graphite. Derivatives with alkyl tails longer than C_{12} self-assembled into linear H-bonded ribbons. For derivatives with tails of intermediate length (from C_6 to C_{10}) no H-bonded supramolecular polymers were formed at the solid-liquid interface. Monolayers of single (non-H-bonded) molecules or H-bonded dimers were observed. Furthermore, we have also studied the metal-templated reversible assembly/reassembly process of a N^9 -alkylguanine into highly ordered quartets and ribbons, achieving a submolecular resolution STM visualization of such a process at the solid-liquid interface on HOPG surfaces. Guanine derivative equipped with C_{18} alkyl chain, was reversibly interconverted at the solid-liquid interface between two highly ordered supramolecular motifs,

that is, H-bonded ribbons and G4-based architectures, upon subsequent addition of [2.2.2]cryptand, potassium picrate, and trifluoromethanesulfonic acid. The visualization of such supramolecular interconversion at the solid–liquid interface represents the first step towards the generation of nanopatterned responsive architectures.

We have utilized STM to visualize large conformational changes of a responsive molecular building block resulting in its dramatically altered self-assembly behavior at the solid–liquid interface. Protonation can successfully be used to overcome the repulsive interaction between the adjacent N atoms present in the neutral “kinked” heteroaromatic BTP molecule and result in the formation of an “extended” conformation on a HOPG surface. This represents the first yet crucial step towards the development of reversible pH triggered switches at the solid–liquid interface.

Finally, we have shown that properly designed fluorene platform, equipped with azobenzene functional unit can undergo *cis-trans* photoisomerisation in large domains at HOPG surfaces. Functional molecules were found to self-assemble into 3D structure at the solid–liquid interface. The entire supramolecular architecture in case of the molecules in their *trans* form was found to be stabilized by the formation of H-bonds between the adjacent molecules and further interdigitation of alkyl chains; in case of the molecules in their *cis* form the self-assembled structures were further stabilized by unspecific weak van der Waals interactions between the azobenzene units, formation of H-bonds between the molecules and partial interdigitation of alkyl chains.

In summary, we have given extensive details on how single molecules, decorated with molecular recognition units, are able to self-organize into 2D supramolecular crystalline materials. This paves the way towards supramolecular scaffolding, i.e. the use of molecular module designed to undergo recognition events and incorporating functional units, to form pre-programmed architectures with a sub-*ångström* resolution, and ultimately functional materials with properties controlled with a high degree of precision. Supramolecular materials, i.e. materials exploiting the use of reversible and dynamic non-covalent interactions, have also the intrinsic ability to both recognize and exchange their constituents; they are constitutionally dynamic materials and may in principle select their constituents in response to external stimuli. Increasing their complexity, being one of the greatest challenges in materials science, can be pursued through self-assembly by exploiting interactions which act in a hierarchical manner,

governing on distinct scales, to achieve a high degree of order on both molecular and mesoscopic dimensions. This leads to the elaboration of smart materials as well as meta-materials. Both smart and meta-materials are defined by their ability to transform energy, i.e. the transformation of external stimuli into the desired smart or meta property (photons into electrons, heat into electrons, electrons into displacement, electrons into algorithms), making supramolecular materials excellent candidates for such colossal tasks. The control of the amplitude of the crystallinity in 2D is one of the first objectives in the reach of future Scanning Tunneling Microscopy studies. Of much interest is also the characterization of 2D self-assembly at curved interfaces, much like micelles, membranes, nanotubes and rough interfaces, which are representative objects of the curved space that we inhabit.

Acknowledgments

It is a great pleasure for me to express my deep gratitude to Prof. Paolo Samorì for giving me the opportunity to work in his group. He has provided exceptional scientific guidance and informal yet stimulating atmosphere.

I am also grateful to the different research groups that collaborated to an interdisciplinary work such as that presented in this thesis. In particular I would like to thank Prof. Jean-Marie Lehn and Prof. Mir Wais Hosseini at the Université de Strasbourg (France), Prof. Gian Piero Spada at the Università di Bologna (Italy), Prof. Stefan Hecht at the Humboldt-Universität zu Berlin (Germany), Prof. Mats Persson at the University of Liverpool (United Kingdom) and all the co-workers in such groups: Dr. Abdelaziz Jouaiti, Dr. Artur R. Stefankiewicz, Dr. Anne Petitjean, Gaël Schaeffer, Dr. Stefano Lena, Prof. Stefano Masiero, Dr. Silvia Pieraccini, Rosaria Perone, Dr. David Bléger, Tamer El Malah, Dr. Felix Hanke.

I am also grateful to all my colleagues and co-workers at ISIS-UdS that have made these three years in Strasbourg an unforgettable and terrific time: Dr. Leszek Zalewski, Dr. Massimo Bonini, Dr. Núria Crivillers, Dr. Jeffrey Mativetsky, Corinna Raimondo, Dr. Emanuele Orgiu, Andrea Cadeddu, Rebecca C. Savage, Dr. Matthias Treier, Dr. Jörn-Oliver Vogel, Dr. Luc Piot, Dr. Anna Llanes Pallas, Marie-Claude Jouati and Prof. Jack Harrowfield.

A special thanks goes to Carlos-Andres Palma for his superb spirit, inspiring and stimulating discussions.

I would also like to acknowledge the French Ministry of Research for the financial support for a predoctoral fellowship.

Last but not least, I want truly acknowledge my family, especially my wife Anna, whose love gave me the *force* to tackle this experience.

Artur

List of Publications

V. Patroniak, J. M. Lehn, M. Kubicki, **A. Ciesielski**, M. Walesa, "Chameleonic ligand in self-assembly and synthesis of polymeric manganese(II), and grid-type copper(I) and silver(I) complexes", *Polyhedron* 25, 2643 (2006)

A. R. Stefankiewicz, M. Walesa, P. Jankowski, **A. Ciesielski**, V. Patroniak, M. Kubicki, Z. Hnatejko, J. M. Harrowfield, J. M. Lehn, "Quaterpyridine ligands forming helical complexes of mono- and dinuclear (helicate) forms", *Eur. J. Inorg. Chem.* 2910 (2008)

A. Ciesielski, M. Wałęsa, V. Patroniak, "Self-assembled grid-type complexes of manganese(II), iron(II), cobalt(II) and zinc(II)", *Pol. J. Chem.*, 82, 1231 (2008)

A. Ciesielski, A. R. Stefankiewicz, M. Wałęsa-Chorab, V. Patroniak, Z. Hnatejko, J. M. Harrowfield, "Association of quaterpyridine complex cations with polyanionometallates", *Supramol. Chemistry*, 21, 48 (2009)

A. Ciesielski, G. Schaeffer, A. Petitjean, J.-M. Lehn, P. Samorì, "STM Insight into Hydrogen-Bonded Bicomponent 1 D Supramolecular Polymers with Controlled Geometries at the Liquid-Solid Interface", *Angew. Chem. Int. Ed.*, 48, 2039 (2009)

A. Ciesielski, L. Piot, P. Samorì, A. Jouaiti, M. W. Hosseini, "Molecular Tectonics at the Solid/Liquid Interface: Controlling the Nanoscale Geometry, Directionality, and Packing of 1D Coordination Networks on Graphite Surfaces", *Adv. Mater.*, 21, 1131 (2009)

A. Ciesielski, A. R. Stefankiewicz, V. Patroniak, M. Kubicki, "Preparation, characterization and crystal structures of three salts of the quaterpyridine ligand", *J. Mol. Struct.*, 930 110 (2009)

A. Ciesielski, S. Lena, S. Masiero, G.P. Spada, P. Samorì "Dynamers at the solid-liquid interface: controlling the reversible assembly/re-assembly process between two highly ordered supramolecular guanine motifs" *Angew. Chem. Int. Ed.* 49, 1963 (2010). (elected as VIP + cover picture, article highlighted in *Nature*, *Nature Chemistry* and *C&EN*)

A. Ciesielski,* A. Gorczyński, P. Jankowski, M. Kubicki, V. Patroniak "Cobalt(II) complex with new terpyridine ligand: an ab initio geometry optimization investigation" *J. Mol. Struct.*, 973, 130 (2010)

A. Ciesielski, R. Perone, S. Pieraccini, G. P. Spada, P. Samorì "Nanopatterning the surface with ordered supramolecular architectures of N9-alkylated guanines: STM reveals" *Chem. Commun.* 46, 4493 (2010).

A. Ciesielski, C.-A. Palma, M. Bonini, P. Samorì "Towards Supramolecular Engineering of Functional Nanomaterials: Pre-Programming Multi-component 2D Self-Assembly at Solid-Liquid Interfaces", *Adv. Mater.* (2010)

Poster presentation

"Molecular tectonics at the solid-liquid interface: controlling the directionality of 1D coordination network forming 2D nanoscale arrays" **A. Ciesielski**, L. Piot, A. Jouaiti, M. W. Hosseini and P. Samorì, 26 -30 May 2008, Strasbourg (France).

"Molecular tectonics on solid-liquid interface: controlling the directionality of 1D coordination network forming 2D nanoscale arrays" **A. Ciesielski**, L. Piot, A. Jouaiti, M. W. Hosseini and P. Samorì, 1st European School on Ellipsometry, September 2008, Ostuni (Italy).

"The Self-Assembly of Guanine Derivatives on Graphite Surface", **A. Ciesielski**, L. Piot, R. Perone, S. Lena, S. Masiero, S. Pieraccini, G. P. Spada and P. Samorì, "Self Assembly of Guanosine Derivatives: From Biological Systems to Nanotechnological Applications" 20-25 June 2009, Obergugl (Austria).

"Dynamers at the solid-liquid interface: controlling the reversible assembly/re-assembly process between two highly ordered supramolecular guanine motifs" **A. Ciesielski**, S. Lena, S. Masiero, G. P. Spada and P. Samorì, "Fundamentals of Guanosine Self-assembly and Quadruplex Formation" 27-29 October 2009, Ischia Island (Italy).

"Nanopatterning the surface with ordered supramolecular architectures of N9-alkylated guanines: Dynamers at the solid-liquid interface." **A. Ciesielski**, R. Perone, S. Pieraccini, S. Lena, S. Masiero, G. P. Spada, P. Samorì, 17th Course of the International School of Liquid Crystals on "Organic Nanomaterials for Electronics and Photonics" 13-20 April 2010, Erice (Italy).

Selected Oral Presentations

"Surface nanopatterning at the solid-liquid interface: controlling the nanoscale geometry of 1-D metalloligand and H-bonded networks on graphite surface", **A. Ciesielski**, G. Schaeffer, A. Petitjean, J.-M. Lehn, M. W. Hosseini and P. Samorì, NANOTECH INSIGHT 2009, 29 March – 2 April 2009, Barcelona (Spain).

“Pre-programmed self-assembly at solid-liquid interfaces: towards 2D supramolecular engineering of functional architectures” **A. Ciesielski**, P. Samorì, 17 December 2009, Poznań (Poland).

“Scanning Tunneling Microscopy (STM) – visualization of the self-assembly at the nano-scale” **A. Ciesielski**, P. Samorì, 18 December 2009, Poznań (Poland).

“Dynamers at the solid-liquid interface: controlling the reversible assembly/re-assembly process between two highly ordered supramolecular guanine motifs” **A. Ciesielski**, S. Lena, S. Masiero, G. P. Spada and P. Samorì, 15 - 19 March 2010, Microscopies a Sonde Locale Forum 2010, Mittelwihr, (France).